

**Development of a fuzzy rule based expert system
for flood forecasts
within the meso-scale Upper Main basin**

Bei der Fakultät Bauingenieur- und Vermessungswesen
der Universität der Bundeswehr München zur Erlangung der Würde eines
Doktor-Ingenieurs (Dr.-Ing.) genehmigte Abhandlung.

Vorgelegt von

Sabine Pakosch

aus Schweinfurt

Hauptberichter:

Prof. Dr.-Ing. Markus Disse

Mitberichter:

Prof. Dr. rer. nat. Dr.-Ing. habil. András Bárdossy

Tag der mündlichen Prüfung: 18. Juli 2011

Neubiberg 2011

Universität der Bundeswehr München
Fakultät für Bauingenieur- und Vermessungswesen

Thema der Dissertation Development of a fuzzy rule based expert system for flood forecasts within the meso-scale Upper Main basin

Verfasser Dipl.-Ing. Sabine Pakosch, M.Sc.

Promotionsausschuss

Vorsitzender Prof. Dr.-Ing. F. Wolfgang Günthert
Universität der Bundeswehr München
Institut für Wasserwesen
Professur für Siedlungswasserwirtschaft und Abfalltechnik

1. Berichterstatter Prof. Dr.-Ing. Markus Disse
Universität der Bundeswehr München
Institut für Wasserwesen
Professur für Wasserwirtschaft und Ressourcenschutz

2. Berichterstatter Prof. Dr. rer. nat. Dr.-Ing. habil. András Bárdossy
Universität Stuttgart
Institut für Wasserbau
Lehrstuhl für Hydrologie und Geohydrologie

Tag der Prüfung 18. Juli 2011

Mit der Promotion erlangter akademischer Grad
Doktor der Ingenieurwissenschaften (Dr.-Ing.)

Neubiberg, den 9. Mai 2011

The more, the fuzzier ...

(Dubois and Prade, 1980)

Acknowledgements

First, I would like to express my gratitude to Prof. Markus Disse (UniBw Munich), who has given me the chance to work in his group, for his continuous support and constructive feedbacks throughout this thesis.

Sincere thanks are given to Prof. András Bárdossy (University Stuttgart) for accepting to co-supervise my thesis and for his invaluable suggestions and discussions.

This work is part of the research project HORIX funded by the German Ministry of Education and Research (BMBF). Many thanks to all co-workers and partners for the good atmosphere and cooperation, in particular to Jan Bliefernicht (University Augsburg) and Jens Grundmann (TU Dresden). The collaboration with the Bayerischen Landesamt für Umwelt is greatly acknowledged.

Furthermore, thanks to all colleagues at the Institute of Hydro Sciences for the overall good working atmosphere and the indispensable coffee breaks. Especially to Wolfgang Rieger and Patrick Keilholz, it was a pleasure for me to work with you.

Many thanks to Dr. Sven Wagner (KIT, IMK-IFU), Claudia Mende and Isabel Hörner for proof-reading the manuscript, giving valuable suggestions and their help with the English language.

I am extremely grateful to my family for their understanding and support throughout my whole life.

Last but not least, I would like to thank my partner Sven for his continuous support, encouragement and understanding. I am looking forward to our common future with our two wonderful children, Norah and Marla.

Contents

Acknowledgements	i
List of Figures	v
List of Tables	xi
List of Abbreviations	xiii
List of Symbols	xv
Kurzfassung	xix
1 Introduction	1
2 Hydrological Modelling	3
2.1 Concepts and classifications	5
2.2 Hydrological model WaSiM-ETH	9
2.3 Algorithm for calibration: Shuffled Complex Evolution	12
3 Fuzzy Modelling	17
3.1 Fuzzy Sets	20
3.1.1 Operations on fuzzy sets	21
3.1.2 Fuzzy numbers	23
3.1.3 Fuzzy sets versus probabilities	25
3.2 Fuzzy Logic and Fuzzy Inference Systems	25
3.2.1 Fuzzy Logic	26
3.2.2 Mamdani inference system	28
3.2.3 Takagi-Sugeno inference system	31
3.2.4 Mamdani versus Takagi-Sugeno inference system.	32
3.2.5 Fuzzy inference systems and artificial neural networks	32
3.3 Training methods for fuzzy inference systems	36
3.3.1 Neuro-Fuzzy	36
3.3.2 Simulated Annealing	38
3.4 Tukey depth function	41
4 The study area: Upper Main	43
4.1 Catchment characteristics	43
4.2 Data basis	47
5 Model development for the Upper Main basin	50
5.1 Hydrological Modelling	50

Contents

5.1.1	Model setup	50
5.1.2	Calibration and validation	52
5.1.3	Simulations of extreme flood scenarios	63
5.2	Fuzzy Modelling	67
5.2.1	Input variables	67
5.2.2	Fuzzy inference systems for the 3 day forecast	71
5.2.3	Fuzzy inference systems for the 6 and 12 hour forecast	80
5.2.4	Fuzzy inference systems for the 48 hour forecast	84
5.3	Mamdani inference system and Tukey depth function	99
5.3.1	Tukey depth of different argument combinations	99
5.3.2	Investigation of Tukey depth as an argument	100
5.3.3	Investigation of the extrapolation behavior of Mamdani inference systems	109
5.4	Performance comparison	113
5.4.1	Mamdani inference systems of observed and generated database	113
5.4.2	Mamdani inference systems and WaSiM-ETH	117
6	Expert System for flood forecasts	121
6.1	Principle concept of the forecast system ExpHo-HORIX	121
6.2	Setup for the Upper Main basin	125
7	Summary and Outlook	127
	Bibliography	133
	Appendix	143
A	Fuzzy arithmetic	145
B	Hydrological Modelling	147
C	Fuzzy Modelling	150
D	Mamdani inference system and Tukey depth	154
E	Mamdani inference systems of observed and generated database	160

List of Figures

2.1	Classification of optimization algorithms	8
2.2	Main modules of the hydrological model WaSiM-ETH Release 6.4 version 2	9
2.3	General scheme of the SCE algorithm for the 2-dimensional case	14
3.1	Four common types of continuous membership functions $\mu(x)$	21
3.2	Schematic diagram of two fuzzy sets, the fuzzy-complement, fuzzy-intersection, and fuzzy-union	22
3.3	Basic scheme of the performed Mamdani inference system	30
3.4	Basic scheme of the performed Takagi-Sugeno inference system	32
3.5	Schematic diagram of a node and general configuration of a simple three layer neural net	34
3.6	Schematic diagram of a cooperative and concurrent Neuro-Fuzzy approach	37
3.7	Schematic diagram of a five layer Mamdani Neuro-Fuzzy inference system	37
4.1	Location of Germany, Europe, and the Upper Main basin in the North-East of the national state Bavaria in Germany	43
4.2	Catchment of the Upper Main river including the three main gauges and the main tributaries	44
4.3	Land use within the Upper Main basin considering the Corine Land Cover Raster Data 2000	48
4.4	Geology within the Upper Main basin considering the soil map BÜK 1000	48
5.1	Derived subcatchments of the WaSiM-ETH model Upper Main and the location of the additional recording points	51
5.2	Illustration of the RMSE response surfaces based on 5000 Monte Carlo simulations for the three subcatchments Heinersdorf, Steinberg, and Ködnitz	55
5.3	GSA results for the subcatchment Heinersdorf considering the WaSiM-ETH parameter K_D , d_r , and k_{rec} as well as the objective functions VE and RMSE	56
5.4	Comparison of the GSA results for the subcatchments Heinersdorf, Ködnitz, and Steinberg considering the WaSiM-ETH parameter d_r and the objective functions VE and RMSE	56
5.5	Comparison of the results of the different SCE setups with the best RMSE Monte Carlo simulation considering subcatchment Ködnitz	60
5.6	Calibration results of the main stations Schwürbitz and Kemmern using SCE setup Upper Main	61
5.7	Validation results of the main stations Schwürbitz and Kemmern using SCE setup Upper Main	62
5.8	Possible realisations of the hourly areal precipitation of an 1000-year extreme event within the Upper Main basin	64

List of Figures

5.9	Examples of simulated hydrographs for five different realisations of the 250-year extreme precipitation event considering wet preconditions in summer and winter at gauge Mainleus	64
5.10	Simulated minimum, maximum, and mean peak with corresponding standard deviation for each considered return period of precipitation in summer and winter under wet precondition at gauge Mainleus	65
5.11	Spatial distributions of the total precipitation volume of the 250-year extreme precipitation summer event within the Upper Main basin considering the WaSiM-ETH model boundaries	65
5.12	Examples for the fuzzification of daily based arguments	72
5.13	Linguistical description of the optimized 5 rule MS inference system considering argument combination D3_4.	73
5.14	Linguistical description of the optimized 5 rule TS inference system considering argument combination D3_4.	73
5.15	Development of the correlation values of D3_1 to D3_5 considering the training / validation sets and both fuzzy inference systems	74
5.16	Examples for the performance of the best fitted MS and TS rule systems considering the 3 day forecast of $Q(t + 3d)$ at gauge Kemmern	75
5.17	Examples for the performance of the best fitted MS and TS rule systems considering the 3 day forecast of $\Delta Q(t, t + 3d)$ at gauge Kemmern	77
5.18	Performance comparison of MS and TS systems for the forecast of $Q(t + 3d)$ at gauges Schwürbitz and Mainleus considering the flood hydrograph	79
5.19	Performance comparison of MS and TS systems for the forecast of $Q(t + 3d)$ at gauges Schwürbitz and Mainleus considering WL 1	79
5.20	Differences between the daily and hourly based membership functions exemplarily shown for the argument/response discharge at gauge Kemmern	81
5.21	Example of a flood event simulated with the best fitted MS and TS inference systems for the 6 and 12 h forecast at gauge Kemmern	82
5.22	Fuzzification of the argument/response discharge performing the pure statistical method and the combination of the statistical and equally-partitioning method	85
5.23	Development of the objective function least-squares and the corresponding correlation values of the training and validation sets considering the four MS optimization setups for H48_1	86
5.24	Development of the objective function least-squares and the corresponding correlation values of the training and validation sets considering the four MS optimization setups for H48_2	86
5.25	Examples for two out of the ten highest flood events simulated with four different MS optimization setup considering 20 rules	87
5.26	Examples for two out of the ten highest flood events simulated with the result of the MS_6MF optimization setup considering 20 rules (left: training; right: validation).	88
5.27	Correlation values of the seven TS inference systems trained for each investigated argument combination and TS optimization setup	90
5.28	Development of the objective function least-squares and the corresponding correlation values considering H48_1 TS_3MF_P and H48_3TS TS_3MF_P	91
5.29	Examples for two out of the ten highest flood events simulated with the reference case of the MS optimization setup and the best fitted TS inference system	92

5.30	Correlation, NS, DPH and DPT values for each investigated argument combination H48_1 to H48_17 performing the MS_6MF (20 rules) optimization setup . . .	94
5.31	Examples for two out of the ten highest flood events simulated with the argument combinations H48_1 to H48_6	95
5.32	Examples for two out of the ten highest flood events simulated with the argument combinations H48_1 and H48_7 to 9	95
5.33	Examples for two out of the ten highest flood events simulated with the argument combinations H48_8 and H48_10 to 17	95
5.34	Examples for the 48 hour forecast at gauges Schwürbitz and Mainleus	97
5.35	Target variable $Q(t + 48h)$ plotted via log-scaled Tukey depth values considering the argument combinations H48_1 or H48_2	100
5.36	$Q_{up}(t)$ and $API12h(t)$ plotted via the target variable $Q(t + 48h)$ considering case H48_1	100
5.37	Fuzzifications of the argument <i>Tukey depth</i> considering optimization setups MS_T1, MS_T2, and MS_T3	102
5.38	Correlation and NS values considering all 30 flood events as well as DPH and DPT values considering the ten highest flood events for each investigated argument combination H48_1 to H48_6 performing the optimization setups MS_6MF, MS_T1, MS_T2, and MS_T3	103
5.39	Examples for two out of the ten highest flood events simulated with the argument combination H48_1 and the different optimization setups MS_6MF, MS_T1, MS_T2, and MS_T3	103
5.40	Extended fuzzification of the argument / response $Q(t)$ and argument $Q_{up}(t)$ for the investigations of the optimization setups MS_T4, MS_T5, and MS_T6	104
5.41	Correlation and NS values considering all 30 flood events as well as DPH and DPT values considering the ten highest flood events for each investigated argument combination H48_1 to H48_6 performing the optimization setups MS_6MF, MS_T4, MS_T5, and MS_T6	105
5.42	Examples for two out of the ten highest flood events simulated with the argument combination H48_1 and the different optimization setups MS_6MF, MS_T4, MS_T5, and MS_T6	106
5.43	Correlation and NS values considering all 30 flood events as well as DPH and DPT values considering the ten highest flood events for each investigated argument combination H48_1 to H48_6 performing the optimization setups MS_6MF, MS_T5, MS_T7, and MS_T8	107
5.44	Examples for two out of the ten highest flood events simulated with the argument combination H48_1 and the different optimization setups MS_6MF, MS_T5, MS_T7, and MS_T8	108
5.45	Generalization of two possible shapes of the cumulative curve based on Tukey depth values.	110
5.46	Cumulative curves based on Tukey depth values calculated on hourly data considering the time period from 01.01.1992 to 31.12.2004 and only the 30 highest flood events for the argument combinations H48_1	110
5.47	Development of the objective function least-squares and the corresponding correlation values of the training and validation sets considering the optimization setups MS_6MF, MS_T5, and MS_T5m for H48_1	111
5.48	Training and validation results considering the extrapolation behavior of MS inference systems H48_1 MS_T5 20 rules and 40 rules	112

List of Figures

5.49	Fuzzification of the argument/response discharge $Q(t)$ for the generated and historical database	113
5.50	Examples for the performance of the inference systems MS_6MF and MS_T5, H48_1s, H48_1w and H48_1a considering generated hydrographs of the validation set	115
5.51	Examples for the simulation of historical flood events performing MS_6MF and MS_T5 (H48_1s, w, a) inference systems.	116
5.52	Examples for the simulation of observed flood events performing WaSiM-ETH, MS_6MF and MS_T5 inference systems (H48_1).	118
5.53	Turning band simulations with WaSiM-ETH.	119
5.54	Fuzzy simulations considering a 30 % of the standard deviation increased and decreased forecasted cumulated areal precipitation	119
6.1	General scheme of the fuzzy rule based forecast system ExpHo-HORIX	123
6.2	Example of the ExpHo-HORIX main configuration file	126
B.1	Simulated minimum, maximum, and mean peak with corresponding standard deviation for each considered (1) return period of precipitation in summer / winter and (2) model precondition at gauge Kemmern	147
B.2	Simulated minimum, maximum, and mean peak with corresponding standard deviation for each considered (1) return period of precipitation in summer / winter and (2) model precondition at gauge Schwürbitz	148
B.3	Simulated minimum, maximum, and mean peak with corresponding standard deviation for each considered (1) return period of precipitation in summer / winter and (2) model precondition at gauge Mainleus	149
C.1	Linguistical description of the best fitted MS inference system considering the direct 3 day forecast of discharge $Q(t + 3d)$: D3_4, 23 rules.	150
C.2	Linguistical description of the best fitted TS inference system considering the direct 3 day forecast of discharge $Q(t + 3d)$: D3_4, 25 rules.	151
C.3	Development of the correlation values for argument combinations dD3_1 to dD3_3 and MS inference systems	152
C.4	Development of the correlation values for argument combinations dD3_3 to dD3_5 and MS inference systems	152
C.5	Development of the correlation values for argument combinations dD3_1 to dD3_3 and TS inference systems	152
C.6	Development of the correlation values for argument combinations H6_1 / H6_3 and MS inference systems	153
C.7	Example of a flood event simulated with the best fitted MS and TS inference systems for the 6 and 12 hour forecast at gauge Mainleus	153
C.8	Example of a flood event simulated with the best fitted MS and TS inference systems for the 6 and 12 hour forecast at gauge Schwürbitz	153
D.1	Examples for a smaller flood event simulated with argument combination H48_1 and the different optimization setups MS_6MF, MS_T1, MS_T2, MS_T3, MS_T4, MS_T5, MS_T6, MS_T7, and MS_T8.	154
D.2	Cumulative curves based on Tukey depth values calculated on hourly data considering the time period from 01.01.1992 to 31.12.2004 and only the 30 highest flood events for the argument combinations H48_2	155

D.3	Cumulative curves based on Tukey depth values calculated on hourly data considering the time period from 01.01.1992 to 31.12.2004 and only the 30 highest flood events for the argument combinations H48_3	155
D.4	Training and validation results considering the extrapolation behavior of MS inference systems for H48_1, MS_6MF, 20 rules, 40 rules, and 23 rules	156
D.5	Training and validation results considering the extrapolation behavior of MS inference systems for H48_1, MS_T5m, 20 rules, 40 rules, and 32 rules	157
D.6	Performance of the inference systems MS_6MF and MS_T5 (H48_1) considering the twelve highest observed flood events and the 48 hour forecast at gauge Kemmern	159
E.1	Development of the correlation values for MS_6MF and MS_T5 (H48_1s, w, a) inference systems	160
E.2	Development of the DPH values for MS_6MF and MS_T5 (H48_1s, w, a) inference systems	161
E.3	Development of the DPT values for MS_6MF and MS_T5 (H48_1s, w, a) inference systems	162

List of Tables

2.1	Fields of application of hydrological models	3
2.2	Objective functions which can be chosen for the SCE optimization of the hydrological model WaSiM-ETH	16
3.1	Essential differences between fuzzy set theory and probability considering the properties of the characteristics functions	26
3.2	Essential Boolean logical and implication operators considering two crisp sets . .	28
3.3	Properties of the Mamdani and the Takagi-Sugeno inference system.	33
3.4	Comparison of fuzzy inference systems and artificial neural networks	35
3.5	Parameters of the Simulated Annealing algorithm	40
4.1	Travel times of flood waves and tributaries of the Upper Main catchment	46
4.2	The five highest observed discharges for the three Upper Main gauges Kemmern, Schwürbitz, and Mainleus	46
4.3	The five highest observed water levels for the three Upper Main gauges Kemmern, Schwürbitz, and Mainleus	46
4.4	Discharges of different flood frequencies for the three Upper Main gauges Kemmern, Schwürbitz, and Mainleus	47
4.5	Warning levels for the three Upper Main gauges Kemmern, Schwürbitz, and Mainleus	47
5.1	WaSiM-ETH 6.4 model configuration applied for the Upper Main basin.	50
5.2	General calibration parameters with respect to the chosen WaSiM-ETH setup. . .	53
5.3	Definition of the sensitivity classes for the General Sensitivity Analysis	53
5.4	Limits of the WaSiM-ETH parameter considering Monte Carlo simulations and the subcatchments Heinersdorf, Steinberg, and Ködnitz	54
5.5	GSA results for the subcatchments Heinersdorf, Steinberg, and Ködnitz considering the evaluated levels of significance and the objective functions VE and RMSE	57
5.6	Parameters of the SCE algorithm	58
5.7	Boundary conditions of three investigated SCE optimization setups.	58
5.8	Limits of the WaSiM-ETH parameter considering the SCE optimization and Monte Carlo simulations as well as the subcatchments Heinersdorf, Steinberg, and Ködnitz	59
5.9	Optimization results for the subcatchments Heinersdorf, Steinberg, and Ködnitz considering three different SCE setups	59
5.10	Performance values of the SCE calibration and validation for all gauges within the Upper Main model	62
5.11	Number of observed trespasses considering the Upper Main gauges Kemmern, Schwürbitz, and Mainleus as well as warning level 1	71
5.12	Combinations of daily based arguments investigated for the direct 3 day forecast of discharge	72

List of Tables

5.13	Evaluation results for the best fitted MS and TS inference systems at gauge Kemmern considering the forecast of $Q(t + 3d)$ and all investigated argument combinations	74
5.14	Combinations of daily based arguments investigated for the forecast of discharge changes $\Delta Q(t, t + 3d)$	76
5.15	Evaluation results for the best fitted MS and TS inference systems considering the forecast of $\Delta Q(t + 3d)$ at gauge Kemmern and all investigated argument combinations	77
5.16	Evaluation results for MS and TS inference systems considering the forecast of $Q(t + 3d)$ at gauges Schwürbitz and Mainleus	79
5.17	Combinations of hourly based arguments investigated for the 6 and 12 hour forecast of discharge	81
5.18	Evaluation results for the best fitted MS and TS inference systems considering the forecast of $Q(t + 6h)$ and $Q(t + 12h)$ at gauge Kemmern	82
5.19	Evaluation results for the best fitted MS and TS inference systems considering the forecast of $Q(t + 6h)$ and $Q(t + 12h)$ at gauges Mainleus and Schwürbitz	83
5.20	Argument combinations considered for the investigation of the four MS optimization setups MS_3MF, MS_6MF, MS_3MF_fR, and MS_6MF_fR.	86
5.21	Evaluation results of the 20 rule MS inference systems considering the MS setup MS_3MF, MS_6MF, MS_3MF_fR, and MS_6MF_fR H48_1 as well as the argument combinations H48_1 and H48_2	88
5.22	Argument combinations considered for the investigation of four different TS optimization setups TS_3MF, TS_6MF, TS_3MF_P, and TS_6MF_P	90
5.23	Evaluation results of the MS reference case and the best fitted TS inference system considering the 48 h forecast	92
5.24	Argument combinations investigated for an improvement of the 48 h forecast performing the MS inference system MS_6MF, 20 rules.	93
5.25	Evaluation results for the best fitted MS_6MF inference systems considering the 48 h forecast at the gauges Schwürbitz and Mainleus	97
5.26	Evaluation results of the best fitted MS_6MF and MS_T5 (H48_1s, w, a) inference systems for the 48 hour forecast	114
5.27	Evaluation results for MS_6MF and MS_T5 (H48_1s, w, a; H48_1) inference systems considering the simulation of 30 observed winterly flood events	115
5.28	Evaluation results for MS_6MF and MS_T5 (H48_1) inference systems as well as WaSiM-ETH considering the simulation of 23 observed flood events	118
5.29	Goodness of fit values for MS_6MF and MS_T5 (H48_1) considering fuzzy simulations with a 30 % of the standard deviation increased and decreased forecasted cumulated areal precipitation	119
6.1	General properties of the fuzzy based forecast system ExpHo-HORIX.	124
6.2	Parameters a and b of the SCEM analyse for the three main gauges Kemmern, Schwürbitz, and Mainleus	125

List of Abbreviations

Abbreviation	Meaning
ANN	Artificial Neural Network
ARMA	Autoregressive Moving Average approach
ARS	Adaptive Random Search optimization algorithm
Bayer. HND	Bavarian administration for flood forecasts (Bayerischer Hochwassernachrichtendienst)
BMBF	Federal Ministry for Education and Research of Germany (Bundesministerium für Bildung und Forschung)
CCE	Competitive Complex Evolution algorithm
ExpHo-HORIX	fuzzy based flood warning system (Expertensystem Hochwasser - HORIX)
FEM	Finite Element Method
FIS	Fuzzy Inference System
GSA	General Sensitivity Analysis
HBV	Hydrologiska Byrans Vattenbalansavdelning (rainfall-runoff model)
HORIX	Development of an operational expert system for flood risk management considering prediction uncertainty
LAI	leaf area index
m.a.s.l.	above sea level
MS	Mamdani inference system
PREVAH	Precipitation-Runoff-Evapotranspiration Hydrological response units model
RIMAX	German abbreviation for Risk Management of Extreme Flood Events (Risikomanagement extremer Hochwasserereignisse)
RS	Rule system
SA	Simulated Annealing optimization algorithm
SA-MS	SA optimization process considering Mamdani inference systems
SA-TS	SA optimization process considering Takagi-Sugeno inference systems
SAC-SMA	Sacramento soil moisture accounting model
SCE	Shuffled Complex Evolution optimization algorithm
SCEM	Shuffled Complex Evolution Metropolis optimization algorithm
SHE	Système Hydrologique Européen
SIXPAR	simplified research version of SAC-SMA
SWAT	Soil and Water Assessment Tool
TOPMODEL	rainfall-runoff model
TS	Takagi-Sugeno inference system
VIC	Variable Infiltration Capacity model
WaSiM-ETH	Water balance Simulation Model ETH

List of Symbols

Symbol	Unit	Definition
α	[-]	α -level sets of a fuzzy set A
α	[-]	level of significance (two sample Kolmogoroff-Smirnov test)
β	[°]	local slope angel (limited to max. $\beta > 45^\circ$)
$\mu_A(x)$	[-]	membership function of fuzzy set A
Ψ	[m]	hydraulic head as sum of the suction and geodetic altitude
\Re	[-]	set of real numbers
Θ	[m ³ /m ³]	water content
a	[-]	ordinary set
b_j	[-]	threshold value of node j (bias)
d	[-]	number of parameters within the parameter vector \mathbf{p}
d_r	[m ⁻¹]	drainage density (scaling parameter)
$f(\cdot)$	[-]	activation function considering neural nets
$h_{geo,0}$	[m.a.s.l.]	geodetic altitude of the soil surface
h_{GW}	[m.a.s.l.]	groundwater table
$i(a,b)$	[-]	t-norm (bivariate function considering intersection)
k	[m/s]	hydraulic conductivity
k_B	[J/K]	Boltzmann constant
k_B	[m]	recession constant for baseflow
k_{rec}	[-]	recession constant for hydraulic conductivity
k_s	[m/s]	saturated hydraulic conductivity
$k_{s,z}$	[m/s]	saturated hydraulic conductivity within depth z
m	[-]	soil layer
\mathbf{p}	[-]	parameter vector (individual)
p	[-]	random number in [0, 1]
p'	[-]	probability of intermediate state
q	[m/s]	specific flux
r	[-]	correlation coefficient
$supp(A)$	[-]	support of a fuzzy number
t	[s]	time
$u(a,b)$	[-]	t-conorm (bivariate function considering union)
x	[-]	crisp input of a fuzzy inference system
y	[-]	crisp output of a fuzzy inference system
z	[m]	vertical coordinate (depth)
A	[-]	fuzzy subset (also fuzzy set)
A	[-]	fuzzy number (special case of a general fuzzy set)

List of Symbols

A	[-]	fuzzified argument
A'	[-]	complement of a fuzzy set A
API	[diverse]	areal antecedent precipitation index
B	[-]	fuzzified response
CP	[-]	circulation pattern
cfP	[diverse]	forecasted cumulated areal precipitation
cNT	[-]	number of correctly forecasted trespasses
D_d	[-]	d-dimensional half-space depth
DOF_j	[-]	degree of fulfillment of rule j
ΣDOF_{fixed}	[-]	minimum sum of the degrees of fulfillment for each rule calculated over all time steps
DPH	[%]	absolute differences of peak heights
DPT	[h]	absolute differences of peak times
DT_a	[-]	decreasing rate of annealing temperature
ΔE	[-]	energy difference between a new and old state
fNT	[-]	number of false forecasted trespasses
fP	[diverse]	forecasted areal precipitation
IS	[-]	initial values for the random number generator
K	[h]	recession constant for runoff
K_D	[h]	recession constant for direct flow
K_I	[h]	recession constant for interflow
$KSTOP$	[-]	maximal number of shuffling loops
LS	[diverse]	least-squares method
M	[diverse]	observed data
MAE	[diverse]	mean absolute error
$MAXN$	[-]	maximal number of evolution steps
mT	[°C]	time-averaged mean areal temperature
N	[-]	number of data
NGS	[-]	number of complexes
NM	[-]	number of temperature changes before temperature decrease rate is modified
NN	[-]	number of iterations used for each temperature
NP	[-]	number of parameter vectors
NPG	[-]	number of parameter vectors within one complex
NPS	[-]	number of parameter vectors within one subcomplex
NS	[-]	Nash-Sutcliffe efficiency
$NSPL$	[-]	number of evolution steps of one complex
NT	[-]	number of observed trespasses
O	[diverse]	objective function
$O(RS)$	[diverse]	performance of an old model
$O(RS')$	[diverse]	performance of a new model
P	[-]	population of parameter vectors
P	[diverse]	areal precipitation
PC	[-]	portion of accepted positive changes (stopping criterion)
$PCENTO$	[-]	convergence criterion (predefined threshold)
Q	[m ³ /s]	current discharge at the forecast gauge
Q_B	[m/s]	baseflow
Q_D	[m/s]	direct runoff

Q_I	[m/s]	interflow
Q_t	[m/s]	runoff component at time t
Q_{t0}	[m/s]	runoff component at time t_0
Q_{up}	[m ³ /s]	current discharge of at the upstream gauge
Q_0	[-]	scaling factor for baseflow
R^j	[-]	response of rule j
$RMSE$	[diverse]	root mean square error
S	[diverse]	simulated data
SSE	[diverse]	sum of square error
T	[°C]	mean areal temperature
T_0	[diverse]	initial annealing temperature
T_a	[diverse]	annealing temperature
VE	[-]	volume error
W	[-]	weight of connection links
WL	[diverse]	warning level
X	[-]	universe set

Kurzfassung

Menschen weltweit werden mit Hochwasserereignissen unterschiedlicher Stärke konfrontiert. Um Eigentum und, noch viel wichtiger, Leben zu retten, ist eine rechtzeitige und zuverlässige Hochwasserwarnung und folglich -vorhersage unerlässlich. Ziel dieser Arbeit ist es deshalb, ein auf Fuzzy-Regeln basiertes Hochwasserwarnsystem für mesoskalige Einzugsgebiete und die Vorhersage von extremen Hochwasserereignissen mit Wiederkehrperioden von 100 Jahren und mehr unter Berücksichtigung von Unsicherheiten zu entwickeln.

Da extreme Hochwasserereignisse mit einer Jährlichkeit von 100 oder mehr Jahren in der Realität nicht in jedem Einzugsgebiet bereits beobachtet und aufgezeichnet wurden, ist eine Erweiterung der Datenbank auf Grund von Modellsimulationen zwingend notwendig. In dieser Arbeit werden hierzu das hydrologische Modell WaSiM-ETH (Wasserhaushalts-Simulations-Modell ETH) sowie von Bliefernicht et al. (2008) generierte Niederschlagsfelder verwendet. Die Kalibrierung des Modells erfolgt mit dem SCE (Shuffled Complex Evolution) Optimierungsalgorithmus. Um reproduzierbare Kalibrierungsergebnisse zu erzielen und die notwendige Kalibrierungszeit möglichst gering zu halten, werden unterschiedliche Optimierungskonfigurationen untersucht und eine Kalibrierungsstrategie für das mesoskalige Einzugsgebiet des Oberen Mains entwickelt.

Um eine kontinuierliche und zuverlässige Vorhersage zu garantieren, ist die Idee entwickelt worden, Fuzzy-Regelsysteme für unterschiedliche Vorhersagehorizonte (3 Tage; 6, 12 und 48 Stunden) für die drei Hauptpegel des Oberen Mains aufzustellen, die im Zusammenspiel eine kontinuierliche Vorhersage sicher stellen. Der Fokus der 3-Tagesvorhersage liegt hierbei in der zuverlässigen Wiedergabe von geringen und mittleren Abflussbedingungen sowie der zuverlässigen und rechtzeitigen Vorhersage von Überschreitungen einer vordefinierten Meldestufe. Eine vorhergesagte Überschreitung der Meldestufe führt zu einem Wechsel der Vorhersagesysteme von der 3-Tages- zu der 6-, 12- und 48-Stundenvorhersage, deren Fokus auf der Vorhersage der Hochwasserganglinie liegt. In diesem Zusammenhang wird die Effizienz der beiden klassischen Regelsysteme, Mamdani und Takagi-Sugeno, sowie die Kombination unterschiedlicher Eingangsgrößen, unter anderem Tukey Tiefenfunktion, näher untersucht. Ein weiterer Effizienzvergleich wird zwischen den Mamdani Regelsystemen der 48-Stundenvorhersage und dem hydrologischen Modell WaSiM-ETH durchgeführt. Für das Training der beiden Regelsysteme wird der SA (Simulated Annealing) Optimierungsalgorithmus verwendet.

Die einzelnen Fuzzy-Regelsysteme werden schließlich in dem entwickelten Hochwasserwarnsystem ExpHo-HORIX (Expertensystem Hochwasser - HORIX) zusammengefügt. Standardmäßig wird für jede Vorhersage die Niederschlagsunsicherheit auf Grund von Ensemble-Vorhersagen innerhalb ExpHo-HORIX analysiert und ausgewiesen. Im Hochwasserfall können für die stündlichen Fuzzy-Regelsysteme Modellunsicherheiten des hydrologischen Modells, das für die Generierung der Datenbank von Extremereignissen verwendet wurde, zusätzlich ausgewiesen werden. Hierzu müssen zusätzlich Ergebnisse der SCEM Analyse (Grundmann, 2009) vorliegen.

1 Introduction

” ... there is an increased risk of tremendous floodings within the next hours and days.”

People worldwide know those news from radio or TV and often pictures of the last serious floods are back in mind. Some of them are well prepared for such situations and need only a few hours to take their flood protection measures. Some are not. For them every minute is most valuable. In both cases, a timely and reliable flood forecast is essential for the people to save goods and, more important, lives.

Recent flood events have shown again that crisis management of this natural hazard still has to be improved. Since 1998 floods in Europe have caused some 700 deaths, the displacement of about half a million people and at least 25 billion Euro in insured economic losses (European Commission, 2011). As reaction the European Water Framework Directive entered into force and introduced the idea of integrated water resources management into catchment planning. Furthermore, after the flood disaster of the Elbe river in the summer of 2002 the German government presented the Five-Point Program in order to improve the prevention of flood damage on a nationwide level. Linked to this program is the BMBF funded initiative *RIMAX - Risikomanagement extremer Hochwasserereignisse*. Among others, one research aspect of RIMAX is the improvement of flood forecasts, in particular, of extreme floods with return periods of 100 years and more.

Nowadays, classical rainfall-runoff models with conceptual and / or physically based approaches are performed for flood forecasts. Often, the processing of precipitation ensembles with these models requires high computation times. Therefore, an analysis of uncertainties, resulting from the precipitation forecasts and the applied hydrological model, can often not be carried out in real cases due to the lack of time. However, if uncertainties are ignored, false alarms are more likely. These false alarms can be very expensive and reduce the public trust in the flood forecast and warning system.

Besides the continuous improvement of classical rainfall-runoff models, new approaches like Artificial Neural Network (ANN) and Fuzzy Inference Systems (FIS) are investigated in conjunction with a timely and reliable flood forecast, including the consideration of uncertainties. In recent years, these approaches have been well-established within various fields of hydrology. Due to their very small computation times they are most attractive for flood forecasts and the corresponding analysis of uncertainties.

In the framework of the RIMAX initiative, the performance of fuzzy inference systems considering timely and reliable flood forecasts is investigated within the project *HORIX - Development of an operational expert system for flood risk management considering prediction uncertainty*.

1 Introduction

One objective of this project is the development of a robust, fuzzy based warning system for meso-scale catchments considering extreme flood events with return periods of 100 years and more.

Considering one river catchment (extreme) flood events, which cause high damages, are seldom. Long observation periods are required to record those events. However, in most cases observation periods are too short and events of higher return periods are not recorded yet. Thus, only flood events of lower return periods are available for the design of flood warning systems. However, these data are not sufficient for a reliable setup of warning systems, in particular considering extreme flood events. In order to overcome this problem, several approaches exist. For example considering reconstructed data of very old extreme flood events beside the recorded ones. Another approach is to extend the observed database by simulations of possible flood events as it is performed within the HORIX project. However, with such an approach uncertainties resulting from the simulations using simplified model descriptions occur in addition to the prediction uncertainties of precipitation. Therefore, the whole model chain *generation of possible rainfall scenarios - modelling the corresponding discharge with a rainfall-runoff model - analysis the uncertainty coming from the rainfall-runoff model* is investigated. Based on the results of the rainfall-runoff model and the uncertainty analysis a robust and reliable fuzzy based forecast system is developed.

Most of the work, which is presented here, has been performed within the framework of the HORIX project. In the context of the project this thesis investigates the following questions:

1. Can unobserved extreme flood events with return periods of 100 years or more be simulated by classical rainfall-runoff models? In particular, is it possible to reduce the calibration time of those rainfall-runoff models by performing optimization algorithm?
2. Can fuzzy inference systems ensure a reliable and continuous flood forecast for different forecast time horizons? How simple and user-friendly are these systems?
3. Can a user-friendly and flexible warning system based on fuzzy inference systems be developed which considers precipitation and model uncertainties?

Based on the questions presented above this work is structured in the following way: After a short review of hydrological modelling, the basic concepts of the performed hydrological model WaSiM-ETH (Water balance Simulation Model) and optimization algorithm SCE (Shuffled Complex Evolution) are introduced in **Chapter 2**. **Chapter 3** starts with a short review of fuzzy modelling, followed by a more detailed introduction of the basic concepts of fuzzy logic and the performed training algorithm SA (Simulated Annealing) as it is not as common in hydrological modelling. Furthermore, the basics of Tukey depth function are presented. Relevant details on the study area chosen for this thesis, the Upper Main basin, and the available data are provided in **Chapter 4**. **Chapter 5** presents the core of this thesis as the first two of the above stated questions are answered for the Upper Main catchment. The developed user-friendly and flexible warning system based on fuzzy inference systems (question 3) is presented in **Chapter 6**. The thesis closes with a summary including some general conclusions and an outlook on future work in **Chapter 7**.

2 Hydrological Modelling

Hydrology is the science of water including its properties and states in the atmosphere, on the ground and in the underground. Thus, it considers the hydrological cycle, the water resources, and the interactions between them. Models are generally a simplified description of the very complex reality, and are used to reproduce the behavior and processes observed in the field. Hydrological models are mathematical descriptions of the underlying physical processes involved within the whole water cycle. They are developed and adjusted for a specific investigation aim (Rosbjerg and Madsen, 2005). With such models values for certain points or future situations which cannot be observed in situ can be investigated. Further fields of application are summarized in Table 2.1. However, a wide variety of processes on different temporal and spatial scales are involved in the cycling of water. Therefore, it is very difficult to find appropriate approximations for the setup of hydrological models. In contrast to hydrological models precipitation models or groundwater models only consider one specific part of the water cycle.

Fields of application	Examples
Planning and design	<ul style="list-style-type: none"> - water resources management (e.g. reservoir control) - forecast of hydrological events (e.g. flood forecast) - investigations of certain effects on the hydrological cycle (e.g. climate change)
Research and exploration	<ul style="list-style-type: none"> - investigation of concepts and hypotheses - development of new approaches for the description of hydrological processes
Visualization and abstraction	<ul style="list-style-type: none"> - illustration of complex interrelations (e.g. impact of climate or land use change on flood events)

Table 2.1: Fields of application of hydrological models (Fleckenstein, 2005).

For the selection of a hydrological model aspects like the investigation aim, the availability of data, the size of the catchment, and the involved hydrological processes have to be considered. Within the frame of this work a hydrological model is required which provides reasonable and reproducible simulations of extreme flood events for observed but also for unobserved events. In particular for the latter, it is important that the hydrological model is able to maintain the main physics of dynamic processes within the unsaturated zone so that simulations beyond the observed data range are more reliable.

2 Hydrological Modelling

In order to achieve a good flood forecast correctly portraying the pre-event catchment conditions (e.g. soil moisture) is a crucial factor at the beginning of the simulations (Niehoff, 2001). Furthermore, the processes of interception, evapotranspiration, snow accumulation and melting as well as infiltration and formation of surface runoff have to be described as precisely as possible for a satisfying representation of the flood formation processes. For the spatial resolution Smith et al. (2004) recommend the use of distributed instead of lumped models for catchments having a high spatial variability of precipitation.

For this investigation the hydrological model WaSiM-ETH has been chosen because (1) it satisfies the mentioned requirements of a model with respect to reliable simulations of observed and unobserved flood events and (2) it has been already successfully applied in the field of flood forecasting.

For example Jasper et al. (2002) investigated the influence of different precipitation predictions on flood forecasts. Thereby, they applied the hydrological model WaSiM-ETH for the simulation of extreme flood events within the complex alpine Ticino-Verzasca-Maggia basin (2627 km², Italy) between 1993 and 2000. The simulations have been based on a 500 times 500 m model grid and an hourly time step. The model was performed in a one way coupled atmospheric-hydrological model environment for the processing of ensemble weather forecasts of five different high-resolution numerical weather prediction (NWP) models.

Cullmann (2006) performed WaSiM-ETH in a similar way as it is used within the frame of the HORIX project. The aim of his investigation was to build up a fast flood forecast system for observed and unobserved flood events based on artificial neural networks. For the generation of the required data the hydrological model WaSiM-ETH was set up for the gauge Kriebstein (Zschopau basin, East German Ore Mountains, 1757 km²) on an hourly time and a 1000 m spatial resolution. Thereby, a new calibration scheme which only takes single flood events into account was developed and the resulting uncertainties were investigated.

A further application of WaSiM-ETH with respect to flood forecast was performed by Marx (2007). Within his developed one-way-coupled meteorological-hydrological forecast system he applied WaSiM-ETH for the alpine Ammer basin (709 km², Germany). For this purpose, WaSiM-ETH was set up with an hourly time step and a spatial resolution of 100 m in order to represent the high spatial differences in a satisfying way.

A successful application of a hydrological model depends on credible model parameter values. But a variety of hydrological models contain not only physically based parameters, but conceptual ones. These parameters cannot be measured directly, and therefore have to be adjusted by the model user. Traditionally this is done by a trial-and-error calibration process which depends strongly on the model understanding (knowledge of the basic approaches and interactions in the model) and the experience of the modeler. Consequently, the manual calibration is subjective and a very time consuming task. Model errors, insufficient process description and measurement errors come along as further uncertainties of the calibration process. Another important fact which complicates the calibration process is that it is not possible to identify an unique parameter set for the model due to the nonlinearity of hydrological processes which are reproduced. That leads to the so-called *equifinality problem* (Beven and Freer, 2001), which means that several sets of model parameter vectors can be found which have similarly good model performances. A further difficulty is the dependency of model parameters on the chosen objective function on the

base of which the model is calibrated (Janssen and Heuberger, 1995; Gupta et al., 1998; Madsen, 2003). The best state of a model is represented by an optimum of the chosen objective function describing the relation between a model output variable and its corresponding measured value. In summary, the calibration of hydrological models is a very complex task which cannot be solved easily. Modern optimization algorithm try to show one way out of this very complex problem.

In recent years the performance of the *Shuffled Complex Evolution* (SCE) algorithm as an optimization algorithm for the calibration process has been proven to be efficient and effective in locating optimal model parameters of different hydrological models. Thereby, it is assumed that the found (local) optimum belongs to a set of optima which are clustered around the global optimum. The first application of the SCE algorithm was performed by Duan et al. (1992) for the conceptual rainfall-runoff model SIXPAR, a simplified research version of the SAC-SMA (Sacramento soil moisture accounting) model used by the North Central River Forecast Center in the USA as an operational flood forecasting model. Further investigations with the SAC-SMA model were performed by Sorooshian et al. (1993) and Hogue et al. (2000) for several study basins in the Upper Mississippi catchment, USA. Kuczera (1997) compared four probabilistic search algorithm (SCE, genetic algorithm using traditional crossover, multiple random start using either simplex or quasi-Newton local searches) in order to calibrate the five model parameter of the modified conceptual rainfall-runoff model SFB for the Chichester river basin (180 km²) in Australia. Madsen (2000) applied the SCE algorithm for the calibration of the Mike 11/NAM rainfall-runoff model for the Danish Tryggevælde catchment (130 km²). For the meso-scale catchment Dietzhölze (81 km²) in central Germany Eckhardt and Arnold (2001) applied the SCE optimization algorithm for an automatic calibration of a modified version of the model SWAT (Soil and Water Assessment Tool). In this study the SCE algorithm was found to be robust and the most efficient.

In this work the SCE algorithm has been chosen for the calibration of the applied rainfall-runoff model WaSiM-ETH because (1) it seems that the algorithm finds robust and reliable results in an acceptable period of time and (2) it has already been successfully applied in combination with hydrological models.

In the following, general concepts and classifications of hydrological models and optimization algorithms are presented first. The basic principles of (1) the chosen hydrological model WaSiM-ETH, and (2) of the optimization algorithm SCE for the calibration process are described afterwards. The performance of both considering the study area Upper Main is discussed in Chapter 5.1.

2.1 Concepts and classifications

Hydrological models. In general, hydrological models are mostly rainfall-runoff models or water balance models. The difference between both is, that the focus of the first lies on the calculation of discharge on the base of occurring rainfall events without considering further major components of the water cycle. The focus of the latter lies on the simulation of all major components of the water cycle including the genesis of discharge as one model component. Due to the fact that the hydrological cycle covers a wide range of physical processes on different temporal and spatial scales several hydrological model approaches are available. Furthermore, the fundamen-

2 Hydrological Modelling

tal problem in studying and modelling hydrological systems is still that most of the action takes place in the underground and that the amount of data not only referring to the subsurface is limited (Beven, 2003). That is the reason why only the most important processes can be taken into account within the setup of the hydrological model in a given application whereas the considered processes themselves depend on the purpose of modelling. For the right choice of hydrological model Rosbjerg and Madsen (2005) state the request for appropriate modelling, in which the actual purpose of the modelling is governing the scales, the sophistication level in process description and parametrization, the calibration and validation procedures as well as the uncertainty assessment.

Historically, the first hydrological model, the Rational Method, was developed by Mulvaney (1851) as a helpful tool for the design of bridges and culverts. Since then, a wide variety of hydrological models has been developed. A comprehensive overview of the most popular ones is given by Singh (1995). For the classification of hydrological models many different schemes have been introduced. A widely-used classification is the one after Dyck and Peschke (1995). They classified hydrological models into three groups according to the degree of physical considerations of involved processes:

1. *Black box models (empirical)*: these simplest models are often derived from system theory in a mostly pure empirical way. They are generally used for event-based modelling purposes. The basic assumption of these models is that rainfall and runoff are related in a reasonable linear way. Examples are the runoff coefficient and the original unit hydrograph models (Sherman, 1932).
2. *Grey box models (conceptual)*: these models are based on process-oriented approaches where the governing physical laws of water flow are not considered explicitly in full detail but through semi-empirical equations. These models are often based on a lumped spatial discretisation. Examples are the Stanford Watershed model (Crawford and Linsley, 1966) or the original HBV model (Bergström, 1995).
3. *White box models (physically based)*: these very complex models try to describe all processes of the system in a complete physically based way. They are both computationally and parametrically demanding as the processes are described by nonlinear partial differential equations and more than one space and time dimension are involved. Although they are physically based some parameters still have to be calibrated because their effective value cannot be measured on the required scale and resolution in the field. A very common example for such a model type is the *Système Hydrologique Européen* (SHE) model (Abbott et al., 1986a,b).

In recent years the differences between grey and white box models have slowly blurred. On the one hand conceptual models have been extended by physically based modules due to the continuously increasing computer power. On the other hand some modules of pure physically based models were reduced to conceptual ones because of the limitation of available data. Due to the rapid development of different hydrological models Beven (2003) introduced two further model groups in addition to the ones after Dyck and Peschke (1995):

1. *Simplified distributed models based on distribution functions*: the models of this group attempt to maintain a distributed description of catchment responses without the de-

tailed process representation of fully distributed models. In order to represent the spatial variability of runoff generation they use a kind of distribution function. Examples of this model group are the well known TOPMODEL (Beven and Kirkby, 1979) and the VIC model (Liang et al., 1994).

2. *Data-based models* or *data-driven models*: the idea of those models is to let the data speak for themselves and to have no prior assumptions about the model structure. Examples are the soft computing approaches like artificial neural networks (ASCE, 2000a,b) and fuzzy logic (Bárdossy, 1996, Chapter 3).

Beside the model classification considering the degree of physical descriptions of involved processes, the classifications according to the temporal and spatial resolution are commonly used. The classification with respect to the temporal resolution differentiates between an *event-based* and a *continuous* time application of the hydrological model. Concerning the spatial resolution the models can be classified considering the degree of representation of the spatial variability of processes, input, boundary conditions and / or system (watershed) geometric characteristics into *lumped*, *semi-distributed* and *fully distributed* models (Singh, 1995). Lumped models simplify the behavior of spatially distributed systems and assume that model parameters have an homogeneous character over the catchment area. An example for a lumped model is the original version of the HBV model (Bergström, 1995). Semi-distributed models as the PREVAH model (Gurtz et al., 1999) subdivide the watershed into hydrological response units with similar hydrological characteristics. Fully distributed models take an explicit account of the spatial heterogeneity of the investigated catchment due to the fact that, depending on the chosen grid size, different responding areas can be spatially differentiated parameterized (e.g. WaSiM-ETH; Schulla and Jasper, 2002). Usually a lumping of small scale physics to the model grid scale occurs in real applications of physically based models (Beven, 1989).

Optimization algorithms. In general, optimization algorithms are logical procedures which are used to search the *response surface* (Singh, 1995), which is described by the objective function in the defined parameter space. They are applied in order to find the model parameter values which optimize, that means minimize or maximize as appropriate, the value of the considered objective function. After Singh (1995) the common optimization algorithms can be classified into *local search* and *global search methods*:

1. *Local search methods*: these methods are designed in order to efficiently find the minimum of unimodal functions. Thereby, the algorithm continuously proceeds downhill, that means in direction of the objective function improvements, and should consequently reach the function minimum, irrespective of where the search is started within the parameter space. The result of the optimization depends on (1) the direction of search, (2) the distance of search in one direction, and (3) the decision, when to stop the optimization because no further improvement can be achieved. There exists a variety of local search methods which differ in the realization of the algorithm with respect to the three boundary conditions. In general, these optimization algorithms can be further classified into *direct search* and *gradient based* methods (Singh, 1995). The difference between them is that the direct search method only uses the function value whereas the gradient based method uses both pieces of information, the function value and the function gradient. In the field of calibrating hydrological models, many direct search methods have been tested, among the first ones were the Rosenbrock method

2 Hydrological Modelling

(Rosenbrock, 1960) and the Simplex method (Nelder and Mead, 1965). Considering the gradient based method the steepest descent approach or the Newton method are widely applied (Singh, 1995). However, the performance of both methods for the calibration of hydrological models was not generally satisfying. One reason for this is the fact that the response surface of the objective function considering the optimization of a hydrological model is not unimodal, but multi-modal. Consequently, the local search method is not appropriate for the calibration of such models.

2. *Global search methods*: in contrast to the local search methods these methods are designed to efficiently find the minimum of multi-modal functions. This group can be further classified into (1) *deterministic* and (2) *stochastic* methods, as well as (3) *combinations* of both. After Singh (1995) only (random) stochastic and combination methods have been performed for the calibration of hydrological models. Due to many model parameters which have to be adjusted during the optimization process a pure random approach is not efficient. Therefore, one widely used stochastic method is the Adaptive Random Search (ARS) approach after Masri et al. (1978) which takes also the probability of searching areas into account. In the field of calibrating hydrological models one simple combination method is the Multi-start Simplex approach (Duan et al., 1992). A further more sophisticated combination approach is the Shuffled Complex Evolution (SCE, Duan et al., 1993) method which is based on the nonlinear simplex approach and belongs to the evolutionary optimization algorithms. Many investigations (Duan et al., 1992; Sorooshian et al., 1993; Kuczera, 1997; Hogue et al., 2000; Madsen, 2000; Eckhardt and Arnold, 2001) show that the SCE optimization algorithm is a good choice for the calibration of hydrological models.

Another classification is proposed by Berlik (2009, Figure 2.1). Thereby, the optimization algorithms are grouped into (1) *gradient based*, (2) *random*, and (3) *enumerative methods*.

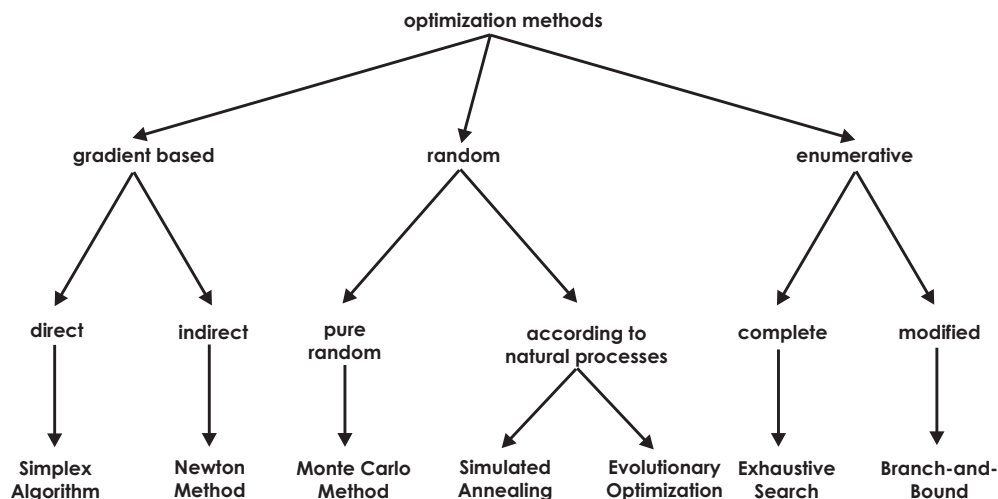


Figure 2.1: Classification of optimization algorithms after Berlik (2009, modified; according to Goldberg, 1989)

Gradient based methods which use the information of the gradient in order to find the optimum are further divided into direct and indirect search algorithms. In contrast to this, random optimization methods take random processes into account as it occurs in nature. They are further grouped into pure random algorithms and algorithms which try to imitate natural processes (e.g. cooling

process of crystals, survival of the fittest). The last group, enumerative optimization methods, evolves the objective function for each possible parameter set within the predefined parameter space and is therefore very time consuming.

2.2 Hydrological model WaSiM-ETH

The hydrological model *Water balance Simulation Model* (WaSiM-ETH) was developed at ETH Zurich (Schulla, 1997) as a deterministic, fully distributed, modular model. The terrestrial water balance is simulated using physically based algorithms for the vertical fluxes and lateral groundwater fluxes (WaSiM-ETH version 2), whereas other lateral fluxes (e.g. surface runoff, interflow) are treated in a lumped manner. In recent years the model has been successfully used in a wide temporal and spatial range, from event-based to continuous simulations. Primarily applied in a small catchment in the Swiss Alps (Schulla, 1997) further investigations using WaSiM-ETH were performed for impact studies of climate or land use change on the terrestrial water balance (WaSiM, 2009). In recent years it has been also successfully applied in the field of flood forecasts in small and medium-size catchments (Jasper et al., 2002; Cullmann, 2006; Marx, 2007). Since its first application WaSiM-ETH has been continuously developed. In the following the main modules of the WaSiM-ETH Release 6.4 version 2 (Figure 2.2), which is performed in this work (Chapter 5.1), are described according to Schulla and Jasper (2002) and Wagner (2008):

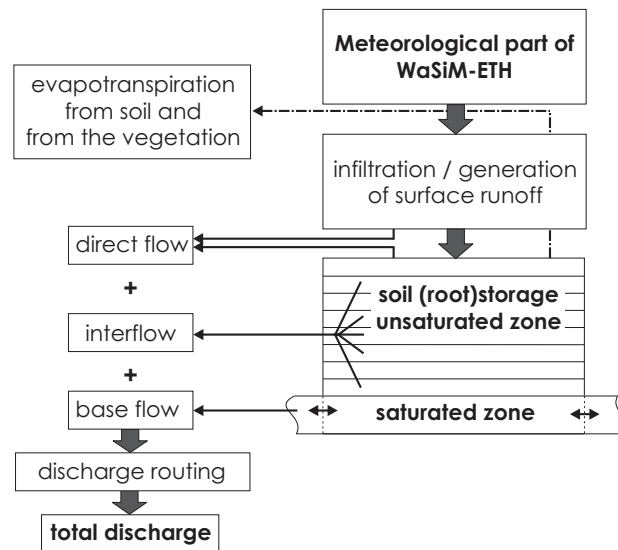


Figure 2.2: Main modules of the hydrological model WaSiM-ETH Release 6.4 version 2 according to Schulla and Jasper (2002).

Interpolation of the meteorological input data. Meteorological information, which is required as driving force of rainfall-runoff models, is usually available as station data. In order to transfer the information of the given data source into the required spatial resolution of the grid-based model WaSiM-ETH following interpolation techniques are provided in WaSiM-ETH:

1. *Inverse distance weighting (IDW) interpolation:* input variables have a stronger horizontal than vertical dependency. All stations within a specified search radius are used for the interpolation.

2 Hydrological Modelling

2. *Thiessen polygon*: a special case of IDW, which considers only the nearest observation station per grid point.
3. *Altitude-dependent regression*: input variables have a stronger vertical than horizontal dependency (e.g. in mountainous catchments). For variables with horizontal and vertical dependency a combination of IDW and altitude-dependent regression can be selected.
4. *Bilinear interpolation*: gridded meteorological data sources are available (e.g. results of a meteorological model).

Topography dependent adjustment of radiation and temperature. A radiation and air temperature adjustment is required to compensate shadowing effects in mountainous regions. The impact of the topography on both variables is considered using the approach after Oke (1987), which calculates a correction factor depending on sunshine duration, incident and zenith angle, and an empirical factor considering diffuse short wave radiation.

Potential and actual evapotranspiration. The potential evapotranspiration can be estimated applying the approach after Penman-Monteith (Monteith, 1975; Brutsaert, 1982), Wendling (1975), or Hamon (Federer and Lash, 1983). In comparison to Penman-Monteith the other methods are less complex and can only be performed on daily time steps. Within WaSiM-ETH version 2 the soil moisture is modeled using Richards-equation (Richards, 1931). Therefore, for the estimation of the real evapotranspiration the relation between the soil water content and the actual capillary pressure of the soil is approximated using the Van Genuchten (1976) equation.

Snow accumulation and snowmelt. The fraction of snow is calculated using the interpolated air temperature, one predefined temperature, at which 50 % of precipitation are falling as snow, and one specified temperature-transition range (Schulla and Jasper, 2002). Snowmelt can be estimated applying the temperature-index approach, the temperature-wind-index approach, or one combined approach after Anderson (1973) and Braun (1985). The later can only be performed on a daily time step.

Interception. The interception is calculated after the snow module. Therefore, the interception storage is able to store melt water as well as rain water on the ground and vegetation. Thereby, a simple bucket approach is used with a capacity depending on the leaf area index (LAI), the vegetation coverage degree, and the maximum height of the water on the leaves. The extraction of water out of the interception storage by evaporation is assumed to be at a potential rate. If the interception storage is filled, further precipitation will fall directly to the soil surface.

Infiltration and generation of surface runoff. The infiltration model is an integrated part of the soil model. Running WaSiM-ETH version 2, infiltration is considered in the calculation of Richards-equation. If precipitation intensities are larger than the actual hydraulic conductivity of the soil surface runoff is generated.

Unsaturated zone. For modelling the vertical fluxes in the unsaturated zone WaSiM-ETH version 2 uses Richards-equation (Richards, 1931, Equation 2.1) instead of the TOPMODEL approach (Beven and Kirkby, 1979, WaSiM version 1). Richards-equation is calculated one-dimensional

in the vertical direction, in the spatially and temporally discretized form for each grid cell.

$$\frac{\partial \Theta}{\partial t} = \frac{\partial q}{\partial z} = \frac{\partial}{\partial z} \left(-k(\Theta) \frac{\partial \Psi(\Theta)}{\partial z} \right) \quad (2.1)$$

with	Θ	[m ³ /m ³]	water content
	t	[s]	time
	k	[m/s]	hydraulic conductivity
	Ψ	[m]	hydraulic head as sum of the suction ψ and geodetic altitude h
	q	[m/s]	specific flux
	z	[m]	vertical coordinate

Hydraulic conductivity and hydraulic head, which are functions of the water content, are parametrized using the approach of Van Genuchten (1976). Thereby, the recession of the saturated hydraulic conductivity k_s with depth z is taken into account by introducing the recession constant k_{rec}

$$k_{s,z} = k_s \cdot k_{rec}^z \quad (2.2)$$

which enables the generation of interflow Q_I . Due to its definition the recession constant k_{rec} can only have values between 0.1 and 1.

For a specific soil layer m the interflow Q_I is calculated as follows:

$$Q_I = k_s(\theta_m) \cdot \Delta z \cdot d_r \cdot \tan \beta \quad (2.3)$$

Thereby, the parameter drainage density d_r represents river density as a scaling parameter and therefore has to be adjusted during the calibration process. β is the local slope angle and limited to 45°. Groundwater recharge is defined as the remaining vertically percolating water. Furthermore, it is assumed that the matrix flow dominates macropore flow. Richards-equation is interpreted as a combination of mass balance and Darcy equation, due to the fact that in general the horizontal resolution of the model is 1 km or larger and therefore not comparable to the original lab scale. Hence, the corresponding parameters of the model are also not fully comparable to laboratory ones. Furthermore, they consider natural heterogeneities within the horizontal resolution and consequently have to be interpreted as effective lumped parameters. Since the mass balance is calculated in an iterative way, the actual conductivity is checked considering the generation of all vertical fluxes.

Groundwater and baseflow. A horizontally two-dimensional groundwater model can be coupled to the unsaturated zone. Interactions between surface water and subsurface water are simulated using the leakage principle. If this module is chosen baseflow, which is the portion of river discharge derived from groundwater, can only be generated when groundwater levels reach the river bed or lake bottom level. If the model is run without the groundwater module baseflow is calculated for each cell of the model grid, and not only at river cells, applying the following approach (Schulla and Jasper, 2002):

$$Q_B = Q_0 \cdot k_s \cdot e^{(h_{GW} - h_{geo,0})/k_B} \quad (2.4)$$

2 Hydrological Modelling

with	Q_B	[m/s]	baseflow
	Q_0	[-]	scaling factor for baseflow
	k_s	[m/s]	saturated hydraulic conductivity
	h_{GW}	[m.a.s.l.]	groundwater table
	$h_{geo,0}$	[m.a.s.l.]	geodetic altitude of the soil surface
	k_B	[m]	recession constant for baseflow

The parameters Q_0 and k_B are conceptual parameters which have to be calibrated. However in practice, the value of k_B is often set to 1 and the value of Q_0 can be estimated to the value of the maximum (observed) baseflow (Schulla, 2006).

Flow concentration within the subcatchment. For an entire subcatchment baseflow is generated as an average value. In contrast to this, interflow is generated for each grid cell separately and then averaged over space. Furthermore, surface runoff is routed to the outlet of the subcatchment according to the flow time zones grid. In order to get the total runoff surface runoff of the lowest flow time zone is added to baseflow and interflow. Considering retention a single linear storage approach is applied to direct runoff Q_D and interflow Q_I . In general, the runoff component Q_t at time t is calculated by runoff component Q_{t_0} at time t_0 and the recession constants K :

$$Q_t = Q_{t_0} \cdot e^{-\Delta t/K} \quad (2.5)$$

with $\Delta t = t - t_0$. During the calibration process the two recession constants K_D (direct flow) and K_I (interflow) have to be adjusted.

Discharge routing. Discharge routing in the river bed channel is performed by a kinematic wave approach using different flow velocities for different water levels in the channel. Thereby, flow times are calculated applying the equation after Manning-Strickler (Schulla and Jasper, 2002). After the translation of the wave, a single linear storage is applied accounting for diffusion and retention. Finally, discharges from different subcatchments are superposed.

2.3 Algorithm for calibration: Shuffled Complex Evolution

In the last two decades the evolutionary approach has emerged as a powerful technique beside the traditional ones (Chapter 2.1). Simonović (2009) gives an overview of the most significant differences between evolutionary and more traditional optimization methods:

- Evolutionary algorithms search not just with a single point, but with a population of points in parallel.
- Evolutionary algorithms are only influenced by the objective function and the corresponding fitness levels, and do not require derivative information or other auxiliary knowledge.

2.3 Algorithm for calibration: Shuffled Complex Evolution

- Evolutionary algorithms do not use deterministic transition rules, but probabilistic ones.
- Evolutionary algorithms have no restrictions for the definition of the objective function and therefore are generally more straightforward to apply.
- Evolutionary algorithms can find a diverse set of model parameter vectors with similar model performances.

In recent years a variety of different evolutionary optimization routines were developed. One of them is the *Shuffled Complex Evolution* (SCE) algorithm which was developed at the University of Arizona (Duan et al., 1992, 1993, 1994). The algorithm belongs to the family of genetic optimization algorithms and is based on the biological evolution process in order to find the *best* adjusted parameter vector. Thereby, a cloud of different individuals try to evolve themselves into the best state (global optimum) by changing the genetic information - the parameter values. For this purpose the following four concepts have been combined: (1) *probabilistic* and *deterministic approaches*, (2) *clustering*, (3) *systematic*, and (4) *competitive complex evolution* (CCE) of a complex of points. The latter is one key component of the SCE method and based on the Nelder and Mead (1965) Simplex downhill search method. Due to this combination of concepts the optimization process does not stick within a local, but a global optimum by theory. In practice, it is assumed that the found optimum belongs to a set of local optima which are clustered around the global optimum.

A *parameter vector* $\mathbf{p} = \{p_1, p_2, \dots, p_d\}$ includes all d parameters of the hydrological model which have to be adjusted. Considering the SCE algorithm a d -dimensional parameter space is defined for the optimization of the parameter vector, and each parameter vector \mathbf{p}_i represents one *individual* within a *population* $P = \{\mathbf{p}_1, \mathbf{p}_2, \dots, \mathbf{p}_{NP}\}$, whereas NP equals the number of parameter vectors. Figure 2.3 illustrates an example for the 2-dimensional case. The parameters X and Y define the parameter space used for the optimization between $[0 \ 5]$ and $[0 \ 6]$. The contour lines represent the surface of the chosen objective function with a local optimum at $(1, 2)$ and a global at $(4, 2)$. In order to reach the best state the following six evolution steps are carried out:

1. *Generation of population P*: NP parameter vectors \mathbf{p}_i are randomly sampled in the feasible d -dimensional parameter space and the corresponding value of the objective function $O_i \in \mathbf{O} = \{O_1, O_2, \dots, O_{NP}\}$ is calculated for each vector (Figure 2.3a with $NP = 10$). If no a priori information is available a uniform probability distribution is used for the generation process.
2. *Ranking of the individuals \mathbf{p}_i* : depending on the chosen objective function the NP generated parameter vectors are ranked in ascending and descending order, respectively. Thus, the first point of the sorted population is the parameter vector with the worst value of \mathbf{O} , the last point the parameter vector having the best value of \mathbf{O} .
3. *Partitioning into complexes*: the population P is classified into NGS complexes each including NPG parameter vectors (Figure 2.3b; $NGS = 2$, asterics and points; $NPG = 5$). The first complex includes every $NGS * (k - 1) + 1$ ranked parameter vector, the second complex every $NGS * (k - 1) + 2$, the third every $NGS * (k - 1) + 3$, and so on ($k = 1, 2, \dots, NPG$).

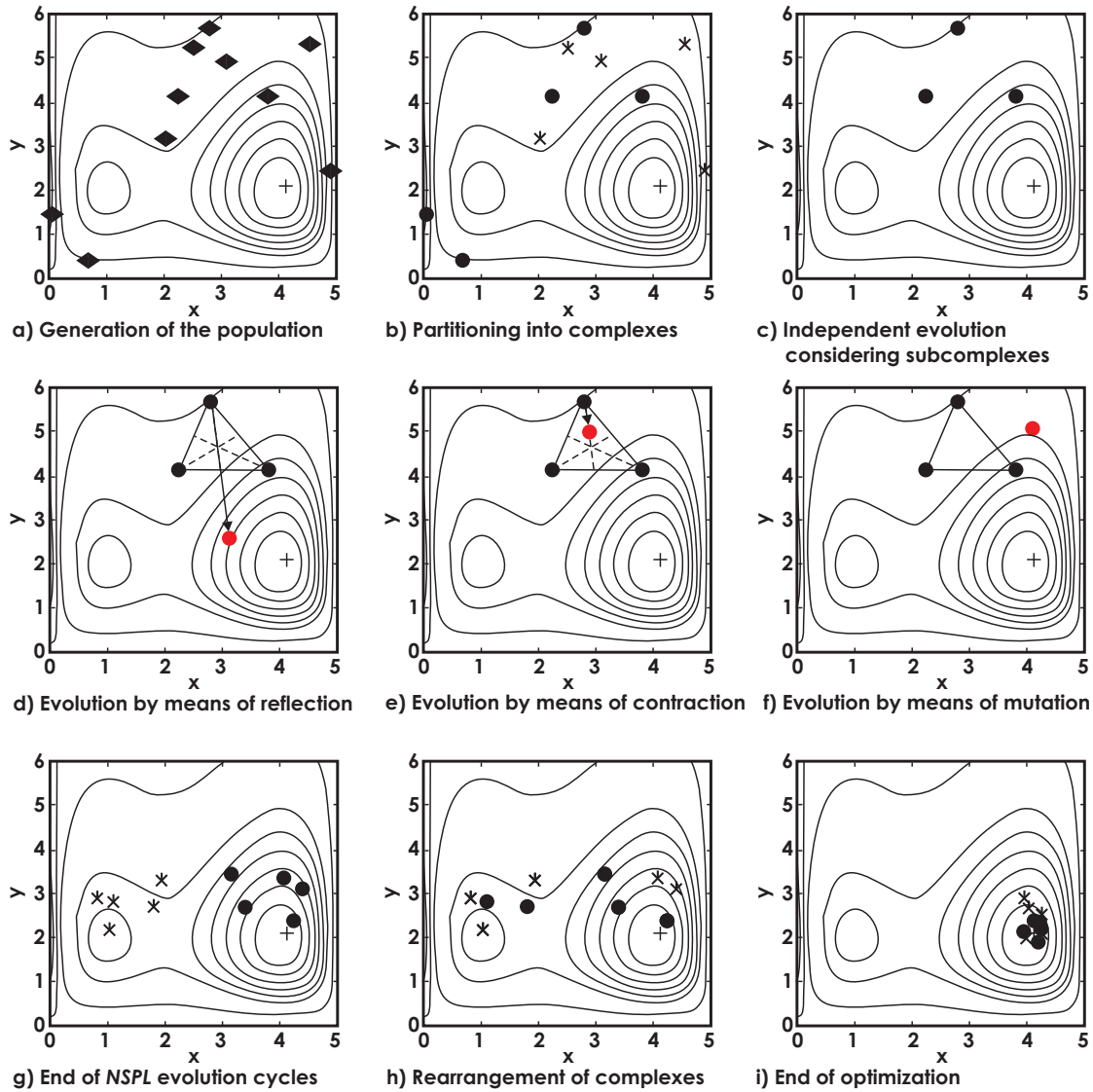


Figure 2.3: General scheme of the SCE algorithm for the 2-dimensional case after Duan et al. (1992, 1993, 1994; modified): Evolution of a population P including $NP = 10$ parameter vectors considering two complexes (points, asterics) with subcomplexes of $NPS = 3$ parameter vectors.

4. *Independent evolution of complexes:* each complex evolves independently from the others $NSPL$ times (e.g. $NSPL = 3$). Within each complex a further subcomplex is sampled according to a trapezoidal probability distribution including NPS parameter vectors (Figure 2.3c; $NPS = 3$). Thereby, the probability distribution is specified such that the parameter vector with the best value of O has the highest chance of being chosen for the subcomplex, and the parameter vector with the worst value of O has the least chance. Then each subcomplex undergoes consecutively the following three evolution steps:
 - a) *Reflection:* considering the subcomplex the parameter vector having the worst value O_i is reflected through the centroid whereby a new parameter vector is generated (Figure 2.3d). If (1) the new parameter vector lies within the parameter space, and (2) the corresponding value of the objective function is better than that of the old one, the old parameter vector is replaced by the new one.

- b) *Contraction*: if no improvement of the objective function is obtained with the reflection step, the contraction step is attempted (Figure 2.3e). Thereby, the new parameter vector is computed halfway between the centroid and the parameter vector having the worst value O_i . If the new parameter vector has a better value of the objective function than the old one, the old parameter vector is refused and the new one is taken.
 - c) *Mutation*: if neither the reflection nor the contraction step lead to an improvement of \mathbf{O} , a free mutation takes place (Figure 2.3f). Within the feasible parameter space a new parameter vector is randomly generated and replaces the parameter vector having the worst value O_i .
5. *Rearrangement of the complexes*: after *NSPL* evolution cycles (Figure 2.3g) the complexes are shuffled. The complex structure is broken up into the single population and the predefined convergence criteria are checked. If no convergence criterion is satisfied the algorithm starts again with the ranking of the individuals (step 2), followed by the partitioning into new complexes (Figure 2.3h).
 6. *End of optimization*: the evolution of the population and the optimization of the parameter vectors, respectively, ends if one of the following convergence criteria is satisfied (Figure 2.3i): (1) the improvement of the objective function is less than a predefined threshold *PCENTO*, (2) the maximal number of evolution steps *MAXN*, or (3) of shuffling loops *KSTOP* is obtained.

For the performance of the SCE optimization algorithm in this work the original SCE Fortran Code (Duan et al., 1992) is modified so that it can be applied for all releases and versions of WaSiM-ETH on a windows and unix platform (Zimmermann and Pakosch, 2008). Theoretically 99 model parameters of different model modules and subcatchments can be optimized simultaneously. Furthermore, it can be chosen if initial grids (e.g. considering the soil moisture) and / or different WaSiM-ETH configuration files should be used for the optimization process. Due to the fact that the objective function has an important influence on the optimization result (Janssen and Heuberger, 1995; Krause et al., 2005) the user can choose between six different objective functions (Table 2.2) and combinations of them depending on the model aim. In addition a user specified weighting of the discharge components (peak, baseflow, overall) for the calculation of the objective function can be performed.

The objective function *root mean square error (RMSE)* measures the deviation of simulated and observed data in a quadratic sense and is sensitive to outliers (Janssen and Heuberger, 1995). A perfect fit of the model would lead to an objective function value of zero. A less sensitive objective function considering outliers is the *mean absolute error (MAE)* which accounts for the deviations in an absolute sense (Janssen and Heuberger, 1995). A perfect fit of the model would lead to an objective function value of zero. The *volume error (VE)* gives dimension of ratio between the overall simulated discharge volume and the corresponding observed one. Due to its definition it is not sensitive to systematic model over- and underestimation. As the perfect fit would be indicated with an objective function value of one a modified version $O = |1 - VE|$ is implemented in the SCE optimization code. For the model efficiency after Nash and Sutcliffe (*NS*, 1970) the objective function ranges between 1.0 (perfect fit) and $-\infty$. If the efficiency is lower than zero a prediction using the mean value of the observed data would lead to better results than

Criterion	abbreviation	equation
Root mean square error	RMSE	$O = \sqrt{\frac{1}{N} \sum_{i=1}^N (S_i - M_i)^2}$
Mean absolute error	MAE	$O = \frac{1}{N} \sum_{i=1}^N S_i - M_i $
Volume error	VE	$O = \sum_{i=1}^N S_i / \sum_{i=1}^N M_i$
Nash-Sutcliffe efficiency	NS	$O = 1 - \frac{\sum_{i=1}^N (S_i - M_i)^2}{\sum_{i=1}^N (M_i - \bar{M})^2}$
Correlation coefficient	r	$O = \frac{\frac{1}{N} \sum_{i=1}^N ((S_i - \bar{S}) \cdot (M_i - \bar{M}))}{\sqrt{\frac{1}{N} \sum_{i=1}^N (S_i - \bar{S})^2} \cdot \sqrt{\frac{1}{N} \sum_{i=1}^N (M_i - \bar{M})^2}}$
Sum of square error	SSE	$O = \sum_{i=1}^N (S_i - M_i)^2$

Table 2.2: Objective functions which can be chosen for the SCE optimization of the hydrological model WaSiM-ETH (Zimmermann and Pakosch, 2008); O : objective function, S : simulated data, M : measured data, N : number of data.

the model itself. One drawback of the NS is that it is not very sensitive to systematic model over- and underestimations (Krause et al., 2005). In this application the model efficiency is modified and calculated as $O = 1 - NS$ during the optimization procedure in order to minimize the objective function (now, perfect fit correspond to 0.0). The *correlation coefficient* is defined according to Bravais-Pearson. More often the *coefficient of determination* (r^2) is used, which estimates the combined dispersion against the single dispersion of the observed and simulated data. The main disadvantage of this objective function is that it only considers the dispersion and is therefore not very sensitive to systematic model over- and underestimations (Krause et al., 2005). For the minimization of the objective function during the optimization process the correlation coefficient is modified and implemented as $O = |1 - r^2|$. The *sum of square error* (SSE) measures the squared discrepancy between the simulated and observed data. A perfect fit of the model leads to a value of zero for the SSE .

3 Fuzzy Modelling

The idea of vagueness, which means it exists something more than just *true* and *false* (classical bivalent logic and ordinary set theory, respectively), is very old and can even be traced back to Aristotle, the "father of logic". The limited, two-valued view dramatically simplifies our world and lacks rapport with reality where complexity is far higher than the principles of the bivalent logic. Nevertheless, it lasted until the early 20th century when the idea of vagueness was discussed anew and solutions for the problem were investigated (e.g. Russel, 1923; Black, 1937; Lukasiewicz, 1957). For example, in 1917 Lukasiewicz established the three-valued logic which accepts the values *true*, *false*, and *unknown*. The formalization of vagueness, the *fuzzy set theory*, was introduced by Zadeh (1965) with his publication "Fuzzy Sets". Fuzzy set theory is basically a theory of classes with *fuzzy*, which means unsharp boundaries and it contains the branches of e.g. fuzzy logic, fuzzy arithmetic, fuzzy data analysis, fuzzy clustering, and fuzzy kriging. With the fuzzy set theory it is possible to define further degrees of truth besides the *absolutely true* and the *absolutely false*, respectively, as intermediate truth degrees.

Since its introduction in the mid 1960ies fuzzy set theory has been further investigated (e.g. Dubois and Prade, 1980; Kaufmann and Gupta, 1991; Zimmermann, 1991; Bárdossy and Duckstein, 1995) and performed within different fields of research. In particular, the development of fuzzy-controllers (Mamdani, 1974) has to be mentioned from which the widely used Mamdani inference system results. On the basis of this inference system the second most common Takagi-Sugeno inference system (Takagi and Sugeno, 1985) was developed. In general, fuzzy inference is the process of formulating the mapping from a given input to an output using fuzzy logic. Fuzzy logic itself is based on IF-THEN rules using fuzzy sets and fuzzy operators. The two mentioned fuzzy inference systems differ in their definition of the rule responses (THEN-part). In recent years both inference systems have been successfully introduced for modelling purposes in the field of hydrology.

For the modelling of the non-linear infiltration process Bárdossy and Disse (1993) applied the Mamdani inference system. They investigated a Green and Ampt based fuzzy model as well as a fuzzy system based on the Richards-equation. Both were applied for a small area on a 5-minute base. The results of the modelled moisture content were compared with those of the Green and Ampt model as well as those of a FEM solution of Richards-equation. They showed that the fuzzy inference systems are an alternative for calculating the infiltration and the movement of the soil moisture in a heterogeneous soil column. The advantages of the set up fuzzy models are that they are transparent for the user due to their structure, and not very sensitive to parameter changes.

In order to improve river level forecasting See and Openshaw (1999) investigated a hybrid multi-model approach by combining a Mamdani type system and an artificial neural network. The assessment of the required rules was done with a genetic algorithm. The results of the 6 hour forecast for the river Ouse, England, were compared with those of an Autoregressive Moving Av-

3 Fuzzy Modelling

erage (ARMA) and a naive prediction model. The study showed that the hybrid model performed well on global statistics, and, more specifically, on predicting key alarm triggering levels. The first results showed a high potential of the system for the improvement of river level forecast and further investigations on this hybrid multi-model approach were carried out (See and Openshaw, 2000; See and Abrahart, 2001; Abrahart and See, 2002).

Xiong et al. (2001) used a Takagi-Sugeno inference system in order to combine the forecast results of different rainfall-runoff models in a systematic way. They applied five rainfall-runoff models to daily data of 11 catchments in different climates and then combined the results in order to achieve better forecast results. The results were compared with those from Shamseldin et al. (1997) who combined the same results of the hydrological models using the simple and weighted average method and the neural network method. The comparison shows that the investigated fuzzy system has behaved almost in the same way as the other methods, but with shorter simulation times. The study confirmed that the Takagi-Sugeno inference system is a very simple and very effective tool for enhancing the accuracy of river forecasts, in the context of model combination.

For the conceptual and modular rainfall-runoff model HBV Hundecha et al. (2001) developed four fuzzy-based modules (Mamdani inference) for the simulation of different processes involved in the generation of runoff from precipitation. The fuzzy-based modules for snowmelt, evapotranspiration, runoff, and basin response were investigated by incorporating only one of them into the conceptual HBV model at a time while retraining the HBV version for the other modules. Finally, all fuzzy-based modules were coupled together. They applied the modified models on the catchment of the river Neckar (13957 km²), Germany, for which daily data were available. The observed discharge could be well reproduced by the fuzzy-based model. The advantage of this model is that no model parameter for the description of the four processes has to be found which makes the approach easier and faster to work with.

In order to deal with parameter uncertainties Özelkan and Duckstein (2001) developed a fuzzy conceptual rainfall-runoff model framework. The uncertainties due to the input data and the model parameters were investigated by applying fuzzy logic and fuzzy regression. They applied their framework to the Lucky Hill sub-watershed of the Walnut Gulch catchment (150 km²), USA. The study showed that the decision makers gain insight about the model sensitivity and the uncertainty due to the model structure by performing this fuzzy logic framework and input data.

Bárdossy et al. (2003) performed the Mamdani inference system for the modelling of nitrogen leaching for three different agricultural soils within the 23687 km² Saale River Basin, Germany, on a monthly time base. For the assessment of rules the Simulated Annealing algorithm was applied. Additional expert knowledge was implemented within the optimization as fixed rules. Although the nitrate leaching is a complex non-linear problem it could be modelled effectively and transparently for the user with the chosen fuzzy inference system.

For the modelling of rainfall-runoff dynamics Vernieuwe et al. (2005) investigated the grid partitioning method, the subtractive clustering and the Gustafson-Kessel clustering for the construction of Takagi-Sugeno inference systems. The study area was the river Zwalm (114 km²), Belgium. The modelling was performed on a daily and hourly time base. The goal was to assess whether these models can be used as a water management tool or not. The results led to the conclusion that fuzzy models can potentially be used as an alternative discharge forecasting tool.

Jacquin and Shamseldin (2006) developed a rainfall-runoff model using the Takagi-Sugeno inference system. Due to the fact that a strong relation between precipitation and discharge exists they investigated five different function combinations (e.g. unit hydrograph) for the definition of the rule response. The global search method was based on the evolutionary algorithm of Sotiropoulos et al. (1998) for the optimization of rules. They applied their fuzzy models for six meso-scale catchments in different climate zones (Nepal, China, Ireland, USA, Australia) on a daily base. The results of this study indicate that fuzzy inference systems are a suitable alternative to the traditional modelling of the non-linear rainfall-runoff process.

For the modelling of the water level - discharge relationship Lohani et al. (2006) used the Takagi-Sugeno inference system. The investigated fuzzy systems were performed for several gauges of the Narmada river system in central India on a daily base. The results of the fuzzy models were compared to those of a back propagation artificial neural network model. They showed that the fuzzy modelling approach is superior compared to the artificial neural network approach.

Another comparison of the artificial neural network and the fuzzy logic approach has been done by Alvisi et al. (2006). For the 1, 3, 6, 9 and 12 hour forecast of the water level at the river Reno (1051 km²), Italy, five neural nets plus the Mamdani and Takagi-Sugeno inference systems were set up individually. For the parameterization an early stopping procedure was used (ASCE, 2000a) for all systems. The forecasting time horizon was limited due to the fact that no rainfall data were considered as known or forecasted within the forecast time horizon.

Gemmar et al. (2006) investigated the Takagi-Sugeno inference system for water level forecasts. At gauge Saarbürg (river Saar, 57 km²), Germany, a set of four fuzzy systems for the 6, 8, 10 and 12 hour water level forecast were optimized semi-automatically. The performed non-negative-least-squares approach ensured that no negative parameters of the Takagi-Sugeno conclusion were achieved as results of the optimization procedure. The study showed that Takagi-Sugeno inference systems are very simple and very effective and have great potential as an alternative tool for water level forecasts besides the traditional rainfall-runoff models.

In order to model catchment scale nitrate dynamics Shrestha et al. (2007) applied the Mamdani inference system on a daily time step for the Weida catchment (100 km²), Germany. Two fuzzy systems were trained on measured and simulated (WaSiM-ETH TOPMODEL version) data for the flow components by applying the Simulated Annealing algorithm. The results were compared with a multiple linear regression model. They showed that the combined process based data driven approach provides an effective methodology for the simulation of catchment scale nitrate dynamics, and that both performed Mamdani inference systems are superior compared to the simple multiple regression model.

Casper et al. (2007) investigated a Takagi-Sugeno inference model in order to predict the actual discharge of the Dürreych catchment (7 km²), Germany, on the basis of soil moisture and rainfall data. In a whole 18 TDR probes were installed at soil depths between 8 and 90 cm. Soil moisture was recorded in time intervals of 1 or 2 hours. Casper et al. (2007) showed that it was possible to predict the system behavior only by using soil moisture in the rule premises. However, the results showed that in order to capture the whole system dynamics, the measurement locations have to represent all relevant runoff generation variables. Due to the fact that the fuzzy system cannot extrapolate, time series of soil moisture have to contain all possible system states in order to predict the runoff at the outlet.

Further fuzzy applications such as water management and decision-making tools are given in Simonović (2009). He discusses among others the application of the fuzzy approach for the management of regional water supply systems and for the sustainable water resources management of aquifers.

The examples given above show that both inference systems, Mamdani and Takagi-Sugeno have been successfully introduced for modelling purposes in the field of hydrology in recent years. Considering flood forecasts the Takagi-Sugeno inference system is more common than the Mamdani one. However, in this work both fuzzy inference systems are performed and compared. In the following the basics of fuzzy sets, fuzzy logic, both fuzzy inference systems and the used optimization algorithm for the rule setup are described. For further details see Dubois and Prade (1980), Zimmermann (1991), Klir and Yuan (1995), as well as Bárdossy and Duckstein (1995).

3.1 Fuzzy Sets

The ordinary set theory is based on the bivalent logic which allows only values of $a = \{0, 1\}$. That means for each point x it can be clearly decided whether it belongs to the set a or not, $x \in a$ or $x \notin a$. In contrast to this, the fuzzy set theory allows all values of a function in the defined interval $[0, 1]$. Therefore, a partial membership of a point x of an universe set X to a fuzzy subset A is possible, whereas the fuzzy subset A (further referred to as fuzzy set) is a set of ordered pairs:

$$A = \{(x, \mu_A(x)) : x \in X; \mu_A(x) \in [0, 1]\} \quad (3.1)$$

$\mu_A(x)$ is called the membership (characteristic) function of the fuzzy set A and represents the grade of membership of x in A by associating each point in X a real number of the interval $[0, 1]$. The closer $\mu_A(x)$ is to 1 the more point x belongs to the fuzzy set A and vice versa. Furthermore, if $\mu_A(x)$ is equal to zero, point x does not belong to the fuzzy set A . If at least one point of a fuzzy set A has a membership value of one, A is a so-called *normal fuzzy set*. Fuzzy sets are often defined by a graphical diagram of its membership function. It is the key component of a fuzzy set, and all operations with fuzzy sets are defined through their membership functions. In order to obtain an approximation of a fuzzy set A it is sometimes advisable to calculate so-called *α -level sets* of a fuzzy set A . It consists of all elements of the fuzzy set A which fulfill the definition of A to at least a degree α . Therefore, it is the ordinary set of points that belongs to the fuzzy set A at least to the degree α :

$$\begin{aligned} A(\alpha) &= \{x \in X, \mu_A(x) \geq \alpha\} \\ A(\alpha_1) &\subset A(\alpha_2) \text{ if } \alpha_1 > \alpha_2 \end{aligned} \quad (3.2)$$

Furthermore, if all α -levels are convex, which means that the membership function consists of an increasing and a decreasing part, the corresponding fuzzy set A is also convex:

$$\mu_A(\lambda x_1 + (1 - \lambda)x_2) \geq \min(\mu_A(x_1), \mu_A(x_2)) \quad (3.3)$$

with $x_1, x_2 \in X$ and $\lambda \in [0, 1]$. Equation 3.3 means that all points which are located on the straight-line segment connecting x_1 and x_2 are in fuzzy set A if A is convex. Depending on the variable to describe, the membership functions may have different shapes and be continuous or discrete. Figure 3.1 shows the four common types of continuous membership function $\mu(x)$ which are described in more detail in Chapter 3.1.2.

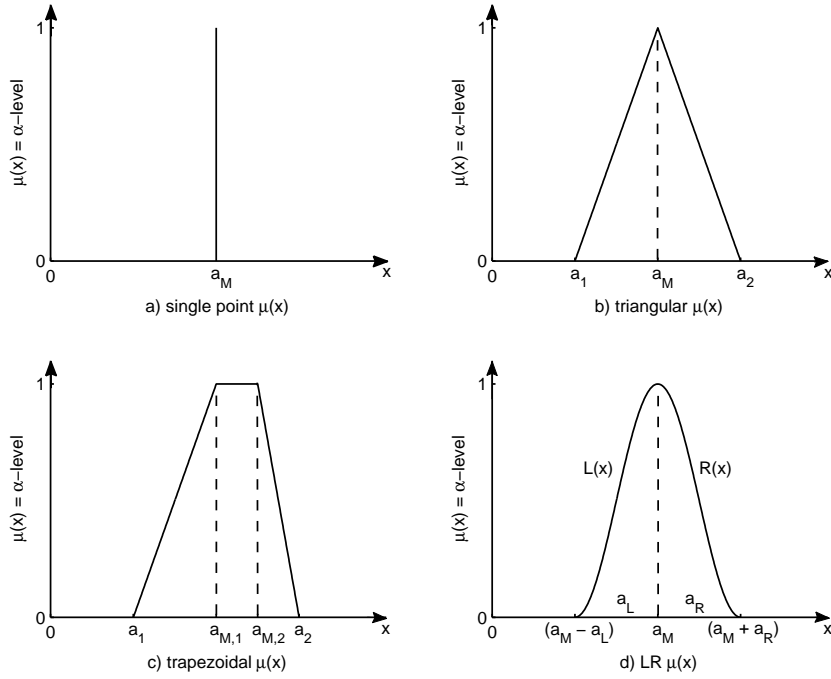


Figure 3.1: Four common types of continuous membership functions $\mu(x)$: a) single point, b) triangular, c) trapezoidal, and d) LR (Left - Right) where $L(x)$ and $R(x)$ are continuous strictly decreasing functions.

3.1.1 Operations on fuzzy sets

For the application of fuzzy sets basic set operations are required. The classical definition for the complement of a fuzzy set as well as the union and the intersection of two fuzzy sets are described in the following (Figure 3.2) as suggested by Zadeh (1965). Thereby, let A and B be two fuzzy sets of the universe X described through their membership functions $\mu_A(x)$ and $\mu_B(x)$ (Figure 3.2a).

Fuzzy-complement: The complement of a fuzzy set A is denoted by A' and its membership function is defined by (Figure 3.2b):

$$\mu_{A'}(x) = 1 - \mu_A(x) \quad (3.4)$$

Fuzzy-union: The union of two fuzzy sets A and B is $C = A \cup B$ and its membership function is defined by (Figure 3.2d):

$$\mu_C(x) = \max(\mu_A(x), \mu_B(x)) \quad (3.5)$$

Fuzzy-intersection: The intersection of two fuzzy sets A and B is $D = A \cap B$ and its membership function is defined by (Figure 3.2c):

$$\mu_D(x) = \min(\mu_A(x), \mu_B(x)) \quad (3.6)$$

The results of the fuzzy complement, union and intersection are again fuzzy sets of the universe set X . Furthermore, if ordinary subsets of X , so called *crisp sets*, are considered the above defined

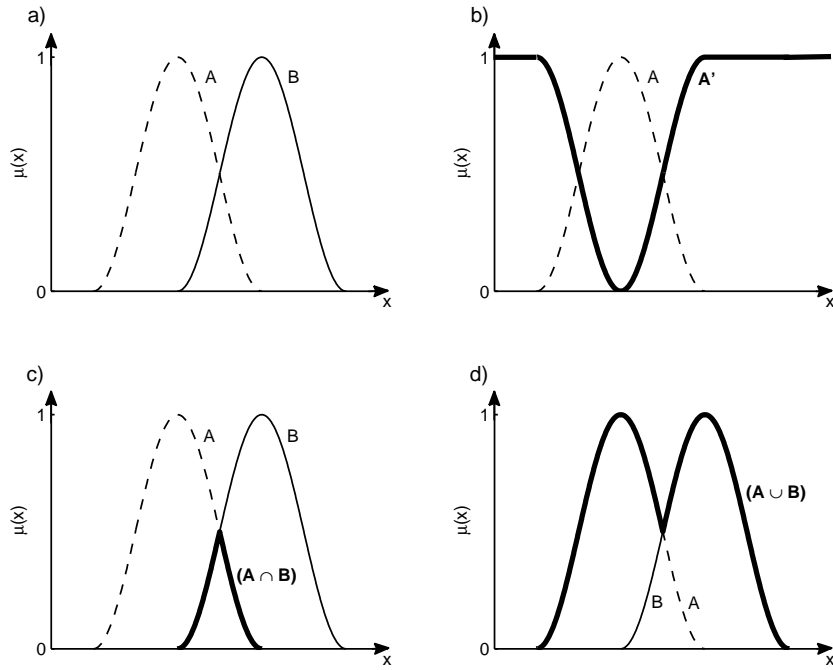


Figure 3.2: Schematic diagram of a) two fuzzy sets A and B ; b) fuzzy set A and its fuzzy-complement A' ; c) fuzzy-intersection $(A \cap B)$ of fuzzy sets A and B ; d) fuzzy-union $(A \cup B)$ of fuzzy sets A and B .

fuzzy operations yield to the usual union and intersection. However, the intersection of a fuzzy set A with its complement A' is not necessary empty (Bárdossy and Duckstein, 1995).

In some cases above definitions for the union and intersections of fuzzy sets are not adequate because their results contradict our intuitions. In these cases other functions can be applied which are generally classified into t-norms (intersection) and t-conorms (union). All functions within the two classes have to fulfill corresponding boundaries as defined in the following.

T-norm: A bivariate function $i : [0, 1] \times [0, 1] \rightarrow [0, 1]$ (i for intersection) is called a t-norm if all following four conditions are fulfilled:

- | | | | |
|----|--|---------------------------------|--------------------|
| 1. | $i(a, 0) = 0, i(a, 1) = a$ | $\forall a \in [0, 1]$ | Boundary condition |
| 2. | $i(a, b) \leq i(c, d)$ if $a \leq c, b \leq d$ | $\forall a, b, c, d \in [0, 1]$ | Monotonicity |
| 3. | $i(a, b) = i(b, a)$ | $\forall a, b \in [0, 1]$ | Symmetry |
| 4. | $i(a, i(b, c)) = i(i(a, b), c)$ | $\forall a, b, c \in [0, 1]$ | Associativity |

T-conorm: A bivariate function $u : [0, 1] \times [0, 1] \rightarrow [0, 1]$ (u for union) is called a t-conorm if all following four conditions are fulfilled:

- | | | | |
|----|--|---------------------------------|--------------------|
| 1. | $u(a, 0) = a, u(a, 1) = 1$ | $\forall a \in [0, 1]$ | Boundary condition |
| 2. | $u(a, b) \leq u(c, d)$ if $a \leq c, b \leq d$ | $\forall a, b, c, d \in [0, 1]$ | Monotonicity |
| 3. | $u(a, b) = u(b, a)$ | $\forall a, b \in [0, 1]$ | Symmetry |
| 4. | $u(a, u(b, c)) = u(u(a, b), c)$ | $\forall a, b, c \in [0, 1]$ | Associativity |

Considering Equation 3.4 each t-norm can be transferred to a t-conorm and vice versa:

$$\text{from t-norm } i \text{ to t-conorm } u \quad u(a, b) = 1 - i(1 - a, 1 - b) \quad (3.7)$$

$$\text{form t-conorm } u \text{ to t-norm } i \quad i(a, b) = 1 - u(1 - a, 1 - b) \quad (3.8)$$

In literature several t-norms with their corresponding t-conorms can be found (Klir and Yuan, 1995). Furthermore, different interpretations of the operations exist. For example, Zimmermann (1991) interprets the intersection operator given in Equation 3.6 as *logical and* (AND), the union operator given in Equation 3.5 as *logical or* (OR). Due to their definition as t-norm and t-conorm, respectively, the minimum operator is an optimistic, the maximum a pessimistic operator (Klir and Yuan, 1995).

3.1.2 Fuzzy numbers

A fuzzy number is a special case of a general fuzzy set and constitutes a generalization of the usual concept of numbers. It is a normal (at least one point has $\mu_A(x) = 1$) and convex (Equation 3.3) fuzzy set of the set of real numbers \mathfrak{R} :

$$A = \{(x, \mu_A(x)) : x \in \mathfrak{R}; \mu_A(x) \in [0, 1]\} \quad (3.9)$$

The convexity assumption ensures that the α -level sets of a fuzzy number are intervals which can be represented in the interval form as

$$A(\alpha) = [x_1(\alpha), x_2(\alpha)] \quad (3.10)$$

with

$A(\alpha)$	fuzzy number at α -level
$x_1(\alpha)$	lower bound of the α -level interval
$x_2(\alpha)$	upper bound of the α -level interval

The 0-level set is defined as the support $supp(A)$ of a fuzzy number which includes all points with an α -level greater than 0:

$$supp(A) = \{x \in X; \mu_A(x) > 0\} \quad (3.11)$$

Because of Equation 3.11 any real number can be considered as a fuzzy number with a single point support and is called a *crisp number* (compare Figure 3.1a) instead of a fuzzy number. Although the definition of fuzzy numbers is very general, only a few types are common. The definition of LR-fuzzy numbers after Dubois and Prade (1980) is very popular and widely-used, in particular, the simplest variants of LR-fuzzy numbers - the triangular and trapezoidal fuzzy numbers.

LR-fuzzy number: A LR-fuzzy number A is defined as $A = (a_M, a_L, a_R)_{LR}$ and its membership function (compare Figure 3.1d) is defined by:

$$\mu_A(x) = \begin{cases} L\left(\frac{a_M - x}{a_L}\right) & \text{if } x \in [(a_M - a_L), a_M] \\ R\left(\frac{x - a_M}{a_R}\right) & \text{if } x \in [a_M, (a_M + a_R)] \\ 0 & \text{else} \end{cases} \quad (3.12)$$

3 Fuzzy Modelling

where $L(x)$ and $R(x)$ are continuously, strictly decreasing functions defined on $[0, 1]$ with values in $[0, 1]$ satisfying the conditions:

$$L(x) = R(x) = 1 \text{ if } x \leq 0 \quad \text{and} \quad L(x) = R(x) = 0 \text{ if } x \leq 1.$$

The support of the LR-fuzzy number A is $supp(A) = [(a_M - a_L), (a_M + a_R)]$.

Triangular fuzzy number: A triangular fuzzy number A is defined as $A = (a_1, a_M, a_2)_T$ and its membership function (compare Figure 3.1b) is defined by:

$$\mu_A(x) = \begin{cases} \frac{x-a_1}{a_M-a_1} & \text{if } x \in [a_1, a_M] \\ \frac{a_2-x}{a_2-a_M} & \text{if } x \in [a_M, a_2] \\ 0 & \text{else} \end{cases} \quad (3.13)$$

where $a_1 \leq a_M \leq a_2$. The support of the triangular fuzzy number A is $supp(A) = [a_1, a_2]$.

Trapezoidal fuzzy number: A trapezoidal fuzzy number A is defined as $A = (a_1, a_{M,1}, a_{M,2}, a_2)_R$ and its membership function (compare Figure 3.1c) is defined by:

$$\mu_A(x) = \begin{cases} \frac{x-a_1}{a_{M,1}-a_1} & \text{if } x \in [a_1, a_{M,1}] \\ 1 & \text{if } x \in [a_{M,1}, a_{M,2}] \\ \frac{a_2-x}{a_2-a_{M,2}} & \text{if } x \in [a_{M,2}, a_2] \\ 0 & \text{else} \end{cases} \quad (3.14)$$

where $a_1 \leq a_{M,1} \leq a_{M,2} \leq a_2$. The support of the trapezoidal fuzzy number A is $supp(A) = [a_1, a_2]$.

Operations on fuzzy numbers. In contrast to the general fuzzy sets for which Boolean operations can be performed, arithmetic operations like addition and subtraction, can only be applied on fuzzy numbers. Furthermore, the union and intersection of fuzzy numbers are usually not themselves fuzzy numbers. Figure 3.2c shows the result of the fuzzy-intersection of the two fuzzy numbers A and B which is a general fuzzy set (no fuzzy number) because the normality assumption is not fulfilled.

The classical (crisp) arithmetic can be transferred to fuzzy sets using the *extension principle* (Zadeh, 1965), which is one of the most basic concepts for the development of fuzzy arithmetic. In general, a set X can be mapped to a set Y using a function $f : X \rightarrow Y$:

$$f : X \rightarrow Y \text{ for every } x \in X, y \in Y \text{ and } f(x) = y \quad (3.15)$$

Considering fuzzy arithmetic, the image of a fuzzy set $A \in X$ with a membership function $\mu_A(x)$ in Y is in demand. The result is the fuzzy set $B \in Y$ with the following membership function:

$$\mu_B(y) = \begin{cases} sup \{ \mu_A(x); y = f(x), x \in X \} & \text{if } f^{-1}(y) \neq \emptyset \\ 0 & \text{else} \end{cases} \quad (3.16)$$

where $f^{-1}(y)$ is the inverse of $f(x)$. Considering the α -level sets, every $A(\alpha)$ can be transformed to a α -level set $B(\alpha)$ by:

$$B(\alpha) = \{y : y = f(x); x \in A(\alpha)\} = f(A(\alpha)) \quad (3.17)$$

Here, $f(A(\alpha))$ is just an ordinary function defined on $A(\alpha)$. Furthermore, a fuzzy vector can be defined, for which the Cartesian product is introduced. If A_1, \dots, A_I are fuzzy sets in X_1, \dots, X_I then the α -level set of the Cartesian product, that is $A_1 \times \dots \times A_I$, is the same as the traditional Cartesian product of the α -level sets:

$$(A_1 \times \dots \times A_I)(\alpha) = A_1(\alpha) \times \dots \times A_I(\alpha) \quad (3.18)$$

With the help of the extension principle, the definition of the Cartesian product, and the definition of α -level sets the classical arithmetic operations can be extended for fuzzy numbers. In the following the four main fuzzy operators (addition, subtraction, multiplication, and division) are defined considering the α -level intervals of any two LR-fuzzy numbers $A(\alpha) = [x_{A,1}(\alpha), x_{A,2}(\alpha)]$ and $B(\alpha) = [x_{B,1}(\alpha), x_{B,2}(\alpha)]$ (Equation 3.10):

$$\text{fuzzy addition} \quad A(\alpha)(+)B(\alpha) = [x_{A,1}(\alpha) + x_{B,1}(\alpha), x_{A,2}(\alpha) + x_{B,2}(\alpha)] \quad (3.19)$$

$$\text{fuzzy subtraction} \quad A(\alpha)(-)B(\alpha) = [x_{A,1}(\alpha) - x_{B,2}(\alpha), x_{A,2}(\alpha) - x_{B,1}(\alpha)] \quad (3.20)$$

$$\text{fuzzy multiplication} \quad A(\alpha)(\cdot)B(\alpha) = [x_{A,1}(\alpha) \cdot x_{B,1}(\alpha), x_{A,2}(\alpha) \cdot x_{B,2}(\alpha)] \quad (3.21)$$

$$\text{fuzzy division} \quad A(\alpha)(/)B(\alpha) = [x_{A,1}(\alpha)/x_{B,2}(\alpha), x_{A,2}(\alpha)/x_{B,1}(\alpha)] \quad (3.22)$$

An example of the four above defined arithmetic operators for fuzzy numbers is given in Appendix A for a better understanding.

3.1.3 Fuzzy sets versus probabilities

At first glance fuzzy set theory is often considered as a very special case of probability theory. Indeed, fuzzy set theory and probability are related and seem to be similar in many respects (e.g. both use the unit interval and describe uncertainty), but their concepts are different. In each case the key component is a characteristic function, namely the membership function $\mu(x)$ in the fuzzy set theory, and the density function $f(x)$ for the probability. Some essential differences of both concepts are listed in Table 3.1 showing the properties of the characteristics functions $\mu(x)$ and $f(x)$ (Bárdossy and Duckstein, 1995). In the case of fuzzy failure the combinations of both concepts are sometimes necessary (see Dubois and Prade, 1980; Zimmermann, 1991; Klir and Yuan, 1995).

3.2 Fuzzy Logic and Fuzzy Inference Systems

Fuzzy inference systems are widely used as fuzzy controllers, fuzzy expert systems, fuzzy pattern recognition, and fuzzy filters. In general, these systems are grouped under the notion of fuzzy decision support systems. As already mentioned fuzzy inference is the process of formulating

fuzzy set theory membership function $\mu(x)$	probability density function $f(x)$
- quantifies similarities to imprecisely defined properties (degree of credibility)	- provides information on expectations over a large number of experiments
- is normalized by its maximum value	- is normalized by the area under the function
- cannot be bimodal due to the convexity assumption	- can be bimodal
- the sum of two fuzzy numbers are calculated with the extension principle	- the sum of two density functions are calculated with some type of convolution integral

Table 3.1: Essential differences between fuzzy set theory and probability considering the properties of the characteristics functions $\mu(x)$ and $f(x)$ (Bárdossy and Duckstein, 1995).

the mapping from a given input to an output using fuzzy logic which itself is based on linguistic IF-THEN rules using fuzzy sets and fuzzy operators. The functionality and structure of fuzzy inference systems are always the same. Basically, a fuzzy inference system can be split into three general parts:

1. *Fuzzification of the crisp inputs:* During the fuzzification process the membership function values $\mu_i(x)$ of the given crisp input x are determined for all defined fuzzy sets i of the argument A (see Chapter 3.1.2).
2. *Application of fuzzy logic:* Depending on the fuzzified inputs the degree of fulfillment DOF_j of each rule j and the corresponding responses R^j are determined applying fuzzy logic operators (IF-THEN rules).
3. *Aggregation to one single output:* Each rule gives one certain response R^j which is finally aggregated to one crisp output y of the inference system. Depending on the type of fuzzy inference system one further step called *defuzzification* has to be applied after the aggregation of all rule responses in order to achieve one crisp output y .

In practice, two different types of fuzzy inference systems are widely-used: the *Mamdani inference system* and the *Takagi-Sugeno inference system*. In both systems the fuzzification process and the application of fuzzy logic are performed in the same way, but the basic difference lies in the definition of the responses R^j . Due to the fact that both inference systems are performed in this work, the basics of fuzzy logic and both inference systems are described in the following.

3.2.1 Fuzzy Logic

One key component of a fuzzy inference system is its fuzzy logic core which uses linguistic IF-THEN rules and the basics of fuzzy set theory. In general, one fuzzy rule is defined as:

$$\text{IF } x_1 \text{ is } A_{i,1} \odot x_2 \text{ is } A_{i,2} \odot \dots \odot x_K \text{ is } A_{i,K} \text{ THEN } y \text{ is } R \quad (3.23)$$

with	x_1, \dots, x_K	crisp input (premise vector $\{x_1, \dots, x_K\}$)
	y	crisp output
	A	fuzzified argument
	R	response of rule
	$i = 1, \dots, I$	index of predefined membership functions
	$1, \dots, K$	number of arguments
	\odot	fuzzy logic operator (e.g. AND, OR)

In case of fuzzy rules (Equation 3.23) the variables within the IF-part are generally named *arguments* (A), the variable of the THEN-part *response* (R). For all types of fuzzy inference systems the arguments are described through several fuzzy numbers and membership functions, respectively (represented by index i). The rule response of the Mamdani inference system (Chapter 3.2.2) is defined as fuzzy numbers R_i , as the arguments. The response of the Takagi-Sugeno inference system is defined as a first order polynomial function $R = f(x_1, \dots, x_K)$ (Chapter 3.2.3). The statement $x_K \text{ is } A_{i,K}$ means that point x belongs to the fuzzy number i of the considered argument K , and is normally replaced by $A_{i,K}$. Furthermore, Equation 3.23 can be defined for a *fuzzy rule system*, in which more than one fuzzy rule are applied in order to represent a process, as:

$$\text{IF } A_{i,1}^j \odot A_{i,2}^j \odot \dots \odot A_{i,K}^j \text{ THEN } R^j \quad (3.24)$$

with	A	fuzzified argument
	R	response of rule
	$i = 1, \dots, I$	index of predefined membership functions
	$1, \dots, K$	number of arguments
	$j = 1, \dots, J$	index of defined rules
	\odot	fuzzy logic operator (e.g AND, OR)

In fuzzy rule systems it is often the case that different fuzzy rules and rule premises, with different responses are fulfilled to a certain degree. Due to the fact that the definition of the *rule premise* (IF-part of each rule) is independent of the type of fuzzy inference system, the truth value and the *degree of fulfillment* (DOF_j) of a rule, are calculated the same way for both considered fuzzy inference systems. Therefore, the logic operators of the above described fuzzy rule system have to be derived from those of the bivalent logic. In Table 3.2 some essential logical operators as well as the implication operator considering two crisp sets A and B are given.

Here, only two values "true" (1) and "false" (0) can be assigned to any rule, and furthermore, no exceptions can be tolerated. Depending on the conditions of the rule premise, the truth level of a binary rule is again a binary function based on 0 and 1 (Table 3.2). In contrast to this a fuzzy rule is not based on a binary function as the rule premise is based on operations of fuzzy numbers (compare Chapter 3.1.2). Consequently, the truth level of such a rule is no longer just 0 or 1,

A	B	$\text{NOT}(A)$ A'	$A \text{ AND } B$ $A \wedge B$	$A \text{ OR } B$ $A \vee B$	$\text{IF } A \text{ THEN } B$ $A \rightarrow B$
1	1	0	1	1	1
1	0	0	0	1	0
0	1	1	0	1	1
0	0	1	0	0	1

Table 3.2: Essential Boolean logical (NOT, AND, OR) and implication (IF - THEN) operators considering two crisp sets A and B .

but also something in between. In order to find the truth level of an applied fuzzy rule premise with the *premise vector* (x_1, \dots, x_K) the degree of fulfillment (*DOF*) is calculated for the interval $[0, 1]$. Equation 3.24 shows that the truth value of a rule depends on the used arguments and fuzzy operations. As pointed out in Chapter 3.1 the generalization of classical bivalent operators for the fuzzy set theory is not unique. Therefore, several possibilities for the definition of the degree of fulfillment for basic logical operators exist, whereas the two most common ones, *product inference* and *min-max inference*, are defined for the two basic logical operators (AND, OR) in the following. Thereby, let A_1 and A_2 be two fuzzy numbers.

Product inference: Considering the product inference, the degree of fulfillment *DOF* of a rule depending on the logical operator and the given premise vector (x_1, \dots, x_K) is defined as:

$$DOF(A_1 \text{ AND } A_2) = \mu_{A_1}(x_1) \cdot \mu_{A_2}(x_2) \quad (3.25)$$

$$DOF(A_1 \text{ OR } A_2) = \mu_{A_1}(x_1) + \mu_{A_2}(x_2) - \mu_{A_1}(x_1) \cdot \mu_{A_2}(x_2) \quad (3.26)$$

Min-max inference: Considering the min-max inference, the degree of fulfillment *DOF* of a rule depending on the logical operator and the given premise vector (x_1, \dots, x_K) is defined as:

$$DOF(A_1 \text{ AND } A_2) = \min(\mu_{A_1}(x_1), \mu_{A_2}(x_2)) \quad (3.27)$$

$$DOF(A_1 \text{ OR } A_2) = \max(\mu_{A_1}(x_1), \mu_{A_2}(x_2)) \quad (3.28)$$

In the case of product inference the order of the arguments have an influence on the calculated *DOF* if no AND operator is used. Furthermore, all arguments of the premise have to be fulfilled in order to achieve a rule response, whereas in the case of the min-max inference only the extremes (minimum, maximum) are important. In practice and also in this work, the combination of the AND operator together with the product inference is widely-used for the calculation of the degree of fulfillment due to its order independence and its simplicity to program.

3.2.2 Mamdani inference system

The most widely used fuzzy system is the Mamdani inference system (Mamdani, 1974, 1977). It was among the first methods which were used for control systems and this is still the main field of its application. Although, it has been successfully introduced in the field of hydrology in recent years its applications for modelling purposes are still restricted to a few specific case studies (e.g.

See and Openshaw, 1999; Bárdossy et al., 2003; Alvisi et al., 2006). In case of the Mamdani inference system Equation 3.24 is written as:

$$\text{IF } A_{i,1}^j \odot A_{i,2}^j \odot \dots \odot A_{i,K}^j \text{ THEN } B_{l,j} \quad (3.29)$$

with	A	fuzzified argument
	B	fuzzified response
	$i = 1, \dots, I$	index of predefined membership functions of arguments
	$l = 1, \dots, L$	index of predefined membership functions of response
	$1, \dots, K$	number of arguments
	$j = 1, \dots, J$	index of defined rules
	\odot	fuzzy logic operator (AND, OR)

The fuzzification and inference steps are performed on the premise vector (x_1, \dots, x_K) as for all fuzzy inference systems. The characteristic feature of this inference system is the definition of the rule responses as fuzzy numbers $R^j = B_{l,j}$ (compare Equation 3.24). Thus, the aggregation step is split into (1) the combination of the rule responses $B_{l,j}$ to one aggregated fuzzy response $B(y)$ and (2) the defuzzification step in which the aggregated fuzzy response $B(y)$ is transferred into a crisp output y . Due to the application of the extension principle there exist several possibilities for both steps. In the following the methods which are used in this work are described .

Combination of rule responses to one aggregated fuzzy response. As the majority of rules are only partly fulfilled the responses $B_{l,j}$ are truncated using the calculated degrees of fulfillments DOF_j . The results of this are no longer fuzzy numbers but fuzzy sets. These fuzzy sets are aggregated to one fuzzy response $B(y)$ by applying fuzzy operators, in this case the *weighted sum additive combination*:

$$\mu_B(y) = \frac{1}{\max_u \sum_{j=1}^J (\mu_{B_{l,j}}(u) \cdot DOF_j)} \sum_{j=1}^J (\mu_{B_{l,j}}(y) \cdot DOF_j) \quad (3.30)$$

where the denominator is the maximum of the sum. That ensures that the resulting membership function is in $[0, 1]$. The advantage of this combination is that as soon as one rule is applicable the response is not empty.

Defuzzification of the aggregated response. The aggregated fuzzy response $B(y)$ is defuzzified to one crisp system output y by using the *center-of-gravity* method:

$$y = C(B) = \frac{\int_{-\infty}^{+\infty} y \mu_B(y) dy}{\int_{-\infty}^{+\infty} \mu_B(y) dy} \quad (3.31)$$

where $C(B)$ stands for the centroid. The crisp output y is defined as the value within the range of $B(y)$ for which the area under the graph of membership function $\mu_B(y)$ is divided into two equal subareas.

For modelling purposes the center-of-gravity generally provides the best results. However, one disadvantage is that if the single truncated rule responses are far apart from each other the calcu-

3 Fuzzy Modelling

lated centroid could be zero wherefore the system response y has the misleading result of zero, too.

Union of aggregation and defuzzification steps. If the weighted sum additive combination and the center-of-gravity method are combined the crisp output of a fuzzy inference system can be calculated directly as a weighted center-of-gravity of the individual rule responses:

$$y = \frac{\sum_{j=1}^J (DOF_j \cdot C(B_{l,j}(y)))}{\sum_{j=1}^J DOF_j} \quad (3.32)$$

with DOF degree of fulfillment
 $C(B_{l,j}(y))$ centroid of fuzzified response
 $l = 1, \dots, L$ index of predefined membership functions of response
 $j = 1, \dots, J$ index of defined rules

That means there is no need to define the aggregated response $B(y)$ as a fuzzy set within a separate step. This combination of methods is simple to program and keeps computation times low. One further advantage is that this combination does not assign great importance to uncertain responses $B_{l,j}(y)$. Figure 3.3 shows the basic scheme of the Mamdani inference system as it is performed within this work.

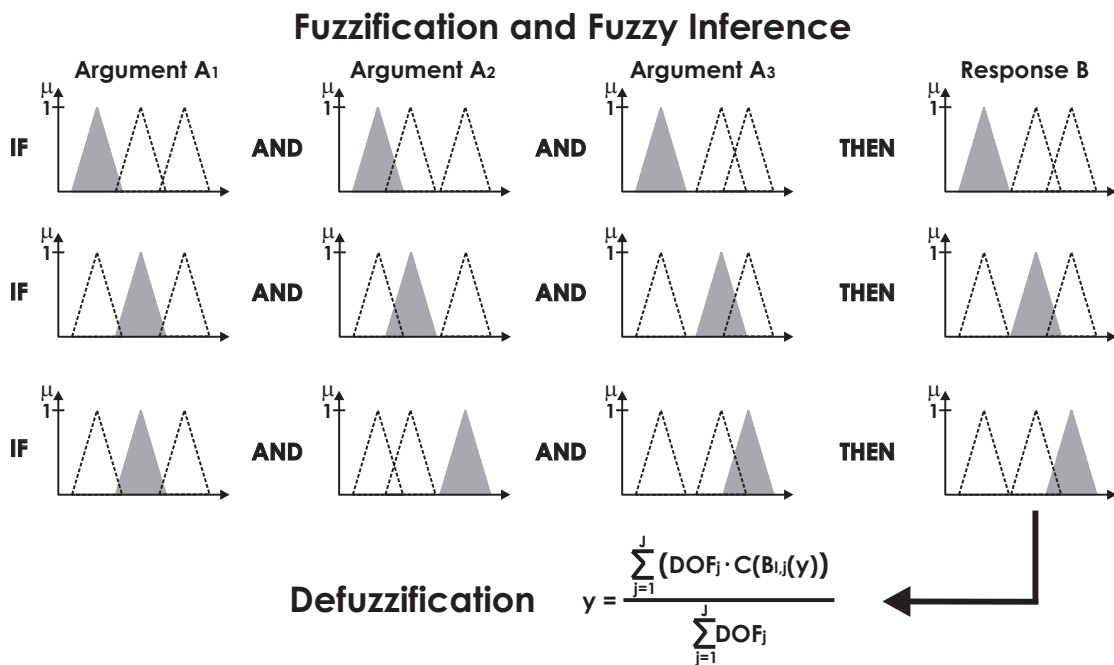


Figure 3.3: Basic scheme of the performed Mamdani inference system (arguments and response are each fuzzified by 3 triangular membership functions; grey shaded membership functions are considered within the corresponding rule).

3.2.3 Takagi-Sugeno inference system

Another type of a fuzzy system is the Takagi-Sugeno inference system which was developed by Takagi and Sugeno (1985) on the basis of the Mamdani inference system. The characteristic feature of this inference system is that the response of each rule is a linear combination of the inputs $R^j = f_j(x_1, \dots, x_K) = b_{0,j} + b_{1,j}x_1 + b_{2,j}x_2 + \dots + b_{K,j}x_K$ (compare Equation 3.24) and thus no fuzzy number. In the case of the Takagi-Sugeno inference system Equation 3.24 is written as:

$$\text{IF } A_{i,1}^j \odot A_{i,2}^j \odot \dots \odot A_{i,K}^j \text{ THEN } f_j(x_1, \dots, x_K) \quad (3.33)$$

with A fuzzified argument
 $f(x_1, \dots, x_K)$ linear function of the premise vector $\{x_1, \dots, x_K\}$
 $1, \dots, K$ number of arguments
 $i = 1, \dots, I$ index of predefined membership functions of arguments
 $j = 1, \dots, J$ index of defined rules
 \odot fuzzy logic operator (e.g. AND, OR)

The fuzzification and inference steps are performed as for all fuzzy inference systems. Within the aggregation step the system output y is calculated as a weighted linear combination of the single rule responses $f_j(x_1, \dots, x_K)$ by considering the corresponding degree of fulfillments DOF_j as the majority of rules are only partly fulfilled:

$$y = \frac{\sum_{j=1}^J (DOF_j \cdot f_j(x_1, \dots, x_K))}{\sum_{j=1}^J DOF_j} \quad (3.34)$$

with DOF degree of fulfillment
 $f(x_1, \dots, x_K)$ linear function of the premise vector $\{x_1, \dots, x_K\}$
 $j = 1, \dots, J$ index of defined rules

Due to the fact that the response is defined as a 1st order polynomial, an optimization algorithm is generally required for the set up of the Takagi-Sugeno inference system (see Chapter 3.3.2). With such an algorithm both (1) the functions constants $b_{0,j}, b_{1,j}, \dots, b_{K,j}$ and (2) the rule premises can be determined. Figure 3.4 shows the basic modules of Takagi-Sugeno inference system as it is performed in this work.

In recent years the Takagi-Sugeno inference system has been successfully introduced in the field of hydrological modelling and is more often used than the Mamdani approach (see introduction of Chapter 3). Due to the fact that a strong relation between precipitation and discharge exist also other functions for the definition of rule responses have been investigated. For example, Jacquin and Shamseldin (2006) have applied the unit hydrograph in order to achieve a better fit.

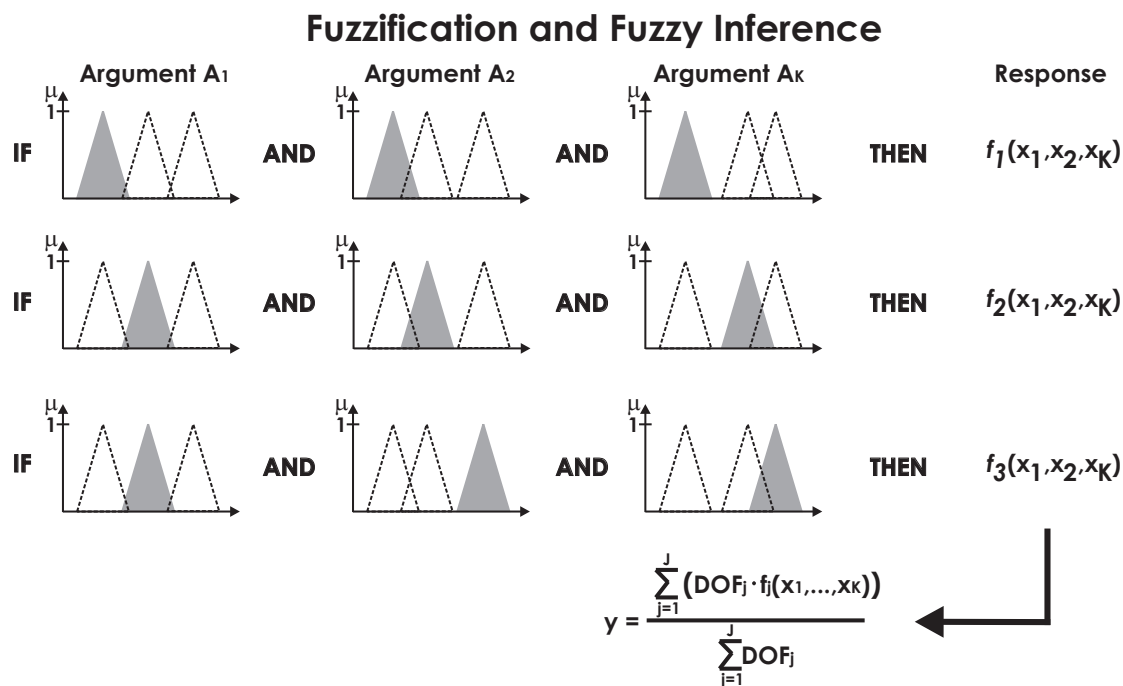


Figure 3.4: Basic scheme of the performed Takagi-Sugeno inference system (arguments are each fuzzified by 3 triangular membership functions; grey shaded membership functions are considered within the corresponding rule).

3.2.4 Mamdani versus Takagi-Sugeno inference system.

Although both presented fuzzy inference systems are very similar essential different system properties exist due to the definition of rule responses. Advantages and disadvantages of both fuzzy inference systems are summarized in Table 3.3.

3.2.5 Fuzzy inference systems and artificial neural networks

Beside the fuzzy inference systems artificial neural networks (further referred to as neural nets) are a further soft computing approach which has become very popular in the field of hydrology in recent years. The role of neural nets in hydrology is concisely overviewed in ASCE (2000a,b) and a vast number of publications considering flood forecast can be found (e.g. Fernando and Jayawardena, 1998; Castellano-Mendez, 2004; Bruen and Yang, 2005; Cullmann, 2006).

In contrast to the fuzzy set approach, which is based on IF-THEN rules, neural nets are based on the functionality of the human brain, the interactions of neurons. Neural nets are massively parallel-distributed information processing systems and their development is based on following two general parts, at and between neurons (ASCE, 2000a):

1. Information processing occurs at many single elements (nodes, neurons). The non-linear transformation of an input to an output signal is performed by applying an activation function $f(\cdot)$.

Mamdani inference system	Takagi-Sugeno inference system
The complete rule system is linguistically interpretable and transparent for the user.	Only the IF-part can be linguistically interpreted by the user whereas the THEN-part is not transparent.
Expert knowledge can be easily integrated by defining additional rules.	Due to the definition of the THEN-part expert knowledge cannot be easily defined as additional rules.
Inference system can be set up straight away by the user.	Optimization procedures are necessary for the definition of the function constants $b_{0,j}, b_{1,j}, \dots, b_{K,j}$.
More than a few rules are necessary for a satisfying reproduction of the considered process.	Only a few rules are necessary for a satisfying reproduction of the considered process as linear relations between input and output can be considered.
Complex processes are reproduced by a non-linear approximation due to the fuzzy rule responses.	Complex processes are reproduced by a weighted linear approximation as the responses are 1st order polynomials.
The system output is limited to the defined membership functions of the responses.	Theoretically, the system output can be extrapolated using the response function, but validity is limited to the cases where the rules are applicable.
In some cases the achieved system output has a misleading result due to the applied defuzzification method.	Continuity of the system output surface is guaranteed.
Additional defuzzification step is necessary which could require more computational time.	No defuzzification step is required which makes it more computationally efficient.

Table 3.3: Properties of the Mamdani and the Takagi-Sugeno inference system.

3 Fuzzy Modelling

- Between neurons signals are passed through connection links. Each of these connection links has an associated weight W that represents the connection strength.

Figure 3.5a shows the schematic diagram of node j within a simple neural net (Figure 3.5b). Here, the input vector $\mathbf{X} = (x_1, \dots, x_n)$ comes from preceding nodes of the net. The weights $\mathbf{W}_j = (w_{1,j}, \dots, w_{n,j})$ represent the connection strength between the considered node j and the nodes in the preceding to this node. The output of node j , y_j , is obtained by computing the activation function $f(\cdot)$ with respect to the inner product of the input vector \mathbf{X} and the weights \mathbf{W}_j :

$$y_j = f \left(\sum_{i=1}^n (X_i \cdot W_{i,j}) - b_j \right) \quad (3.35)$$

where b_j is the threshold value, so called *bias*, of node j , which has to be exceeded before the node can be activated. The most commonly used activation function is the sigmoid function. Further examples of common activation functions are given in Reyhani-Masouleh (2008). There exists a wide variety of different neural nets, e.g. feedforward neural nets, Kohonen self-organizing nets, and recurrent nets, which differ in how single nodes are connected with each other.

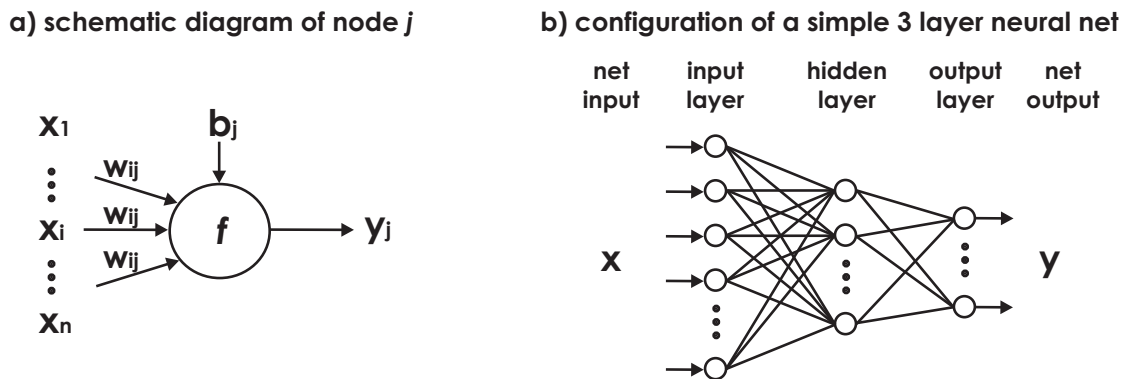


Figure 3.5: Schematic diagram of a node (a) and general configuration of a simple three layer neural net (b) after ASCE (2000a).

Although both, fuzzy inference systems and neural nets, belong to the same group of models, their concepts are totally different. Table 3.4 gives an overview of general advantages and disadvantages of both soft computing approaches (Nauck et al., 1994; Bárdossy and Duckstein, 1995).

In the field of flood forecast several investigations (e.g. Alvisi et al., 2006) have been performed, which compare the neural nets and the fuzzy approach in order to achieve a higher forecast accuracy. As in case of traditional modelling of the rainfall-runoff process the choice of the performed soft computing approach depends on the question of investigation. For solving complex problems Abraham (2001) advises (1) to performed fuzzy inference systems if knowledge can or is expressed in linguistic variables and rules, and (2) to use artificial neural nets if a certain amount of measured or simulated data is available.

Fuzzy inference systems	Artificial neural networks
<p>Both systems copy the instinctive human way of connecting causes with their effects by creating a quantitative inner chain of links between input and output without justifying the physical reasons.</p>	
<p>Both systems are able to describe the non-linear behavior of natural systems as universal approximators without using a complex mathematical model.</p>	
<p>Both work well even when the training sets contain noise and measurement errors.</p>	
<p>Rule structure is transparent and linguistic interpretable for the user.</p>	<p>Model structure has a black-box behavior.</p>
<p>Due to the application of linguistic variables rule systems are easy to model.</p>	<p>The strength of neural nets lies in their learning aptitude.</p>
<p>Robust fuzzy systems can be set up even if scarce data sets are available.</p>	<p>A certain amount of data is required for the neural net learning.</p>
<p>A priori expert knowledge can be included.</p>	<p>No a priori expert knowledge can be considered.</p>
<p>If input data are outside the range of training data no system output is achieved due to the predefined fuzzy numbers and used fuzzy operators (critical conditions are recognisable).</p>	<p>The system gives always an output and critical conditions might be missed.</p>
<p>More and more optimization algorithms are available and can be significantly improved if a priori knowledge is available.</p>	<p>Various learning algorithms are available and often give the impression that the user only has to feed data into the model. However, the learning process might not always converge.</p>
<p>The problem of overfitting might occur but can be overcome if the right number of rules is used.</p>	<p>Neural nets often face the problem of overfitting which leads to a poor predictive performance.</p>

Table 3.4: Comparison of fuzzy inference systems and artificial neural networks (Nauck et al., 1994; Bárdossy and Duckstein, 1995).

3.3 Training methods for fuzzy inference systems

In case of soft computing methods the term *calibration* is generally substituted by the term *learning* and *training*, respectively, as it comes from the human learning and training process. Basically, there exist four methods for the assessment of fuzzy inference systems (Bárdossy et al., 2003):

1. Directly by using experimental data and / or expert knowledge.
2. Genetic optimization algorithms.
3. Neuro-fuzzy approaches.
4. Simulated Annealing.

For the setup of fuzzy controller the direct method is mostly applied which requires interviews of workers in many cases. The learning of fuzzy control rules using genetic algorithms is presented in e.g. Herrera et al. (1998). For modelling purpose the last two are common as they can handle great amounts of data. Because of its popularity a short description of the neuro-fuzzy approach is given first. However, in this work the Simulating Annealing (Kirkpatrick et al., 1983; Guély et al., 1999) approach is used as it has been already successfully applied as shown by Bárdossy et al. (2002, 2003) and Alvisi et al. (2006). The goal is to find the rule system with the optimal performance which includes the function parameters $b_{0,j}, b_{1,j}, \dots, b_{K,j}$ (Chapter 3.2.3) in the case of the Takagi-Sugeno inference system. The definitions of the required fuzzy numbers and membership functions, respectively, are done manually.

3.3.1 Neuro-Fuzzy

As shown in Chapter 3.2.5 both approaches, fuzzy inference systems and neural nets, have different advantages and disadvantages. The central argument for a combination of both, which can be done in two ways, is the enhanced ability to learn. In general, there exists a significant difference between Neuro-Fuzzy and Fuzzy neural networks. The first is more or less an optimization procedure for the setup of fuzzy inference systems in which the learning capability of neural nets is utilised for the assessment of fuzzy inference systems (Abraham, 2005). In contrast to this, Fuzzy neural networks are neural nets whose inputs, weights and outputs are fuzzy numbers (Klir and Yuan, 1995). As only different training methods for fuzzy inference systems are considered in this chapter, the three classical Neuro-Fuzzy approaches - *cooperative*, *concurrent*, and *integrated (hybrid)* - are briefly presented in the following.

The simplest Neuro-Fuzzy setup is the cooperative approach (Abraham, 2005, Figure 3.6a). This learning method is in some view comparable with the Simulated Annealing method as the general structure of the fuzzy inference system stays untouched. Here, the neural net learning mechanism determines the membership functions or the rules of the fuzzy system based on the given training data. Usually, the rule base is set up by applying a clustering approach (e.g. self organizing maps). After the assessment of the fuzzy inference system the neural net goes to the background.

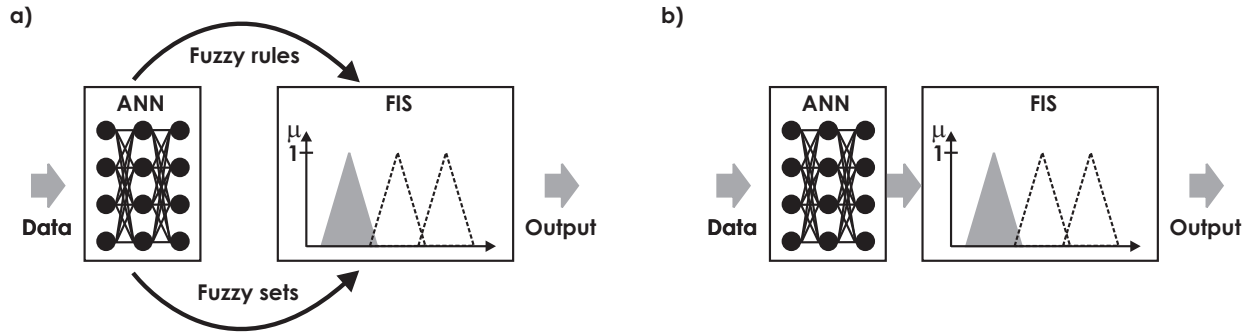


Figure 3.6: Schematic diagram of (a) a cooperative and (b) concurrent Neuro-Fuzzy approach after Abraham (2005, ANN: neural net, FIS: fuzzy inference system).

In contrast to the cooperative Neuro-Fuzzy system the neural net within the concurrent approach does not optimize the fuzzy system in one step and goes not to the background (Abraham, 2005). The neural net assists the fuzzy inference system continuously and aids to improve the performance of the overall system. That means that the predefined fuzzy inference system remains untouched and the learning progress of the overall system takes place only in the neural net. Depending on the data, the neural net can act as a pre- (Figure 3.6b) or postprocessor of the fuzzy inference system.

Integrated (hybrid) Neuro-Fuzzy systems are neural nets which imitate the structure and the functionality of fuzzy inference systems (Nauck et al., 1994; Abraham, 2005). Figure 3.7 exemplarily illustrates a hybrid Mamdani Neuro-Fuzzy system which consists of five neural net layers which represent the general structure of the Mamdani system. However, a classical Mamdani inference system as described in Chapter 3.2.2 does not exist any longer since only the single layers and their connections are interpreted as a fuzzy inference system. Thereby, L1 represents the crisp input which is fuzzified within L2 through the consideration of several nodes. The fuzzy rule premise (IF-part) is described by the connections of L2 and L3. Furthermore, the connections of L3 and L4 are interpreted as the THEN-part of a rule system whereby the nodes of L4 represent the fuzzified responses. Finally, the defuzzification step is performed considering the last layer L5 of the neural net. The same holds true for the integrated Neuro-Fuzzy systems considering the Takagi-Sugeno inference system.

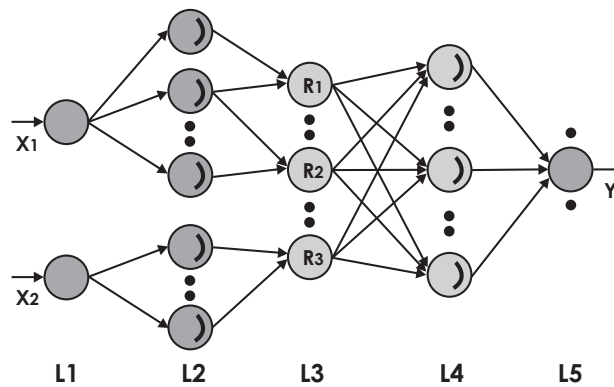


Figure 3.7: Schematic diagram of a five layer Mamdani Neuro-Fuzzy inference system after Abraham (2005); L1: input layer, L2: fuzzification layer, L3: rule antecedent layer, L4: rule consequent layer, L5: defuzzification layer.

It is obvious that the optimized cooperative, concurrent, and integrated (hybrid) Neuro-Fuzzy systems are not fully interpretable due to the fact that the neural net is still present after the training process and cannot be uncoupled. That means that no stand-alone fuzzy inference system is obtained for modelling purposes. Furthermore, the complexity of these systems are not very practical in the context of the development of a user-friendly and transparent flood warning system as it is one aim of this thesis. Therefore, no Neuro-Fuzzy approach is performed for the optimization of the fuzzy inference systems.

3.3.2 Simulated Annealing

Simulated Annealing is used for optimization problems which exclude the testing of all possibilities and simple mathematical methods due to their complexity. It is a meta-heuristic optimization method considering combinatorial problems. The basis of the optimization algorithm is the Metropolis-Hasting approach. The Simulated Annealing method provides an acceptably good solution in a fixed amount of time, rather than the best possible solution. The origin of the Simulated Annealing method lies in materials science (Kirkpatrick et al., 1983). There it is used as a cooling schedule (annealing) of materials in order to achieve the best configuration of the molecules. That means the internal energy of the system has to be minimized. Hence, all parameters of the optimization algorithm still have notations considering the cooling process (e.g. temperature, energy). On the way to the best molecule configuration, worse intermediate states of the molecules are allowed and local minima can be overcome. Time and temperature are key parameters of this cooling process and play an important role within the transformed optimization algorithm. One further key component is the probability to allow worse intermediate states to occur (Equation 3.36 written in molecules energy notation and model performance notation).

$$p' = e^{\left(\frac{-\Delta E}{k_B T_a}\right)} = e^{\left(\frac{-(O(RS') - O(RS))}{T_a}\right)} \quad (3.36)$$

with	p'	probability of an intermediate state (Boltzmann factor)
	ΔE	energy difference between a new and old state
	k_B	Boltzmann constant
	T_a	annealing temperature
	$O(RS')$	performance of the new model (rule system)
	$O(RS)$	performance of the old model (rule system)

The *traveling salesman problem* (Pfeiffer, 2003) is one of the most common example for the application of the Simulated Annealing algorithm. The task consists in finding the (nearly) shortest path connecting a number of cities visited by a traveling salesman on his sales route. Due to the fact that there exists a great amount of possible itineraries this combinatorial problem is very difficult to solve. For example, if the route goes through 15 cities and it does not matter in which direction in time the salesman visits the cities, there exists $14! / 2 = 43589145600$ possibilities for his route.

The training of fuzzy rule systems is a similar problem as the traveling salesman problem. If K arguments each with I membership functions are used $\prod_K I_K$ rules can be set up in a whole. Even

if the number of rules is fixed to J , $(\prod_K I_K)$ possibilities for the setup of the rule system exist. In case of the Mamdani inference system the amount of possibilities even increases to $(\prod_K I_K \times L)$ as the response is also defined by L membership functions.

For the setup of a rule system the Simulated Annealing algorithm is applied as it was already performed by Bárdossy (1998); Bárdossy et al. (2002, 2003) and Alvisi et al. (2006). Below the general steps of this procedure are briefly described. Table 3.5 summarizes the parameters of the Simulated Annealing algorithm which have to be defined in advance as boundary conditions. Furthermore, it is assumed that the number of rules are fixed to J and the K (and L) membership functions of all arguments (and the response) are predefined.

1. An initial rule system RS is randomly generated and its performance $O(RS)$ is evaluated.
2. The initial annealing temperature T_0 is selected and set to the annealing temperature T_a .
3. One membership function of an argument within the rule system is randomly changed to another defined membership function of this argument, whereby a new rule system RS' is achieved. In case of the Mamdani inference system the generation of the new rule system is extended by the membership functions of the response.
4. The sum $\sum_{t=1}^N DOF_j(t)$ is calculated for each rule over all time steps N :
 IF $\sum_{t=1}^N DOF_j(t) < \sum DOF_{fixed}$ then the algorithm continues with step 3.
 ELSE the algorithm continues with step 5.
5. The performance of the new rule system $O(RS')$ is evaluated with respect to the minimization of the objective function:
 IF $O(RS') < O(RS)$ then the new rule system replaces the old one $RS := RS'$ and the algorithm continues with step 3.
 ELSE the probability of acceptance p' (Equation 3.36) is evaluated and compared with a generated random number p in $[0, 1]$:
 IF $p' > p$ then the old system is replaced by the new one $RS := RS'$.
6. Steps 3 to 5 are repeated NN times.
7. The annealing temperature T_a is decreased by the scale factor DT_a given as a boundary condition.
8. Steps 3 to 7 are repeated NM times.
9. The temperature scale factor DT_a is modified and the algorithm continues with step 3.
10. Steps 3 to 9 are repeated until one of the following termination conditions is fulfilled: (1) the final annealing temperature is reached, (2) the portion of accepted positive changes PC becomes smaller than a predefined threshold.

3 Fuzzy Modelling

In order to achieve satisfying optimization results the initial temperature has to be high enough to ensure that the result is not dependent on this boundary condition. The higher the annealing temperature T_a , more worse intermediate states are accepted. This is important to overcome a local minima, in particular, right after the beginning of the optimization process. The more the system cools down, the smaller is the probability of acceptance and only a few negative variations can occur. For the application on fuzzy systems Bárdossy et al. (2002) advise that the number of attempted changes NN at a given annealing temperature should be at least as many as the number of arguments multiplied by the number of rules. In general, there exist several different cooling schedules considering T_a as shown in Reyhani-Masouleh (2008). Step 4 ensures that the sum $\sum_{t=1}^N DOF_j(t)$, calculated for each rule over all time steps, never becomes smaller than a fixed value $\sum DOF_{fixed}$ given as a boundary condition. This is an additional feature introduced to the common optimization algorithm to achieve more generally applicable than event depending rules. Considering the objective function the least-squares method is chosen in this work. In contrast to Gemmar et al. (2006) who applied a non-negative least-squares approach, the SA algorithm can result in negative parameters of the response function considering the TS systems which makes this inference system once more less interpretable. If the probability of acceptance p' is generally set to zero the Simulated Annealing algorithm corresponds to the local search concept which sticks to the first local minimum.

Notation	Simulated Annealing parameter
T_0	initial annealing temperature
DT_a	decreasing rate of annealing temperature (scale factor)
NN	number of iterations used for each temperature
NM	number of temperature changes before temperature decrease rate DT_a is modified
$\sum DOF_{fixed}$	minimum sum of DOF which is calculated for each rule over all time steps
PC	portion of accepted positive changes (stopping criterion)
IS	initial value for the random number generator

Table 3.5: Parameters of the Simulated Annealing algorithm

According to Pfeiffer (2003) the advantages of Simulated Annealing can be summarized as followed:

1. It is easy to program.
2. Good optimization results are located about 1 to 10 % apart from the optimum.
3. It is one of the best investigated meta-heuristic optimization methods.
4. There exist several hundred applicabilities of the algorithm.

The disadvantage is the difficulty to find the right combination of parameters as boundary conditions for the performed Simulated Annealing optimization. In general, an optimized fuzzy rule system is considered as good, if:

1. it is complete. That means that in case of the Mamdani inference system for every input vector the corresponding response is a non-empty fuzzy set and all questions concerning the modeled process can be answered.
2. the rules are representative and transparent.
3. the modeled output fits the observed variable well.

3.4 Tukey depth function

Data depth is a concept which recently receives increasing interest and is more and more used in multivariate statistics. Dyckerhoff (2004) overviews the most important depth function, e.g. the Mahalanobis depth (Mahalanobis, 1936), the half-space depth (Tukey, 1975), the simplicial depth (Liu, 1988), the majority depth (Singh, 1991), and the zonoid depth (Koshevoy and Mosler, 1997). These functions are successfully applied in the field of multivariate statistics including among others multivariate rank tests and quality control (Liu and Singh, 1993), outlier detection (Cramer, 2003), cluster analysis and classification (Hoberg, 2003). In the field of hydrology the use of data depth is very limited so far. Chebana and Ouarda (2008) used the Tukey data depth to define weights for the regional estimation of hydrological extremes. Bárdossy and Singh (2008) applied the same data depth to find a set of robust parameter vectors for a hydrological model. Bliefernicht (2010) investigated the performance of the L_1 -depth function for the detection of precipitation extremes.

In general, data depth is a concept that measures the centrality of a point \mathbf{z} in a given data cloud $\mathbf{x}_1, \mathbf{x}_2, \dots, \mathbf{x}_n \in \mathfrak{R}^d$. Tukey (1975) introduced in his pioneering work the half-space depth as a tool for visualizing bivariate data sets and to identify the center of a multivariate dataset as an analogous to the univariate rank, respectively. Further investigations were advanced by Donoho and Gasko (1992), Ruts and Rousseeuw (1996), Rousseeuw and Struyf (1998), Zuo and Serfling (2000), and others. Considering the simplest case, the depth D_1 of a value z in an one-dimensional data set $X = \{x_1, x_2, \dots, x_n\}$ is the minimum of number of data points (#) lying on the left and on the right side of z :

$$D_1(z; X) = \min(\#\{i : x_i \leq z\}, \#\{i : x_i \geq z\}) \quad (3.37)$$

That means that in one-dimension the minimum and the maximum of a data set have the depth equal to 1, the second lowest and the last-second highest the depth 2, and so on. Furthermore, the upper and lower quartiles have a depth of $\cong n/4$, and the median a depth of $\cong n/2$. Considering the d-dimensional case, the half-space depth D_d of a point $\mathbf{z} = \{z_1, z_2, \dots, z_d\} \in \mathfrak{R}^d$ relative to the d-dimensional data cloud $X = \{\mathbf{x}_1, \mathbf{x}_2, \dots, \mathbf{x}_n\}$ with $\mathbf{x}_i = \{x_1, x_2, \dots, x_d\}$ is the least depth of \mathbf{z} in any one-dimensional projection or view of the data set. That means that the depth of a point \mathbf{z} gives an indication of how deep the point is inside the d-dimensional data cloud. Furthermore, the half-space depth can be seen as the smallest number of data points in any closed half-space with boundary through \mathbf{z} , and therefore it can be written as (Donoho and Gasko, 1992):

$$D_d(\mathbf{z}; X) = \min_{\|\mathbf{u}\|=1} \#\{i : \mathbf{u}^T \mathbf{x}_i \geq \mathbf{u}^T \mathbf{z}\} \quad (3.38)$$

where \mathbf{u} ranges over all vectors in \mathfrak{R}^d with $\|\mathbf{u}\| = 1$.

Depth is not equivalent to density. A point with maximal depth can be thought of as a multidimensional median and the deepest point, respectively. Due to its definition the half-space depth is a nested convex, nonnegative and bounded function which satisfies the following four important properties (Zuo and Serfling, 2000):

1. *Affine invariance*: the depth of a point $\mathbf{z} \in \mathfrak{R}^d$ is independent of the underlying coordinate system and of the scales of the underlying measurements.
2. *Maximality at center*: the depth function obtains maximum value at center (equates deepest point) for distributions having a uniquely defined one (e.g. point of symmetry).
3. *Monotonicity relative to the deepest point*: the depth at a point \mathbf{z} increases monotonically as it moves toward the deepest point along any fixed ray through the center.
4. *Vanishing at infinity*: the depth of a point \mathbf{z} approaches zero as $\|\mathbf{z}\|$ approaches infinity.

One further advantage of depth functions are their robustness in higher dimensions. By adding k bad data points to the d -dimensional data set X , only the k -outermost depth contours can at most be corrupted, whereas the inner ones have to reflect the shape of the good data as before.

In the context of this thesis, Tukey depth is investigated as an additional source of information for the assessment of different flood events. Thereby, ordinary and unusual conditions can be classified with the help of Tukey depth based on the argument combinations under investigation. Ordinary argument combinations are represented through high depth values. In contrast to this seldom argument conditions are interpreted as outliers and own very small depth values according to the definition of Tukey depth function. Here, the application of Tukey depth function as an additional source of information is investigated in two ways: First, it is considered as an additional argument within the Mamdani inference systems in order to improve the 48 hour forecast ability of these systems (Chapter 5.3.2). Second, the extrapolation behavior of Mamdani inference systems is investigated based on Tukey depth (Chapter 5.3.3).

4 The study area: Upper Main

4.1 Catchment characteristics

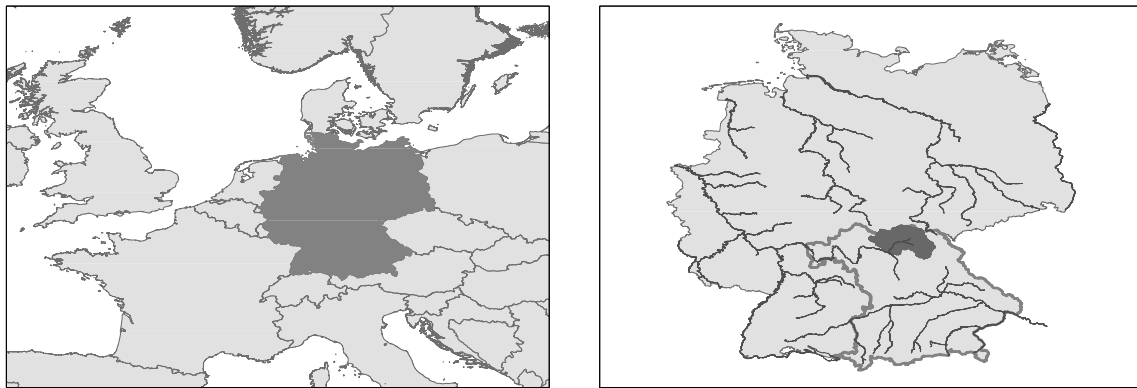


Figure 4.1: Location of Germany, Europe (dark gray, left), and the Upper Main basin in the North-East of the national state Bavaria in Germany (dark gray, right).

The river catchment of the Upper Main is part of the Rhine basin and is located in the North-East of the national state Bavaria in Germany (Figure 4.1). It refers to the rather dry region of Bavaria. It covers an area of about 4646 km², and stretches approximately from latitude 49.8 N to 50.5 N and longitude 10.5 E to 11.8 E, with a mean North-South extension of approximately 70 km, and a mean West-East extension of about 90 km (LfW, 1978). It is enclosed by the low mountain range of the Thuringian Forest in the North, the Haßberge in the West, the Franconian Switzerland in the South, the Franconian Forest and the foothills of the Fichtelgebirge in the South-East and East. The highest point lies with 1044 m.a.s.l. in the South-East of the catchment, and the lowest with 230 m.a.s.l. in the South-West near the outlet gauge Kemmern. The mean elevation is about 429 m.a.s.l.. About 75 % of the area has an elevation between 200 and 500 m.a.s.l., and about 25 % of the area is a low mountain region with a height between 500 to 850 m.a.s.l.. The Upper Main river itself arises by the confluence of the two headwaters White and Red Main (near gauge Mainleus), and ends with the confluence of the river Regnitz in the South-West of the catchment (about 6 km downstream of gauge Kemmern, Figure 4.2). The springs of the White and the Red Main are located in the low mountain range of the Fichtelgebirge in the South-East, where the highest annual precipitation of the catchment occurs. The White Main rises at 887 m.a.s.l. and has a flow distance of 45 km before it converges with the Red Main, whose spring is located at 581 m.a.s.l. and has a flow length of 55 km. After the confluence of the two headwaters the Upper Main itself has a flow distance of about 70 km. Two climatic and geological very different sides characterise the course of the river: (1) the Upper Main valley and its bigger tributaries with less precipitation, and (2) the spring regions with high precipitation, often in combination with

4 The study area: Upper Main

snowmelt, which causes flood events. The main tributaries are river Rodach, Itz and Baunach from the North, and less important the tributary Weismain from the South (Figure 4.2).

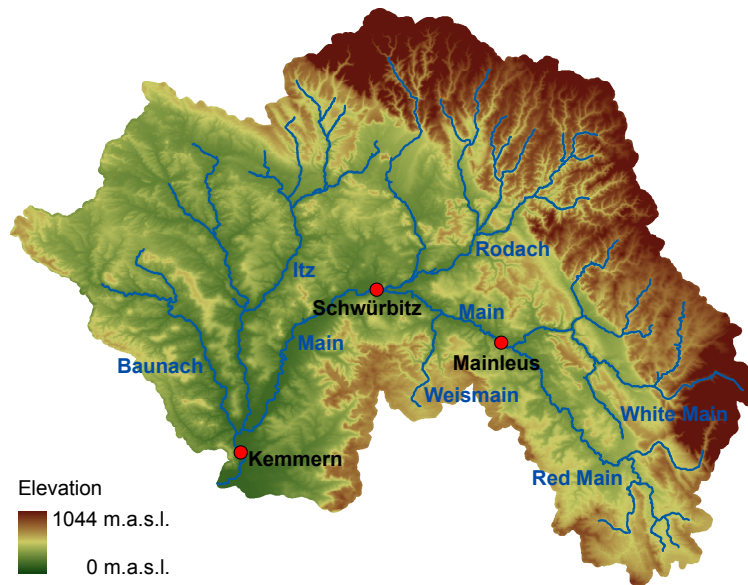


Figure 4.2: Catchment of the Upper Main river including the three main gauges Kemmern (4244 km²), Schwürbitz (2419 km²), and Mainleus (1166 km²) as well as the main tributaries Baunach, Itz, Rodach, Weismain, White and Red Main.

For thousands of years the Upper Main was a typical river for the low mountain range with vast meander and flood plains. Since the 12th century the river was used as a route of transportation for felled timber coming from the Franconian Forest. To satisfy the requirements of timber rafting the course of the river was changed dramatically: the river was straightened, the river bed was narrowed, and the river banks were fixed. Today, the consequences of these measures are still serious: The flood risk has been increased for people living in downstream areas, the enforced flood wave propagation causes erosions of the riverbed, and natural habitats have been lost (LfU, 2008).

Climate: Spatial differences of the mean annual precipitation are very distinctive. With 1100 mm the highest annual precipitation occurs at the West hillside of the Fichtelgebirge in the East, followed by 700 mm in the Red Main valley in the South-East, and 550 mm in the Upper Main valley in the Western part of the catchment. Except for the Fichtelgebirge precipitation is equally distributed over the year. In case of the Fichtelgebirge slightly more precipitation occurs in winter. The mean annual temperature ranges between 6 °C in the high mountain range of the Fichtelgebirge and 7 °C in the Upper Main valley (HAP, 2008).

Land use: With about 53 % of the catchment area agriculture is the dominant land use type. Further 41 % of the area is covered by forests. Only 5 % of the area is urbanized, which is far below the nationwide average of 12.8 %, and also below the Bavarian average of 10.8 % (StBA, 2004). The rest of the area belongs to natural grassland with bush banks.

Geology and soil: The investigation area is subdivided into three geological units: (1) the Mesozoic overburden in the West and South-West of the catchment consists of Fränkische Sandsteinkeuper (Haßberge), and Jurassic rock layers of the Franconian Alb. (2) The East Bavarian Bruch-

schollenland, which stretches out over the Red Main valley, consists of Bunter, Muschelkalk, Keuper, Black, Brown, and White Jura. (3) The crystalline bedrock extends over the Franconian Forest and the Fichtelgebirge in the East and South-East of the catchment. It mainly consists of metamorphic rocks as Gneiss and Mica, however, in the region of the Fichtelgebirge it is Granite. The two dominant soil types are (1) Cambic Podzols from sandstone and quartzite, and (2) Vertic Cambisols from marlstone and claystone weathering. They are alternating on the top of bedrocks Sandsteinkeuper and Lias. Because of this soil structure of alternating clay and loam layers the permeability into the lower soil horizon is moderate to low.

Groundwater: Except for the aquifers underneath the flood plains of the larger rivers, which consist of sands and gravel, and the karst aquifer in the South (Fränkische Alb) fractured aquifers are predominant within the catchment area. Important aquifers are the Fränkische Keuper and the Bunter of the Bruchschollenland. Both are fractured aquifers, which have been made available for drinking water supply using springs but mainly deep wells. The karst aquifer of the Fränkische Alb is only tapped by springs. The delivery of such springs can exceed 100 l/s. Because of the marginal thickness of the soil layers, the bad filter property, and the high flow velocity karst areas are very sensible regions for water supply, in particular to pollutants. The schist and crystalline rocks of the Thuringian-Franconian uplands refer to the fractured aquifers and have been made available mainly by small springs. Partially larger groundwater occurrences are within the quaternary sands and gravels of the Main valley.

Discharge and flood events: For the Upper Main area, flood events appear predominantly as consequences of long-lasting precipitation events during winter, often in combination with snowmelt. They occur straight after the causative weather pattern, have a short time of concentration, and therefore short advance warning times. The Upper Main area is characterized through asymmetric discharges with high flood and low low water contributions due to low storage capacities of the soil and high precipitation events. During flood events water levels of rivers rise very quickly having steep and short-lived flood peaks. Within the White Main area surface runoff is dominant because of the low storage capacity of the crystalline fractured aquifer. Here, flood events occur periodically as a consequence of high precipitations onto marginal to medium snow covers. Because of their local characteristics thunderstorms have no great impacts during summertime. The mean travel time of flood waves from gauge Bad Berneck (downstream of the White Main spring) to the gauge Mainleus amounts to about 9.5 hours. The slope of the Red Main valley is flatter than that of the White Main. The Sandsteinkeuper also has a lower storage capacity as the crystalline fractured aquifer. Marginal snow cover in combination with frozen or saturated soil layers causes the risk of flooding during wintertime. In contrast to the White Main, mean flood events occur in response to heavy thunderstorms during summertime at the Red Main. The mean travel time of flood waves from gauge Bayreuth (downstream of the Red Main spring) to the gauge Mainleus amounts to approximately 8 hours. In Table 4.1, travel times of flood waves, based on investigations of past flood events, and important tributaries are given.

For 54 gauges of the investigation area current water levels with corresponding discharges as well as measurements of the last six days are available online. Only for the three Upper Main gauges Mainleus (1166 km²), Schwürbitz (2419 km²) and Kemmern (4244 km²) flood forecast is performed by the Bavarian Administration (Bayerische Hochwassernachrichtendienst: Bayer. HND). For these three gauges the five highest observed discharges are given in Table 4.2, the five highest observed water levels in Table 4.3 (Bayer. HND, 2005).

4 The study area: Upper Main

flow distance	river	length [km]	travel time [h]	tributaries
gauge Bad Berneck - gauge Mainleus	White Main	38	9 to 10	Weismain, Rodach Itz, Baunach
gauge Bayreuth - gauge Mainleus	Red Main	33	6 to 10	
gauge Mainleus - gauge Schwürbitz	Upper Main	22.8	3 to 6	
gauge Schwürbitz - gauge Kemmern	Upper Main	47.3	10 to 20	

Table 4.1: Travel times of flood waves and tributaries of the Upper Main catchment (Bayer. HND, 2005).

Rank	Kemmern		Schwürbitz		Mainleus	
	date	Q [m ³ /s]	date	Q [m ³ /s]	date	Q [m ³ /s]
1	25.12.1967	1000	24.12.1967	764	26.01.1995	357
2	07.01.1982	771	28.12.1947	676	21.12.1993	263
3	24.02.1970	749	09.02.1946	616	31.12.1986	255
4	04.01.2003	731	06.01.1982	605	01.04.1988	249
5	29.01.2002	712	03.01.2003	576	13.02.2005	247

Table 4.2: The five highest observed discharges (Bayer. HND, 2005) for the three Upper Main gauges Kemmern (4244 km², observation period: 1931 - 1998), Schwürbitz (2419 km², observation period: 1941 - 1999), and Mainleus (1166 km², observation period: 1983 - 1999).

Rank	Kemmern		Schwürbitz		Mainleus	
	date	W [cm]	date	W [cm]	date	W [cm]
1	07.01.1982	687	06.01.1982	546	26.01.1995	442
2	02.11.1998	668	26.01.1995	538	21.12.1993	414
3	27.01.1995	667	10.03.1981	531	01.11.1998	408
4	24.02.1970	664	02.11.1998	529	31.12.1986	408
5	11.03.1981	664	03.03.1999	489	01.04.1988	406

Table 4.3: The five highest observed water levels (Bayer. HND, 2005) for the three Upper Main gauges Kemmern (4244 km², observation period: 1931 - 1998), Schwürbitz (2419 km², observation period: 1941 - 1999), and Mainleus (1166 km², observation period: 1983 - 1999).

For a better classification of the occurred flood events (Table 4.2, 4.3) discharges of different flood frequencies (Table 4.4) as well as different warning levels (Table 4.5) of the three Upper Main gauges are given (Bayer. HND, 2005). Since for the latter only water levels are given by the Bayer. HND the corresponding discharges are calculated considering the corresponding rating curve (Bayer. HND, 2005).

Considering the discharges it becomes obvious that except for one flood event in the year 1967 only smaller flood events around HQ_{20} occurred within the Upper Main basin. Furthermore, looking at the water levels flood events exceeding warning level 4 (large-scale overflowing of urban areas and large-scale dike improvements are necessary) only occurred within the two smaller gauge catchments Schwürbitz (2419 km²) and Mainleus (1166 km²) owing flood frequencies around 2 and 5 years.

	Kemmern		Schwüribitz		Mainleus	
	$[m^3/s]$	$[mm/h]$	$[m^3/s]$	$[mm/h]$	$[m^3/s]$	$[mm/h]$
HQ_1	300	0.26	250	0.37	125	0.39
HQ_2	400	0.34	325	0.48	165	0.51
HQ_5	510	0.43	410	0.61	210	0.65
HQ_{10}	640	0.55	520	0.77	260	0.80
HQ_{20}	780	0.66	640	0.95	320	0.99
HQ_{50}	980	0.83	800	1.19	400	1.24
HQ_{100}	1150	0.98	950	1.41	460	1.42
HQ_{1000}	1800	1.53	1500	2.23	730	2.25

Table 4.4: Discharges of different flood frequencies HQ (Bayer. HND, 2005) for the three Upper Main gauges Kemmern (4244 km²), Schwüribitz (2419 km²), and Mainleus (1166 km²).

Warning level	Kemmern		Schwüribitz		Mainleus	
	$W [cm]$	$Q [m^3/s]$	$W [cm]$	$Q [m^3/s]$	$W [cm]$	$Q [m^3/s]$
WL 1	420	151	350	138	250	55
WL 2	480	216	400	209	290	80
WL 3	570	326	450	306	320	99
WL 4	700	766	530	513	400	182

Table 4.5: Warning levels (Bayer. HND, 2005) for the three Upper Main gauges Kemmern (4244 km²), Schwüribitz (2419 km²), and Mainleus (1166 km²). Discharges are calculated considering the corresponding rating curve (Bayer. HND, 2005, WL 1: overflowing in some minor places; WL 2: overflowing of agricultural areas and some traffic obstructions; WL 3: overflowing of some houses / basements, closure of main roads, and some dike improvements are necessary; WL 4: large-scale overflowing of urban areas and large-scale dike improvements are necessary).

4.2 Data basis

For a successful calibration and validation of a deterministic and fully distributed hydrological model (WaSiM-ETH) as well as of fuzzy inference systems meteorological and hydrological observation data are required. These historical data records should consist of long and ideally continuous time series. In case of the fully distributed hydrological model further grid based data as topology, land use and soil are necessary.

The grid based data used for the setup of the hydrological model WaSiM-ETH in this study is provided by the Bayerischen Landesamt für Umwelt (LfU, 2005) with Gauss-Krüger coordinates (12° central meridian). As topographic data the DGM 25 of Bavaria and Thuringia (Figure 4.2), as land use data the Corine Land Cover Raster Data 2000 (Figure 4.3), and as soil data the Bodenübersichtskarte 1000 (Figure 4.4) are given with a resolution of 50 m. Latter is parameterized after Schulla (1997). The required coordinates of the gauge locations are taken from Bayer. HND (2005).

Considering the meteorological input the preprocessed data of Bliefernicht et al. (2008) are used for both modelling systems. For the calibration and validation phase precipitation, temperature, global radiation, air humidity, and wind data of a temporal resolution of one hour and a spatial

4 The study area: Upper Main

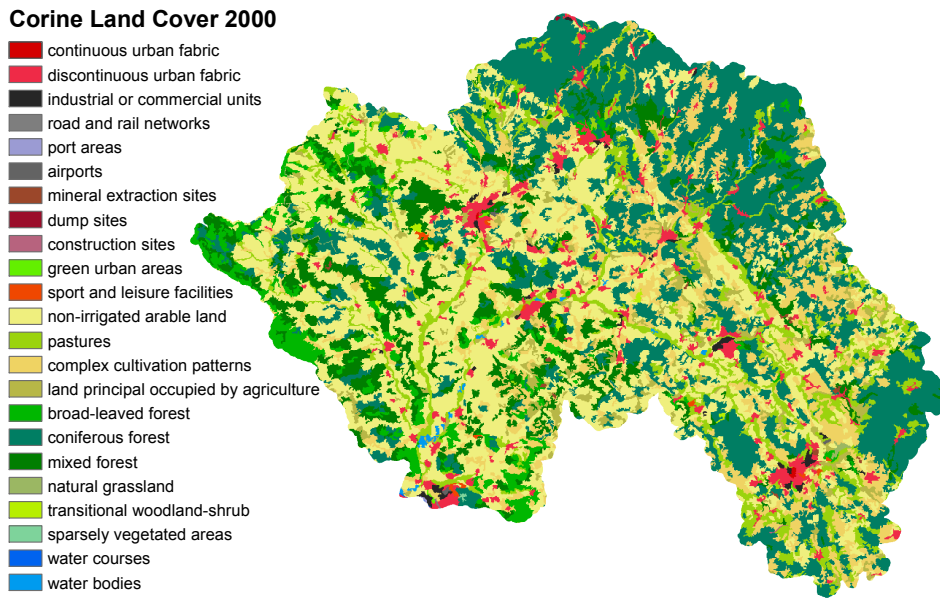


Figure 4.3: Land use within the Upper Main basin considering the Corine Land Cover Raster Data 2000 (DLR, 2000).

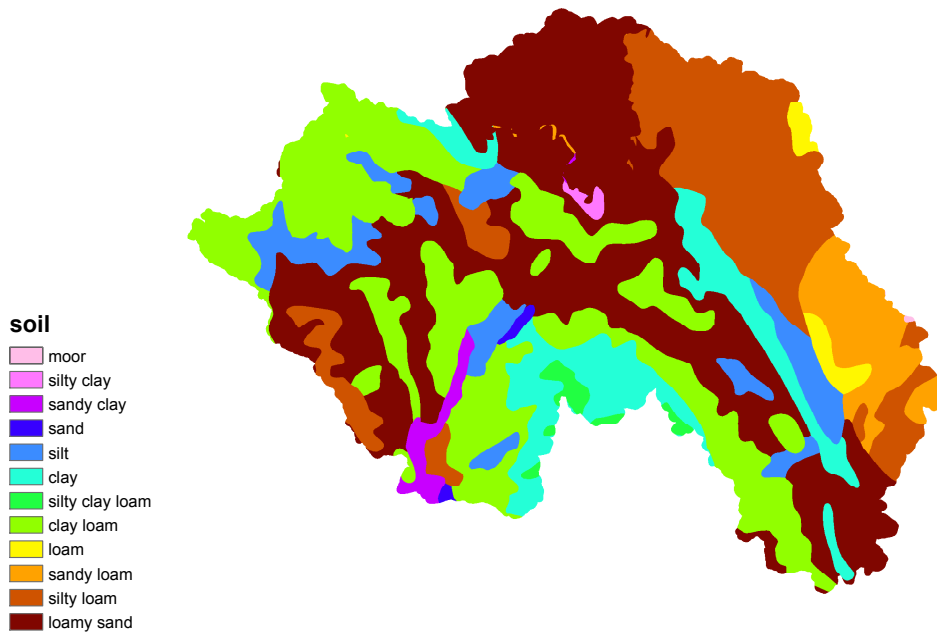


Figure 4.4: Geology within the Upper Main basin considering the soil map BÜK 1000 from 1995 (LfU, 2005).

resolution of 1000 m x 1000 m are provided. Furthermore, the same data are given as areal data on an one hour and daily time resolution for the fuzzy inference systems. In order to investigate the robustness and the uncertainties of the hydrological model WaSiM-ETH, different turning band realisations are available (1 hour, 1000 x 1000 m², 10.09.1998 - 31.12.1998). For the simulation of unobserved extreme flood events (Chapter 5.4.1) 1400 turning band realisations for seven different precipitation frequencies (10, 25, 50, 100, 250, 500, 1000 a) have been generated by Bliefernicht et al. (2008) and preprocessed as input data for the hydrological model (1 hour, and 1000 x 1000 m² spatial resolution) and for the fuzzy inference systems (1 hour and daily temporal resolution, mean areal values).

Discharge data are provided by the LfU (2005) on a daily and an one hour time resolution for 14 gauges within the Upper Main basin (compare Figure 5.1):

Kemmern ($A_E = 4244 \text{ km}^2$)	Schwüribitz ($A_E = 2419 \text{ km}^2$)
Unterlangenstadt ($A_E = 715 \text{ km}^2$)	Unterzettlitz ($A_E = 508 \text{ km}^2$)
Leucherhof ($A_E = 380 \text{ km}^2$)	Heinersdorf ($A_E = 379 \text{ km}^2$)
Coburg ($A_E = 368 \text{ km}^2$)	Bayreuth ($A_E = 332 \text{ km}^2$)
Ködnitz ($A_E = 313 \text{ km}^2$)	Horb ($A_E = 254 \text{ km}^2$)
Untersteinach ($A_E = 245 \text{ km}^2$)	Neukenroth ($A_E = 139 \text{ km}^2$)
Steinberg ($A_E = 96 \text{ km}^2$)	Wallenfels ($A_E = 96 \text{ km}^2$)

For these gauges daily discharge records are provided as of 1982. Discharge data with an one hour time resolution are available for all 14 gauges from 1989 to 2005. For the investigation of fuzzy inference systems hourly data of gauge Mainleus (1166 km²) are provided from 1991 to 2005.

5 Model development for the Upper Main basin

5.1 Hydrological Modelling

Records of (extreme) flood events are very seldom within the Upper Main basin. However, those data are essential for a successful setup of a timely and reliable warning system considering extreme flood events. Since only 30 flood events are hourly recorded between 1991 and 2004 and the highest one corresponds to a return period of around 20 years the database has to be extended. In this work, the database is extended by simulations with the hydrological model WaSiM-ETH. In this context, an optimization strategy considering the SCE algorithm is developed for the calibration of the WaSiM-ETH model Upper Main in order to keep computation times low.

The performance of the hydrological model WaSiM-ETH within the Upper Main basin including the calibration and validation phase, as well as the simulations of possible extreme flood events are presented in the following.

5.1.1 Model setup

The setup of the hydrological model WaSiM-ETH release 6.4 version 2 is presented as it is required for successful simulations of flood events in the meso-scale Upper Main basin within the framework of the HORIX project. Table 5.1 summarizes the chosen WaSiM-ETH modules.

WaSiM-ETH module	Approach
Evapotranspiration	Penman-Monteith
Snow	Temperature-Index approach
Interception	Storage approach after MORECS
Infiltration and Soil	Richards-equation
Groundwater	Conceptual
Discharge routing	Kinematic wave approach
Temporal resolution	1 h
Spatial resolution	1000 m

Table 5.1: WaSiM-ETH 6.4 model configuration applied for the Upper Main basin.

Temporal resolution. For a good reproduction of a discharge hydrograph, in particular for flood events, a high temporal resolution is adequate, but restricted by the availability of measurement

data during the calibration and validation period. Since the 1990ies both, measured precipitation and discharge data are available on a hourly time discretization. Thus, the model temporal resolution is one hour.

Spatial resolution. The spatial resolution used in this study is $1000 \times 1000 \text{ m}^2$, which results in a regular grid of 105×81 grid points for the Upper Main basin.

Subcatchments. Current discharge data are available online for 54 gauges. However, the delineation of the Upper Main catchment into 14 subcatchments is based on the partition of an existing WaSiM-ETH version 1 model (Blasy and Øverland, 2004) to enable performance comparisons (Pakosch and Disse, 2006). Figure 5.1 shows the 14 subcatchments which have been used for the calibration. The gauges Mainleus, Rodach, Weismain, and Itz (Figure 5.1, red points) are required for the recording of simulated discharges, among others for an offline coupling with the hydrodynamic model SOBEK (Disse et al., 2009). For the setup of the fuzzy inference systems simulated data of gauge Kemmern, Schwürbitz and Mainleus are considered. Due to a missing gauging station at the confluence of the rivers Upper Main and Regnitz (about 6 km downstream of gauge Kemmern), the outlet of this setup is set to the gauge Kemmern.

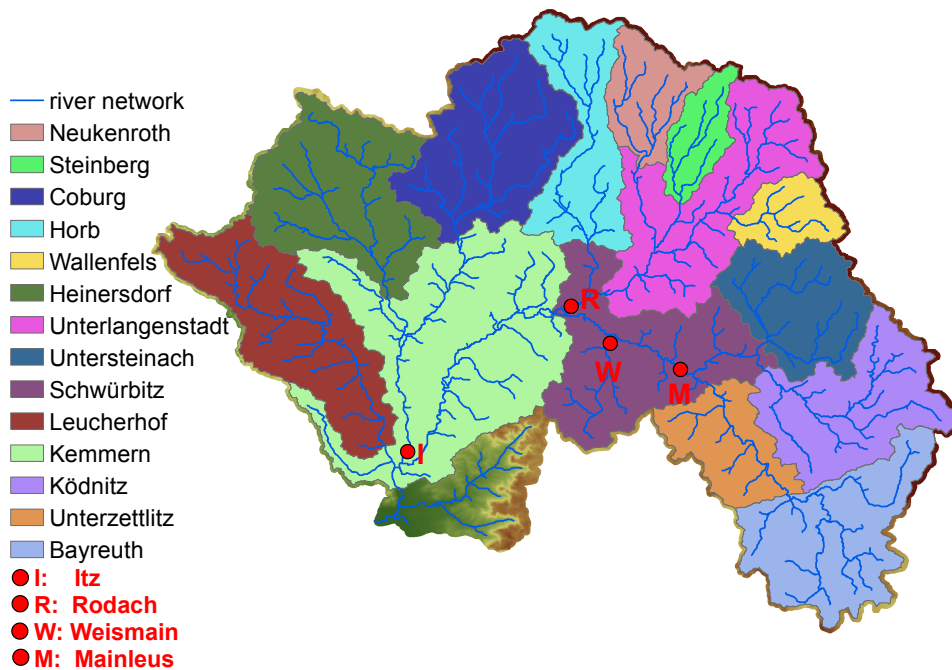


Figure 5.1: Derived subcatchments of the WaSiM-ETH model Upper Main and the location of the additional recording points Itz, Rodach, Weismain, and Mainleus (red points).

Meteorological input. Considering the meteorological input data no data interpolation and no data correction is performed since these data are preprocessed by Bliedernicht et al. (2008) within the HORIX project (Chapter 4.2). Therefore, $1000 \times 1000 \text{ m}^2$ interpolated data grids are available for the calibration and validation.

Soil parameterization. Vertically, the soil is represented by 30 equidistant layers of 0.33 m thickness each. The soil hydraulic properties are taken from Schulla and Jasper (2002). The soil column is less precisely discretized, because the soil column is saturated during (extreme) flood events and therefore has no impact on the flood hydrograph itself. Furthermore, due to the

modelling purpose WaSiM-ETH is considered as a pure rainfall-runoff instead of a hydrological model.

Hydrogeology. Due to further research objectives within the HORIX project (Disse et al., 2009) the two dimensional groundwater module is not performed for the derivation of baseflow. Instead baseflow is calculated by applying the conceptual approach after Schulla and Jasper (2002, Equation 2.4).

Discharge routing. The properties of the river network are derivated with the WaSiM-ETH preprocessing tool *Tanalis* and aligned with the existing river network of a previous study (Blasy and Øverland, 2004).

5.1.2 Calibration and validation

Before the hydrological model WaSiM-ETH can be performed for the simulation of extreme flood events in the Upper Main basin the model parameters have to be adjusted to the catchment characteristics. As mentioned in Chapter 2 this can be done either by manual calibration (trial-and-error) or as in this work by applying the SCE optimization algorithm (Chapter 2.3). The focus of the calibration lies primarily on the good representation of flood events. However, the right simulation of the entire flow spectrum should also be ensured to a certain degree. The calibration and validation of the WaSiM-ETH model is performed based on the available meteorological and discharge data (Chapter 4.2). No verification of the simulated evaporation, interception, snow storage, groundwater level or single runoff components can be carried out due to the lack of observed data.

Calibration and validation period

With respect to the investigation aim the calibration period is not set to one specific flood event, but over a two year period, from 01.11.1997 to 31.10.1999. Within the chosen calibration period both representative runoff characteristics of the Upper Main basin are included, one of the highest winter flood event and low to medium flow conditions during summer. For the validation the period from 01.11.1993 to 30.10.1997 is chosen. Furthermore, single flood events within the validation period are considered for the evaluation of the model performance as the focus of the model lies predominately on the simulation of flood events.

Main WaSiM-ETH calibration parameters

The parameterization of the evapotranspiration, snow and interception modules are taken from the existing WaSiM-ETH version 1 model (Blasy and Øverland, 2004) and are not further considered in the calibration process. Furthermore, no parameter considering the soil hydraulic functions (e.g. pedotransfer functions) is calibrated since WaSiM-ETH is interpreted as a rainfall-runoff instead of a hydrological model for the modelling purpose, simulation of extreme flood events. Table 5.2 summarizes the remaining model parameters which generally have to be calibrated specifically for each of the 14 subcatchments.

Considering the unsaturated zone, the drainage density d_r which linearly controls the strength of interflow (Equation 2.3), and the recession constant k_{rec} which accounts for the reduction of the saturated hydraulic conductivity with depth (Equation 2.2) have to be calibrated. Due to

Notation		WaSiM-ETH calibration parameters
d_r	$[\text{m}^{-1}]$	drainage density
k_{rec}	$[-]$	recession constant for saturated hydraulic conductivity with depth
Q_0	$[-]$	scaling factor for baseflow
k_B	$[\text{m}]$	recession constant for baseflow
K_D	$[\text{h}]$	recession constant for direct runoff
K_I	$[\text{h}]$	recession constant for interflow

Table 5.2: General calibration parameters with respect to the chosen WaSiM-ETH setup.

the setup without a groundwater model the scaling factor Q_0 and the recession constant k_B of the conceptual baseflow approach (Equation 2.4) are calibrated in addition. Furthermore, the calibration of the two recession constants K_D (direct flow) and K_I (interflow), which account for retention by applying a single linear storage approach (Equation 2.5), is required.

Investigation of the WaSiM-ETH parameter space

The boundaries of the parameter space considering the WaSiM-ETH model parameters (Table 5.2) have a significant influence on the optimization results. Within a first step of this work (Pakosch and Disse, 2007; Pakosch, 2006) the parameter space of the general calibration parameters considering the chosen WaSiM-ETH modules is investigated. Based on these results different SCE setups are explored in order to make the optimization of the hydrological model WaSiM-ETH more efficient (e.g. short computation times).

The behavior of the WaSiM-ETH model parameters is investigated considering the *General Sensitivity Analysis* (GSA, Madsen, 2000, 2003; Spear and Hornberger, 1980). This method is based on traditional *Monte Carlo* simulations and combined with the statistical *two sample Kolmogoroff-Smirnov* test (Plate, 1993). For each parameter set of the Monte Carlo simulations WaSiM-ETH is performed and six different objective functions (Table 2.2) are calculated based on the results. For each objective function separately the parameter sets are sorted in a way so that the parameter set in first position has the worst, the last the best value of the objective function. Afterwards two subsets are formed consisting of the 100 worst and the 100 best parameter sets. After Madsen (2000) the degree of parameter sensitivity can be determined based on the two sample Kolmogoroff-Smirnov test. Thereby, the empirical distribution functions for the two subsets are plotted as well as the maximum distance between both and the level of significance α , respectively, are calculated (Table 5.3). If the distribution of a parameter for the best subset is identical to the distribution for the worst subset, the parameter is insensitive to the model response or objective function considered. One drawback of the method is that it only considers single parameter and no interactions between the parameters under investigation can be analysed.

Level of significance	Property of the parameter
$\alpha \leq 1\%$	high sensitive
$1\% < \alpha \leq 10\%$	medium sensitive
$10\% < \alpha$	low sensitive

Table 5.3: Definition of the sensitivity classes for the General Sensitivity Analysis after Madsen (2000).

For the investigation of the parameter space and the behavior of the model parameters three sub-catchments (compare Figure 5.1) Heinersdorf (379 km²), Steinberg (96 km²), and Ködnitz (313

km²) are chosen because of their different catchment sizes and characteristics. For the Monte Carlo simulations the parameter spaces of the WaSiM-ETH parameters are identically defined for the three subcatchments (Table 5.4). Because of their definitions (Chapter 2.2) the boundaries of the parameters k_{rec} , k_B , and Q_0 are set very narrow. In contrast to this, the values of the parameters d_r , K_I , and K_D range over several magnitudes due to missing experiences in the Upper Main basin. 5000 WaSiM-ETH parameter sets are sampled within the 6-dimensional parameter space for the Monte Carlo simulations by using the *Uniform Latin Hypercube Sampling* method (Iman et al., 1981) for each subcatchment separately.

WaSiM-ETH parameter		Limits of the parameter space	
		<i>minimum</i>	<i>maximum</i>
d_r	[m ⁻¹]	0.01	100
k_{rec}	[-]	0.1	1.0
Q_0	[-]	0.05	0.15
k_B	[m]	0.5	1.5
K_D	[h]	0.01	100
K_I	[h]	0.01	100

Table 5.4: Limits of the WaSiM-ETH parameter considering Monte Carlo simulations and the subcatchments Heinersdorf (379 km²), Steinberg (96 km²) and Ködnitz (313 km²).

Figure 5.2 shows an illustration of the Monte Carlo simulations. Thereby, depending on the chosen parameter pairs the values of the objective function, in this case RMSE, are plotted over the whole parameter range. The resulting surface, which is described by the objective function in the parameter space and which is called *response surface* (Singh, 1995), gives an overview of local and global optima. The dark blue areas indicate local optima and the red diamonds represent the locations of global optima based on the 5000 Monte Carlo simulations considering the corresponding RMSE values.

Considering the parameters k_{rec} , k_B , and Q_0 (Figure 5.2, rows 2, 4, 6) satisfying RMSE values occur over the whole defined parameter range. In contrast to this, more or less clear structures of the response surfaces are distinguishable for the other three parameters d_r , K_I , and K_D (Figure 5.2, rows 1, 3, 5). Therefore, this illustration of the Monte Carlo results may indicate that the parameters k_{rec} , k_B , and Q_0 are less sensitive than the parameters d_r , K_I , and K_D considering objective function RMSE. Furthermore, if the parameter values of the global optimum are close to the boundary an extension and new limits of the parameter space should be considered.

In addition to Figure 5.2 the empirical functions of the parameters are plotted for the different subcatchments as described above for the GSA. Figure 5.3 shows exemplary the results for the parameters K_D , d_r , and k_{rec} considering the objective functions VE and RMSE for the subcatchment Heinersdorf (379 km²). The impacts of the different parameters on the discharge become apparent in the figure. For example it shows, that the parameter K_D has no influence on the discharge volume because both empirical functions are aligned (Figure 5.3a). But the RMSE evaluation shows that the parameter K_D has an important impact on the shape of the modelled hydrograph (Figure 5.3d). Therefore, both results confirm the defined characteristic of the conceptual parameter K_D to be insensitive with respect to discharge volume, but sensitive to the shape of the hydrograph. Figure 5.3b and 5.3e show that the parameter d_r influences both, the discharge volume and the shape of the hydrograph. In contrast to this, parameter k_{rec} has almost

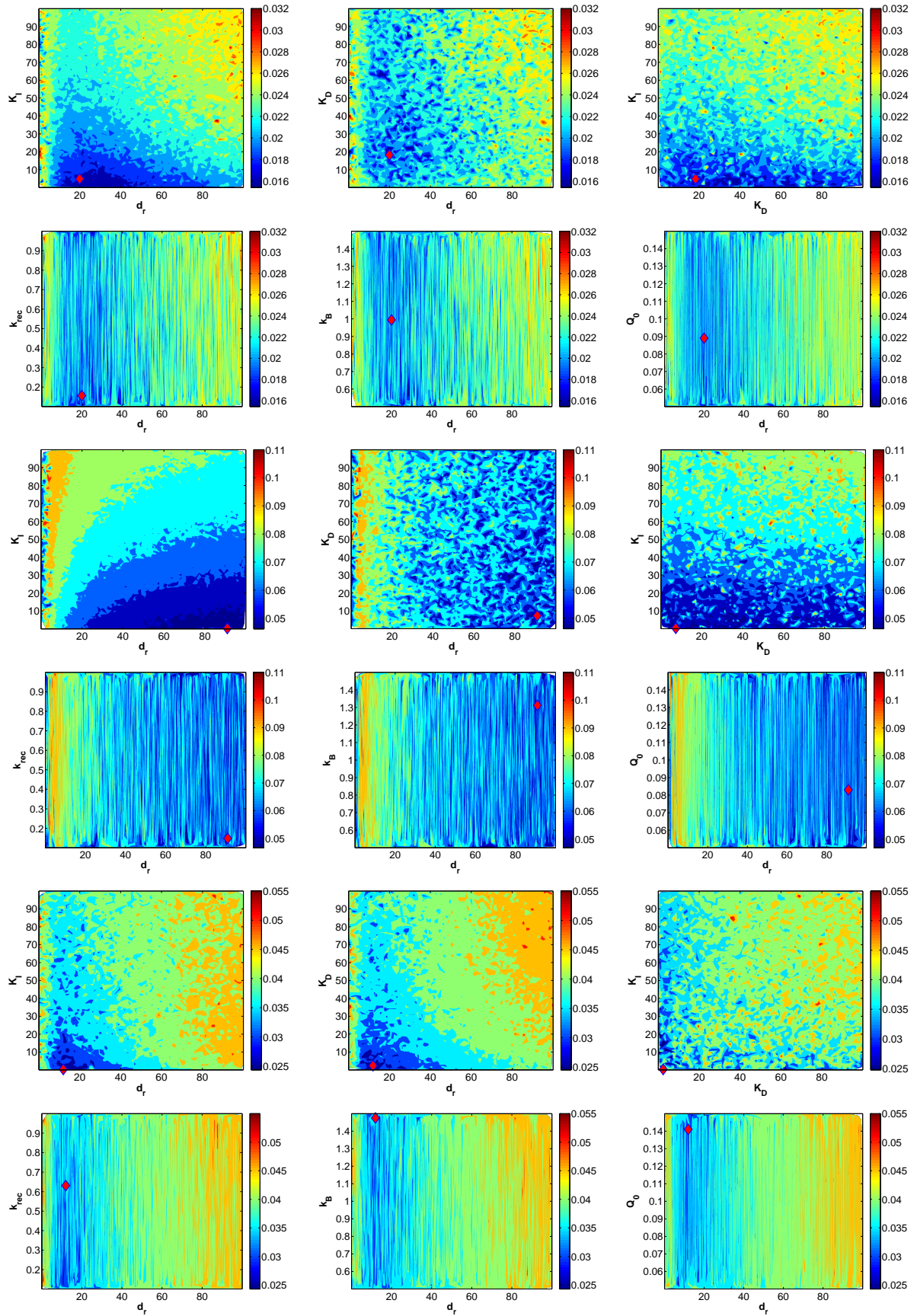


Figure 5.2: Illustration of the RMSE response surfaces based on 5000 Monte Carlo simulations for the three subcatchments Heinersdorf (379 km², top 6 plots), Steinberg (96 km², 6 plots at centre), and Ködnitz (313 km², bottom 6 plots).

5 Model development for the Upper Main basin

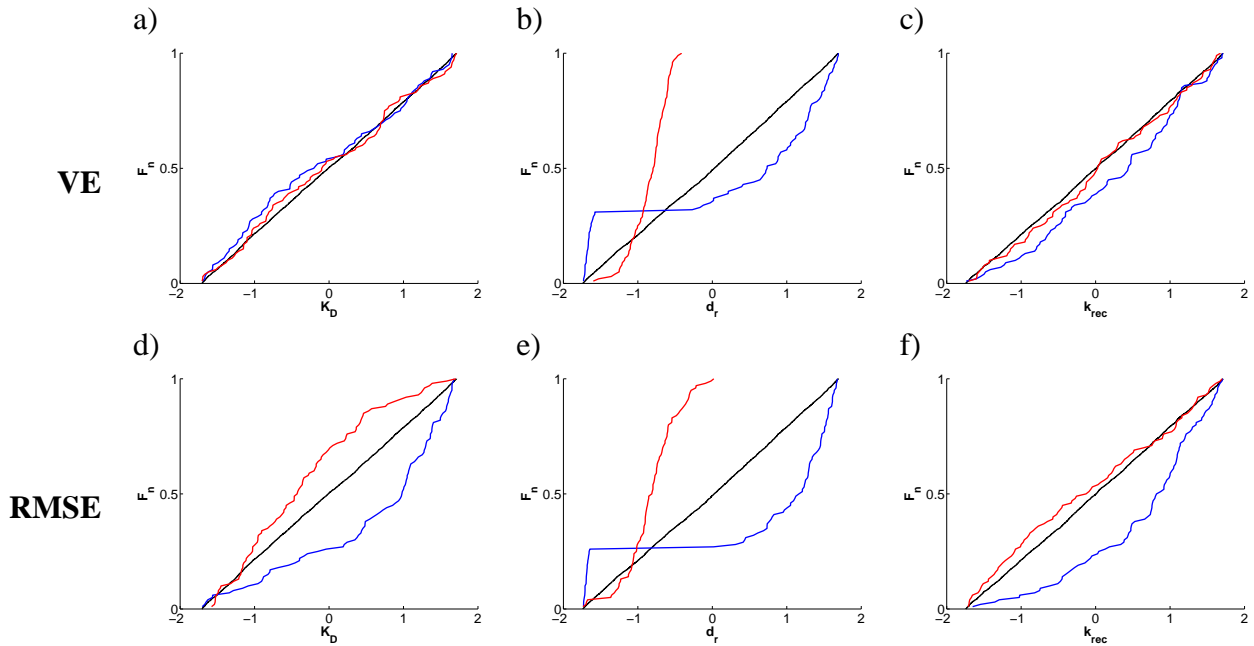


Figure 5.3: GSA results for the subcatchment Heinersdorf (379 km²) considering the WaSiM-ETH parameter K_D (left), d_r (centre), and k_{rec} (right) as well as the objective functions VE (a - c) and RMSE (d - f) (F_n : empirical distribution function; blue: 100 worst parameter sets; red: 100 best parameter sets; black: all parameter sets; parameter values are normalized).

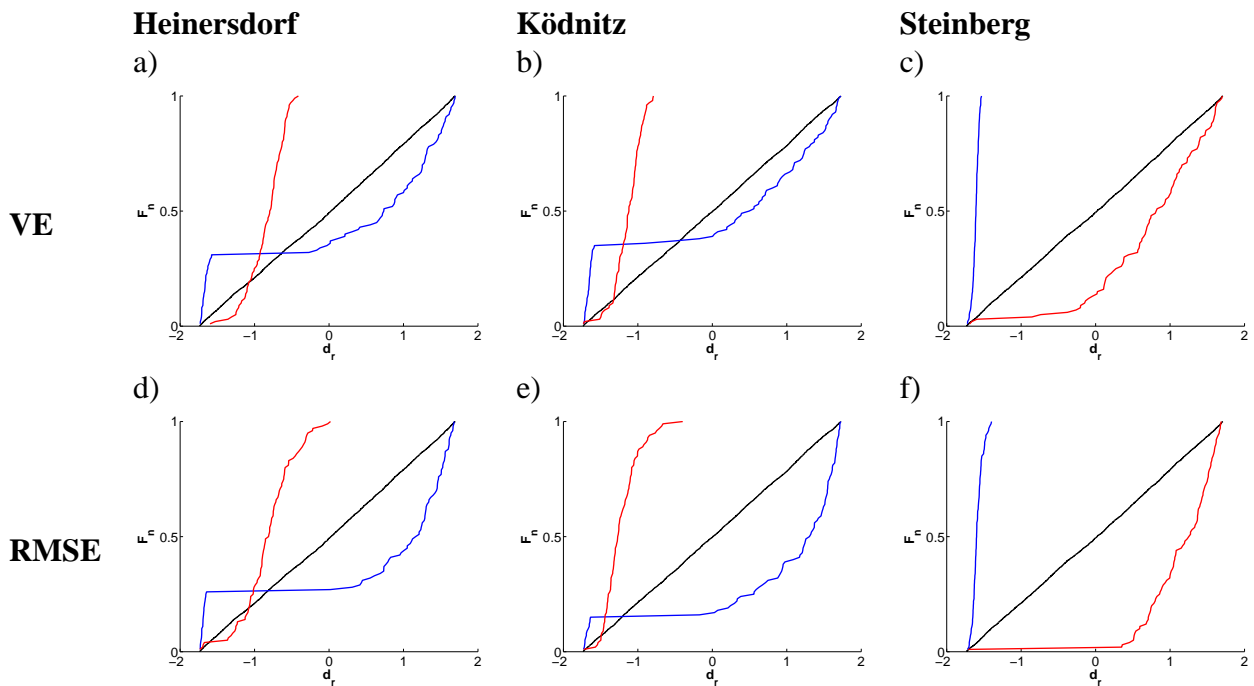


Figure 5.4: Comparison of the GSA results for the subcatchments Heinersdorf (379 km²), Ködnitz (313 km²), and Steinberg (96 km²) considering the WaSiM-ETH parameter d_r and the objective functions VE (a - c) and RMSE (d - f) (F_n : empirical distribution function; blue: 100 worst parameter sets; red: 100 best parameter sets; black: all parameter sets; parameter values are normalized).

no impact on the volume and shape of the hydrograph, and therefore is a low sensitive parameter (Figure 5.3c, f). These RMSE results confirm the interpretations of Figure 5.2.

Figure 5.4 shows the dependency of the parameter space on the catchment characteristics exemplary for parameter d_r . Considering the subcatchment Heinersdorf (379 km²) which is characterized by wide floodplains it can be expected that the adjusted value of parameter d_r is located in the lower half of the investigated parameter space (Figure 5.4a, d). The same result holds for the subcatchment Ködnitz (313 km², Figure 5.4b, e) which has around the same catchment size and is mainly characterized by wide floodplains, but also some higher reaches. In contrast to this, the subcatchment Steinberg (96 km²) is considerably smaller than the other two and characterized by higher mountain reaches of the Franconian Forest. For this subcatchment it can be expected that the adjusted parameter value of d_r is located in the upper half of the investigated parameter space (Figure 5.4c, f). Furthermore, it seems that the parameter space for d_r has to be extended to even higher values for the SCE optimization because the empirical function representing the 100 best parameters does not flatten at the upper end. Later, this assumption is affirmed by the results of the SCE optimization (see Table 5.9).

WaSiM-ETH parameter		Parameter sensitivity					
		Heinersdorf		Ködnitz		Steinberg	
		VE	RMSE	VE	RMSE	VE	RMSE
d_r	[m ⁻¹]	H	H	H	H	H	H
k_{rec}	[-]	M	H	L	H	H	H
Q_0	[-]	H	M	L	L	H	L
k_B	[m]	H	H	H	H	H	L
K_D	[h]	L	H	L	H	L	H
K_I	[h]	L	H	L	H	L	H

Table 5.5: GSA results after Madsen (2000) for the subcatchments Heinersdorf (379 km²), Steinberg (96 km²) and Ködnitz (313 km²) considering the evaluated levels of significance (Table 5.3) and the objective functions VE and RMSE (H: high sensitive; M: medium sensitive; L: low sensitive).

Table 5.5 summarizes the GSA results after Madsen (2000) considering the evaluated levels of significance (Table 5.3) and the two objective functions VE and RMSE for each model parameter of the three subcatchments. Depending on the objective function the sensitivity of the model parameter can range over all three sensitivity classes and over the whole defined parameter space. Furthermore, the GSA results contradict the visual interpretation of the corresponding response surface in some cases (e.g. k_{rec}). In particular for the three model parameters k_{rec} , k_B , Q_0 a higher dimensional sensitivity analysis should be carried out, but also for the other three, as the dimension of the investigated parameter space is extremely reduced with the applied projections. Since no clear statements about the parameter sensitivities of all parameters can be derived from the GSA results it is not advisable to reduce the parameter space considering the SCE optimization.

Investigation of the SCE boundary conditions

Beside the definition of the parameter space for the WaSiM-ETH parameters the definition of the six SCE parameters has an important influence on the optimization procedure (Chapter 2.3). Table 5.6 summarizes the parameters of the SCE algorithm which have to be set in advance.

As mentioned in Chapter 2.3 an appropriate objective function (Table 2.2) for the optimization

Notation	Parameters of the SCE algorithm
<i>MAXN</i>	maximal number of evolution steps
<i>KSTOP</i>	maximal number of shuffling loops
<i>PCENTO</i>	convergence criterion
<i>NGS</i>	number of complexes
<i>NPS</i>	number of parameter vectors within one subcomplex
<i>NSPL</i>	number of evolution steps before shuffling

Table 5.6: Parameters which set the boundary conditions of the SCE optimization algorithm.

has to be additionally chosen depending on the investigation aim (simulation of the whole discharge spectrum or only single flood / drought periods, etc.). Due to the number of SCE boundary parameters and the available objective functions a variety of possible setups for the SCE optimization are investigated in order to find one SCE setup with which a reliable and efficient, in terms of computation times, optimization of the hydrological model WaSiM-ETH can be performed. In the following the results of three SCE setups (default, recommended, Upper Main, Table 5.7) are presented and discussed in more detail. Thereby, the default SCE setup uses the fixed boundary conditions which are deposited within the source code. However, in the publications of Duan et al. (1992, 1993, 1994) advices for the definition of the boundary conditions depending on the number of model parameters are given and considered within the recommended SCE setup. After the investigation of a variety of different SCE setups, the Upper Main setup is found as the one which fulfills all requirements of the calibration (short computation times, etc.) in the best manner.

SCE boundary conditions	Investigated cases		
	<i>default</i>	<i>recommended</i>	<i>Upper Main</i>
<i>MAXN</i>	15000	15000	15000
<i>KSTOP</i>	5	5	5
<i>PCENTO</i>	0.001	0.001	0.001
<i>NGS</i>	3	4	3
<i>NPS</i>	5	5	3
<i>NSPL</i>	9	8	4
<i>Objective Function</i>	SSE	RMSE	RMSE

Table 5.7: Boundary conditions of three investigated SCE optimization setups.

As the investigation of the parameter space the investigation of the SCE boundaries is performed within the three subcatchments Heinersdorf (379 km²), Steinberg (96 km²), and Ködnitz (313 km²) within a first step (Pakosch and Disse, 2007; Pakosch, 2006). Since WaSiM-ETH requires a long initial phase of about two years initial model grids for soil moisture, etc. are generated in advance to keep computation times further low. However, a time lag of further two months is chosen before the objective function is calculated to reduce transient oscillation effects at the beginning of the simulation.

The defined parameter spaces are given in Table 5.8. Except for the subcatchment Steinberg the parameter boundaries for the investigation of the different SCE setups are identical to those of the Monte Carlo simulations. Based on the interpretation of the Monte Carlo simulations and the GSA results the upper boundary for parameter d_r is extended for the subcatchment Steinberg. Table 5.9

WaSiM-ETH parameter	Limits of the parameter space					
	SCE optimization				Monte Carlo	
	Heinersdorf & Ködnitz		Steinberg		minimum	maximum
minimum	maximum	minimum	maximum			
d_r [m ⁻¹]	0.01	100	0.01	200	0.01	100
k_{rec} [-]	0.1	1.0	0.1	1.0	0.1	1.0
Q_0 [-]	0.05	0.15	0.05	0.15	0.05	0.15
k_B [m]	0.5	1.5	0.5	1.5	0.5	1.5
K_D [h]	0.01	100	0.01	100	0.01	100
K_I [h]	0.01	100	0.01	100	0.01	100

Table 5.8: Limits of the WaSiM-ETH parameter considering the SCE optimization and Monte Carlo simulations as well as the subcatchments Heinersdorf, Steinberg, and Ködnitz.

Subcatchment	WaSiM-ETH parameter	SCE setup			Monte Carlo ¹⁾
		default	recommended	Upper Main	
Heinersdorf	d_r [m ⁻¹]	19.939	20.043	21.603	19.960
	k_{rec} [-]	0.800	0.843	0.786	0.156
	Q_0 [-]	0.020	0.019	0.034	0.089
	k_B [m]	0.988	0.993	1.073	0.994
	K_D [h]	0.161	0.147	1.093	18.289
	K_I [h]	0.089	0.098	0.080	4.878
	<i>RMSE</i>	0.0132	0.0132	0.0133	0.0154
	<i>NS</i>	0.8254	0.8253	0.8116	0.7865
	<i>runs</i> ²⁾	713	783	114	5000
Steinberg	d_r [m ⁻¹]	165.827	165.200	165.180	90.937
	k_{rec} [-]	0.901	0.789	0.802	0.148
	Q_0 [-]	0.127	0.148	0.028	0.083
	k_B [m]	1.036	1.203	0.991	1.312
	K_D [h]	9.681	12.079	13.353	7.267
	K_I [h]	0.026	0.129	0.082	0.299
	<i>RMSE</i>	0.0508	0.0508	0.0508	0.0562
	<i>NS</i>	0.8694	0.8694	0.8693	0.8435
	<i>runs</i> ²⁾	455	598	184	5000
Ködnitz	d_r [m ⁻¹]	8.799	8.874	8.776	11.955
	k_{rec} [-]	0.776	0.804	0.769	0.631
	Q_0 [-]	0.076	0.073	0.068	0.141
	k_B [m]	1.146	0.906	1.008	1.475
	K_D [h]	0.126	0.142	0.260	2.385
	K_I [h]	0.054	0.104	0.018	0.299
	<i>RMSE</i>	0.0227	0.0227	0.0228	0.0243
	<i>NS</i>	0.8682	0.8681	0.8675	0.8256
	<i>runs</i> ²⁾	719	981	230	5000

Table 5.9: Optimization results for the subcatchments Heinersdorf (379 km²), Steinberg (96 km²), and Ködnitz (313 km²) considering three different SCE setups (¹⁾ Results of the Monte Carlo simulation representing the lowest RMSE value; ²⁾ number of WaSiM-ETH simulations).

5 Model development for the Upper Main basin

summarizes the results for the three optimization runs for each subcatchment and compares it with the results of the Monte Carlo simulations.

Although the objective function values of the SCE and Monte Carlo simulations are of comparable quality, significant differences with respect to single parameter values occur. This can be traced back to the fact that it is not possible to identify an unique parameter set for the model due to the nonlinearity of hydrological processes which are reproduced. This means that several sets of model parameter vectors can be found which have similarly good model performances, which leads to the so-called equifinality problem (Beven and Freer, 2001).

Comparing the results of the three different SCE setups it becomes apparent that the adjusted WaSiM-ETH parameter sets are grouped around the same values, all having satisfying and comparable Nash-Sutcliffe values. The only difference lies in the number of required simulations which is minimized in the case of the Upper Main setup. Furthermore, Figure 5.5 exemplarily shows that almost no differences between the three SCE optimized hydrographs are visually distinguishable as they are all aligned. However, some drawbacks with respect to the simulation of low and medium discharge conditions occur, which are acceptable considering the WaSiM-ETH setup of the soil column and the calibration aim. Due to these results the Upper Main setup is selected for the calibration of all subcatchments in the Upper Main basin with the SCE algorithm.

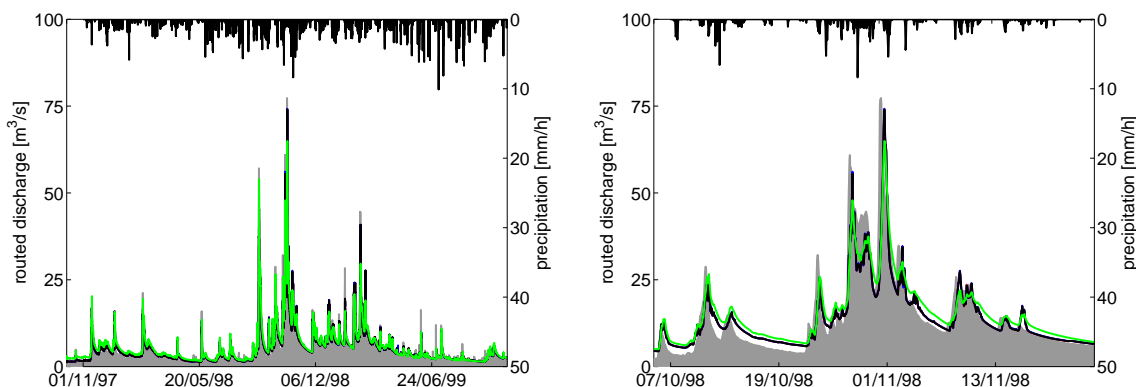


Figure 5.5: Comparison of the results of the different SCE setups (default: red, recommended: blue, Upper Main: black) with the best RMSE Monte Carlo simulation (green) considering subcatchment Ködnitz (313 km²; grey: observed discharge).

Performance of the SCE calibration for the Upper Main model.

As already mentioned the focus of the calibration lies primarily on the good representation of flood events. However, the correct simulation of the entire flow spectrum should be ensured to a certain degree. Therefore, an optimization strategy is developed with which the calibration of the WaSiM-ETH parameters is carried out in an iterative way (Duan, 2010): Since WaSiM-ETH requires a long initial phase of about 2 years in case of the Upper Main basin model grids considering soil moisture, etc. are generated in advance to keep simulation times additionally low. However, a time lag of a further two months is chosen before the objective function is calculated to reduce transient oscillation effects. The optimization is then performed considering the initial model grids. The resulting parameters are compared with the initial one. If the parameter values used for the model initialisation differ significantly, new initial model grids are generated considering the results of the SCE optimization. Afterwards a new optimization process is started considering the new initial model grids. These steps are repeated until no significant differences

between the parameter values occur. For all subcatchments the parameter space is defined as for the subcatchment Steinberg (Table 5.8).

Figure 5.6 shows the hourly time series of the calibration results for the two main stations along the Upper Main river, Schwürbitz (2419 km²) and Kemmern (4244 km²). The overall performance is satisfying, and the discharge hydrographs are simulated in a reasonable way. Nash-Sutcliffe efficiencies and RMSE values of the SCE optimizations for all considered gauges within the Upper Main basin are given in Table 5.10.

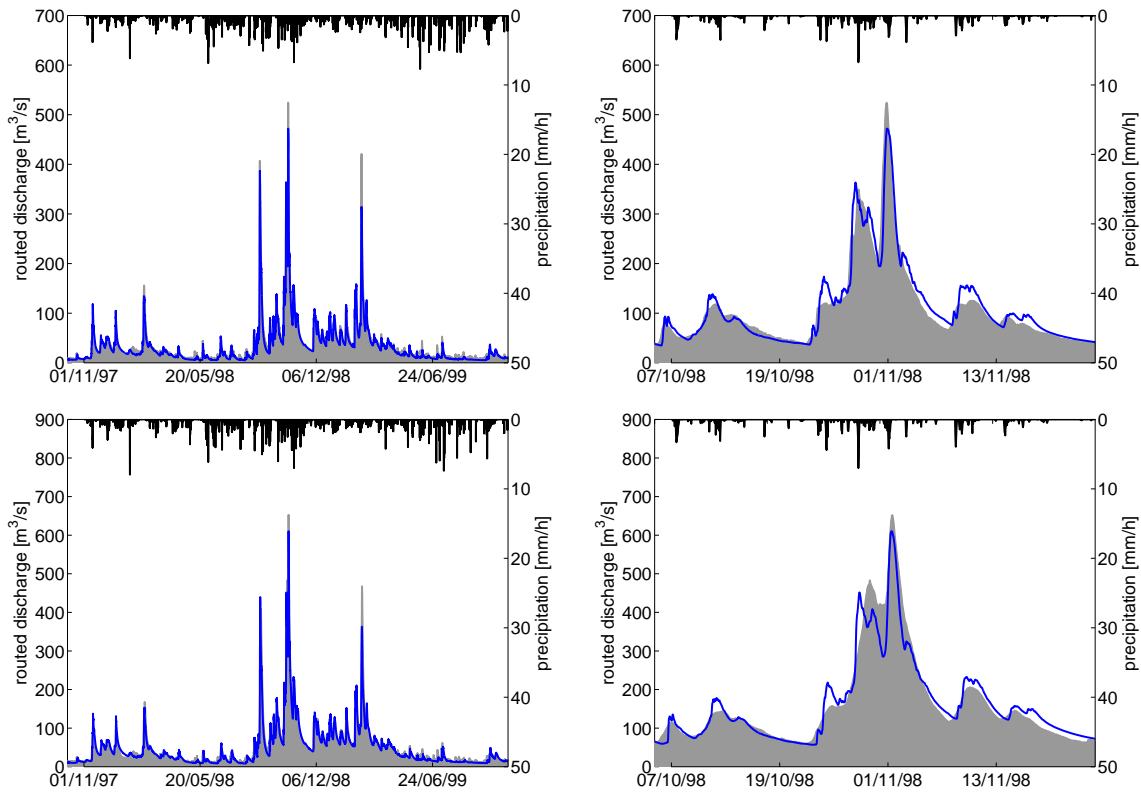


Figure 5.6: Calibration results of the main stations Schwürbitz (2419 km², top) and Kemmern (4244 km², bottom) using SCE setup Upper Main (left: 01.11.1997 - 31.10.1999; right: 07.10.1998 - 24.11.1998; gray: observed; blue: simulated).

Figure 5.7 shows the hourly time series of the validation results for the two main stations Schwürbitz (2419 km²) and Kemmern (4244 km²). The performance of the validation is comparable to the one of the calibration period (Table 5.10). For the head and smaller basins model performances vary in both directions between calibration and validation period. For the complete basin model efficiencies are in the same range. But considering the lin NS values of the three smallest subcatchments Neukenroth (139 km²), Steinberg and Wallenfels (both 96 km²) for the shown flood event a significant performance degradation is recognizable. However, they have no great impact on the simulation of flood hydrographs at the gauges Schwürbitz (2419 km²) and Kemmern (4244 km²). This is also the case for other flood events within the validation period: e.g. flood event 04.02.1997 - 09.03.1997: lin NS(Neukenroth) = 0.61, lin NS(Steinberg) = 0.55, lin NS(Wallenfels) = 0.66. Since for the other gauges the model efficiencies are within the same range for the whole validation period and for single flood events it is assumed that the setups of the WaSiM-ETH model and the SCE optimization are chosen in an acceptable way for these gauges. Considering the three smallest subcatchments it is assumed that the setup of the WaSiM-

5 Model development for the Upper Main basin

Gauge	A_E [km ²]	Calibration		Validation <i>lin NS</i>	
		RMSE	<i>lin NS</i>	whole period	flood event 19.02.94 - 20.04.94
Kemmern	4244	0.0134	0.90	0.88	0.78
Leucherhof	380	0.0115	0.83	0.74	0.77
Heinersdorf	379	0.0113	0.82	0.73	0.85
Coburg	368	0.0262	0.86	0.85	0.83
Schwürbitz	2419	0.0149	0.95	0.90	0.91
Horb	254	0.0381	0.89	0.83	0.86
Unterlangenstadt	715	0.0348	0.87	0.86	0.85
Neukenroth	139	0.0506	0.86	0.80	0.64
Steinberg	96	0.0508	0.87	0.80	0.65
Wallenfels	96	0.0450	0.84	0.79	0.68
Untersteinbach	245	0.0360	0.84	0.82	0.85
Ködnitz	313	0.0230	0.87	0.80	0.79
Unterzettlitz	508	0.0163	0.89	0.85	0.85
Bayreuth	332	0.0198	0.87	0.80	0.74

Table 5.10: Performance values of the SCE calibration (RMSE, *lin NS*) and of the validation (*lin NS*) for all gauges within the Upper Main model (for the validation phase the *lin NS* values for the whole time period and an example of a flood event are given).

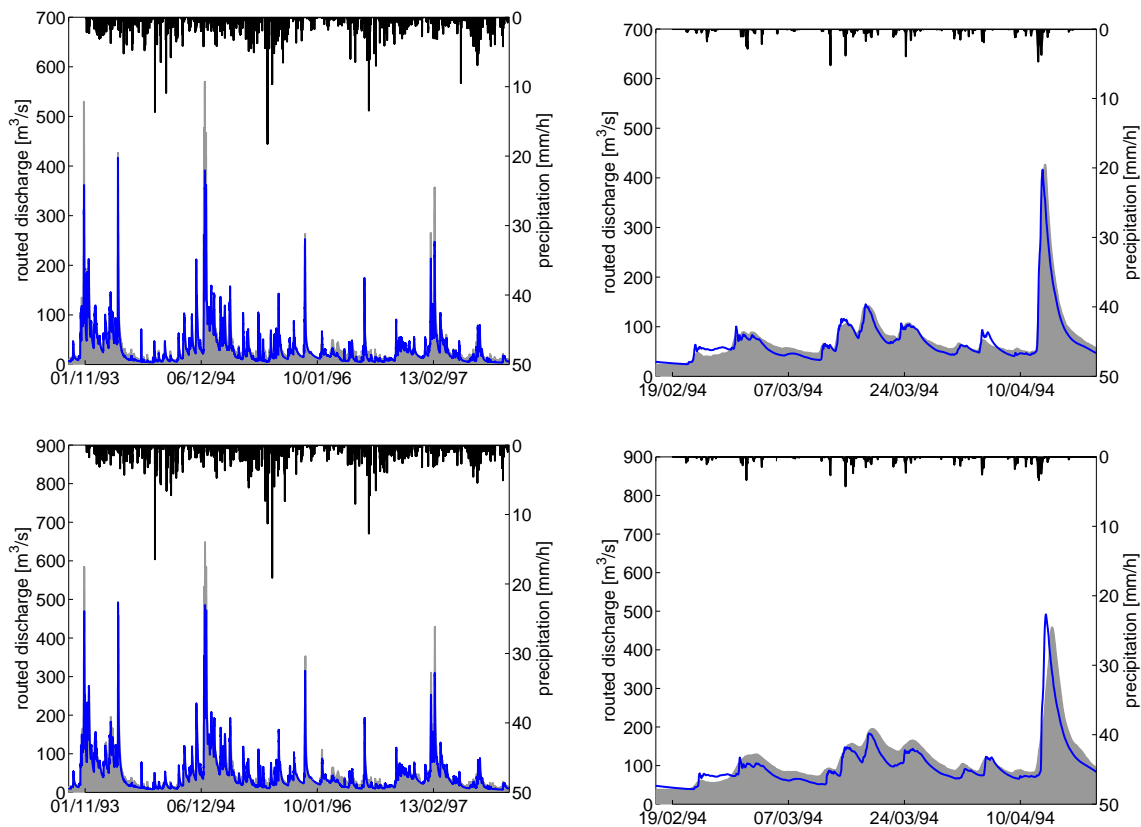


Figure 5.7: Validation results of the main stations Schwürbitz (2419 km², top) and Kemmern (4244 km², bottom) using SCE setup Upper Main (left: 01.11.1993 - 31.10.1997; right: 19.02.1994 - 20.04.1994; gray: observed; blue: simulated).

ETH model has to be improved since the performance of the SCE setup Upper Main is satisfying and reasonable for the other subcatchments. In this context the uncertainty of the precipitation input should be checked for these subcatchments due to their locations within the low mountain region (compare Figure 5.1, 4.2). Because of missing observation stations the estimation of the precipitation is difficult for these regions.

5.1.3 Simulations of extreme flood scenarios

For the setup of fuzzy rule based forecast systems considering extreme flood events (Chapter 5.4.1) a database is generated by simulations with the calibrated WaSiM-ETH model Upper Main. The performance and the results of these simulations are presented in the following.

In a first step extreme precipitation events are generated by Bliefernicht et al. (2008) as input for the rainfall-runoff model WaSiM-ETH. In order to keep the variability of precipitation, a stochastic simulation is performed in four steps. (1) The areal precipitation of an extreme event is estimated by an extreme value distribution based on block maxima (e.g. annual) of areal precipitation of the whole considered catchment. (2) Hourly precipitation fields in a spatial resolution of 1 km x 1 km are simulated by a three-dimensional turning band method (Mantoglou and Wilson, 1987). A more detailed description of this step is also given in Bliefernicht et al. (2008). (3) The amount of areal precipitation is disaggregated according to the spatial and temporal distribution of the simulated hourly precipitation fields. (4) Finally, step two and three are repeated to derive an ensemble of different realisations. The strong interannual variability of the precipitation process is accounted by splitting the data into two classes (summer and winter term). For both classes only the hourly observations of extreme events are used to estimate the statistical properties needed for the simulation. Based on this methodology 100 realisations of extreme summer and winter events are generated for seven return periods (10, 25, 50, 100, 250, 500 and 1000 a). The event duration is 48 hours for a summer event and 72 hours for a winter event. It is assumed, that the temporal distribution of an extreme event is not known. That is also the reason why ensembles of precipitation should be taken into account for real flood forecasts. Possible realisations of the hourly areal precipitation of an 1000-year extreme event within the Upper Main basin in summer and in winter are shown in Figure 5.8. It has to be emphasised that the return period and the resulting amount of areal precipitation always refer to the whole Upper Main basin. Thus, considering the precipitation amount within single subcatchments large differences can occur.

Within the second step the rainfall-runoff model is performed using the generated extreme precipitation events as input. In order to ensure the modelling of the whole flood hydrograph, that means the increasing and decreasing branch, the simulations of the summer extreme events are performed over a seven, the winter events over an eight day time period. Furthermore, two different sets of initial model grids considering dry and wet conditions are generated for both seasons separately. Since most of the high flood events are influenced by snowmelt a third initial condition ensuring a certain snow amount within the Upper Main basin is generated for the winter season. Examples of simulated hydrographs for different realisations of the 250-year extreme precipitation event considering wet preconditions in summer and winter at gauge Mainleus (1166 km²) are shown in Figure 5.9. Furthermore, the simulated minimum, maximum, and mean peak with corresponding standard deviation (σ) for each considered return period of precipitation in summer and winter under wet precondition are exemplarily given in Figure 5.10 for gauge Mainleus

5 Model development for the Upper Main basin

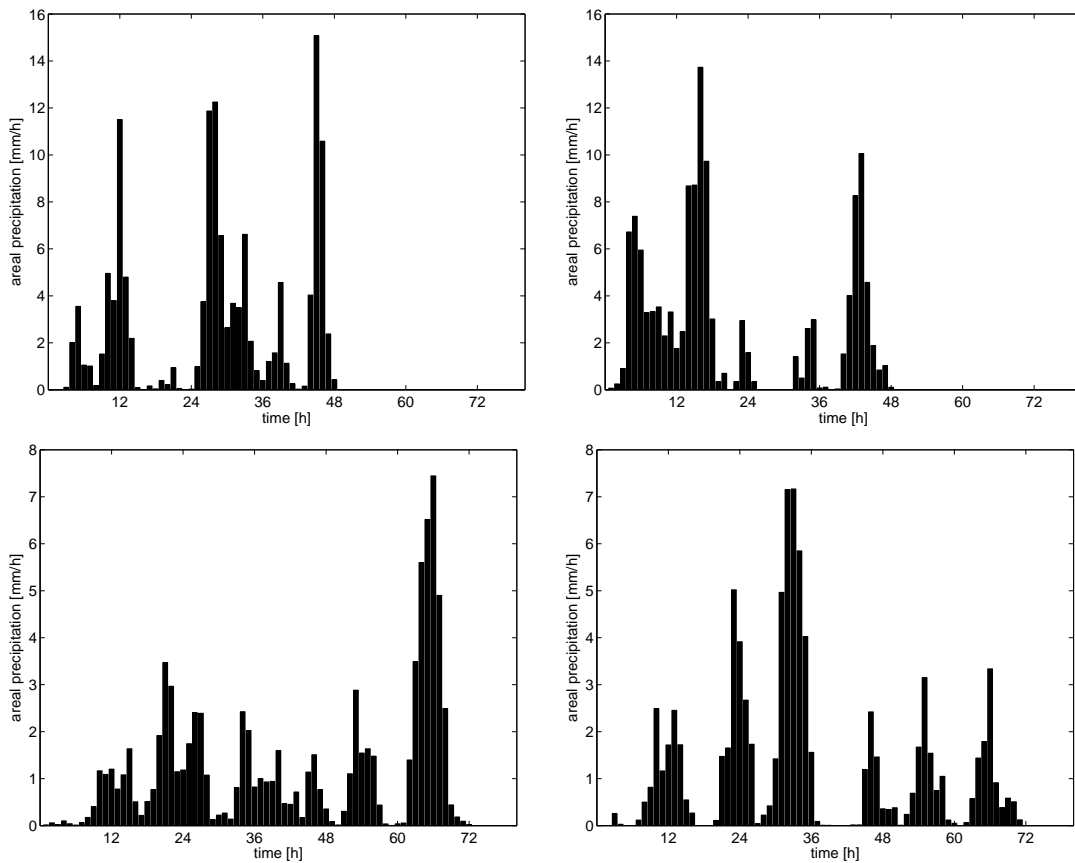


Figure 5.8: Possible realisations of the hourly areal precipitation of an 1000-year extreme event within the Upper Main basin in summer (top) and in winter (bottom).

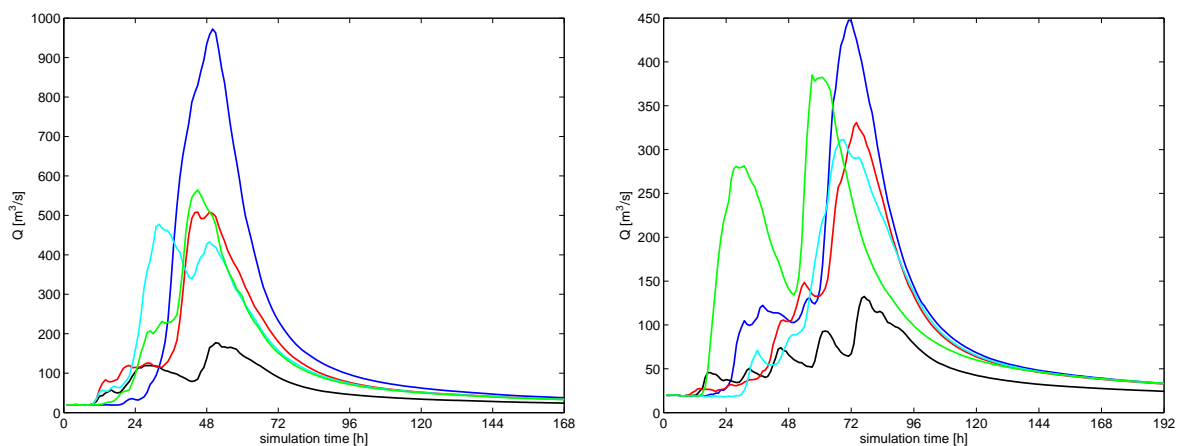


Figure 5.9: Examples of simulated hydrographs for five different realisations of the 250-year extreme precipitation event considering wet preconditions in summer (left) and winter (right) at gauge Mainleus (1166 km^2).

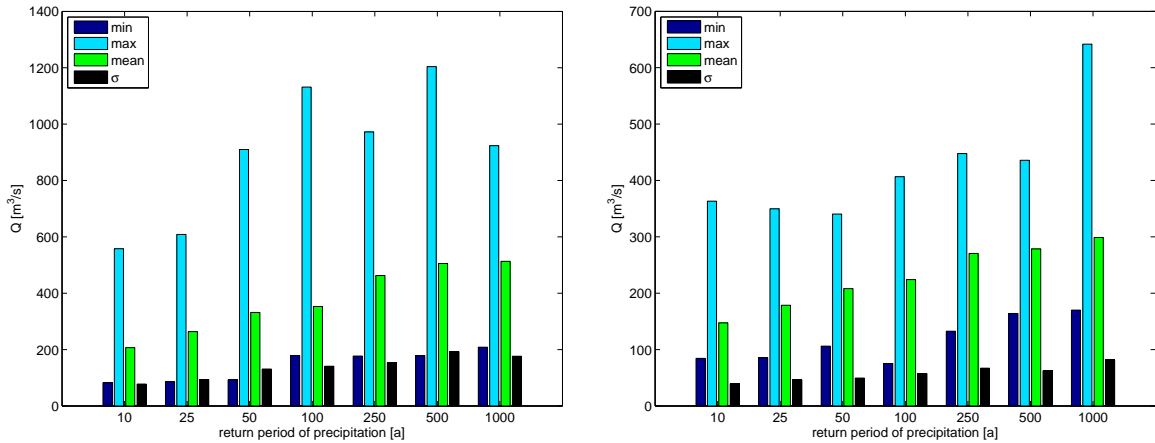


Figure 5.10: Simulated minimum, maximum, and mean peak with corresponding standard deviation (σ) for each considered return period of precipitation in summer (left) and winter (right) under wet precondition at gauge Mainleus (1166 km²).

(see Appendix B for all preconditions at the gauges Kemmern, Schwürbitz, and Mainleus).

The comparison of Figure 5.10, B.1 to B.3 with the discharge values of different flood frequencies (Table 4.4) shows that (realistic) extreme flood events ($HQ_{>100}$) can be simulated with the applied rainfall-runoff model. Considering the three main gauges Mainleus, Schwürbitz, and Kemmern the variability of the peak heights within one and between the different precipitation return periods are caused by the temporal and spatial distribution of the generated extreme precipitation events as well as the interactions of the different tributaries. Furthermore, the total precipitation volume of different realisations of one return period can vary within different subcatchments meanwhile the total volume of the overall areal precipitation stays constant within the Upper Main basin. This results in different flood hydrographs considering the shape and the volume within single subcatchments. However, this influence becomes less significant with the increase of the subcatchment size. Figure 5.11 exemplarily shows spatial distributions of the total precipitation volume of the 250-year extreme precipitation summer event within the Upper Main basin.

Considering the maximum values of the extreme peaks and the different precipitation return pe-

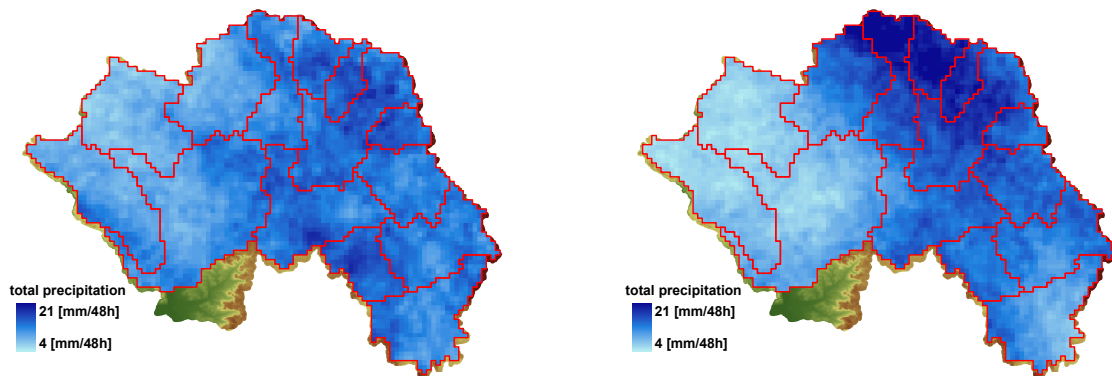


Figure 5.11: Spatial distributions of the total precipitation volume of the 250-year extreme precipitation summer event within the Upper Main basin considering the WaSiM-ETH model boundaries.

5 Model development for the Upper Main basin

riods the maximum ones occur mainly during summertime as a single peak event caused by an extreme convective precipitation event. Furthermore, the mean values of the simulated peaks resulting from precipitation events of lower return periods show that in average higher peaks occur during multiple peak events in combination with snowmelt in wintertime. This confirms the observed flood events of the last decades. Furthermore, the simulated peak heights are consistent with those of the classical statistics (Table 4.4). Based on these results it can be assumed that (realistic) extreme flood events are simulated with the rainfall-runoff model WaSiM-ETH. Therefore, these simulations can be used for the training of a fuzzy forecast system (Chapter 5.4.1).

5.2 Fuzzy Modelling

Fuzzy inference systems own many degrees of freedom which have to be adjusted for modelling purposes (Chapter 3). Having fixed the type of fuzzy inference system, that means the general structure and calculation rules (Mamdani or Takagi-Sugeno), a decision on the form, the number, the support and the peak of the membership functions for each argument and, in the case of the Mamdani inference system (MS), each response is required. Furthermore, the number of rules and the IF-THEN rules themselves have to be defined. For the Takagi-Sugeno inference system (TS) the definition of the linear response equations is necessary, that means, a decision on the arguments used for the response equation is required which increases the degree of freedom further.

Due to the many degrees of freedom a fuzzification and optimization strategy has to be developed to ensure the comparability of different investigation results. Thereby, the parameter values of the SA optimization process for MS and TS inference systems (SA-MS, SA-TS) are based on the findings of Reyhani-Masouleh (2008) and remain unaffected throughout the whole time. In the following the different investigations considering the setup of fuzzy inference systems for four different forecast time horizons are presented and their application for the three Upper Main gauges Mainleus (1166 km²), Schwürbitz (2419 km²), and Kemmern (4244 km²) are discussed.

Objectives of different forecast time horizons.

Within the framework of the HORIX project (Chapter 1) a flood forecast system is developed which ensures a satisfying and reliable short and medium term forecast of both, low and medium discharge conditions as well as of extreme flood events. Therefore, the idea is developed to perform the forecast for four different time horizons (6, 12, and 48 hours, 3 days) to ensure a continuous forecast. That means that for each time horizon one fuzzy inference system has to be trained and validated since only one response can be modeled per system. The focus of the 3 day forecast (based on daily data) lies on the appropriate representation of the low and medium discharge conditions as well as on the reliable forecast of trespasses considering a predefined warning level. A trespass of the warning level results in the switching to the three systems with hourly time resolution. Therefore, the representation of flood peaks is less important for the 3 day systems, but essential for the hourly ones. In literature, several studies using fuzzy inference systems for discharge forecast on a daily basis and for the 6 and 12 hour time horizons can be found (Chapter 3). However, since the memory of the catchment Upper Main has no great impact on the 48 hour forecast and no references can be found in literature for this time horizon, the setup of fuzzy inference systems considering the 48 h forecast is a great challenge. That is one reason why it is investigated in more detail than the other three within the framework of this thesis.

5.2.1 Input variables

In general, the severity of flood events is dependent on extreme combinations of different environmental factors. For example, extreme convective precipitation can cause floods during summer-time, whereas the combination of snowmelt and additionally long-lasting precipitation are often the main causes for winter flood events. Therefore, an investigation of different environmental factors, which are responsible for flood events, has to be carried out in order to find significant

arguments for the setup of fuzzy inference systems considering the corresponding study area. This has been done in a first step by Bengelstorf (2009), who characterized the Upper Main basin and investigated some different environmental factors on daily data. The result of this recommendations of different environmental factors of interest are further investigated as arguments for the Upper Main basin during the training phase of the fuzzy inference systems. Considering the hourly forecast systems, the selection of the arguments are based on the results of the daily fuzzy forecast systems and on findings in literature (e.g. See and Openshaw, 1999; Xiong et al., 2001; Alvisi et al., 2006; Casper et al., 2007). They are only investigated during the training phase of the fuzzy inference systems.

In general, the selection of the different environmental factors are based on the following three ideas and additionally on the results of the literature research:

1. The environmental factors should be available (online) at all times. Due to the fact, that most of the time during high flood events recording points at gauges are out of order and / or report wrong measurements the environmental factor discharge should not be used as argument, if possible, but has to be investigated as it is used as response (target variable).
2. The environmental factors should be representative for the catchment area of the considered gauge. Thus, the arguments should be able to describe the past and present catchment conditions.
3. The environmental factors should be independent of hydrological and hydrodynamic models. The calculation of environmental factors which are based on other environmental factors (e.g. snow storage) does not rely on the application of a complex model.

Based on the above mentioned requirements for the fuzzy input and considering the response, *direct forecast of discharge* ($Q(t+X)$) and *forecast of discharge changes* ($\Delta Q(t,t+X)$), with $X = 3$ days; 6, 12, 48 hours) the following environmental factors are investigated to find suitable arguments for flood forecasts:

Discharge.

In general, discharge $Q(t)$ is one essential environmental factor as it represents the overall present conditions within the catchment the best (e.g. droughts through low flow). However, most of the time during flood events recording points at gauges are out of order, wherefore this environmental factor should not be used as argument, if possible. The argument $Q(t)$ considers the current discharge at the forecast gauge itself, whereas $Q_{up}(t)$ is the current discharge measured at the corresponding upstream gauge.

Change of discharge.

The change of discharge within the past $\Delta Q(t-X,t)$ allows conclusions to be drawn about the change of past to present conditions within the catchment and is defined as:

$$\Delta Q(t-n,t) = Q(t-n) - Q(t) \quad (5.1)$$

Depending on the time resolution of the fuzzy inference system several time intervals n have been investigated as arguments ($n = 3, 7, 14, 21$ days and $n = 6, 12, 18$ hours) and named as $\Delta Q(t-3d,t)$, $\Delta Q(t-7d,t)$, and so forth.

Areal precipitation.

As the areal precipitation $P(t)$ is the driving force of discharge forecasts three different environmental factors have been defined and investigated as possible arguments:

1. areal precipitation of the past:

$$P(t-i) \quad \text{with } i = 1, \dots, 12 \text{ hours} \quad (5.2)$$

2. forecasted areal precipitation:

$$fP(t+i) \quad \text{with } i = 1, 2, 3 \text{ days; } 1, \dots, 48 \text{ hours} \quad (5.3)$$

3. forecasted cumulated areal precipitation:

$$cfP((t+n) - (t+m)h, t) = \sum_{i=n}^m P(t+i) \quad \text{e.g. } cfP(25 - 48h, t) \quad (5.4)$$

As no real forecasts of the areal precipitation were available for this work, actual measurements of the areal precipitation have been taken as ideal forecasts. Consequently, as soon as real forecasts of this environmental factor are available, it is advisable to repeat the training of the fuzzy inference systems.

Areal antecedent precipitation index.

The areal antecedent precipitation index $API(t)$ is an indicator of the soil moisture and remaining infiltration capacity. Based on the areal precipitation $P(t)$ and the recession constant c it is defined as

$$API(t) = \sum_i^n P(t-i) \cdot c^i \quad (5.5)$$

In this case the recession constant is set to 0.9. Furthermore, depending on the time resolution of the fuzzy inference system several API time intervals n have been investigated as arguments ($n = 3, 7, 14, 21$ days and $n = 6, 12, 18$ hours) and named as $API3d(t)$, $API7d(t)$, ..., $API12h(t)$, $API18h(t)$.

Temporal dissymmetry coefficient.

The temporal dissymmetry coefficient $S(t)$ indicates the position of the rainfall peak within a certain time interval and is defined as (Alvisi et al., 2006):

$$S(t) = \frac{\sum_{n=1}^N \left[\left(-\frac{N+1}{2} + n \right)^3 \cdot P(t-n\Delta t, t-(n-1)\Delta t) \right]}{\sum_{n=1}^N P(t-n\Delta t, t-(n-1)\Delta t)} \quad (5.6)$$

thereby N is the number of time steps with respect to the time interval $[t-N\Delta t, t]$ and $P(t-n\Delta t, t-(n-1)\Delta t)$ is the areal precipitation measured in the time interval $[t-n\Delta t, t-(n-1)\Delta t]$. This environmental factor was only investigated for the hourly time resolution.

Circulation pattern.

The circulation pattern $CP(t)$ represents the large scale condition of a flood event. Consequently, certain circulation pattern indicate a high potential of occurring flood events. In this work the

5 Model development for the Upper Main basin

classification of circulation pattern within the Upper Main basin on a daily base is taken from Bliefernicht et al. (2008). Furthermore, it has been only investigated for the daily forecast horizon.

Mean areal temperature and time-averaged mean areal temperature.

Both environmental factors are investigated with respect to their potential to indicate seasonal (winter, summer) as well as icy, snowy or rainy conditions during wintertime, in particular. Thereby, the time-averaged mean areal temperature $mT(t)$ is defined based on the mean areal temperature $T(t)$ as

$$mT(t) = \frac{1}{n} \sum_{i=1}^n T(t-i) \quad (5.7)$$

and named depending on the considered time intervals n ($n = 3, 7, 14, 21$ days and $n = 6, 12, 18$ hours) as $mT3d(t)$, $mT7d(t)$, ..., $mT12h(t)$, $mT18h(t)$.

Areal snow storage and snow discharge.

Due to the fact that the biggest flood events within the considered time period of 1991 - 2004 occurred during wintertime the environmental factors areal snow storage $snowst(t)$ and snow discharge $qsnow(t)$ are investigated. As no measurements of these variables were available, they were calculated using the formulae of the hydrological model WaSiM-ETH (Schulla and Jasper, 2002) to ensure comparable inputs. Thereby, the areal snow storage $snowst(t)$ is calculated by considering the snow fraction p_{snow} :

$$p_{snow} = \frac{T_{R/S} + T_{trans} - T(t)}{2 \cdot T_{trans}} \quad \text{for } (T_{R/S} - T_{trans}) < T(t) < (T_{R/S} + T_{trans}) \quad (5.8)$$

with

p_{snow}	[—]	fraction of snow with respect to the total precipitation (0, ..., 1)
$T(t)$	[°C]	areal temperature
$T_{R/S}$	[°C]	temperature, at which 50 % of precipitation are falling as snow (here: 0.5)
T_{trans}	[°C]	one half of the temperature-transition range from snow to rain (here: 1.0)

The areal snow storage $snowst(t)$ is then the sum of that fraction of precipitation which falls as snow. Furthermore, snowmelt M and the resulting snow discharge $qsnow(t)$ is calculated based on the temperature-index approach and the calibrated parameters of the hydrological model WaSiM-ETH as follows:

$$M = c_0 \cdot (T(t) - T_{0,m}) \cdot \frac{\Delta t}{24} \quad (5.9)$$

with

M	[mm/Δt]	melting rate for $T(t) > T_{0,m}$, otherwise $M = 0$
c_0	[mm/(°C · d)]	temperature dependent melt factor (here: 1.8)
$T_{0,m}$	[°C]	temperature for the onset of snowmelt (here: -0.5)
Δt	[h]	time step

Potential evapotranspiration.

Since potential evapotranspiration $ETP(t)$ plays no role for the hourly forecast of winter flood events this environmental factor was only investigated as a possible argument for the daily forecast

(Bengelstorf, 2009). As in case of snow storage and snowmelt no measurements were available and, therefore, the variable was calculated separately after Penman-Monteith as it is implemented within the hydrological model WaSiM-ETH in order to ensure comparability.

5.2.2 Fuzzy inference systems for the 3 day forecast

As mentioned before the aim of the 3 day forecast systems is the early indication of an occurring flood event to ensure a well-timed switching to the hourly forecast systems. Therefore, the focus of these systems and their training lies on the appropriate representation of low and medium discharge conditions as well as on reliable forecasts of trespasses considering a predefined warning level. The forecast of the flood hydrograph above the predefined threshold is less important because this is performed with the hourly forecast systems. Table 5.11 gives the number of observed trespasses considering warning level 1 (compare Table 4.5) as well as the Upper Main gauges Kemmern (4244 km²), Schwürbitz (2419 km²), and Mainleus (1166 km²), separately for the training (01.01.1984 - 31.12.1994) and validation (01.01.1995 - 31.12.2004) period. A further requirement of the 3 day forecast systems is that they should be user friendly. Thus, simple fuzzy inference systems have to be developed. Furthermore, only meteorological and no discharge data should be considered as arguments, if possible, because most of the time recording points at gauges are out of order and / or report wrong measurements during high flood events.

	Kemmer		Schwürbitz		Mainleus	
	WL 1 [m^3/s]	NT	WL 1 [m^3/s]	NT	WL 1 [m^3/s]	NT
Training	151	31	138	25	55	26
Validation	151	29	138	20	55	26

Table 5.11: Number of observed trespasses (NT) considering the Upper Main gauges Kemmern (4244 km²), Schwürbitz (2419 km²), and Mainleus (1166 km²) as well as warning level 1 (WL 1, compare Table 4.5; training / validation period, 01.01.1984 - 31.12.1994 / 01.01.1995 - 31.12.2004).

Both fuzzy inference systems, MS and TS, are investigated for the 3 day forecast because no reference and generally accepted statements could be found in literature which clarify the question whether one system is superior or not. Due to the system requirements mentioned above, the fuzzification of arguments (MS, TS) and response (MS) is performed with a pure statistical method only considering the minimal, maximal and mean values of the corresponding variable and triangular shapes (Figure 5.12). Furthermore, only the number of rules, which are optimized, is set in advance and no further restrictions with respect to the automatic rule setup applying Simulated Annealing (SA, Chapter 3.3.2) are defined. Thus, the initialisation of the rule system and its optimization is performed by the SA algorithm itself, whereas the shape and number of the predefined membership functions remain unaffected during the optimization process.

Performance comparison of MS and TS with respect to $Q(t+3d)$.

In a first step a performance comparison of both fuzzy inference systems is carried out for the direct 3 day forecast of discharge $Q(t+3d)$. Based on the findings of Bengelstorf (2009) and other literature different combinations of daily based environmental factors (Chapter 5.2.1) are investigated as arguments for both fuzzy inference systems. Some of these argument combinations, including the final one, are presented in the following. Table 5.12 summarizes the different

5 Model development for the Upper Main basin

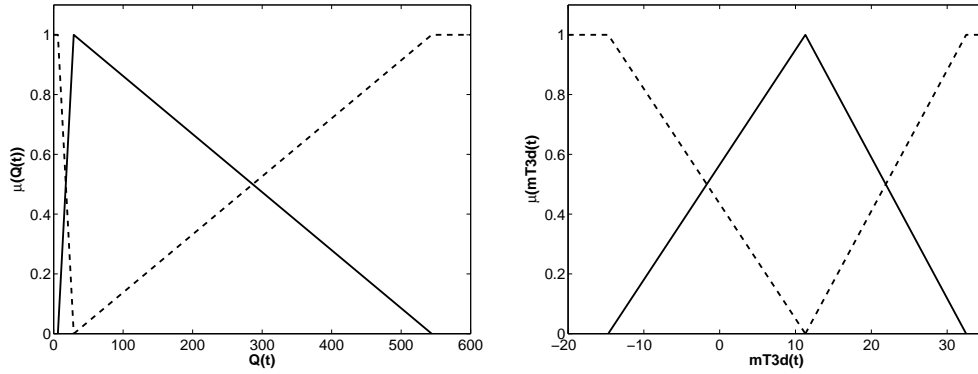


Figure 5.12: Examples for the fuzzification of daily based arguments (left: discharge, right: time-averaged mean areal temperature) considering the 3 day forecast (dashed left: minimal value, solid: mean, dashed right: maximal value of the corresponding variable).

argument combinations, in which each argument is fuzzified through three triangular membership functions as mentioned before (Figure 5.12).

Argument	D3_1	D3_2	D3_3	D3_4	D3_5
$Q(t)$	X	X	X	X	
$Q_{up}(t)$	X	X	X		
$API3d(t)$	X				
$API7d(t)$		X			
$API14d(t)$			X	X	X
$mT3d(t)$	X				
$mT7d(t)$		X			
$mT14d(t)$			X	X	X
$P(t)$	X	X	X	X	X
$fP(t+1d)$	X	X	X	X	X
$fP(t+2d)$	X	X	X	X	X
$fP(t+2d)$	X	X	X	X	X
Σ	8	8	8	7	6

Table 5.12: Combinations of daily based arguments (D3_1 to D3_5) investigated for the direct 3 day forecast of discharge $Q(t+3d)$ ($Q(t)$: current discharge at the forecast gauge; $Q_{up}(t)$: current discharge at the corresponding upstream gauge).

For each argument combination (Table 5.12) fuzzy inference systems with 5 to 30 rules (continuously increasing by 1) are trained and validated with no further restrictions in order to find the best fitted rule system for the 3 day forecast. Except for the arguments areal antecedent precipitation index API and time-averaged mean areal temperature mT the arguments are considered within both, the IF-part and the linear response functions of the THEN-part of each rule in case of the TS systems. The time-averaged mean areal temperature occurs only within the IF-part of the TS systems because it is not directly related with the discharge volume. The argument API is not considered within the THEN-part as the corresponding coefficients of the linear response functions are zero after the SA-TS optimization process. In Figure 5.13 and 5.14 the linguistic description of both inference systems, MS and TS, are exemplarily given for the optimized 5 rule system, which does not represent the best fitted one. The first rule in Figure 5.13 means that inde-

pendent from the argument inputs mean discharge is always forecasted. In combination with the other rules a divergence can be achieved resulting in the forecast of lower or higher discharges. Therefore, the plausibility of one rule has always to be evaluated in combination with the other rules. For this, the DOF values are considered in this work. Through the linguistic description of the arguments and hence of the model process, the transparency of the systems is ensured for the user in both cases. However, the TS inference system is less transparent because the coefficients of the linear response functions within the THEN-part cannot be linguistically interpreted.

IF	Q(t)	&	API14d(t)	&	mT14d(t)	&	P(t)	&	fP(t+1d)	&	fP(t+2d)	&	fP(t+3d)	THEN	Q(t+3d)
IF		&		&		&		&		&		&		THEN	mean
IF	max	&		&		&		&		&		&		THEN	min
IF		&		&		&	max	&	max	&		&		THEN	max
IF		&		&	min	&	max	&		&		&		THEN	max
IF	mean	&		&	mean	&		&		&	max	&		THEN	max

Figure 5.13: Linguistical description of the optimized 5 rule MS inference system considering argument combination D3_4.

IF	Q(t)	&	API14d(t)	&	mT14d(t)	&	P(t)	&	fP(t+1d)	&	fP(t+2d)	&	fP(t+3d)	THEN	Q(t+3d) =
IF		&		&		&	max	&	mean	&	max	&	min		
IF		&	mean	&	min	&		&		&	min	&			
IF		&		&	min	&		&	min	&	min	&			
IF		&		&	min	&	min	&	min	&		&	max		
IF		&	mean	&	max	&	max	&	mean	&	max	&	max		
THEN	Q(t+3d) =														
	a0		+ a1 * Q(t)		+ a2 * P(t)		+ a3 * fP(t+1d)		+ a4 * fP(t+2d)		+ a5 * fP(t+3d)				
THEN	0.03		0.01		-0.03		-0.02		1.17		-0.33				
THEN	0.00		0.12		0.12		0.21		0.11		0.58				
THEN	0.03		-0.14		0.22		-0.69		0.13		0.44				
THEN	-0.33		23.17		-59.71		2.88		0.41		3.81				
THEN	-0.07		-0.04		0.11		0.18		0.08		1.81				

Figure 5.14: Linguistical description of the optimized 5 rule TS inference system considering argument combination D3_4.

For the evaluation of the 26 inference systems each, the value of the objective function of the optimization process (least-square method), the correlation coefficient and the well-timed forecasts of trespasses (cNT, fNT) considering the corresponding warning level 1 are investigated. For the latter, a three day window from t to $t + 3d$ is analysed in which the trespass should occur otherwise the forecast fails. For gauge Kemmern Figure 5.15 shows the development of the correlation values for the training and validation sets for the argument combinations D3_1 to D3_3 (left), and D3_3 to D3_5 (right) for both fuzzy inference systems.

In case of MS all 26 rule systems can be set up for each argument combination considering the forecast of direct discharge $Q(t + 3d)$ at gauge Kemmern. That means that satisfying rule systems have been optimized so that the rules are able to reproduce the whole discharge range. Thus, all responses could be simulated with a value unequal zero at all time. In contrast to this, the TS inference systems show a sensitive behavior considering both, the rule number to be optimized and the chosen argument combination. It could not be totally clarified if these sensitivities occur due to the performed SA-TS optimization setup or if they reflect a general behavior of TS inference systems. As indicated through the worse correlation values, not all responses are simulated at all time and the corresponding $Q(t + 3d)$ values are set to zero. However, in case of argument combination D3_4 and the 25 rule TS inference system all responses have values unequal zero, and the rules are able to reproduce the whole discharge range.

Table 5.13 summarizes the optimization results considering the best fitted MS and TS inference systems for the 3 day forecast (Disse et al., 2009). The linguistic descriptions of the corresponding rules are given in Appendix C. Furthermore, Figure 5.16 shows two examples for the forecast

5 Model development for the Upper Main basin

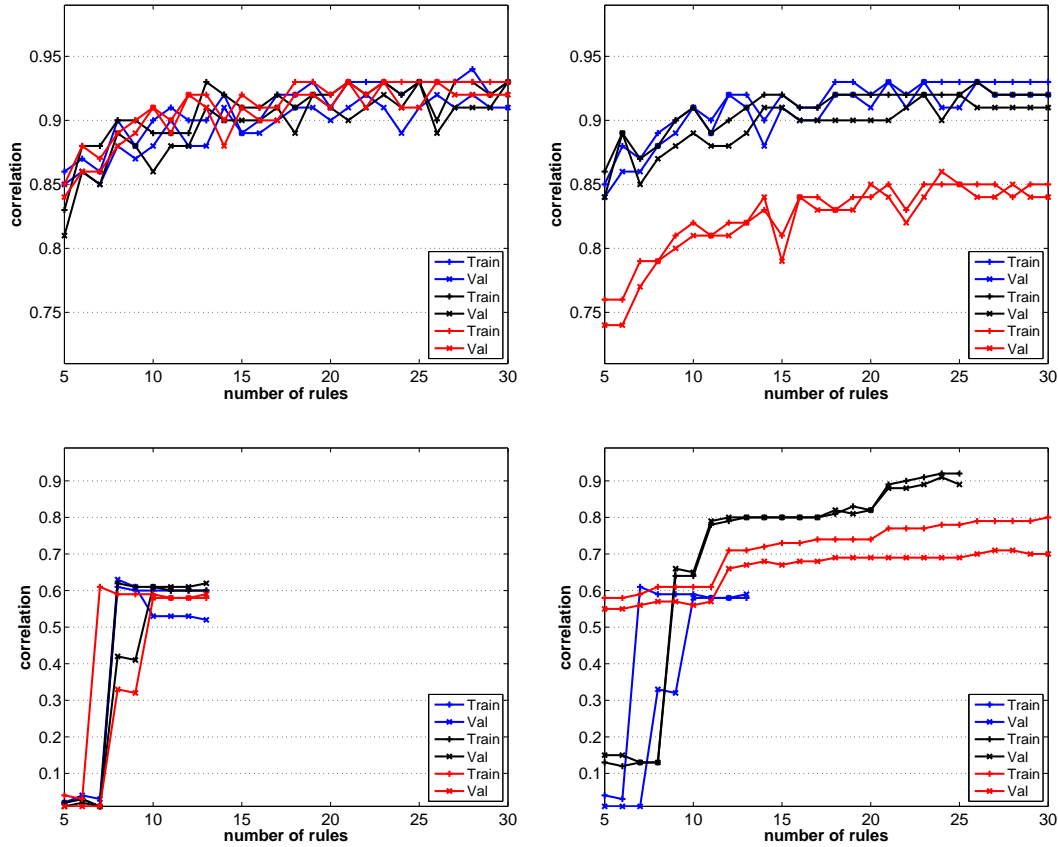


Figure 5.15: Development of the correlation values for the training and validation sets and both fuzzy inference systems (top: MS; bottom: TS) considering left the argument combinations D3_1 (blue), D3_2 (black), D3_3 (red), and right D3_3 (blue), D3_4 (black), D3_5 (red).

performance of these two fuzzy inference systems for gauge Kemmern. The crucial factors for the rating of the different fuzzy inference systems are the reproduction of the hydrograph considering low and medium discharge conditions as well as the number of false and correctly forecasted trespasses (fNT , cNT) of warning level 1 (see also Table 5.11). Thereby, a false forecasted trespass is counted if (1) an observed one is missed or (2) a trespass is forecasted although none occurs.

FIS			Training			Validation		
			r	cNT	fNT	r	cNT	fNT
MS	D3_4	23 rules	0.92	26	9	0.91	25	7
TS	D3_4	25 rules	0.91	21	17	0.89	21	14

Table 5.13: Evaluation results for the best fitted MS and TS inference systems at gauge Kemmern considering the forecast of $Q(t + 3d)$ and all investigated argument combinations (r: correlation coefficient; cNT / fNT: correctly / false well-timed forecasts of trespasses; observed NT (training / validation): 31 / 29).

Considering the MS inference systems the optimized 23 rule system for D3_4 represents the best fitted one because less arguments are required in order to achieve results of comparable quality considering the correlation value (Figure 5.15) as well as the relation of false and correctly forecasted trespasses (D3_1: Training cNT/fNT = 27/9, Validation cNT/fNT = 26/9 ; D3_2: 27/10, 25/8; D3_3: 27/10, 25/8).

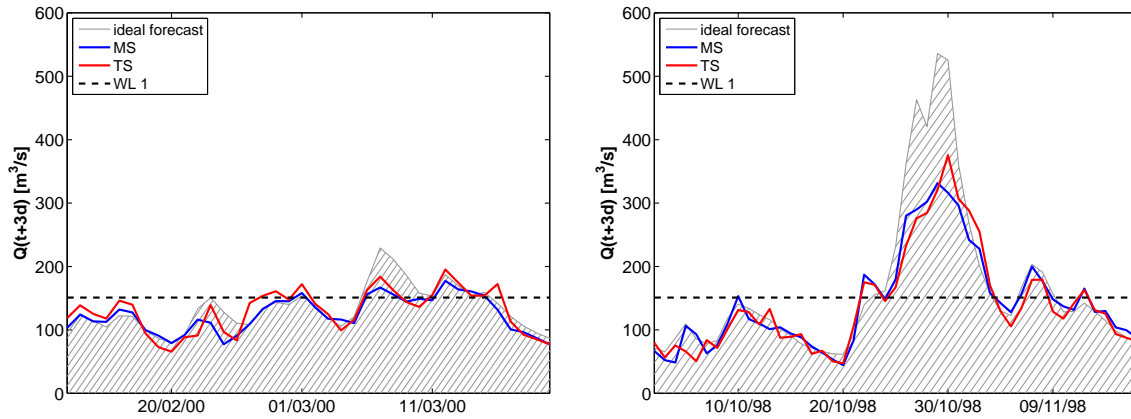


Figure 5.16: Examples for the performance of the best fitted MS and TS rule systems considering the 3 day forecast of $Q(t + 3d)$ at gauge Kemmern (validation period; MS: D3_4, 23 rules; TS: D3_4, 25 rules).

The performance of the best fitted MS and TS inference systems is of comparable quality, whereas the well-timed forecasts of trespasses is better performed with the MS inference system. Failures of the well-time forecast of trespasses occur mostly in situations, when the discharge oscillates around the predefined warning level for a certain time period (Figure 5.16, left). Low and medium flow conditions are well reproduced, but drawbacks for high discharges occur which are acceptable considering the forecast aim (Figure 5.16, right). Comparing the optimization process of both fuzzy inference systems much more computation time is required in case of TS because the coefficients of the linear response functions have to be determined within all optimization steps. Furthermore, the sensitive behavior of the TS inference systems within the chosen SA-TS optimization setup (number of rules and argument combination) makes their optimization more difficult and more time consuming in comparison to MS inference systems.

The correlation values (Figure 5.15) show that the environmental factor *discharge at the forecast gauge* is an essential argument and cannot be neglected in any of both fuzzy inference systems in this case. Furthermore, discharge information of the upstream gauge is not as important for the presented argument combinations and can be neglected. Thus, the above stated requirement for the 3 day forecast systems cannot be totally fulfilled since the argument *current discharge at the forecast gauge* provides too much information of the actual catchment conditions and has to be considered. This argument cannot be replaced by other investigated arguments.

Performance comparison of MS and TS with respect to $\Delta Q(t, t+3d)$.

The performance comparison of both fuzzy inference systems considering the direct 3 day forecast of discharge $Q(t + 3d)$ shows that the argument discharge is very significant and cannot be neglected within these systems. However, one restriction for the 3 day forecast systems is to ignore this environmental factor as argument if possible. Therefore, the forecast of discharge changes $\Delta Q(t, t + 3d)$ are investigated. The major difference between both forecast strategies is that the forecast of discharge changes $\Delta Q(t, t + 3d)$ focuses more on the forecast of dynamic changes within the catchment, wherefore the argument discharge should fade into the background.

As in case of the direct 3 day forecast of discharge different combinations of environmental factors (Chapter 5.2.1) are investigated. A selection of considered argument combinations including the final one are given in Table 5.14. The fuzzification of arguments (MS, TS) and response (MS) is

5 Model development for the Upper Main basin

performed with the pure statistical method as before (triangular shapes, Figure 5.12) in order to ensure comparable results and simple fuzzy inference systems.

Argument	dD3_1	dD3_2	dD3_3	dD3_4	dD3_5
API3d(t)	X				
API7d(t)		X			
API14d(t)			X	X	X
mT3d(t)	X				
mT7d(t)		X			
mT14d(t)			X	X	X
P(t)	X	X	X	X	X
fP(t+1d)	X	X	X	X	X
fP(t+2d)	X	X	X	X	X
fP(t+2d)	X	X	X	X	X
CP(t)				X	
snowst(t)					X
Σ	6	6	6	7	7

Table 5.14: Combinations of daily based arguments (cases dD3_1 to dD3_5) investigated for the forecast of discharge changes $\Delta Q(t, t + 3d)$.

For each combination both fuzzy inference systems with 5 to 30 rules (continuously increasing by 1) are trained and validated with no further restrictions in order to find the best fitted system as in case of $Q(t + 3d)$. Additionally, all arguments are considered within both, the IF-part and the linear response functions of the THEN-part of each rule, except of the time-averaged mean areal temperature mT . Since it is not directly related to the discharge volume, the argument mT occurs only within the IF-part of the TS inference systems.

In case of TS all 26 rule systems can only be set up for dD3_1 to dD3_3 with the performed SA-TS optimization setup. In contrast to this, all 26 MS rule systems are successfully optimized for each argument combination. In Appendix C the development of the correlation values for the training and validation sets for the presented argument combinations considering gauge Kemmern are shown. The evaluation of each of the 26 inference systems is performed as for the direct 3 day discharge forecast. For the rating of the different fuzzy inference systems the correlation coefficient, the reproduction of low and medium discharge conditions as well as the number of false and correctly forecasted trespasses are considered. Since with both inference systems negative forecasted discharges can occur resulting from far too large forecasted discharge changes, $Q(t + 3d) = Q(t) + \Delta Q(t, t + 3d)$, their number is further taken into account for the evaluation.

Considering the correlation values of argument combinations dD3_2 to dD3_5 and the MS inference systems (Figure C.3, C.4) no significant differences occur. Since the number of correctly and false forecasted trespasses of all optimized MS inference systems differs by maximal 2, the number of negative forecasted discharges is the crucial factor for the determination of the best fitted MS inference system. Consequently, the 20 rule MS inference system for argument combination dD3_3 represents the best fitted one because only 185 (113) instead of 269 (173) or more negative discharges are forecasted. For the same reasons the best fitted TS inference system is chosen. The number of forecasted trespasses differs by maximal 2, but less negative discharges are forecasted (124/92 instead of 131/101 or more). Table 5.15 summarizes the optimization re-

sults of the best fitted MS and TS inference systems. Figure 5.17 shows two examples for the forecast performance of these two fuzzy inference systems for gauge Kemmern.

FIS			Training					Validation				
			r_{Δ}	r	cNT	fNT	nd	r_{Δ}	r	cNT	fNT	nd
MS	dD3_3	20 rules	0.73	0.88	24	14	185	0.75	0.88	22	12	113
TS	dD3_3	12 rules	0.55	0.86	22	16	124	0.51	0.84	20	16	92

Table 5.15: Evaluation results for the best fitted MS and TS inference systems considering the forecast of $\Delta Q(t+3d)$ at gauge Kemmern and all investigated argument combinations (r : correlation coefficient; cNT / fNT: correctly / false well-timed forecasts of trespasses; nd: number of negative forecasted discharge; Δ : considering the forecast of $\Delta Q(t, t+3d)$, otherwise of $Q(t+3d) = Q(t) + \Delta Q(t, t+3d)$; observed NT: 31 / 29).

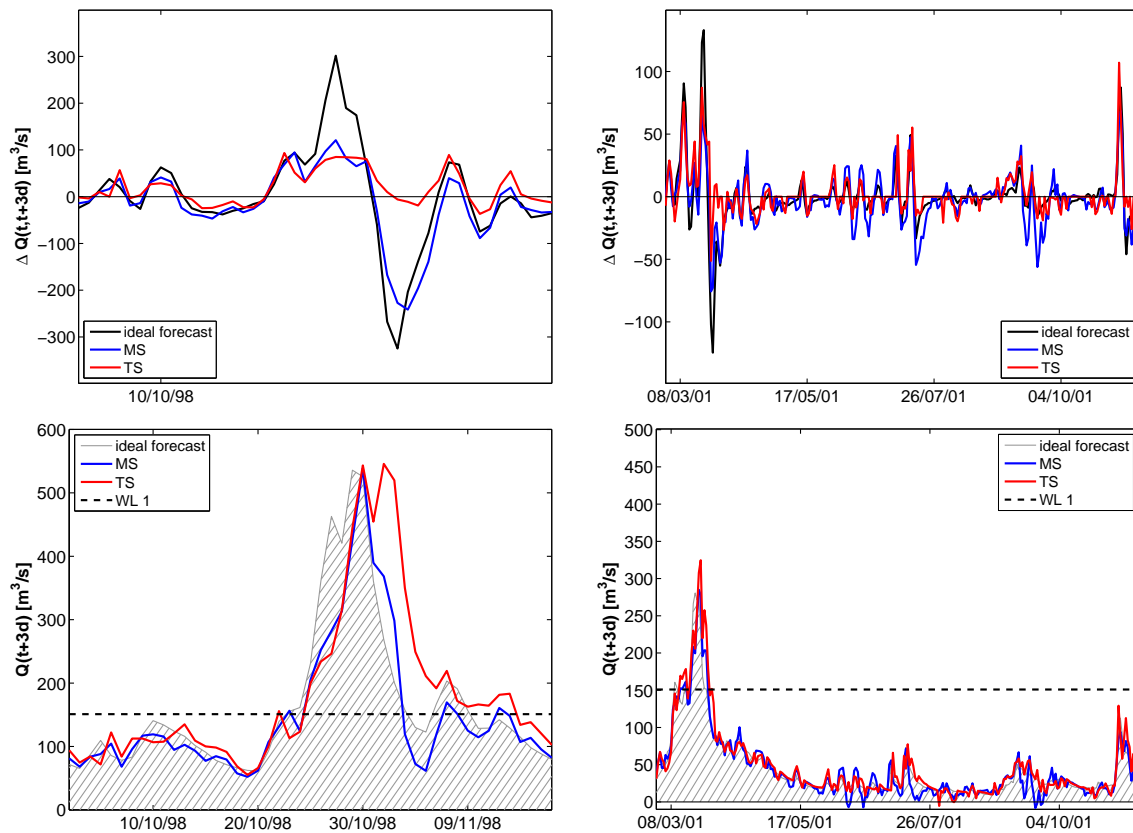


Figure 5.17: Examples for the performance of the best fitted MS and TS rule systems considering the 3 day forecast of $\Delta Q(t, t+3d)$ at gauge Kemmern (validation period; MS: dD3_3, 20 rules; TS: dD3_3 12 rules; top: forecast of $\Delta Q(t, t+3d)$; bottom: resulting forecast of $Q(t+3d) = Q(t) + \Delta Q(t, t+3d)$).

The performance of both best fitted fuzzy inference systems is of comparable quality. Furthermore, comparing the well-timed forecasts of trespass of both forecast strategies, direct $Q(t+3d)$ and discharge changes $\Delta Q(t, t+3d)$, the number of failures and correct forecasts are comparable (Table 5.13, 5.15) considering cNT. This can be traced back to the addition of $Q(t)$ to the forecasted $\Delta Q(t, t+3d)$ which acts as an autotracking of the forecast model and, therefore, attenuates worse forecasts of $\Delta Q(t, t+3d)$ most of the time. However, the forecast of trespasses is slightly better as in the case of a persistence forecast, for which the current observed discharge is taken as the forecast.

Considering the simulation of low and medium discharge conditions the performance of the $\Delta Q(t, t + 3d)$ forecast is less satisfying than in case of $Q(t + 3d)$. Far too large negative forecasted changes cause an overall negative and consequently wrong forecast of discharge (Figure 5.17, right). This drawback cannot be attenuated if other arguments are additionally considered to dD3_3 (compare correlation values Figure C.4). Thus, the best fitted fuzzy inference systems considering the forecast of $\Delta Q(t, t + 3d)$ are not adequate for a performance within the framework of the forecast system ExpHo-HORIX in this case.

Despite of the discussed drawbacks, much potential still lies in the forecast of discharge differences $\Delta Q(t, t + 3d)$ as mostly time-averaged areal environmental factors, fuzzified through three membership functions, have been investigated in this work. Among others, the following aspects should be considered in the future:

1. Training and validation data can be further divided into training and validation sets considering only positive and only negative discharge changes. Then, separate fuzzy inference systems can be trained for the positive and negative data samples. Together with the setup of fuzzy inference systems for negative data samples, the performance of a simple storage constant can be investigated as response for the description of the decreasing part of the hydrograph. However, the major challenge, but also drawback of this approach is the merging of both separate performing fuzzy inference systems and the well-timed forecast of the switching between both.
2. Instead of time-averaged mean areal environmental factors, spatial distributed environmental factors can be investigated. Thereby, also other methods of fuzzification should be considered (compare Chapter 5.2.4). However, this approach requires more detailed knowledge about the catchment characteristics (dynamics). This means, that the setup of fuzzy inference systems is less simple for an unexperienced user.

Performance of the optimal setups at the gauges Schwürbitz and Mainleus.

In order to verify the results of the above discussed performance comparisons and to investigate the transferability of the optimal MS and TS inference systems at gauge Kemmern, both fuzzy inference systems have been trained for two further Upper Main gauges, Schwürbitz (2419 km²) and Mainleus (1166 km²). Thereby, the optimal MS and TS setups for the forecast of $Q(t + 3d)$ (D3_4, 23 rule MS, 25 rule TS) are considered. Since negative discharges occur for the forecast of $\Delta Q(t, t + 3d)$ at gauge Kemmern with both fuzzy inference systems, they are not presented here (see Pakosch et al., 2008a).

The optimization of the fuzzy inference systems is performed as for gauge Kemmern. That means that they are trained and validated with no further restrictions. Within the TS systems all arguments are considered within the IF-part and the linear response functions of the THEN-part of each rule, except of the time-averaged mean areal temperature. The time-averaged mean areal temperature occurs only within the IF-part of the TS systems. Table 5.16 summarizes the evaluation results considering the correlation coefficients and well-timed forecasts of trespasses.

Both fuzzy inference systems have been successfully set up with focus on low and medium discharge conditions for the 3 day forecast of $Q(t + 3d)$ at both gauges, Schwürbitz and Mainleus. That means that all responses are simulated at all times and both fuzzy inference systems are able to reproduce the whole range of discharge with some drawbacks considering the flood events

FIS				Training			Validation		
				r	cNT	fNT	r	cNT	fNT
Schwüribitz	MS	D3_4	23 rules	0.92	19	10	0.87	15	10
	TS	D3_4	25 rules	0.89	20	13	0.89	15	11
Mainleus	MS	D3_4	23 rules	0.89	23	9	0.89	23	8
	TS	D3_4	25 rules	0.88	23	12	0.88	20	8

Table 5.16: Evaluation results for MS and TS inference systems considering the forecast of $Q(t + 3d)$ at gauges Schwüribitz (2419 km²) and Mainleus (1166 km²; r: correlation coefficient; cNT / fNT: correctly / false well-timed forecasts of trespasses; observed NT: 25 / 20 at Schwüribitz, 26 / 26 at Mainleus).

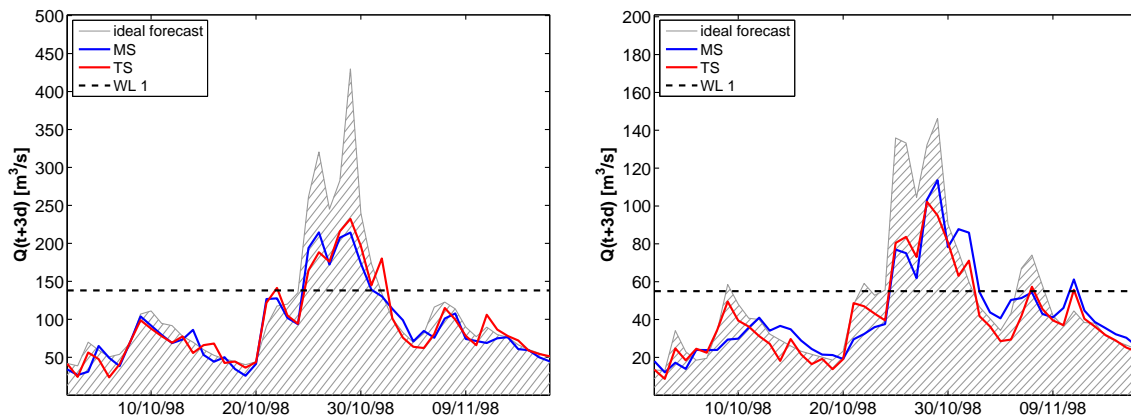


Figure 5.18: Performance comparison of MS and TS systems for the forecast of $Q(t + 3d)$ at gauges Schwüribitz (left) and Mainleus (right) considering the flood hydrograph.

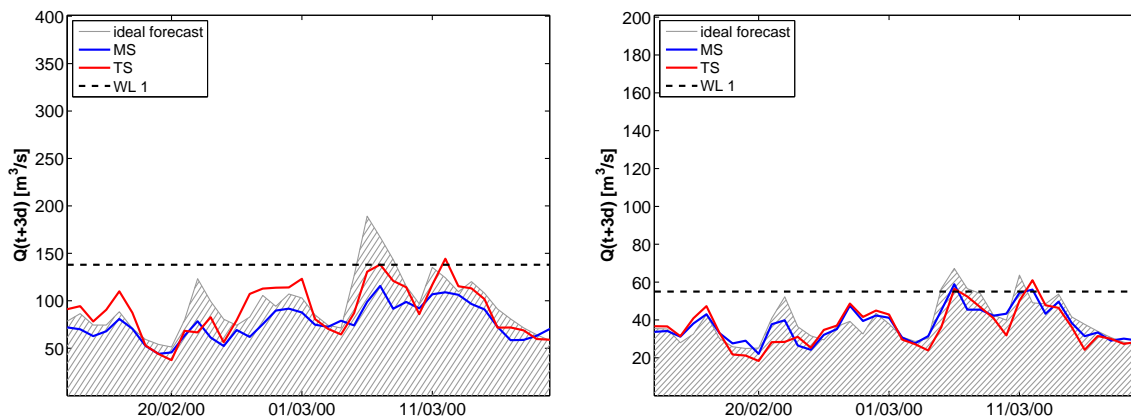


Figure 5.19: Performance comparison of MS and TS systems for the forecast of $Q(t + 3d)$ at gauges Schwüribitz (left) and Mainleus (right) considering WL 1.

(Figure 5.18). Failures of the well-timed forecast of trespasses occur only within acceptable situations, when the hydrograph oscillates around the predefined warning level for a certain time period as in case of gauge Kemmern (Figure 5.19).

Overall, the results of gauges Schwürbitz and Mainleus confirm the results of gauge Kemmern, which are the following:

1. It is possible to set up simple MS and TS inference systems for a 3 day forecast of discharge $Q(t + 3d)$ for the three main gauges within the Upper Main basin.
2. No significant performance differences between both fuzzy inference systems occur (Figure 5.18, 5.19). However, the sensitivity behavior of the SA-TS optimization process has to be pointed out.

Conclusions for the following investigations on a hourly time resolution.

Due to the discussed drawbacks of the forecast of discharge changes $\Delta Q(t, t + 3d)$, which arise mainly from the chosen environmental factors, the forecast of $\Delta Q(t, t + Xh)$ on a hourly time resolution is not further investigated within the framework of this thesis. However, much potential still lies in this forecast strategy, as mentioned before.

Both fuzzy inference systems are further investigated for the hourly time resolution because (1) no general statements about significant performance differences can be made and (2) the sensitivity behavior of the SA-TS optimization process is not totally clarified. Further investigations for TS inference systems at gauge Mainleus show, that if the arguments are normalized with their corresponding maximum values and fuzzified through more than 3 membership functions (1) the sensitive behavior of the SA-TS optimization process vanishes, and (2) the forecast performance considering the discharge changes $\Delta Q(t, t + 3d)$ is enhanced (Pakosch et al., 2008b).

5.2.3 Fuzzy inference systems for the 6 and 12 hour forecast

The focus of the 3 day forecast systems lies on the reliable and well-timed forecast of a predefined warning level. In contrast to this, the hourly based fuzzy inference systems should ensure a reliable and satisfying forecast of the flood hydrograph itself. In literature, several studies using fuzzy inference systems for discharge forecast for a 6 and 12 hour time horizons can be found (e.g. Alvisi et al., 2006; Gemmar et al., 2006; Casper et al., 2007). That is not the case considering a 48 hour forecast horizon. Furthermore, in contrast to the 6 and 12 h forecast the memories of the catchments have no great impact on the 48 h forecast. Consequently, it is a challenge to find appropriate argument combinations for the 48 h forecast. Therefore, the essential results of both fuzzy inference systems for the 6 and 12 hour forecast are shortly presented in this chapter, whereas those of the 48 hour ones are discussed in more detail in the following one.

As in case of daily fuzzy inference systems, very user friendly and consequently simple fuzzy inference systems should be developed. Therefore, the fuzzification is performed with the pure statistical method using triangular shapes, as before. Figure 5.20 exemplarily shows the differences between the daily and hourly based membership functions of the argument/response discharge, which results due to the different time resolutions and corresponding accuracies.

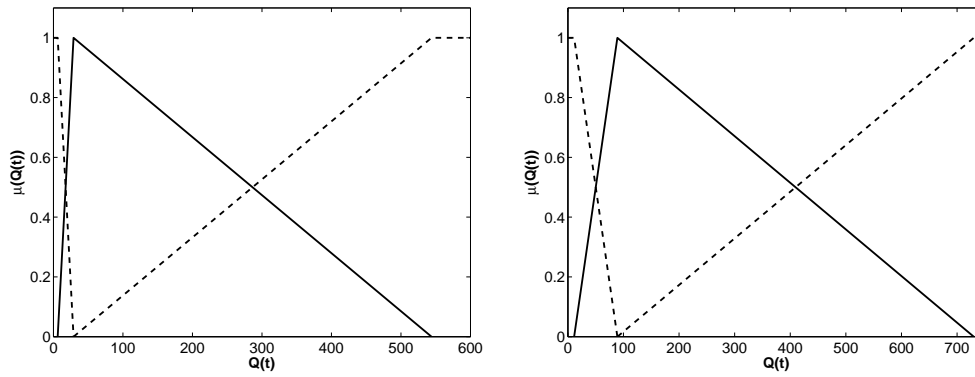


Figure 5.20: Differences between the daily (left) and hourly (right) based membership functions exemplarily shown for the argument/response discharge at gauge Kemmern (dashed left: minimal value, solid: mean, dashed right: maximal value of the corresponding variable).

As the focus lies on the forecast of the flood hydrograph itself, only data of observed flood events are taken into account for the training and validation of the fuzzy inference systems. Therefore, time periods, in which predominantly low and medium flow conditions exist, are ignored. A consideration of these data would profoundly influence the training process as their number is by far larger than those corresponding to single flood events. In whole 30 flood events between 1991 and 2004 are selected, whereat 26 occur during wintertime and 4 during the transition period between wintertime and summertime (hydrological year).

The selection of environmental factors as arguments for the direct 6 and 12 hour forecast of discharge, $Q(t + 6h)$ and $Q(t + 12h)$, is primarily based on findings in literature and the results of the daily forecast systems. Table 5.17 shows examples of investigated argument combinations including the final one, which are briefly discussed. Thereby, argument combinations H6_1 and H12_1 represent a straight forward extension of the 3 day forecast argument combination D3_4. H6_2 is based on literature findings, and H12_2 is a straight forward extension of it.

Argument	H6_1	H6_2	H6_3	H12_1	H12_2
$Q(t)$	X	X		X	X
$API12h(t)$	X	X	X	X	X
$mT12h(t)$	X	X	X	X	X
$P(t-1h)$ to $P(t-6h)$		X			X
$P(t)$	X	X	X		X
$cfP(0-6h,t)$				X	
$fP(t+1h)$ to $(t+6h)$	X	X	X		X
$fP(t+7h)$ to $(t+12h)$				X	X
Σ	10	16	9	10	22

Table 5.17: Combinations of hourly based arguments investigated for the 6 and 12 hour forecast of discharge $Q(t + 6h)$ and $Q(t + 12h)$ ($Q(t)$: current discharge at the forecast gauge).

Similar to the 3 day forecast 5 to 40 rules systems (continuously increased by 1) are trained and validated for both inference systems and argument combinations. In case of TS inference systems only the arguments $Q(t)$, $API12h(t)$, and $mT12h(t)$ occur within the IF-part of the rule systems. Within the THEN-part all arguments except of $mT12h(t)$ are considered.

5 Model development for the Upper Main basin

Although MS inference systems can be set up for each investigated argument combination of the 3 day forecast, this is not the case here. Both inference systems show a certain sensitivity considering the chosen argument combination. Furthermore, the sensitive behavior of the SA-TS optimization due to the chosen rule number still exists, but is less grave than for the 3 day forecast. With the performed SA-MS optimization setup no MS inference systems could be set up in case of H6_2, which is able to simulate all data of the flood events. A reason for this is the huge number of arguments, which are considered within this case. In contrast to this, the SA-TS optimization is successful for H6_2, but fails for H6_1, and H6_3. Due to the huge number of arguments neither MS nor TS inference systems can be optimized with the corresponding SA setups for argument combination H12_2, but for H12_1.

FIS			Training				Validation					
			r	DPH		DPT		r	DPH		DPT	
				\bar{x}	σ	\bar{x}	σ		\bar{x}	σ	\bar{x}	σ
MS	H6_1	17 rules	0.99	2	3	4	2	0.98	3	4	5	2
	H12_1	20 rules	0.96	9	5	9	2	0.96	9	5	9	3
TS	H6_2	6 rules	0.99	4	3	4	2	0.98	5	5	3	3
	H12_1	6 rules	0.97	7	5	8	2	0.96	10	5	10	2

Table 5.18: Evaluation results for the best fitted MS and TS inference systems considering the forecast of $Q(t + 6h)$ and $Q(t + 12h)$ at gauge Kemmern (4244 km²; r: correlation coefficient; DPH [%] and DPT [h]: absolute differences of peak heights and times; \bar{x} : mean; σ : standard deviation).

Table 5.18 summarizes the optimization results of the best fitted MS and TS inference systems. For the rating of the single fuzzy inference systems correlation values as well as mean absolute differences of peak heights (DPH) and peak times (DPT) are considered. The high correlation values can be traced back to a very good performance of both inference systems considering the lower discharge range. However, as indicated by the DPH values the forecast of the peaks is slightly worse. Since the discharge is over- and underestimated, no systematic error is apparent. Figure 5.21 shows two examples for the forecast performance of the best fitted fuzzy inference systems for gauge Kemmern.

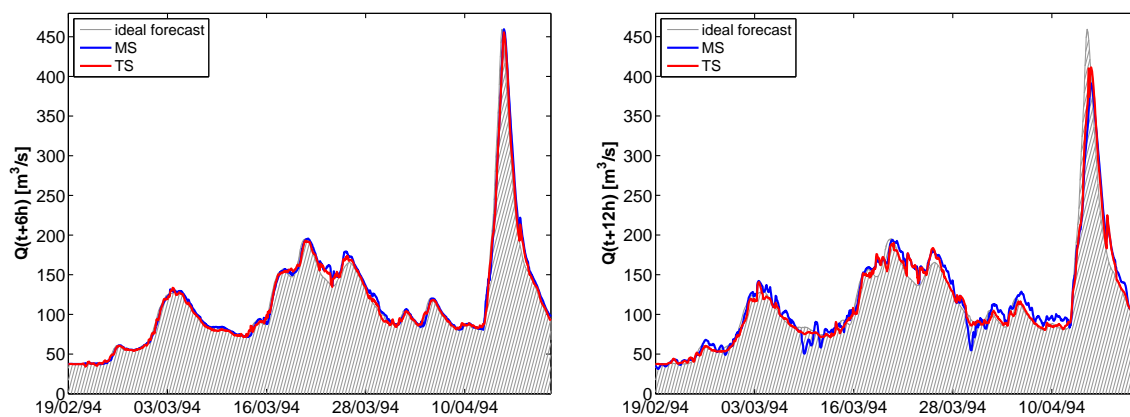


Figure 5.21: Example of a flood event simulated with the best fitted MS and TS inference systems for the 6 (left) and 12 (right) hour forecast at gauge Kemmern (4244 km²).

Indicated by the degradation of the correlation values considering MS inference systems (Figure C.6) the environmental factor discharge cannot be neglected as argument as in case of the 3

day forecast. This confirms the findings in literature. Furthermore, no TS inference systems could be optimized for this argument combination H6_3.

Performance of the optimal setups at the gauges Schwürbitz and Mainleus.

For the verification of the above presented results their transferability performance is investigated considering the two other Upper Main main gauges Mainleus (1166 km²) and Schwürbitz (2419 km²). The optimization of the MS and TS inference systems are performed as for gauge Kemmern. All arguments are described through three membership functions (statistical method). The optimizations are carried out without any further restrictions. Table 5.19 summarizes the evaluation results of the best fitted MS and TS inference systems considering the forecast of $Q(t + 6h)$ and $Q(t + 12h)$ at both gauges. Examples for the performance of the corresponding best fitted inference systems are shown in Figure C.7 and C.8.

FIS				Training					Validation				
				r	DPH		DPT		r	DPH		DPT	
					\bar{x}	σ	\bar{x}	σ		\bar{x}	σ	\bar{x}	σ
Mainleus	MS	H6_1	15 rules	0.97	4	3	5	2	0.95	10	7	5	2
		H12_1	16 rules	0.97	15	7	3	5	0.91	18	10	9	3
	TS	H6_2	7 rules	0.98	6	5	5	2	0.96	10	9	5	2
		H12_1	6 rules	0.96	13	9	7	4	0.92	17	11	9	2
Schwürbitz	MS	H6_1	21 rules	0.98	5	4	5	2	0.98	4	4	5	2
		H12_1	24 rules	0.96	14	8	8	4	0.94	13	8	8	4
	TS	H6_2	6 rules	0.98	6	5	5	2	0.96	10	6	5	2
		H12_1	6 rules	0.96	13	9	8	3	0.92	17	11	10	2

Table 5.19: Evaluation results for the best fitted MS and TS inference systems considering the forecast of $Q(t + 6h)$ and $Q(t + 12h)$ at gauges Mainleus (1166 km²) and Schwürbitz (2419 km²; r: correlation coefficient; DPH [%] and DPT [h]: absolute differences of peak heights and times; \bar{x} : mean; σ : standard deviation).

As for gauge Kemmern, no MS inference system can be trained for argument combinations H6_2 and H12_2, as well as no TS inference system for H6_1, H6_3, and H12_2 considering gauge Schwürbitz and Mainleus. Thus, the sensitive behavior of both fuzzy inference systems considering the argument combinations and the number of arguments, respectively, is confirmed. Furthermore, the same sensitivity of the SA-TS optimization process occurs as for gauge Kemmern, and for the optimization of the 3 day forecast systems.

The high correlation values can be traced back to a very good performance of both inference systems considering the lower discharge range as for gauge Kemmern. However, the forecast of the peaks is also slightly worse. Since the discharge is over- and underestimated, no systematic error within both fuzzy inference systems is apparent.

Overall, the results of gauges Schwürbitz and Mainleus verify those of gauge Kemmern. The forecast performance of the best fitted MS and TS inference systems are of comparable quality as for gauge Kemmern. No significant differences between those inference systems occur. These results also confirm the findings in literature.

Conclusions for the further investigation of the 48 h forecast.

As in case of the 3 day forecast satisfying and reliable results with respect to the 6 and 12 h forecast are achieved with both fuzzy inference systems, MS and TS, which confirm the findings in literature. Since the performances of both fuzzy inference systems are of comparable quality considering the high discharge range, they are both further investigated for the 48 h forecast.

One advantage of the MS is its much more simpler and faster setup due to the fact that less arguments have to be considered. However, looking at the lower discharge range smoother hydrographs are forecasted in case of TS due to the linear response functions. Considering the forecasted peak heights better results are achieved with the TS in some cases. This can be also traced back to the behavior of the linear response functions. In this case MS inference systems are slightly more conservative due to the definition of the response as membership functions.

5.2.4 Fuzzy inference systems for the 48 hour forecast

Since the application performances of both fuzzy inference systems are of comparable quality for the 6 and 12 h discharge forecast, both are also investigated for the 48 h forecast. However, one general problem is the limitation of arguments as it became apparent before. That means, among others, that the number of the argument forecasted areal precipitation has to be manageable in order to ensure a reasonable optimization of the rule system. Therefore, the straight forward proceeding of the 6 and 12 h forecast cannot be applied since an hourly input of the forecasted areal precipitation cannot be performed with the corresponding SA optimization setups.

In the following, the development steps for the setup of fuzzy inference systems for the 48 h forecast are exemplarily discussed for gauge Kemmern (4244 km²) since further investigations presented in Chapter 5.3 and 5.4 are also related to this gauge and forecast time horizon. Furthermore, the transferability and performance of the optimal 48 h setup is discussed considering the other two gauges Schwürbitz (2419 km²) and Mainleus (1166 km²).

Development of a fuzzification and optimization strategy.

Due to their definitions fuzzy inference systems own many degrees of freedom which have to be adjusted for modelling purposes. In a first step further fuzzification and optimization strategies are investigated beside the simplest one, which has been performed for the other forecast time horizons before. Thereby, the aim is to find an optimization strategy with which comparable fuzzy inference systems can be trained without investigating a certain number of rules for each argument combination in order to keep computation times low. This is done for both fuzzy inference systems, MS and TS, whereas for MS the following four optimization setups are compared:

MS_3MF:

This optimization setup corresponds to the setups performed for the 3 day, 6 and 12 hour forecast. The fuzzification of the arguments and the response is done with a pure statistical method (triangular shape; Figure 5.22 left). Furthermore, only the number of rules is continuously increasing by 1 from 5 to 50 and an automatic training of the whole rule systems using SA is applied. The initialisation of the whole rule system and its optimization is performed by the SA algorithm itself, whereas the shape and number of the predefined membership functions remain unaffected during the optimization process.

MS_6MF:

Except of the fuzzification method this setup corresponds to the same restrictions as MS_3MF. In this case the fuzzification is a combination of the statistical and the equally-partitioning method as it is similarly performed by Shrestha et al. (2007). Thereby, the arguments and the response are described through six membership function in a whole, considering the minimal, maximal and mean values and further three symmetric membership functions equally spaced between the minimal and maximal values (triangular shape; Figure 5.22 right).

MS_3MF_fR:

Except for one restriction considering the optimization process this setup corresponds to MS_3MF. The arguments and the response are fuzzified through three membership functions (pure statistical method). However, the responses and therefore the membership functions applied within the THEN-part are defined in advance by the user and remain unaffected during the optimization process. Only an initialisation of the IF-part (considering the arguments) and its optimization is performed by the SA algorithm, whereas the THEN-part stays untouched. The shape and number of the predefined membership functions of the arguments also remain unaffected, as before.

MS_6MF_fR:

This setup is a combination of MS_6MF and MS_3MF_fR. The arguments and the response are described through six membership functions using the combination of the statistical and equally-partitioning method (MS_6MF). Furthermore, the responses are set in advance by the user and remain unaffected during the optimization process (MS_3MF_fR).

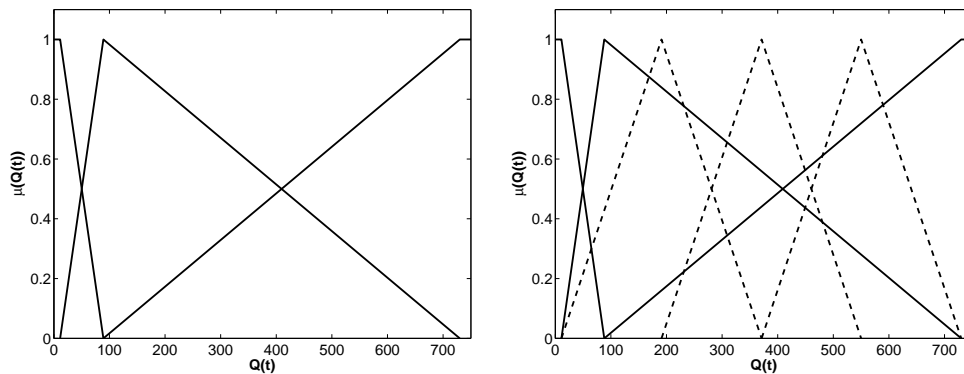


Figure 5.22: Fuzzification of the argument/response discharge performing the pure statistical method (left) and the combination of the statistical (solid lines, right) and equally-partitioning method (dashed lines, right).

For the investigation of the four different MS optimization setups two different combinations of arguments are examined (Table 5.20). These argument combinations consider the results of the daily and the 6 and 12 h forecast systems. Furthermore, 45 fuzzy inference systems (5 to 50 rules, continuously increasing by 1) are trained for each argument combination and each optimization setup. Figure 5.23 shows the development of the objective function *least-squares* (LS) and the corresponding correlation values of the training and validation sets for the four different setups considering argument combination H48_1. The same is presented in Figure 5.24 for argument combination H48_2.

5 Model development for the Upper Main basin

Argument	H48_1	H48_2
$Q(t)$	X	X
$Q_{up}(t)$	X	X
API12h(t)	X	X
mT12h(t)	X	X
API21d(t)		X
cfP(0-24h,t)	X	X
cfP(25-48h,t)	X	X
Σ	6	7

Table 5.20: Argument combinations considered for the investigation of the four MS optimization setups MS_3MF, MS_6MF, MS_3MF_fR, and MS_6MF_fR.

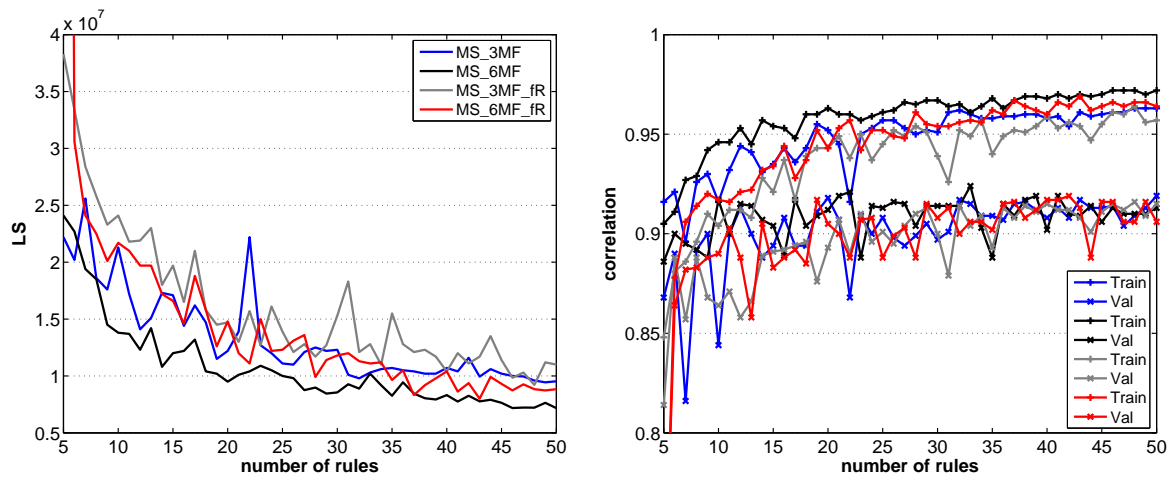


Figure 5.23: Development of the objective function least-squares (LS) and the corresponding correlation values of the training and validation sets considering the four MS optimization setups for H48_1.

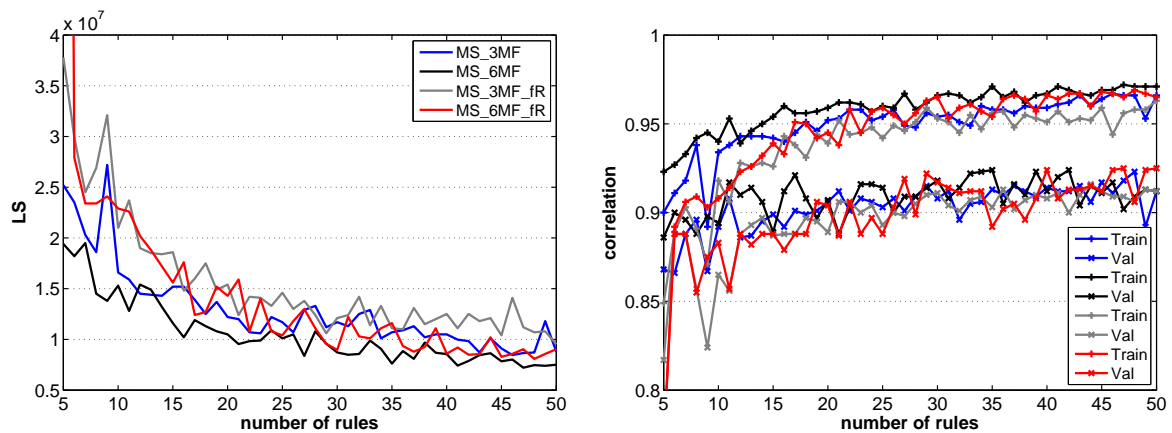


Figure 5.24: Development of the objective function least-squares (LS) and the corresponding correlation values of the training and validation sets considering the four MS optimization setups for H48_2.

Considering the LS values of both argument combinations H48_1 and H48_2, all curves show a similar shape. Furthermore, better LS values are generally achieved with optimization setup MS_6MF. However, the points where overfitting occurs cannot be determined by only considering the LS values. The overfittings of the fuzzy inference systems are recognisable by the stagnation of the correlation curves corresponding to the validation sets. Thereby, an overfitting is reached as soon as the gap between the correlation values of the training and validation set becomes larger. That means, that no improvements can be achieved by a further increase of the rule number considering the validation set. In this case, the overfitting occurs for the different optimization setups and argument combinations as soon as the correlation values of the validation set starts to oscillate around 0.90 and the gap between the correlation values of the training and validation sets are still small.

In the following, fuzzy inference systems consisting of 20 rules are considered for the comparison of the different argument combinations and MS optimization setups because these systems are around the point where overfitting occurs. Figure 5.25 shows the optimization results of the four MS setups for two out of the ten highest flood events (HQ₃ - HQ₂₀) simulated with the 20 rules fuzzy inference systems (case H48_1). It exemplarily points out that considering the ten highest flood events the peak heights are underestimated. However, one has to keep in mind that these fuzzy inference systems do not always reflect the best optimized fuzzy inference system for all investigated cases due to the restriction of 20 rules.

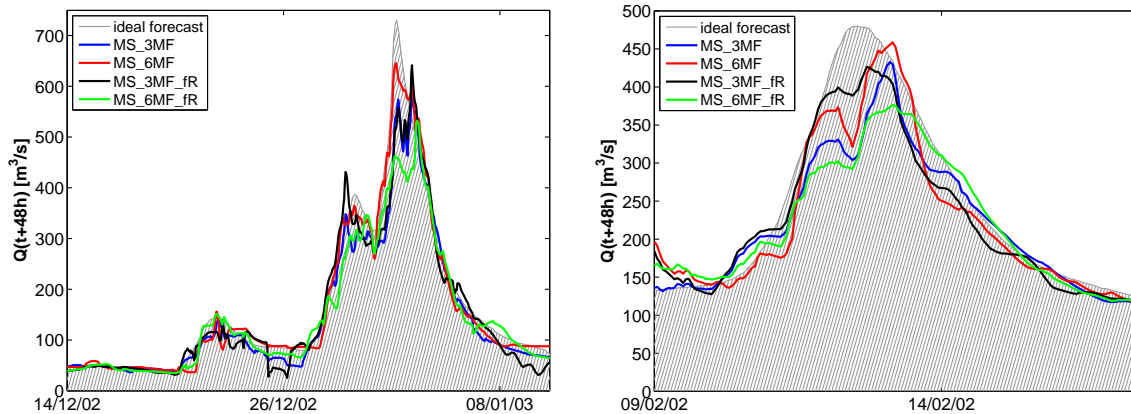


Figure 5.25: Examples for two out of the ten highest flood events simulated with with four different MS optimization setup considering 20 rules (left: training; right: validation; case H48_1).

Table 5.21 summarizes the mean absolute differences of peak heights (DPH) and peak times (DPT) considering the ideal and simulated forecast for all MS optimization setups and the two argument combinations, H48_1 and H48_2. The table shows, that no significant differences between the DPT values of the investigated argument combinations occurs except for case MS_6MF_fR H48_1. Comparing the DPH values, it becomes apparent that the performance of the two optimization setups MS_3MF_fR and MS_6MF_fR is worse than those of the others. Considering the two setups MS_3MF and MS_6MF no significant differences between the DPH values of the corresponding training and validation sets occur except for the validation set of H48_2.

Since the aim is to find an optimization strategy with which comparable fuzzy inference systems can be trained without investigating a certain number of rules for each argument combination the following restrictions are defined for the further investigations of the MS inference system based on the results presented above:

MS setup		DPH		DPT		DPH ₁₀		DPT ₁₀	
		\bar{x}	σ	\bar{x}	σ	\bar{x}	σ	\bar{x}	σ
MS_3MF	H48_1	18	17	11	10	11	10	14	9
		23	21	12	9	16	9	15	8
	H48_2	18	12	11	11	13	9	15	8
		30	20	11	9	18	11	11	12
MS_6MF	H48_1	16	14	9	11	10	5	8	9
		23	16	11	9	17	9	12	9
	H48_2	22	12	12	10	16	8	14	7
		21	17	15	8	22	9	12	8
MS_3MF_fR	H48_1	29	24	13	12	13	6	15	11
		29	23	10	9	18	8	12	10
	H48_2	25	20	12	12	16	8	15	8
		32	23	8	9	22	14	8	10
MS_6MF_fR	H48_1	21	11	15	12	22	8	23	9
		19	14	14	12	26	4	20	10
	H48_2	23	14	11	11	29	8	9	7
		23	13	16	9	27	9	17	5

Table 5.21: Evaluation results of the 20 rule MS inference systems considering the MS setup MS_3MF, MS_6MF, MS_3MF_fR, and MS_6MF_fR H48_1 as well as the argument combinations H48_1 and H48_2 (gauge Kemmern; DPH [%] and DPT [h]: absolute differences of peak heights and times; ₁₀: considering the ten highest flood events; \bar{x} : mean; σ : standard deviation; first training, second validation).

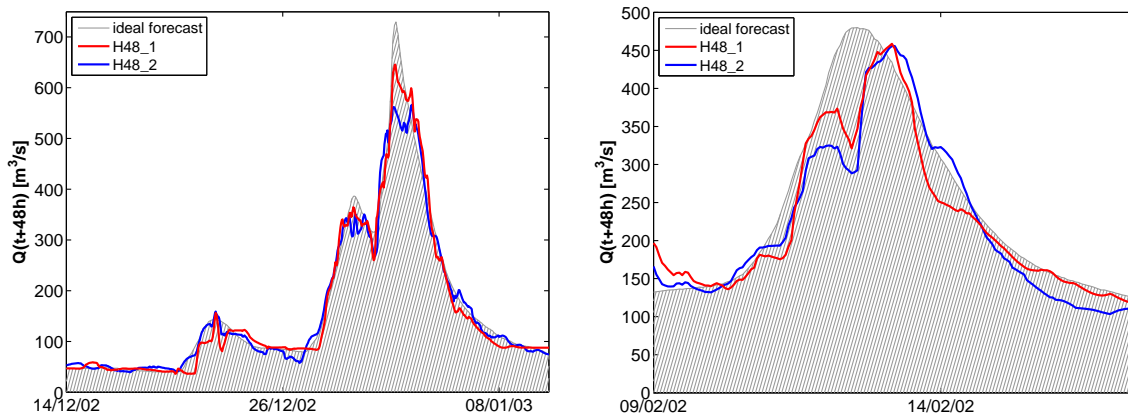


Figure 5.26: Examples for two out of the ten highest flood events simulated with the result of the MS_6MF optimization setup considering 20 rules (left: training; right: validation).

1. The argument combination H48_1 is set as the reference case for the following investigations because the corresponding values of the objective functions (LS, correlation, DPH, DPT) are slightly better for this case than for H48_2. Furthermore, the visual comparison of single simulated flood events (e.g. Figure 5.26) confirms that decision.
2. Considering further optimizations of fuzzy inference systems the MS optimization setup MS_6MF is performed because of the same reasons as in case of argument combination H48_1. That means, that the arguments and the response are fuzzified through six membership functions (Figure 5.22 right) and no restrictions for the SA optimization are defined.
3. In order to keep the number of optimizations manageable only fuzzy inference systems consisting of 20 rules are trained in the following investigations. It is assumed that those systems are around the point where overfitting occurs even if the number of arguments changes significantly. However, it has to be pointed out that these optimized fuzzy inference systems do not always reflect the best fitted systems for the corresponding argument combination and fuzzification under investigation but performs nearly as good.

Until now only the development of a fuzzification and optimization strategy for the MS fuzzy inference system is presented. However, the conclusion for the MS system cannot be directly applied for the TS inference system because of the different definition of the responses applying linear functions instead of membership functions. Furthermore, the results of the 6 and 12 hour forecasts show that different argument combinations and rule numbers have to be considered in order to find a satisfying TS inference system. Therefore, the following optimization setups together with five different argument combinations (Table 5.22) are investigated for TS:

TS_3MF:

The fuzzification of the arguments is done with a pure statistical method (triangular shape; Figure 5.22 left). Furthermore, all arguments which are based on precipitation and / or discharge are considered within both, the IF-part and the linear response functions of the THEN-part of each rule. Other arguments as time-averaged mean areal temperature occur only within the IF-part of the TS inference systems.

TS_6MF:

Except for the fuzzification method this setup corresponds to the same restrictions as TS_3MF. In this case the fuzzification is a combination of the statistical and the equally-partitioning method as it is also performed for MS_6MF and MS_6MF_fR (triangular shape; Figure 5.22 right).

TS_3MF_P:

Except for one restriction considering the IF-part of the TS inference systems this setup corresponds to TS_3MF. The arguments are fuzzified through three membership functions (pure statistical method). However, the arguments of the forecasted (cumulated) areal precipitation are only considered within the THEN-part of each rule, not within the IF-part. Arguments which are not related to precipitation and discharge are only applied within the IF-part. All other arguments are performed within the IF- and THEN-part of each rule.

TS_6MF_P:

This setup is a combination of TS_6MF and TS_3MF_P. The arguments are described through six membership functions using the combination of the statistical and equally-partitioning method (TS_6MF). The consideration of arguments within the IF- and THEN-part is identical to setup TS_3MF_P.

Argument	H48_1	H48_2TS	H48_3TS	H48_4TS	H48_5TS
Q(t)	X	X	X	X	X
Q _{up} (t)	X	X	X		
API12h(t)	X	X	X	X	X
mT12h(t)	X	X	X	X	X
cfP(0-24h,t)	X	X			
cfP(0-12h,t)			X	X	X
cfP(13-24h,t)			X	X	X
cfP(25-48h,t)	X				
cfP(25-36h,t)		X	X	X	X
cfP(37-42h,t)		X	X	X	
cfP(43-48h,t)		X			
cfP(37-48h,t)					X
fP(t+43h) to fP(t+48h)			X	X	
Σ	6	8	14	13	7

Table 5.22: Argument combinations considered for the investigation of four different TS optimization setups TS_3MF, TS_6MF, TS_3MF_P, and TS_6MF_P (H48_1: only argument combination which is also investigated for the MS setups).

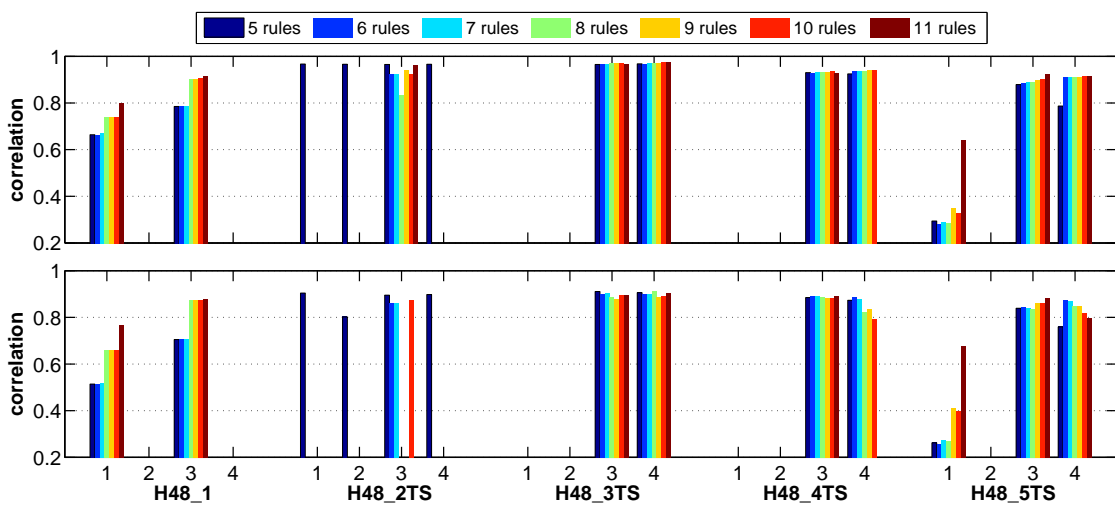


Figure 5.27: Correlation values of the seven TS inference systems (5 to 11 rules) trained for each argument combination H48_X (X: 1, 2TS, 3TS, 4TS, 5TS) and optimization setup (1: TS_3MF; 2: TS_6MF; 3: TS_3MF_P; 4: TS_6MF_P; top: training; bottom: validation).

Based on the results of the 6 and 12 hour forecast, seven TS inference systems (5 to 11 rules, continuously increasing by 1) are trained and validated for each argument combination and optimization setup. The initialisation of the whole rule system and its optimization are performed by the SA algorithm itself, whereas the shape and number of the predefined membership functions remain unaffected during the optimization process. The resulting correlation values of the training and validation phase are shown in Figure 5.27.

Figure 5.27 shows that in many cases no TS inference system can be optimized with the performed SA-TS setup (no bars) and that partly large differences considering the increasing rule number of one setup and argument combination occur (compare H48_1). Only in case of setup TS_3MF_P rule systems can be trained and validated for each argument combination, but not always for all considered rules (compare H48_2TS). However, it has to be emphasized that not all responses can be simulated for those fuzzy inference systems optimized with TS_3MF_P although the correlation values indicate satisfying optimization results in some cases. Only for argument combination H48_3TS together with the TS setups TS_3MF_P (5, 6, 7, 9, 10, 11 rules) and TS_6MF_P (5, 7, 9, 10, 11 rules) all responses can be satisfyingly simulated.

Based on the results shown in Figure 5.27 no point where overfitting occurs can be determined. In particular, considering H48_1 TS_3MF_P it seems that with a further increase of rules the point where overfitting occurs can be detected. Therefore, further 14 fuzzy inference systems (12 to 25 rules, continuously increasing by 1) are trained and validated for case H48_1 TS_3MF_P. The same is done for case H48_3TS TS_3MF_P, since the best optimization results are achieved with this combination. Figure 5.28 shows the resulting development of the objective function of the SA optimization (LS) and the corresponding correlation values for both cases.

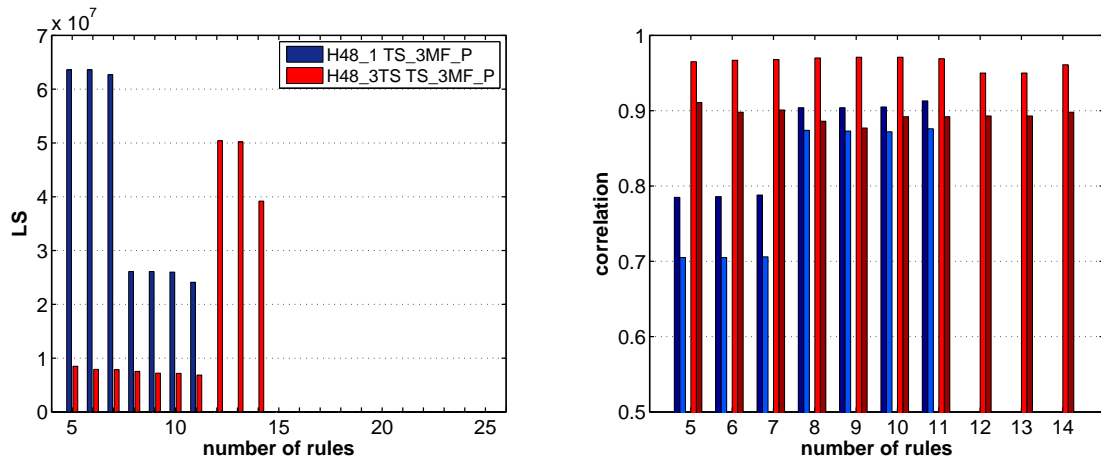


Figure 5.28: Development of the objective function least-squares (LS , left) and the corresponding correlation values (right) considering H48_1 TS_3MF_P and H48_3TS TS_3MF_P (left bar of one color: training, right bar: validation).

As indicated by the development of the LS values no TS inference system can be trained for a rule number higher than 14 in both cases (no bars). Therefore, no improvement of the fuzzy rule systems can be achieved with a further increase of rules. However, not all responses can be simulated with the remaining fuzzy inference systems although the correlation values indicate satisfying optimization results. Thereby, the number of false simulated responses responds very sensitive to changes considering the rule number. In this case, it is advisable to train TS inference systems in the range of at least 8 to 11 rules performing the TS_3MF_P and SA-TS optimization setup,

5 Model development for the Upper Main basin

if different argument combinations are investigated for the 48 hour forecast in order to achieve a satisfying base for comparisons. However, this comes along with very high computation and evaluation times which make the performance of the TS fuzzy inference systems less attractive for further investigations within this work.

Since the aim is to find an optimization strategy with which comparable fuzzy inference systems can be trained without investigating certain rule numbers for each argument combination no general restrictions as in case of the MS inference system can be defined for TS inference systems. The main reason for this is the high sensitivity of the chosen SA-TS setup to changes considering the number of rules and argument combination which requires the investigation of a range of rules and consequently very high computation times. That means that the number of rules should be continuously increasing by 1 until no rule system could be optimized (compare Figure 5.28). Consequently, the investigation of different argument combinations is difficult to perform. For this reason the performance of the TS inference system and SA-TS system, respectively, is rejected for further investigations within the framework of this thesis, although the application performance of the TS (H48_3TS TS_3MF_P, 6 rules) and the MS (H48_1 MS_6MF, 20 rules) systems are of comparable quality (Figure 5.29, Table 5.23).

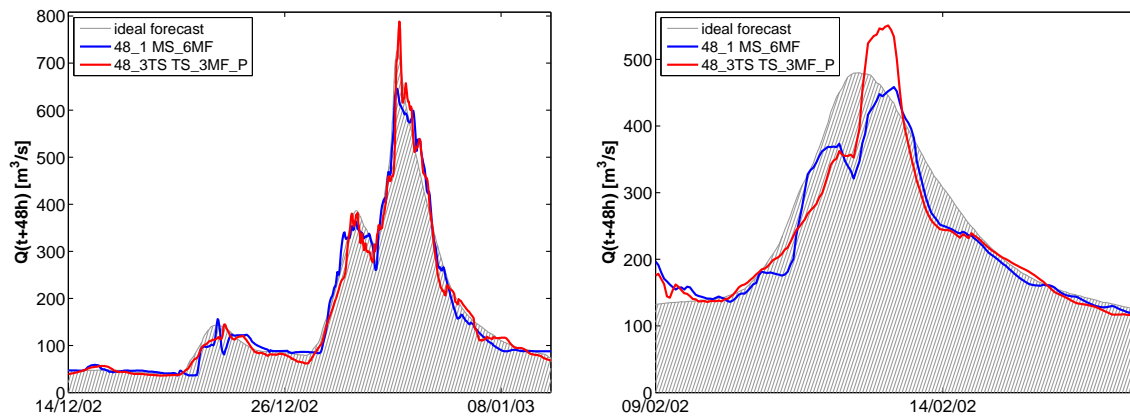


Figure 5.29: Examples for two out of the ten highest flood events (left: training; right: validation) simulated with the reference case of the MS optimization setup (H48_1 MS_6MF, 20 rules) and the best fitted TS inference system (H48_3TS TS_3MF_P, 6 rules).

FIS			r	DPH		DPT		DPH ₁₀		DPT ₁₀	
				\bar{x}	σ	\bar{x}	σ	\bar{x}	σ	\bar{x}	σ
MS_6MF	H48_1	20 rules	0.96	16	14	9	11	10	5	8	9
			0.91	23	16	11	9	17	9	12	9
TS_3MF	H48_3TS	6 rules	0.97	14	12	11	13	8	6	9	8
			0.90	30	16	14	10	20	4	20	10

Table 5.23: Evaluation results of the MS reference case (H48_1 MS_6MF, 20 rules) and the best fitted TS inference system (H48_3TS TS_3MF_P, 6 rules) considering the 48 h forecast (gauge Kemmern; DPH [%] and DPT [h]: absolute differences of peak heights and times; ₁₀: considering the ten highest flood events; \bar{x} : mean; σ : standard deviation; first training, second validation).

Investigation of different argument combinations performing the MS inference system MS_6MF, 20 rules.

As presented before, the chosen SA-TS optimization setup is not really suitable for a comprehensive investigation of different argument combinations within the framework of this thesis because of its sensitivity considering changes of rule number and argument combinations. Therefore, only MS inference systems are performed for further investigations of different argument combinations in order to (1) improve the direct 48 hour discharge forecast $Q(t + 48h)$ and (2) to investigate the influence of the argument $Q_{up}(t)$. Thereby, the MS inference system H48_1 MS_6MF (20 rules) is set as the reference case for the evaluation of the forecast improvement. Table 5.24 summarizes some of the investigated argument combinations including the reference case H48_1.

Argument	H48_																
	1	2	3	4	5	6	7	8	9	10	11	12	13	14	15	16	17
Q(t)	X	X	X	X	X	X	X	X	X	X	X	X	X	X	X	X	X
$Q_{up}(t)$	X	X	X	X	X	X											
API12h(t)	X	X	X	X	X	X	X	X	X	X	X	X	X	X	X	X	X
mT12h(t)	X	X	X	X	X	X	X	X	X	X	X	X	X	X	X	X	X
API21d(t)		X						X		X	X	X	X	X	X	X	X
snowst(t)			X						X								
cfP(0-24h,t)	X	X	X	X	X	X	X	X	X	X	X	X	X	X			
cfP(0-12h,t)															X	X	X
cfP(13-24h,t)															X	X	X
cfP(25-48h,t)	X	X	X				X	X	X								
cfP(25-42h,t)				X						X			X				
cfP(25-36h,t)					X	X				X	X		X	X	X	X	X
cfP(37-42h,t)						X					X		X		X	X	X
cfP(43-48h,t)				X		X				X		X				X	
cfP(37-48h,t)					X						X				X		
fP(t+43h) to fP(t+48h)													X	X			X
Σ	6	7	7	7	7	8	5	6	6	7	7	8	12	14	8	9	14

Table 5.24: Argument combinations investigated for an improvement of the 48 h forecast performing the MS inference system MS_6MF, 20 rules.

For each argument combination a 20 rule MS inference system is trained and validated performing the MS_6MF optimization setup in order to ensure comparable results. The correlation, NS, DPH and DPT values are shown in Figure 5.30. In case of H48_7 not all responses within the low and medium discharge range can be simulated with the optimized MS inference system, which is why the results of the 19 rule MS inference system are given in Figure 5.30 (marked with *) instead.

The partly large differences between the objective function values of the training and validation phase can be mainly traced back to the restrictions of the optimization setup MS_6MF 20 rules. For some cases an overfitting of the fuzzy inference systems considering the training data set already occurs. Therefore, the focus of the performance comparison of different argument combinations lies on the objective function values of the validation data set and on the visual comparison of the simulated hydrographs.

5 Model development for the Upper Main basin

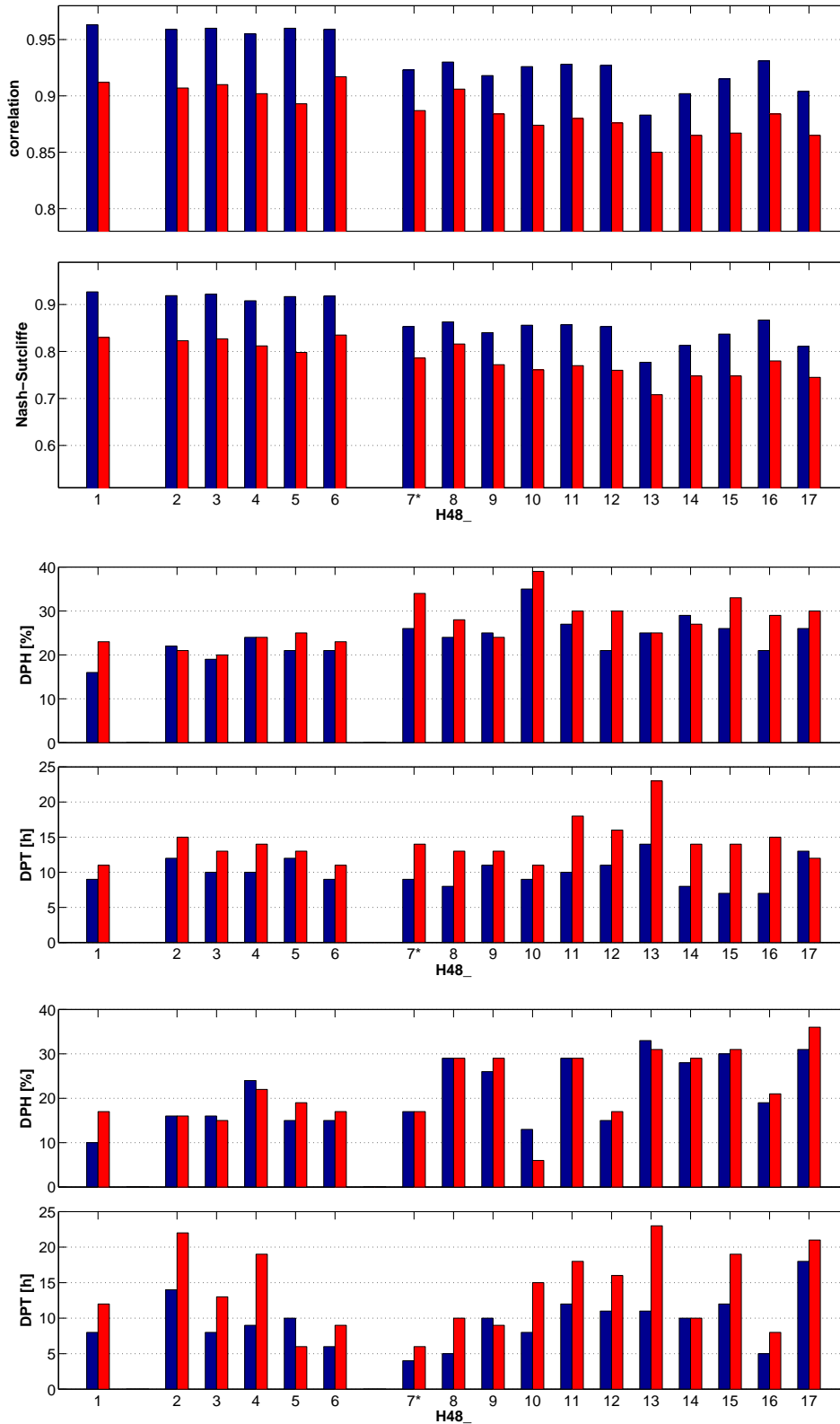


Figure 5.30: Correlation, NS, DPH and DPT values for each investigated argument combination H48_1 to H48_17 performing the MS_6MF (20 rules) optimization setup (last two: considering the ten highest flood events, otherwise all 30 flood events; blue: training; red: validation; *: 19 rules).

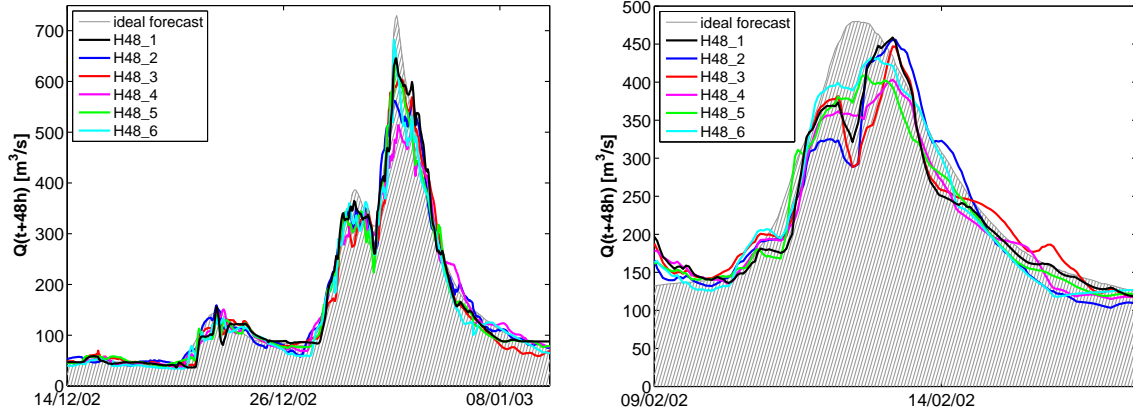


Figure 5.31: Examples for two out of the ten highest flood events simulated with the argument combinations H48_1 to H48_6 (MS_6MF 20 rules; left: training; right: validation).

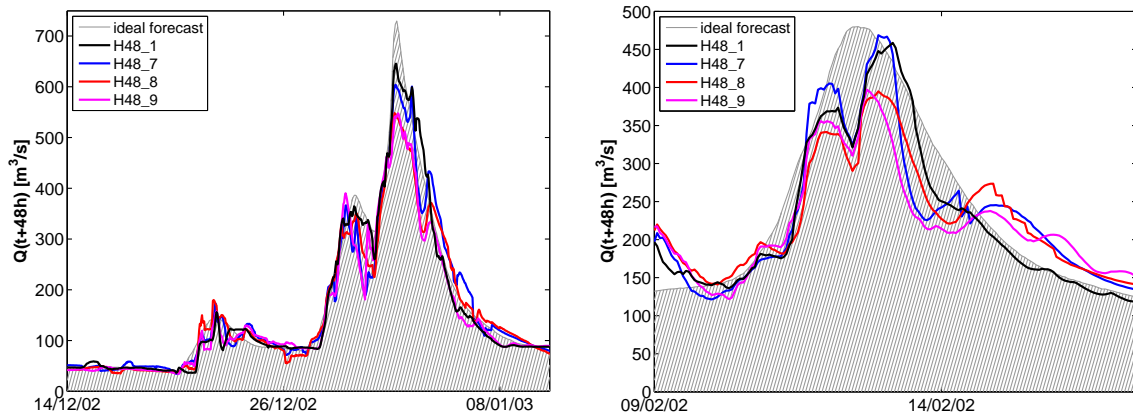


Figure 5.32: Examples for two out of the ten highest flood events simulated with the argument combinations H48_1 and H48_7 to 9 (MS_6MF 20 rules; in case of H48_7: 19 rules; left: training; right: validation).

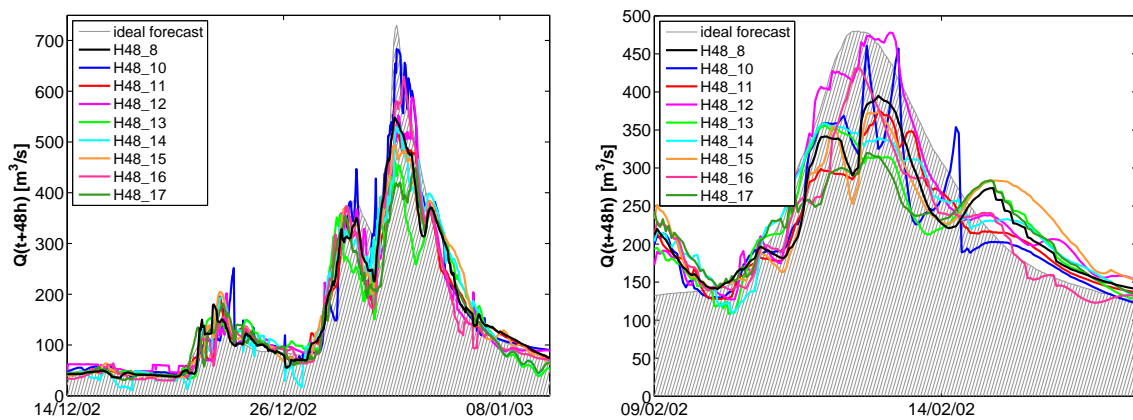


Figure 5.33: Examples for two out of the ten highest flood events simulated with the argument combinations H48_8 and H48_10 to 17 (MS_6MF 20 rules; left: training; right: validation).

5 Model development for the Upper Main basin

Comparing the results of the argument combinations H48_1 to H48_6 no significant differences occur except for the DPT values considering the 10 highest flood events. Furthermore, the performance of the fuzzy inference systems are of comparable quality. No significant improvements of the 48 hour forecast can be achieved by considering (1) the arguments $API21d(t)$ (H48_2) or $snowst(t)$ (H48_3) or (2) a finer temporal discretized forecast of the cumulated areal precipitation (H48_3 to 6) in this case. The visual evaluation of the simulated hydrographs confirms these results (Figure 5.31). The fluctuations of the hydrograph from one to another time step occur due to the fact that the simulated time steps are independent from each other.

The significant difference between H48_1 to 3 and H48_7 to 9 is that the argument $Q_{up}(t)$ is ignored. Consequently, a general degradation of the forecast performance occurs for all flood events. Comparing the 10 highest flood events the performance of H48_1 and H48_7 is of comparable quality. However, DPH values of up to 131% occur for smaller single flood events in case of H48_7.

Considering the results of all flood events, the general degradation of the forecast systems can be slightly attenuated by performing argument $API21d(t)$ (H48_8), whereas the consideration of argument $snowst(t)$ has no influence (Figure 5.32). Therefore, argument combination H48_8 is investigated in more detail by considering finer temporal discretized forecasts of the cumulated areal precipitation (H48_10 to 17). However, no significant improvement of the forecast system H48_8 is achieved by applying finer temporal discretized forecasts of the cumulated areal precipitation (Figure 5.30, 5.33).

Summarizing the results presented above, the MS setup MS_6MF H48_1 is still one of the best fitted systems for the simulation of the whole range of flood events. Therefore, it is further considered as the reference case. However, MS inference systems of comparable quality can be optimized considering the argument combinations H48_2 to 6. Therefore, these systems are also further considered within Chapter 5.3 beside H48_1. Furthermore, it has been proven that the information content of the argument $Q_{up}(t)$ is essential for the 48 hour forecast with MS fuzzy inference systems in this case. A disregard of this argument results in a general degradation of the forecast quality of the MS inference systems as in case of the daily forecast. Finally, a general improvement of the MS forecast systems considering all flood events and the performance of finer temporal discretized forecasts of the cumulated areal precipitation cannot be proven in this case. Even considering only the 10 highest flood events, no significant improvement with respect to DPH and DPT can be detected except for DPH of case H48_10.

Performance of the ideal 48 h setup at gauges Schwürbitz and Mainleus.

In order to verify the results of the 48 hour forecast at gauge Kemmern, the transferability of the optimal MS inference system MS_6MF H48_1 is investigated considering the gauge Schwürbitz (2419 km²). Since no single gauge within the main Upper Main river is located more than 30 km upstream of gauge Mainleus (1166 km²) the MS setup MS_6MF H48_1 cannot be verified at this gauge. In fact two gauges within the tributaries White and Red Main (Unterzettlitz and Ködnitz, Figure 5.1) are located upstream. However, these gauges are situated very closely to gauge Mainleus. A forecast system considering these two gauges would not make much sense. Therefore, the current discharges at these gauges are not considered as arguments for the MS inference system and argument combination H48_7 (Table 5.24) is verified for gauge Mainleus instead.

Considering gauge Schwürbitz it turns out that argument combination H48_1 has to be slightly modified (H48_1m) in order to ensure a satisfying 48 hour forecast performance. Thereby, the arguments $API12h(t)$ and $mT12h(t)$ of the original setup have to be replaced with the arguments $API6h(t)$ and $mT6h(t)$. Reasons for this are the reduced catchment size and changed catchment characteristic. Furthermore, the assumption that a satisfying forecast performance can be achieved with a 20 rule system is no longer adequate. In this case 37 rules are needed. Among others this can be traced back to the fact that the flood events are more diverse (shape, duration) considering gauge Schwürbitz than in case of gauge Kemmern. However, with the modified setup a MS inference system can be trained, which is of comparable quality as in case of gauge Kemmern (Table 5.25, Figure 5.34 left).

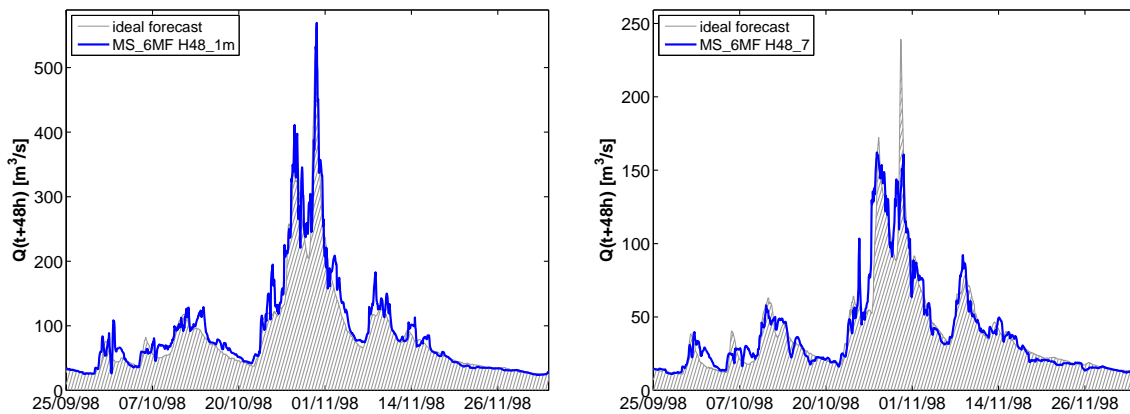


Figure 5.34: Examples for the 48 hour forecast at gauges Schwürbitz (2419 km², left) and Mainleus (1166 km², right).

FIS			r	DPH		DPT		DPH ₁₀		DPT ₁₀	
				\bar{x}	σ	\bar{x}	σ	\bar{x}	σ	\bar{x}	σ
Schwürbitz	H48_1m	37 rules	0.93	20	18	9	7	15	12	4	4
			0.90	16	15	8	5	10	9	5	5
Mainleus	H48_7	36 rules	0.92	24	15	8	9	23	13	7	5
			0.85	26	19	10	10	26	17	7	10

Table 5.25: Evaluation results for the best fitted MS_6MF inference systems considering the 48 h forecast at the gauges Schwürbitz (2419 km²) and Mainleus (1166 km²; r: correlation coefficient; DPH [%] and DPT [h]: absolute differences of peak heights and times; ₁₀: considering the ten highest flood events; \bar{x} : mean; σ : standard deviation; first training, second validation).

Because of missing information given by argument $Q_{up}(t)$ the performance of the forecast system Mainleus (MS_6MF, H48_7) is degraded in comparison to the MS inference systems Schwürbitz and Kemmern (Table 5.25, Figure 5.34 right). In particular, larger errors occur considering the forecast of peak heights. Even if the argument combinations are slightly modified, as in case of gauge Schwürbitz, or a finer temporal resolution of the forecasted mean areal precipitation are considered, no improvements can be achieved in this case. This in turn confirms the results of the investigations at gauge Kemmern. Furthermore, more rules have to be optimized in case of gauge Mainleus (H48_7) in order to ensure a optimization result of comparable quality to gauge Kemmern (H48_7).

In contrast to the investigation results of the 3 day, 6 and 12 hour forecasts appropriate argument

5 Model development for the Upper Main basin

combinations for gauge Kemmern cannot be directly transferred to other gauges considering the 48 hour forecast. However, they can be considered as a base on which 48 hour forecast systems of other gauges can be adapted to current catchment characteristics. Thereby, the temporally modification of arguments (e.g. $API6h(t)$ instead of $API12h(t)$) as well as the modification of the number of rules should be taken into account.

In order to reduce the performance degradation, if upstream discharge informations are missing (compare gauge Mainleus), a more detailed investigation should be carried out considering spatial distributed instead of mean areal environmental factors. Disse et al. (2009) presented one possible approach for the consideration of spatial distributed information. However, their approach results in much more complex forecast systems than those presented in this work because the forecast at single gauges is based on a forecast chain. Considering the philosophy of the developed warning system ExpHo-HORIX (Chapter 6) this approach is not adequate in this case due to its complexity.

5.3 Mamdani inference system and Tukey depth function

With the help of Tukey depth (Chapter 3.4) current argument conditions of flood events can be characterized as ordinary or unusual. Thereby, seldom argument conditions own very small depth values as they are interpreted as outliers, whereas common ones own high depth values. Furthermore, low Tukey depth values correspond not necessarily to seldom conditions considering the target variable $Q(t + 48h)$. Nevertheless, Tukey depth function is investigated as a possible source of information considering MS inference systems in the framework of this thesis. First, it is considered as an additional argument within the MS inference systems in order to improve their 48 hour forecast ability, in particular, the forecast of the ten highest flood events. Second, the general extrapolation behavior of MS inference systems is investigated based on Tukey depth. As mentioned in Chapter 5.2.4 these investigations are only performed for the 48 hour forecast at gauge Kemmern (4244 km²) and presented in the following.

5.3.1 Tukey depth of different argument combinations

Considering the 48 h forecast time horizon MS inference systems of comparable quality can be set up with the argument combinations H48_1 to H48_6 (Table 5.24, Chapter 5.2.4) at gauge Kemmern. Although case H48_1 is set as the reference case, the other five argument combinations are also investigated in conjunction with Tukey depth as their corresponding depth values differ from each other due to the combination of different arguments. For the determination of the different depth values the ideal forecasted 48 hour discharge at gauge Kemmern, which is equal to the measured one, is considered as the target variable. The depth values themselves are calculated based on the corresponding argument values for the different argument combinations separately. Thereby, the data of all 30 flood events are considered as one data set and no differentiation between a training and validation set is made.

Figure 5.35 shows exemplarily the target variable $Q(t + 48h)$ plotted via the Tukey depth values considering the argument combinations H48_1 or H48_2. Comparing both plots, almost no differences with respect to the general shape of the scatterplot are recognisable. However, it is apparent that not only extreme discharges at gauge Kemmern correspond to a depth value of nearly zero, but also ordinary smaller ones. This fact occurs due to the multi-dimensional investigation of the argument combination. Therefore, unusual (extreme) events can be detected not necessarily for the target variable $Q(t + 48h)$ but for one argument of the argument combination under investigation. This is exemplarily shown in Figure 5.36 for case H48_1. On the left side, the argument $Q_{up}(t)$ is plotted via the target variable $Q(t + 48h)$, whereas on the right the argument $API12h(t)$ is plotted via the target variable. The color of the markers represents the corresponding depth values (log-scaled). Although the multi-dimensional behavior of Tukey depth is extremely reduced within such projections it can be recognised that extreme discharges at gauge Kemmern are not inevitably related to extreme discharges at its upstream gauge Schwürbitz (left plot), but to an extreme situation considering the other argument $API12h(t)$ (right plot).

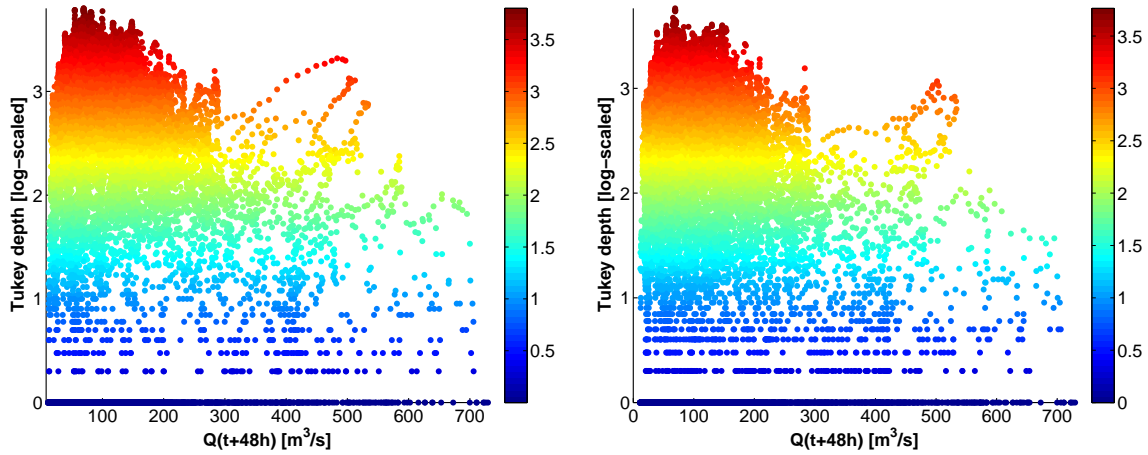


Figure 5.35: Target variable $Q(t + 48h)$ plotted via log-scaled Tukey depth values considering the argument combinations H48_1 (left) or H48_2 (right; marker color represents the corresponding log-scaled depth values).

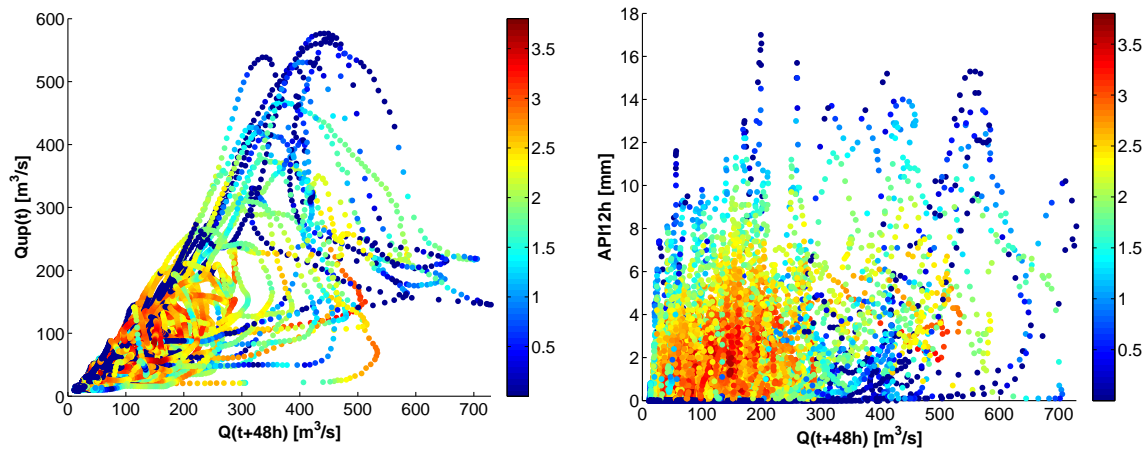


Figure 5.36: $Q_{up}(t)$ (left) and $API12h(t)$ (right) plotted via the target variable $Q(t + 48h)$ considering case H48_1 (marker color represents the corresponding log-scaled depth values).

5.3.2 Investigation of Tukey depth as an argument

In order to improve the 48 hour MS forecast systems of argument combinations H48_1 to H48_6 (Chapter 5.2.4), in particular, considering the ten highest flood events, Tukey depth values are taken into account as an additional source of information. Hereby, the assumption is investigated if the performance of the argument *Tukey depth* causes a shift within the rule system so that less rules are considered for the description of ordinary argument conditions and more for unusual ones. Since a classification of argument conditions (ordinary or unusual) can be performed based on depth values a fuzzification using only two membership functions seems more adequate than that of the before developed strategy MS_6MF (Chapter 5.2.4). Therefore, two different fuzzification strategies considering Tukey depth are investigated in addition to MS_6MF in a first step. Furthermore, in order to keep the number of optimizations manageable and based on the previously shown results (Chapter 5.2.4), it is assumed that MS inference systems consisting of 20 rules are still around the point where overfitting occurs, even if the fuzzification strategy of one single argument changes. The different optimization strategies can be summarized as follows:

MS_T1:

This optimization setup corresponds to the optimal one performed for the setup of 48 hour MS forecast systems (MS_6MF, Chapter 5.2.4). The fuzzification of all arguments, including *Tukey depth*, is a combination of the statistical and the equally-partitioning method (triangular shape; Figure 5.37 top).

MS_T2:

Except for the fuzzification method considering the argument *Tukey depth*, this setup corresponds to the same restrictions as MS_T1. In this case, only the argument *Tukey depth* is fuzzified through two instead of six membership functions based on the visual interpretation of projections as shown in Figure 5.35 and 5.36. Since high discharges considering $Q(t + 48h)$ own depth values of 0 to around 50 and not significant higher depth values, two membership functions are defined in order to represent this boundary. Thereby, one is defined as $(0,10,50)_T$ which corresponds to high discharges, whereas the other completes the whole range of depth values (triangular shape; Figure 5.37 bottom left). The fuzzification of the other arguments and the response is still performed with the combination of the statistical and the equally-partitioning method.

MS_T3:

In this setup a further fuzzification of the argument *Tukey depth* is performed. Considering the definition of Tukey depth, outliers are generally marked by a depth value of zero. Therefore, the fuzzification of the argument *Tukey depth* as shown in Figure 5.37 (bottom right) is investigated. With this fuzzification a clear boundary instead of a smooth transition as in case of MS_T2 is defined. Note that due to rounding errors occurring within the depth algorithm the boundary is not set between 0 and 1 according to the mentioned definition of outliers, but between 1 and 2. The other arguments and the response are again fuzzified with the combination of the statistical and the equally-partitioning method.

For the investigation of the different fuzzification approaches a 20 rule MS inference system is optimized for each argument combination H48_1 to H48_6. Furthermore, an automatic training of the whole rule systems using SA is performed without any further restrictions. The initialisation of the whole rule system and its optimization is performed by the SA algorithm itself, whereas the shape and number of the predefined membership functions remain unaffected during the optimization process.

For the investigated setups the corresponding correlation and NS values considering all 30 flood events as well as the resulting DPH and DPT values considering only the ten highest flood events are shown in Figure 5.38. For comparison, the results of the corresponding MS_6MF 20 rule MS inference systems without considering Tukey depth are additionally given in both figures. In the case of H48_4 MS_T2 and MS_T3 not all responses of the validation set can be simulated with the corresponding optimized 20 rule MS inference system, which is why the results of the 19 rule MS inference systems are shown in Figure 5.38 instead.

The partly large differences considering the objective function values of the training and validation phase can mainly be traced back to the general restriction of 20 rules. That means, that for some cases an overfitting of the MS inference systems considering the training data set already occurs.

5 Model development for the Upper Main basin

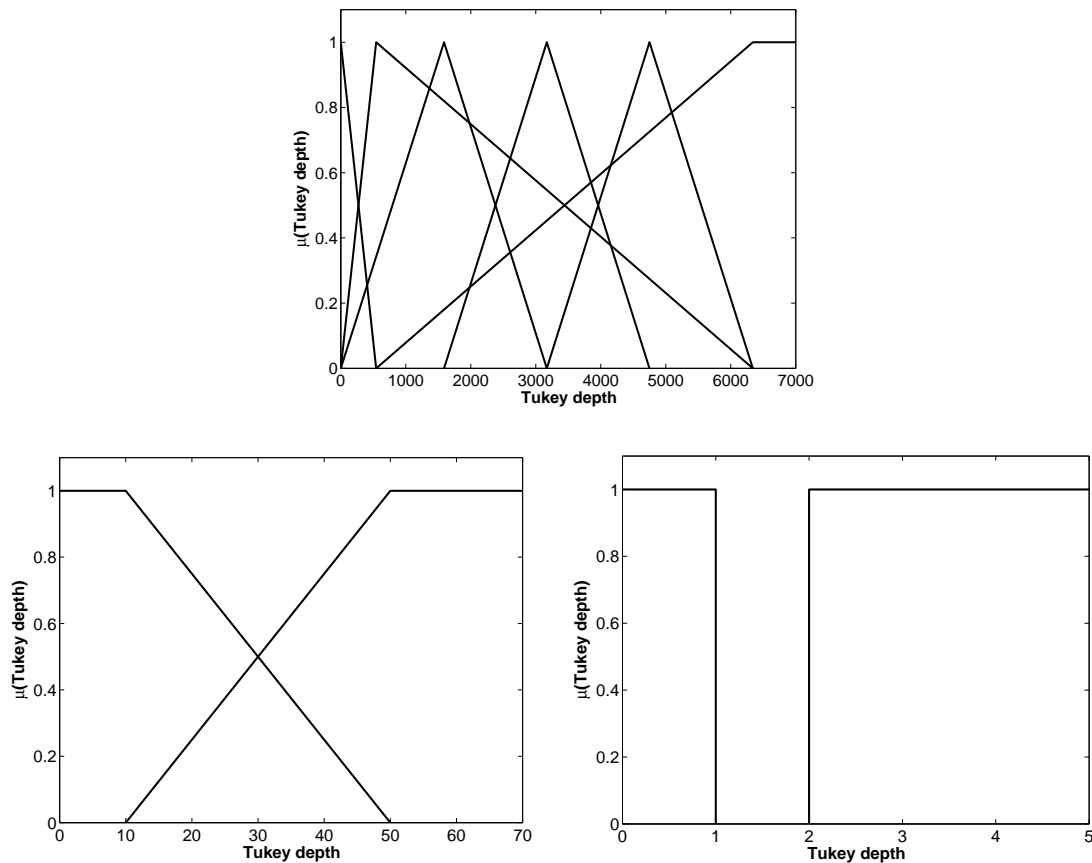


Figure 5.37: Fuzzifications of the argument *Tukey depth* considering optimization setups MS_T1 (top), MS_T2 (bottom left), and MS_T3 (bottom right).

Comparing the correlation and NS values of the different fuzzification setups MS_6MF, MS_T1, MS_T2, and MS_T3 for case H48_1 no significant differences can be detected. The visual evaluation of the flood hydrographs confirms this result (Figure 5.39). Furthermore, these MS inference systems represent all 30 as well as the ten highest flood events of comparable quality and more satisfying than the other ones. No significant improvement of reference case MS_6MF H48_1 can be achieved by any other argument combination and MS_T1 to MS_T3 setup.

However, considering only the ten highest flood events the fuzzification strategy MS_T3 of H48_1 reproduces the flood peak slightly better than H48_1 MS_6MF, but has some drawbacks with the satisfying simulation of smaller flood events. This can be traced back to the restriction of 20 rules. In the case of H48_1 MS_6MF 8 of 20 rules are set up by the SA algorithm for the description of high discharges, whereas 12 rules define the conditions of small (9 rules) and medium (3 rules) discharges. In contrast to this, only 6 and 4 rules are optimized for the simulation of small and middle discharges in case of H48_1 MS_T3 as the corresponding argument conditions are marked as ordinary through the argument *Tukey depth*. For the unusual conditions 10 rules are optimized, and consequently improvements considering the simulation of the highest discharges are achieved with the described shift within the optimized rule system.

Although, no general improvement of the 48 hour forecast of discharge considering all 30 flood events could be achieved with the setups MS_T1, MS_T2, and MS_T3, a further investigation with another fuzzification strategy is reasonable. Since the arguments $Q(t)$ and $Q_{up}(t)$ have a

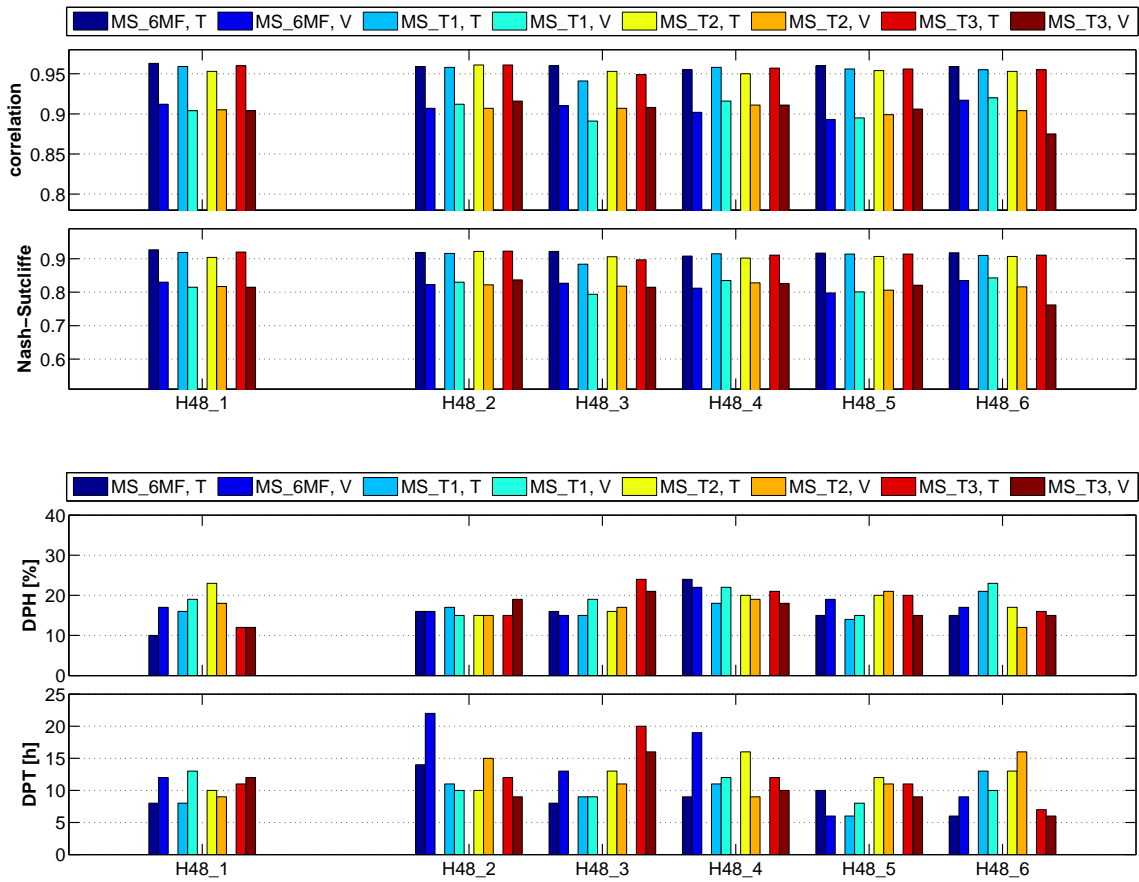


Figure 5.38: Correlation and NS values considering all 30 flood events as well as DPH and DPT values considering the ten highest flood events for each investigated argument combination H48_1 to H48_6 performing the optimization setups MS_6MF, MS_T1, MS_T2, and MS_T3 (T: training; V: validation).

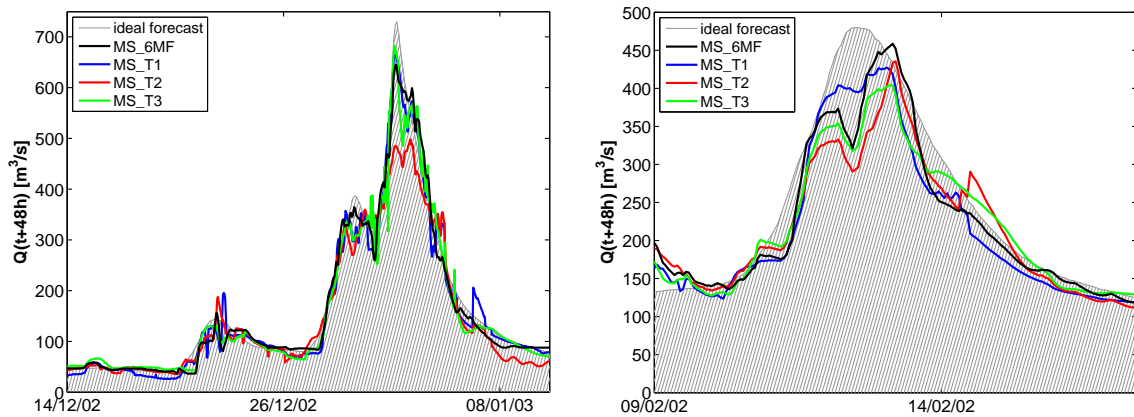


Figure 5.39: Examples for two out of the ten highest flood events simulated with the argument combination H48_1 and the different optimization setups MS_6MF, MS_T1, MS_T2, and MS_T3 (left: training; right: validation).

great impact on the forecast quality of the MS inference systems, these two arguments are additionally considered within an extended fuzzification strategy. Thereby, further two membership functions are defined based on Tukey depth scatterplots (Figure 5.35, 5.36). Considering argument $Q(t)$ the membership functions $(-\infty, 400, 500)_T$ and $(300, 400, \infty)_T$, considering argument $Q_{up}(t)$ the membership functions $(-\infty, 300, 400)_T$ and $(300, 400, \infty)_T$ are added (Figure 5.40 solid lines). Since the argument $Q(t)$ and the response $Q(t + 48h)$ are the same environmental factor, the modification considering the extended fuzzification holds for both. The new fuzzifications of $Q(t)$ and $Q_{up}(t)$ are investigated together with the argument *Tukey depth* in the following setups:

MS_T4:

Except for the fuzzification of the arguments $Q_{up}(t)$ and $Q(t)$, this optimization setup corresponds to optimization setup MS_T1: Tukey depth is fuzzified through six (Figure 5.37 top), $Q(t)$ and $Q_{up}(t)$ are fuzzified through eight (Figure 5.40) instead of six (Figure 5.22 right) membership functions. All other arguments are still defined by six membership functions (Figure 5.22 right).

MS_T5:

This optimization setup is a combination of MS_T2 and MS_T4. Tukey depth is defined by two (Figure 5.37 bottom left), $Q(t)$ and $Q_{up}(t)$ by eight (Figure 5.40), and all other by six membership functions (Figure 5.22 right).

MS_T6:

Except for the fuzzification of the argument Tukey depth this optimization setup is identical to MS_T5. Tukey depth is fuzzified as in case MS_T3 (two membership functions, Figure 5.37 bottom right).

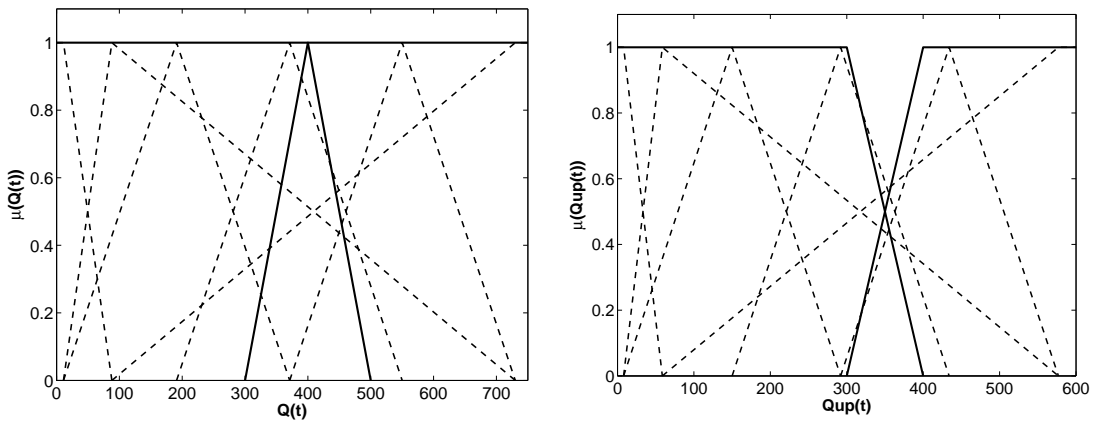


Figure 5.40: Extended fuzzification of the argument / response $Q(t)$ (left) and argument $Q_{up}(t)$ (right) for the investigations of the optimization setups MS_T4, MS_T5, and MS_T6.

For the investigation of the different extended fuzzification strategies a 20 rule MS inference system is optimized for each argument combination H48_1 to H48_6 without any further restrictions as for MS_T1 to MS_T3. Figure 5.41 presents the corresponding correlation and NS values considering all 30 flood events as well as the resulting DPH and DPT values considering only the ten highest flood events. For comparison, the results of the corresponding MS_6MF 20 rule systems are also given in the figures. Except for H48_3 MS_T6, satisfying 20 rule MS inference systems are optimized and all responses of the training and validation sets can be simulated. For H48_3 MS_T6 the results of the 19 rule MS inference system are shown instead.

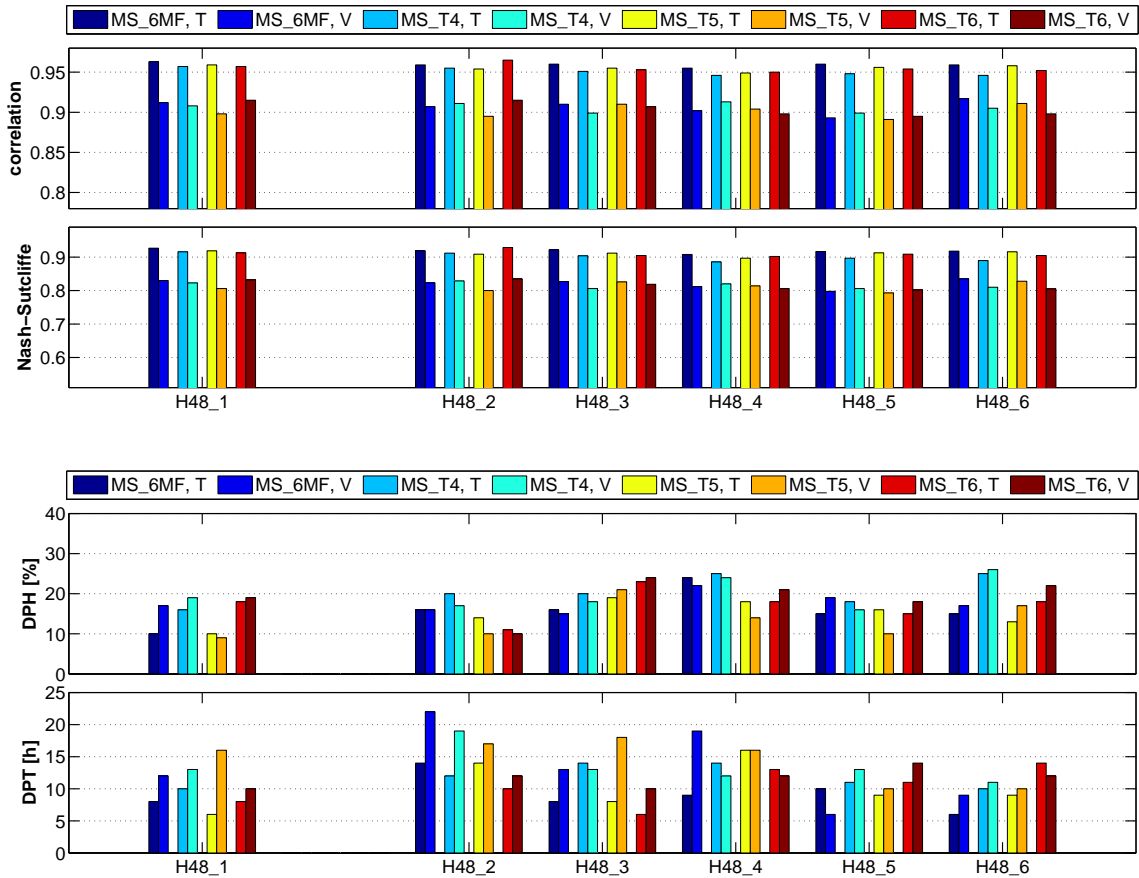


Figure 5.41: Correlation and NS values considering all 30 flood events as well as DPH and DPT values considering the ten highest flood events for each investigated argument combination H48_1 to H48_6 performing the optimization setups MS_6MF, MS_T4, MS_T5, and MS_T6 (T: training; V: validation).

As before, the partly large differences considering the objection function values of the training and validation phase can be traced back to the fact that in some cases an overfitting of the MS inference systems already occurs.

Considering the correlation and NS values (Figure 5.41) no significant differences and therefore, no general improvements of the 48 hour forecast can be detected considering all 30 flood events. However, an improvement with respect to the 48 hour forecast of the flood peak heights of the ten highest flood events is achieved with the fuzzification strategy MS_T5 (Figure 5.41). Performing this fuzzification strategy the DPH values considering the validation phase of all argument combinations except of H48_3 are reduced to below 15 % and even in three cases (H48_1, H48_2, H48_5) to below 10 %. This improvement again can be traced back to a shift within the corresponding rule system based on the extended fuzzification strategy. But in comparison to the fuzzification strategies presented before, this improvement comes along with the degradation of the DPT values in case of H48_1 to H48_4. Furthermore, the DPT values considering the ten highest flood events show a certain variability, which is why no statement about which fuzzification strategy is superior with respect to the forecast quality of the peak times can be made. Nevertheless, considering the visual evaluation and the peak heights of the ten highest flood events (Figure 5.42) an extended investigation of the fuzzification strategy MS_T5 is reasonable.

5 Model development for the Upper Main basin

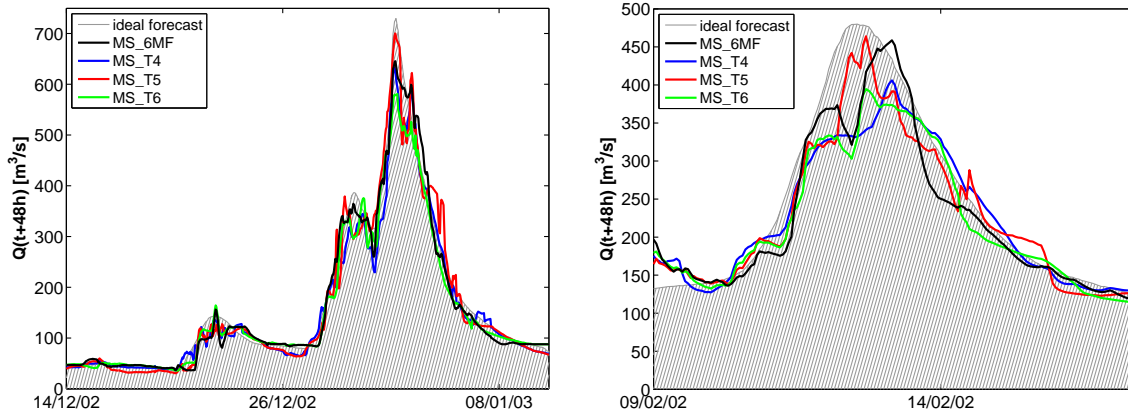


Figure 5.42: Examples for two out of the ten highest flood events simulated with the argument combination H48_1 and the different optimization setups MS_6MF, MS_T4, MS_T5, and MS_T6 (left: training; right: validation).

Until now, different fuzzifications of the arguments *Tukey depth*, $Q(t)$ and $Q_{up}(t)$ have been investigated for an improvement of the 48 hour forecast of discharge, whereas the optimization setup is kept as it is performed for MS_6MF: the optimization of a 20 rule MS inference system is always performed without any further restrictions. Within a last investigation step, these optimization restrictions are slightly modified by expert knowledge.

Since a certain structure can be recognized within the projections as shown in Figure 5.35 and 5.36 the rule parts considering the arguments *Tukey depth* and $Q_{up}(t)$ as well as the response $Q(t+48h)$ of three rules are defined in advance and remain untouched during the SA optimization procedure. However, it is possible that different membership functions of other arguments are added to these partly fixed rules during the SA-MS optimization process. This is reasonable because low depth values do not only indicate seldom conditions considering $Q_{up}(t)$ and $Q(t)$, but also for other arguments which are taken into account for the calculation of the corresponding *Tukey depth*. In this case the three partly fixed rules are defined as:

IF $Q_{up}(t) (300,400,\infty)_T$ *AND* *Tukey* $(-\infty,10,50)_T$ *THEN* $Q(t+48) (300,400,\infty)_T$

IF $Q_{up}(t) (-\infty,300,400)_T$ *AND* *Tukey* $(-\infty,10,50)_T$ *THEN* $Q(t+48) (300,400,\infty)_T$

IF $Q_{up}(t) (-\infty,300,400)_T$ *AND* *Tukey* $(10,50,\infty)_T$ *THEN* $Q(t+48) (-\infty, 400,500)_T$

These predefined, partly fixed rules are investigated together with the fuzzification strategy MS_T5 in the following setups:

MS_T7:

Since until now, 20 rule MS inference systems are optimized for the different argument combinations H48_1 to H48_6, only 17 rules are now completely automatically trained so that the rule number of the whole rule system remains constant in comparison to the previous setups. The initialisation of 17 rules and their optimization together with the three partly fixed rules are performed without any further restrictions by the SA algorithm automatically.

MS_T8:

Except of the number of rules this optimization setup corresponds to MS_T7. In this case a 23 rule MS inference system is trained. 20 rules are automatically optimized in addition to the three predefined, partly fixed rules in order to keep the number of fully automatically optimized rules constant in comparison to the previous setups.

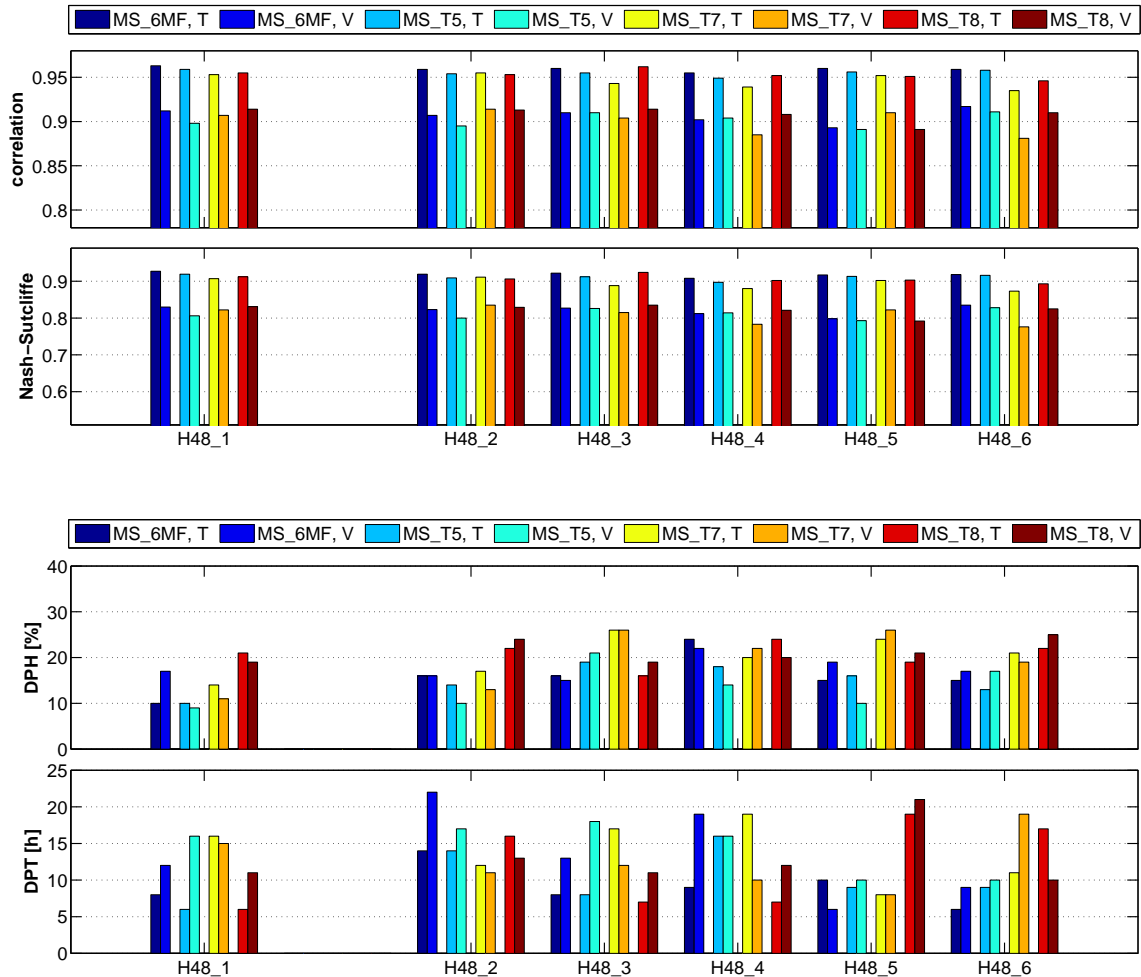


Figure 5.43: Correlation and NS values considering all 30 flood events as well as DPH and DPT values considering the ten highest flood events for each investigated argument combination H48_1 to H48_6 performing the optimization setups MS_6MF, MS_T5, MS_T7, and MS_T8 (T: training; V: validation).

For comparison, the resulting correlation and NS values considering all 30 flood events are given in Figure 5.43 for the optimization setups MS_T7 and MS_T8 considering the different argument combinations H48_1 to H48_6 together with those of MS_6MF and MS_T5. Furthermore, the corresponding DPH and DPT values considering the ten highest flood events are shown in this figure. For H48_6 MS_T8 not all responses of the validation set can be simulated with the optimized 23 rule MS inference system. Therefore, the results for the 22 rule system are given in Figure 5.43 instead.

The partly large differences considering the objective function values of the training and valida-

5 Model development for the Upper Main basin

tion phase are due to the fact that in some cases an overfitting of the MS inference systems already exists. Furthermore, no significant differences within the correlation and NS values considering all 30 flood events can be detected. Therefore, no general improvement of the 48 hour forecast considering all 30 flood events could be achieved with the chosen optimization setups MS_T7 and MS_T8.

Considering the ten highest flood events no improvements with respect to the 48 hour forecast of the peak heights occur by performing MS_T7 and MS_T8 (Figure 5.43). The visual evaluation of the flood hydrographs confirms this result (Figure 5.44). The DPT values considering the ten highest flood events also show a certain variability. Therefore, no statement about which fuzzification strategy is superior with respect to the forecast quality of the peak times can be made.

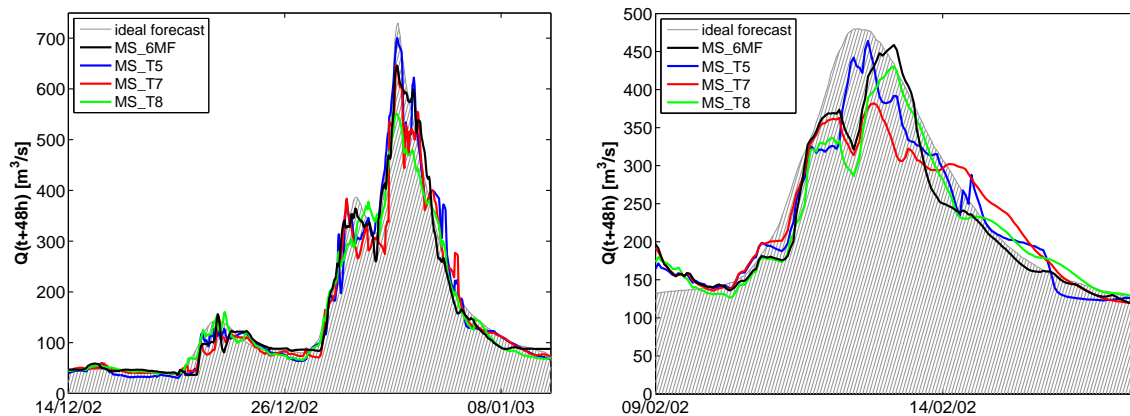


Figure 5.44: Examples for two out of the ten highest flood events simulated with the argument combination H48_1 and the different optimization setups MS_6MF, MS_T5, MS_T7, and MS_T8 (left: training; right: validation).

Summary and further discussion.

The aim of the investigation of Tukey depth as an additional argument focused on the possible improvement of the MS inference systems for the 48 hour discharge forecast. Considering all 30 flood events, no general and significant improvements can be achieved with one of the discussed optimization setups MS_T1 to MS_T8 and argument combinations H48_1 to H48_6. Therefore, reference setup H48_1 MS_6MF (Chapter 5.2.4) is still one of the best fitted MS inference system for 48 hour forecast of the whole range of considered flood events. Furthermore, it is most attractive as its performance is manageable for an inexperienced user.

Considering only the peak heights of the ten highest flood events a certain improvement can be achieved with the optimization setup MS_T5. A reason for this is, that through the argument *Tukey depth* common argument conditions are marked as ordinary, why less rules are trained for those conditions. Consequently, a shift within the corresponding rule systems occurs. Within these rule systems more rules consider the description of higher discharges compared to MS_6MF (11 instead of 8). Nevertheless, this improvement comes along with certain degradations considering the peak times (Figure 5.41) and the simulations of smaller flood events (Figure D.1). In general, it is recommended to perform the H48_1 MS_6MF MS inference system at gauge Kemmern since its forecast performance considering the whole range of flood events is one of the best and simplest one in this case.

Nevertheless, it is promising to perform Tukey depth as an indicator and additional tool for the quantifications of the forecast quality in combination with the performed MS forecast system. The idea behind is that based on the current conditions and argument values Tukey depth is calculated. Then based on the determined Tukey depth the upcoming conditions are classified as ordinary or unusual and conclusions for the forecast quality of an MS inference system can be probably drawn. In this context, it has to be investigated in more detail, if in general better forecast qualities correspond to higher Tukey depth values, as they indicate ordinary argument conditions, and suboptimal qualities to low depth values. Based on these results it is further interesting to study if any general conclusions and recommendations considering a switching between the MS inference systems H48_1 MS_6MF and MS_T5 for the 48 hour forecast can be drawn. However, one has to keep in mind that the above discussed results are based on the restrictions of a 20 rule MS inference system and do not always represent the best optimized one in all cases. Therefore, the performance ability of the developed fuzzification and optimization strategies have to be checked in conjunction with the proposed investigation.

5.3.3 Investigation of the extrapolation behavior of Mamdani inference systems

Due to its structure and the general definition of arguments and response as membership functions the extrapolation behavior of MS inference systems is limited. However, due to ongoing discussions among others with respect to climate changes and the resulting increase of extreme events (droughts, floods) forecast systems which own a certain extrapolation ability are in demand. Therefore, the general extrapolation behavior of MS inference systems is investigated based on the previous results. Thereby, the need for extrapolation considering MS inference systems within the Upper Main basin (gauge Kemmern) is studied based on Tukey depth values.

The general question whether MS inference systems within the Upper Main basin (gauge Kemmern) require a certain extrapolation behavior or not is investigated first. To answer this question Tukey depth values are considered, and a cumulative curve over time based on these values is calculated. Thereby, seldom argument conditions with depth values of 0 or 1 are counted by one, ordinary conditions with higher depth values by zero. Depending on the number of unusual and ordinary conditions two general shapes of the cumulative curves can be distinguished (Figure 5.45). If the cumulative curve continuously increases over time, then it can be assumed that the MS inference systems still have to face unusual argument conditions in the future (Figure 5.45, dashed line). In contrast to this, if the cumulative curve flattens it can be assumed that the probability of unusual argument conditions becomes smaller in the future (Figure 5.45, solid line). For the latter case the extrapolation behavior of a flood forecast system is less important than for the first case.

Figure 5.46 shows the development of the cumulative curves based on Tukey depth values for argument combination H48_1 calculated on hourly data considering (1) the time period from 01.01.1992 to 31.12.2004 and (2) only the 30 highest flood events. Since Tukey depth values depend on the chosen arguments further plots are exemplarily given for argument combinations H48_2 and H48_3 in Appendix D.

In case of the 30 flood events the shape of the cumulative curves corresponds to a step function

5 Model development for the Upper Main basin

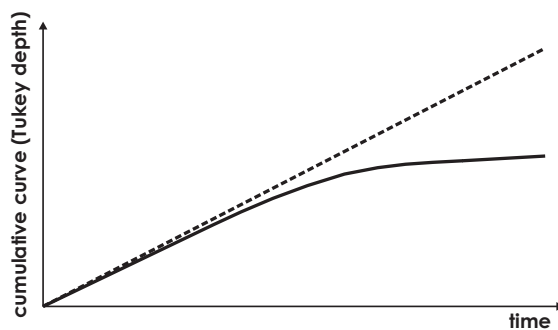


Figure 5.45: Generalization of two possible shapes of the cumulative curve based on Tukey depth values.

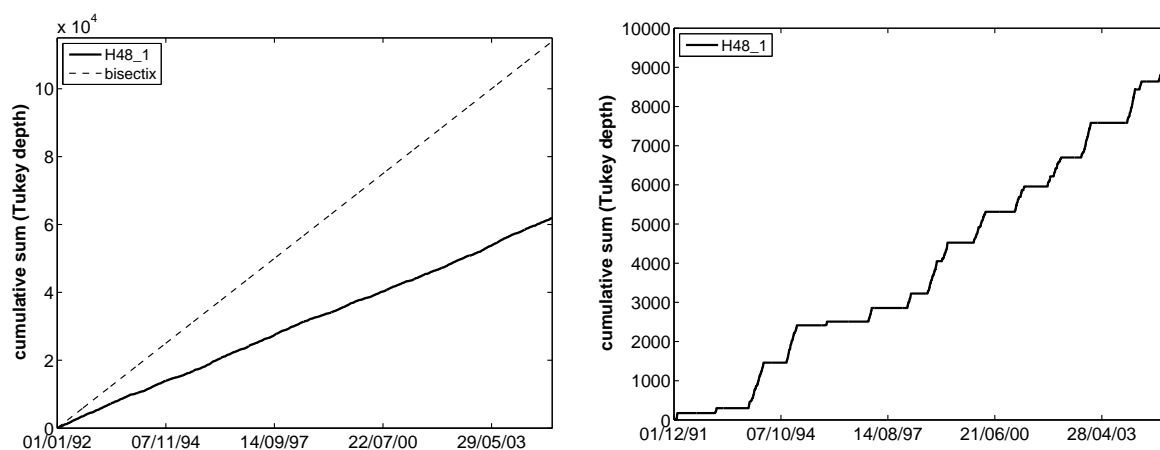


Figure 5.46: Cumulative curves based on Tukey depth values calculated on hourly data considering the time period from 01.01.1992 to 31.12.2004 (left) and only the 30 highest flood events (right) for the argument combinations H48_1.

because of lacking data between single flood events. Furthermore, although 30 flood events are considered only 17 steps can be clearly distinguished because (1) for some smaller events almost all data are marked as ordinary and (2) some floods occurred shortly one after another. Therefore, they cannot be differentiated in these diagrams.

In all figures a continuous increase of the cumulative sum over time is apparent and it can be assumed that the MS inference systems still have to face unusual argument conditions in future within the Upper Main basin (gauge Kemmern). A reason for this is the limited database including a small number of flood events (30 greater WL 1; only 5 greater WL 3). Consequently, an adequate forecast system for the Upper Main basin will require a certain extrapolation ability. Therefore, the extrapolation behavior of MS inference systems presented before is investigated in the following.

The investigation of the extrapolation behavior is based on measured data of the 30 flood events. However, these data are split into a training and validation set considering warning level 3 at gauge Kemmern (570 m³/s, Table 4.5) instead of single flood events. The training set includes all discharges which are below this warning level and the remaining ones belong to the validation set. Based on the training set MS inference systems are optimized and their extrapolation behavior is investigated based on the validation set.

Considering the Tukey depth data of the training and validation sets are not mixed together but analysed separately. The depth values of the training set are calculated with respect to the target variable $Q(t + 48h)$ as before, but without considering the data of the validation set. Since the data of the validation set virtually represent up to now unknown extreme discharges, their Tukey depth values are calculated with respect to the data of the training set.

Based on the results of Chapter 5.2.4 and 5.3.2 the MS inference system setups MS_6MF and MS_T5 are considered together with argument combination H48_1 for the investigation of the extrapolation ability. However, because the setups MS_T7 and MS_T8 have shown a certain sensitivity with respect to the performed number of rules, these are also considered in the following.

The optimization restriction of 20 rule MS inference systems seems not necessarily adequate any longer because the point where overfitting occurs is not clear, but essential for this investigation. Therefore, 46 inference systems (5 to 50 rules, continuously increasing by 1) are optimized considering MS_6MF and MS_T5 for H48_1. Since MS_T7 and MS_T8 are identical except for the number of optimized rules and represent a modified setup of MS_T5, both are summarized to and named as MS_T5m in the following. As in case of MS_6MF and MS_T5 46 MS inference systems are optimized for setup MS_T5m.

Considering the fuzzification of the arguments and the response, the definitions of the different membership functions are kept as in the investigations before. That means, that the membership functions are not defined based on the new training set, but on the whole database of 30 flood events. Therefore, a certain extrapolation ability based on the membership functions is ensured.

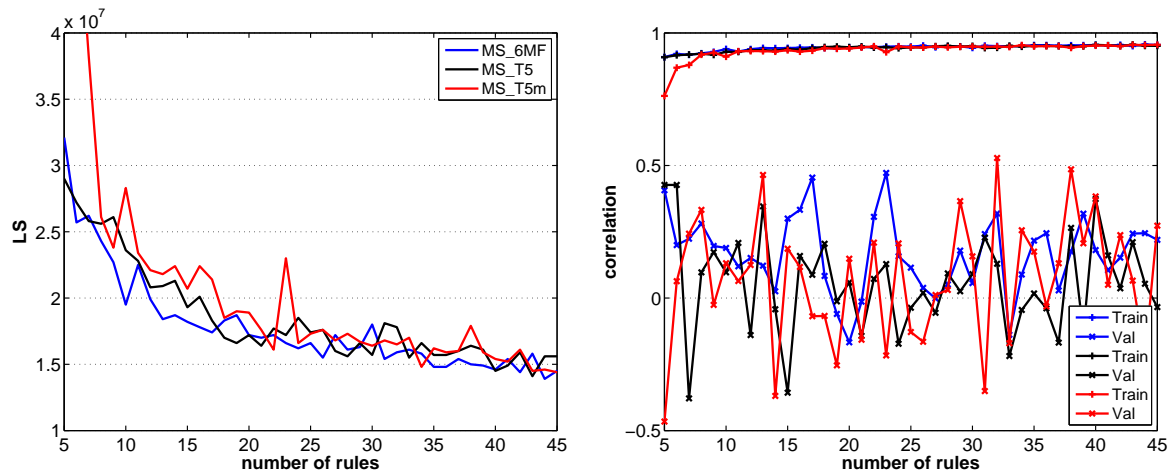


Figure 5.47: Development of the objective function least-squares (LS) and the corresponding correlation values of the training and validation sets considering the optimization setups MS_6MF (blue), MS_T5 (black), and MS_T5m (red) for H48_1.

Figure 5.47 presents the development of the objective function LS and the corresponding correlation values of the training and validation sets for the three considered optimization setups. All LS curves show a similar shape and a continuous improvement of the MS inference systems with increasing rule numbers. However, the correlation values of the validation set do not confirm this result. No clear development (improvement or degradation) is apparent, but a certain sensitivity with respect to the performed number of rules. Furthermore, no satisfying optimization of at least one MS inference system is achieved based on the correlation values. Figure 5.48 and the figures

in Appendix D confirm these result.

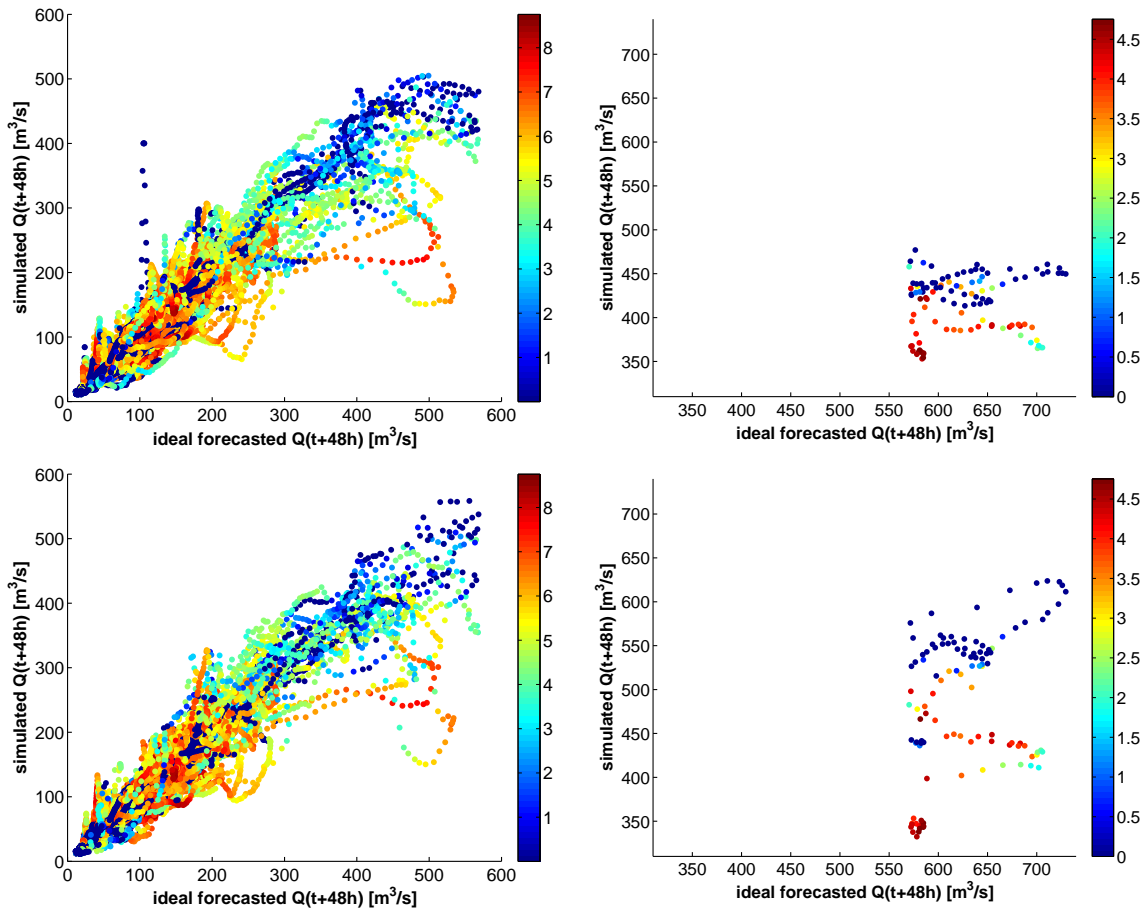


Figure 5.48: Training (left) and validation (right) results considering the extrapolation behavior of MS inference systems H48_1 MS_T5 20 rules (top) and 40 rules (bottom; best optimization result; marker color represents the corresponding log-scaled depth values).

However, looking in more detail at the data behind Figure 5.48, D.4, and D.5, it turns out that extreme discharges with low depth values generally belong to the increasing part of the hydrograph and are more often better forecasted than those with high depth values which refer to the decreasing part of the hydrograph. Furthermore, high (extreme) discharges considering the increasing part of the hydrograph are more often better forecasted with setup MS_T5 than with the other two. This fact verifies the result of Chapter 5.3.2, that with the performance of Tukey depth as argument extreme discharges (ten highest flood events) are better forecasted than with the other setups. Therefore, it is assumed that a slight improvement of the extrapolation behavior can be achieved with the performance of MS_T5 and a further splitting of the database. Thereby, only discharges of the increasing part of the hydrograph should be considered within the training and validation sets. Nevertheless, all results demonstrate the limited extrapolation behavior of MS inference systems which can be traced back to the general properties of the Mamdani approach.

The results of this investigation show (1) the need for a certain extrapolation ability of MS inference systems within the Upper Main basin (gauge Kemmern), and (2) the limits of the performed MS inference systems with respect to this requirement. With the generation of a new database which includes unobserved, but possible (extreme) events, this problem can be overcome and is investigated in the following chapter.

5.4 Performance comparison

5.4.1 Mamdani inference systems of observed and generated database

As shown in Chapter 5.3.3 a MS forecast system within the Upper Main basin (gauge Kemmern) requires a certain extrapolation ability. However, the extrapolation behavior of MS inference systems is limited. To overcome this problem the application of a generated database including unobserved, but possible (extreme) flood events is investigated in the following.

In this work the new database is generated by performing the hydrological model WaSiM-ETH. As presented in Chapter 5.1.3 (also Appendix B) 3500 possible flood events are simulated, whereby 2100 scenarios represent winter and 1400 summer flood events. Since the highest flood events occur during wintertime within the Upper Main basin the training of the MS inference systems is performed based on (1) only generated winter flood events (in the following labeled as w), (2) only generated summer flood events (s), and (3) all generated data (a). Thereby, it can be investigated, whether MS inference systems, trained on pure generated wintertime events, perform a better forecast of the 30 observed wintery flood events (Chapter 4) than those, trained on the whole database. All three database are equally split into training and validation sets so that the amount of flood events considering the corresponding precipitation frequency is equal in both.

For the fuzzification of the arguments observed and generated data are considered. This is necessary because the optimized MS inference systems, which are trained and validated based on only generated data, are further verified considering the observed flood events. Figure 5.49 shows exemplarily the defined membership functions for argument/response discharge $Q(t)$ applied for this investigation (left), and for the previous ones (right). With the new fuzzification less membership functions describe the range of observed data as a shift to higher discharges occurs.

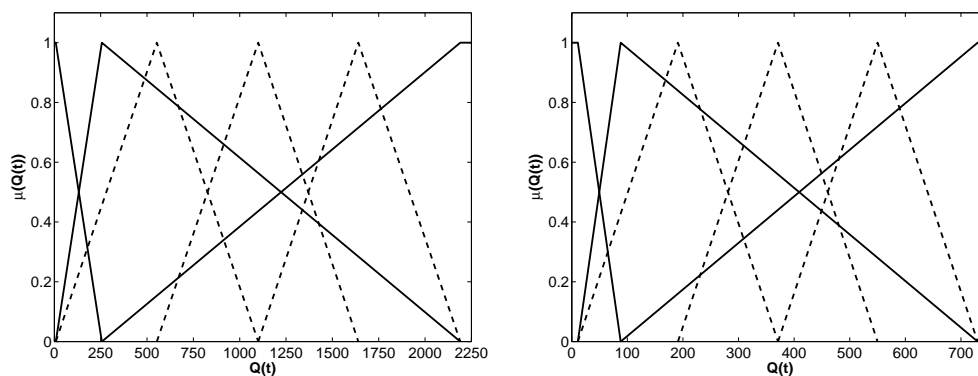


Figure 5.49: Fuzzification of the argument/response discharge $Q(t)$ for the generated (left) and historical database (right).

Considering the results of Chapter 5.2.4 and Chapter 5.3.2 the 48 hour forecast should be performed with one of both MS inference systems, MS_6MF or MS_T5, together with argument combination H48_1 (Table 5.24) within the Upper Main basin (gauge Kemmern). Therefore, both setups are considered for this investigation and trained for the generated database. Over-

5 Model development for the Upper Main basin

all six different setups are investigated: H48_1s, H48_1w, H48_1a together with MS_6MF and MS_T5. Since the new database (H48_1a) includes around 20 times more data than the historical one, the assumption that the point where overfitting occurs is around 20 rules is not longer adequate. Thus, 36 MS inference systems (5 to 40 rules, continuously increasing by 1) are optimized for each setup and database.

For the rating of the optimized MS inference systems correlation values as well as mean absolute differences of peak heights (DPH) and times (DPT) of (1) all peaks, (2) 100, and (3) 50 highest peaks are considered. The development of these quantities are given in Appendix E. A further rating criterion is the general ability to simulate all data of the historical database. Table 5.26 summarizes the evaluation results for the best fitted MS inference system for each investigated setup.

FIS			r	DPH		DPT		DPH ₁₀₀		DPT ₁₀₀		DPH ₅₀		DPT ₅₀	
				\bar{x}	σ	\bar{x}	σ	\bar{x}	σ	\bar{x}	σ	\bar{x}	σ	\bar{x}	σ
MS_6MF	H48_1s	25 rules	0.95	22	20	4	6	13	10	4	4	16	8	4	4
			0.95	21	16	5	5	14	8	5	4	19	10	5	4
	H48_1w	23 rules	0.94	17	18	9	7	18	9	5	4	22	9	6	4
			0.94	17	16	9	9	18	10	6	5	23	9	6	5
	H48_1a	37 rules	0.94	26	21	3	6	16	9	4	4	19	9	4	5
			0.94	24	20	4	7	16	10	4	5	20	18	4	5
MS_T5	H48_1s	28 rules	0.95	21	20	6	5	14	8	5	5	19	8	5	5
			0.95	21	20	6	5	16	8	6	5	23	9	6	5
	H48_1w	34 rules	0.95	17	18	7	8	16	9	5	4	18	8	6	4
			0.95	17	18	8	8	16	9	7	4	19	9	7	4
	H48_1a	23 rules	0.93	21	17	4	4	15	10	5	5	19	9	5	5
			0.93	21	17	4	4	17	9	5	5	21	10	5	5

Table 5.26: Evaluation results of the best fitted MS_6MF and MS_T5 (H48_1s, w, a) inference systems for the 48 hour forecast (r: correlation coefficient; DPH [%] and DPT [h]: absolute differences of peak heights and times; ₁₀₀ / ₅₀: considering the 100 / 50 highest peaks; \bar{x} : mean; σ : standard deviation; first training, second validation).

Comparing the correlation, DPH and DPT values, no significant performance degradation between the training and validation set occurs. Furthermore, the performance of the different best fitted MS inference systems is of comparable quality. The application of the MS_T5 setup does not necessarily result in a better simulation of the highest peak as it was the case in Chapter 5.3.2. A reason for this is the regular shape of almost all generated hydrographs with a very steep increasing part (Figure 5.50). Therefore, a certain variability of the data is missing considering gauge Kemmern. Long drawn-out hydrographs, as they also occur within the Upper Main basin, are rare within the generated database. In terms of Tukey depth this means that many conditions are marked as ordinary and as an argument, Tukey depth fades into the background within the rule systems. Examples of generated hydrographs and the performance of the best fitted MS inference systems are shown in Figure 5.50 for the validation set.

The transferability of the best fitted MS inference systems is tested with the observed database. Thereby, all 30 observed winterly flood events are considered. In Table 5.27 the resulting correlation, DPH and DPT values are given. For comparison the results from Chapter 5.2.4 and

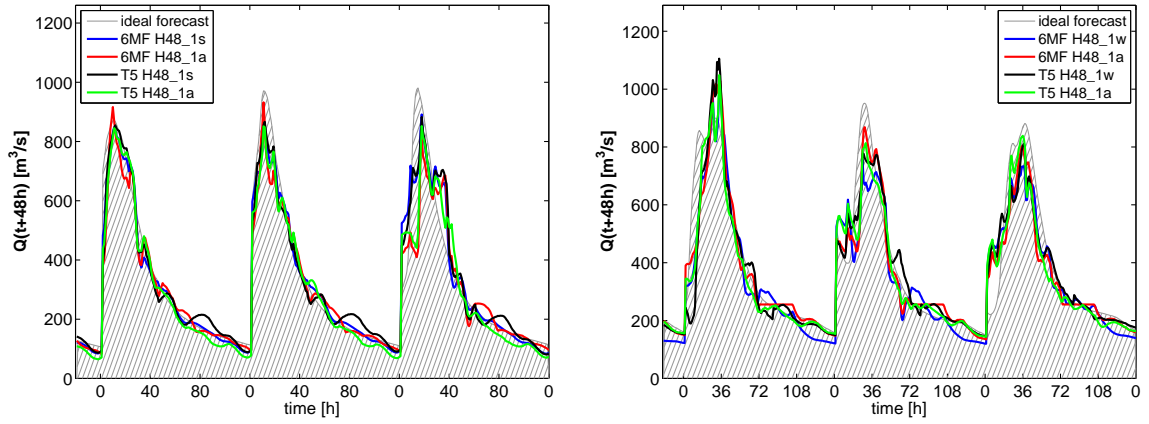


Figure 5.50: Examples for the performance of the inference systems MS_6MF and MS_T5, H48_1s / H48_1a (summer events, left) and H48_1w / H48_1a (winter events, right) considering generated hydrographs of the validation set.

FIS			r	DPH		DPT		DPH ₁₀		DPT ₁₀	
				\bar{x}	σ	\bar{x}	σ	\bar{x}	σ	\bar{x}	σ
MS_6MF	H48_1s	25 rules	0.76	100	68	12	16	67	38	4	6
	H48_1w	23 rules	0.88	22	15	16	12	26	15	11	5
	H48_1a	37 rules	0.76	59	56	12	13	15	11	6	7
MS_T5	H48_1s	28 rules	0.81	63	66	12	12	30	25	8	7
	H48_1w	34 rules	0.77	38	42	18	16	26	13	18	8
	H48_1a	23 rules	0.69	43	52	7	13	35	46	5	6
MS_6MF	H48_1	20 rules	0.96	16	14	9	11	10	5	8	9
			0.91	23	16	11	9	17	9	12	9
MS_T5	H48_1	20 rules	0.96	22	20	8	10	10	7	6	7
			0.91	25	16	16	12	9	9	15	13

Table 5.27: Evaluation results for MS_6MF and MS_T5 (H48_1s, w, a; H48_1) inference systems considering the simulation of 30 observed wintery flood events (r: correlation coefficient; DPH [%] and DPT [h]: absolute differences of peak heights and times; ₁₀: considering the ten highest flood events; \bar{x} : mean; σ : standard deviation; last two MS setups: first training, second validation).

5 Model development for the Upper Main basin

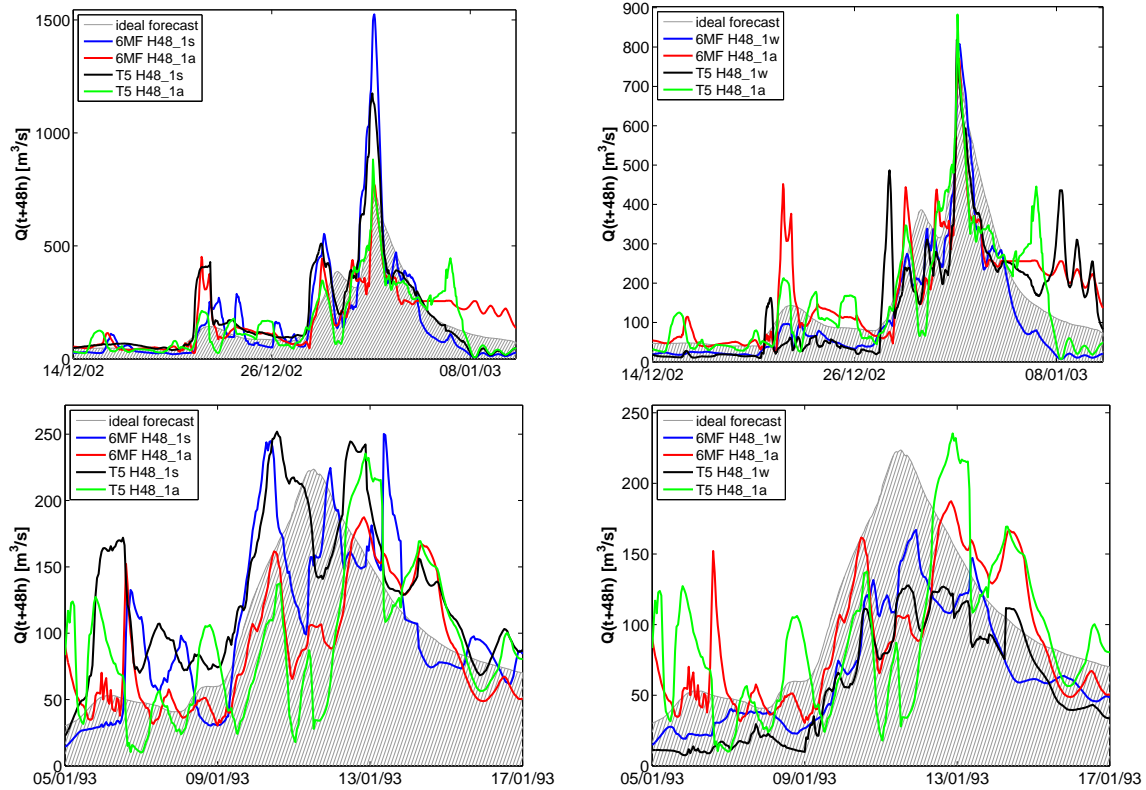


Figure 5.51: Examples for the simulation of historical flood events performing MS_6MF and MS_T5 (H48_1s, w, a) inference systems.

Chapter 5.3.2 for training and validation are also listed within the table. Furthermore, Figure 5.51 shows two examples for the performance of these MS inference systems considering a high and a small flood event.

The performance degradation of the MS_6MF and MS_T5 (H48_1s, w, a) inference systems considering the 30 observed winterly flood events is significant. None of the optimized systems is able to simulate the observed hydrographs in a satisfying way. However, if only the peaks of the highest flood events are considered both MS systems, trained on the winter and overall database, are able to reproduce these peaks in a satisfying way (Figure 5.51, top, right). This circumstance can be traced back to the properties of the generated and observed database as well as the limited extrapolation behavior of MS inference systems. Considering the generated database the highest observed flood events (approximately HQ_{20}) belong to the smallest ones and is very rarely presented. Therefore, their influence on the training of the MS inference systems is less significant and less rules are optimized for this discharge range with the performed SA-MS setup. That is the reason why the performance of the optimized MS inference systems degrades considering the simulation of observed flood events of small return periods.

Nevertheless, the MS inference systems only based on the observed and generated database, respectively, complement each other. Therefore, the performance of these MS inference systems ensures a continuous forecast of flood events considering both ranges, usual and extreme. Thereby, in case of ordinary flood events MS inference systems, which are trained on the observed database, should be performed for the 48 h forecast. However, as soon as these MS inference systems indicate an upcoming extreme flood event, the MS inference systems, which are trained on the

generated database, should be additionally taken into account for the forecast.

In order to improve the forecast property of the presented MS inference systems (H48_1s, w,a) considering the simulation of observed flood event the generated database should be extended. As described in Chapter 5.1.3, the generated precipitation events are implemented within three specific time windows and two different preconditions. Therefore, the trained MS inference systems are less flexible if significant differences within the input of the systems occur (limited extrapolation behavior). However, a random implementation of different precipitation events within the observed time series would increase the variability of the generated flood events considering shape, occurrence, and duration. Therefore, it is assumed that for MS inference systems based on a more variable generated database the performance of the forecast of observed flood events will be improved.

As presented in Chapter 5.1.3, the generated precipitation events of one frequency differ in both, time and space. However, only mean areal environmental factors are considered as arguments in this work. Consequently, less information is provided to the MS inference systems. Therefore, it is assumed that a spatial distributed consideration of arguments could improve the forecast ability once more. First results presented by Disse et al. (2009) confirm this assumption.

5.4.2 Mamdani inference systems and WaSiM-ETH

The 48 hour forecast performances of the classical rainfall-runoff model WaSiM-ETH (Chapter 5.1) and the Mamdani inference systems are compared in the following at gauge Kemmern considering observed flood events. Since the Mamdani inference systems, which are trained on the generated database (Chapter 5.4.1), fail for the observed flood events, only the MS_6MF and MS_T5 inference systems together with H48_1 (Chapter 5.2.4, 5.3.2) are taken into account for the comparison.

Considering the 48 hour forecast with WaSiM-ETH the hydrograph simulated for the calibration and validation period is shifted forward by 48 hour. This is possible, because no real precipitation forecasts are available for both modelling approaches (rainfall-runoff model, fuzzy inference system) and the observed data are taken as ideal forecasts in both cases. Therefore, the comparability of both modelling approaches is ensured. However, due to missing input data for the hydrological modelling with WaSiM-ETH only simulations from end of 1991 to begin of 2002 are considered.

Since no long time periods, but single flood events are simulated with the MS inference systems the comparison of the model performance considering the 48 hour forecast is investigated based on 23 single flood events. Furthermore, as the calibration / training and validation time periods are not identical, the overall performance is compared, considering the correlation coefficient and the mean absolute differences of peak heights DPH and times DPT (Table 5.28). Figure 5.52 shows two examples for the 48 hour forecast of flood events with WaSiM-ETH and MS inference systems.

The performance of the different modelling approaches is of comparable quality considering the goodness of fit values and the visual evaluations. However, the hydrograph simulated by WaSiM-ETH is smoother than that of the MS inference systems, in particular, within the lower discharge

FIS			r	DPH		DPT		DPH ₁₀		DPT ₁₀	
				\bar{x}	σ	\bar{x}	σ	\bar{x}	σ	\bar{x}	σ
MS_6MF	H48_1	20 rules	0.94	19	15	9	10	13	8	8	7
MS_T5	H48_1	20 rules	0.93	17	15	10	11	10	8	6	5
WaSiM-ETH			0.91	19	20	12	10	9	7	8	5

Table 5.28: Evaluation results for MS_6MF and MS_T5 (H48_1) inference systems as well as WaSiM-ETH considering the simulation of 23 observed flood events (r: correlation coefficient; DPH [%] and DPT [h]: absolute differences of peak heights and times; 10: considering the ten highest flood events; \bar{x} : mean; σ : standard deviation).

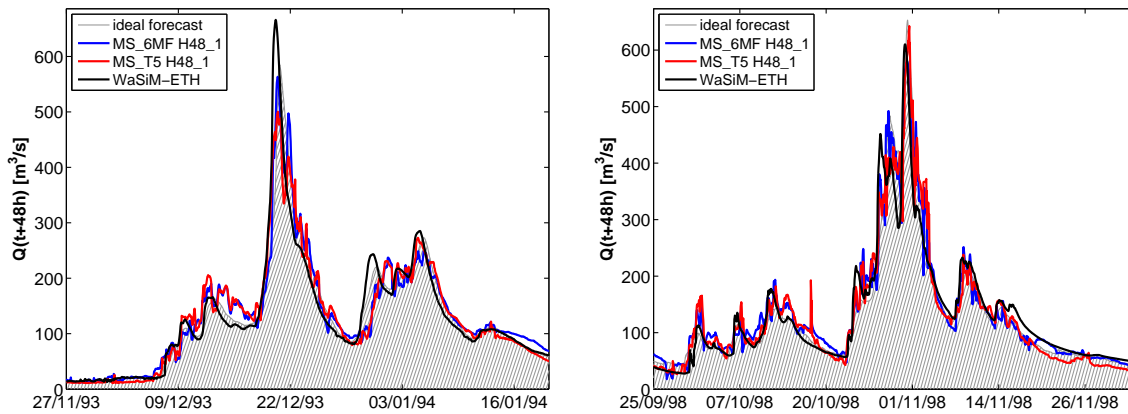


Figure 5.52: Examples for the simulation of observed flood events performing WaSiM-ETH, MS_6MF and MS_T5 inference systems (H48_1).

range. Considering WaSiM-ETH each simulation step is based on the previous one, which results in a smooth hydrograph. In contrast to this, the simulated time steps are independent from each other with the chosen MS setups. Therefore, larger fluctuations of the hydrograph from one to another time step can occur.

The robustness of both modelling approaches is further investigated for the performance comparison. Thereby, 100 turning band realisation of the measured precipitation are taken into account for WaSiM-ETH (Chapter 4.2). These realisations do not differ in terms of temporal, but spatial distribution. Figure 5.53 shows the resulting simulated hydrographs. Considering the highest peak in the figure discharges are simulated within the range between 541 and 718 m³/s (observed peak: 653 m³/s).

Since only mean areal environmental factors are performed within the MS inference systems, no spatial sensitivity can occur as for WaSiM-ETH. Therefore, the chosen setups of MS inference systems are more robust considering the spatial variability. Even if the forecasted cumulated areal precipitation is increased and decreased by 30 % of the corresponding standard deviation the MS inference systems respond less sensitive considering the highest peaks than WaSiM-ETH in case of turning band simulations (Figure 5.54) in this case. Considering setup MS_6MF H48_1 the highest peaks within the shown figure range between 563 and 593 m³/s, in case of MS_T5 H48_1 between 638 and 643 m³/s. Due to the interaction of single rules within the MS inference systems and the defined membership functions an increase and decrease of the forecasted cumulated areal precipitation has no great impact on the MS inference output considering the shown flood

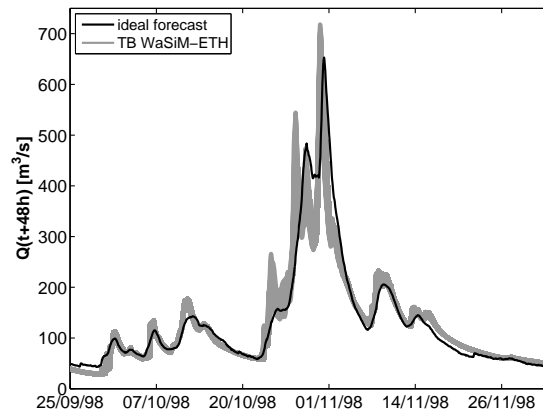


Figure 5.53: Turning band simulations with WaSiM-ETH.

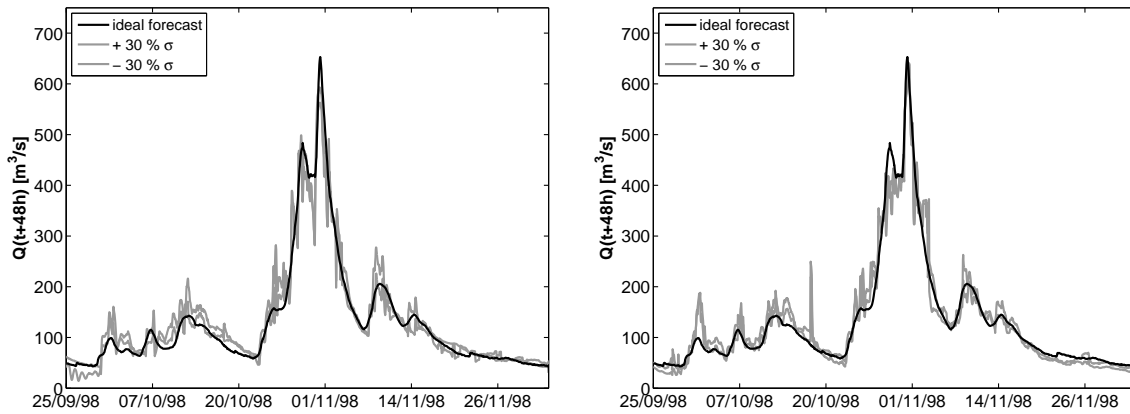


Figure 5.54: Fuzzy simulations considering a 30 % of the standard deviation increased and decreased forecasted cumulated areal precipitation (left: MS_6MF; right: MS_T5; both: H48_1).

FIS			r	DPH		DPT		DPH ₁₀		DPT ₁₀	
				\bar{x}	σ	\bar{x}	σ	\bar{x}	σ	\bar{x}	σ
MS_6MF	H48_1	20 rules	0.94	19	15	9	10	13	8	8	7
		+ 30 % σ	0.94	22	18	10	10	12	8	8	7
		- 30 % σ	0.93	18	12	14	12	16	7	13	11
MS_T5	H48_1	20 rules	0.93	17	15	10	11	10	8	6	5
		+ 30 % σ	0.92	25	26	13	14	9	6	9	11
		- 30 % σ	0.93	23	26	12	13	8	6	6	5

Table 5.29: Goodness of fit values for MS_6MF and MS_T5 (H48_1) considering fuzzy simulations with a 30 % of the standard deviation increased and decreased forecasted cumulated mean areal precipitation (r: correlation coefficient; DPH [%] and DPT [h]: absolute differences of peak heights and times; 10: considering the ten highest flood events; \bar{x} : mean; σ : standard deviation).

5 Model development for the Upper Main basin

event. The same holds for the other flood events. Table 5.29 presents the overall performance of the two MS inference systems considering the changed conditions and all 23 flood events. In addition to the shown results, it should be investigated to which amount of forecasted cumulated areal precipitation the MS inference systems own their robustness. In this context, it should be discussed to which amount of forecasted cumulated areal precipitation a robustness of the MS inference system is reasonable and adequate.

The performance comparison between the classical rainfall-runoff model WaSiM-ETH and the Mamdani inference systems considering the 48 h forecast of flood events can be summarized as follows:

1. The performance of both modelling approaches is of comparable quality considering the 48 h forecast at gauge Kemmern.
2. In contrast to the hydrological model the presented MS inference systems are less time consuming and always applicable because no tracking of the model has to be performed between single flood events. However, the hydrograph simulated by WaSiM-ETH is much more smoother than those of the MS inference systems and corresponds more to the notion of a user.
3. The developed MS inference systems are more robust than WaSiM-ETH considering the spatial distribution of precipitation in this case. A reason for this is the definition of arguments as mean areal environmental factors. In addition to this, a certain uncertainty of the input data can be attenuated through the fuzzification of the crisp input. However, this robustness of the performed MS inference systems can be a drawback e.g. considering alpine catchments. Furthermore, the robustness of the MS inference systems with respect to the amount of forecasted cumulated areal precipitation is not totally clear and requires further investigations.
4. Since mean areal arguments are performed as inputs the preprocessing for the MS inference systems are less time consuming than for WaSiM-ETH in this case, because all WaSiM-ETH inputs have a spatial resolution of 1000 m x 1000 m. Furthermore, less meteorological information has to be considered for the developed MS inference systems.

6 Expert System for flood forecasts

One goal of the multidisciplinary project HORIX has been the development of a very fast and robust forecast system for extreme flood events which is also able to quantify uncertainties (Chapter 1). Here, the notion of extreme floods includes the already observed flood events and, in addition, extremes which have not occurred yet but may probably occur in the future due to precipitation and catchment properties. For this purpose the observed data base has to be extended by simulated data as presented in Chapter 5.1.3. However, this enlargement of data introduces additional uncertainties beside those of the measured data. The model uncertainties occur due to the model structures and the corresponding assumptions of the chosen hydrological model and have to be considered. Therefore, one important feature of the new forecast system is the quantification of uncertainties coming from (1) precipitation predictions and (2) model structure separately and as an overall uncertainty. In addition, the new forecast system should be easy to handle and flexible with respect to modifications at individual gauges. As shown in Chapter 5.2 fuzzy inference systems can be satisfactorily trained for flood forecasts at individual gauges of a river basin for each forecast time horizon separately. That means that the amount of necessary fuzzy inference systems increases linearly with the number of considered gauges of a river basin and forecast time step. This results in an unmanageable amount of fuzzy inference systems for an (operational) application. In order to overcome this problem and to provide the user a manageable and fast forecast system including the quantification of uncertainties the program *Expertensystem Hochwasser – HORIX* (ExpHo-HORIX; Pakosch, 2008; Pakosch et al., 2008a; Disse et al., 2009) was developed within the framework of this thesis.

In the following first a brief overview of the properties of the forecast system ExpHo-HORIX is given and second an example of a program setup for the Upper Main basin is described.

6.1 Principle concept of the forecast system ExpHo-HORIX

The two most important properties of the forecast system ExpHo-HORIX are (1) the ability to account for uncertainties and (2) to provide the user a manageable, transparent and fast forecast system which ensures an easy integration into an existing environment. Here, two kinds of uncertainties are distinguished: (1) uncertainties coming from precipitation predictions and (2) uncertainties which arise due to model structure if the data base for the fuzzy inference systems is extended by hydrological simulations. Within the HORIX project both kinds of uncertainties were investigated in detail by two HORIX project partners, Bliefernicht (2010, precipitation uncertainties) and Grundmann (2009, model uncertainties).

Consideration of precipitation uncertainties. Adequate areal precipitation prediction is an important issue in flood forecasting. Unfortunately, such predictions have a high uncertainty concerning intensity and location especially during extreme flood events which forces high uncertainties regarding discharge forecasts. Bliefernicht et al. (2008) developed a precipitation forecast system for areal precipitation whose results can be performed as input. For a daily forecast the analogue method is applied, whereas for the hourly prediction both the analogue and the turning bands method are performed. During a flood event this precipitation forecast system provides a certain amount of different precipitation ensembles and scenarios. The resulting uncertainties concerning the corresponding forecasted discharge are statistically quantified by default using the ExpHo-HORIX program (e.g. mean forecasted discharge \bar{Q}_p).

Consideration of model uncertainties. First it has to be emphasized that model uncertainties only have to be taken into account if the database for the training and validation of the single fuzzy inference systems is extended by hydrological simulations. Grundmann (2009) shows that model uncertainties can be investigated for individual gauges within an existing hydrological model by using the *Shuffled Complex Evolution Metropolis* (SCEM) algorithm. He found a functional relation between the mean forecasted discharge concerning precipitation \bar{Q}_p and the corresponding confidence intervals with respect to model uncertainties (Equation 6.1). On this basis he defined an overall forecast uncertainty (Equation 6.2) including both precipitation and model uncertainties:

$$Q_{m,q} = \bar{Q}_m \pm z_{crit} \cdot s_m = \bar{Q}_p \pm z_{crit} \cdot (a \cdot \bar{Q}_p^b) \quad (6.1)$$

$$Q_{o,q} = Q_{p,q} + Q_{m,q} - \bar{Q}_o = Q_{p,q} + Q_{m,q} - \bar{Q}_p \quad (6.2)$$

with	\bar{Q}	$[m^3/s]$	mean forecasted discharge
	p		concerning precipitation
	m		concerning hydrological modelling
	o		concerning overall uncertainty
	q		quantile of the corresponding confidence interval
	z_{crit}		quantile of the standard normal distribution
	s	$[m^3/s]$	standard deviation
	a, b		gauge specific parameters (results from SCEM)

The two basic assumptions for these relations are (1) that the uncertainty is normally distributed and (2) that the mean forecasted discharge is equal for all three uncertainties, $\bar{Q}_p = \bar{Q}_m = \bar{Q}_o$. The results of this study is implemented within the developed forecast system ExpHo-HORIX and can be activated for each gauge as soon as the required results of the investigation (Grundmann, 2009) are available.

Required preprocessing. The preprocessing step consists of the training and validation of fuzzy inference systems for individual gauges of a river basin for each forecast time horizon separately (Chapter 5.2). If only observed data are used this preprocessing includes, beside the classical steps of modelling (data preparations, training/calibration, validation), the investigation of appropriate input variables (arguments). Thereby, the number of arguments can differ in individual fuzzy inference systems due to catchment characteristics and chosen forecast time horizons. Further, for each gauge and time resolution one of both fuzzy inference systems, Mamdani or

Takagi-Sugeno, can be chosen for integration in the program ExpHo-HORIX. The training of these fuzzy inference systems can be performed by applying the Simulated Annealing method (Chapter 3.3.2). If the database is enlarged through hydrological simulations like in the HORIX project the data preparation step includes additionally the generation of possible extreme precipitation events (Bliefernicht et al., 2008), the calibration, validation and performance of a hydrological model (Chapter 5.1), as well as an uncertainty analysis concerning the hydrological model (Grundmann, 2009). The preprocessing of further individual gauges can be performed in parallel to an already existing ExpHo-HORIX setup for a river basin due to the fact that individual fuzzy inference systems are trained separately and bundled within the program frame ExpHo-HORIX afterwards. This is one main advantage in comparison to classical hydrological models and the PAI-OFF system (Cullmann, 2006).

Processing the program ExpHo-HORIX. After the preprocessing step all trained fuzzy inference systems are joined within the framework of ExpHo-HORIX depending on their time resolution (daily, hourly). Figure 6.1 shows the general (operational) scheme and Table 6.1 summarizes the general properties of the program ExpHo-HORIX.

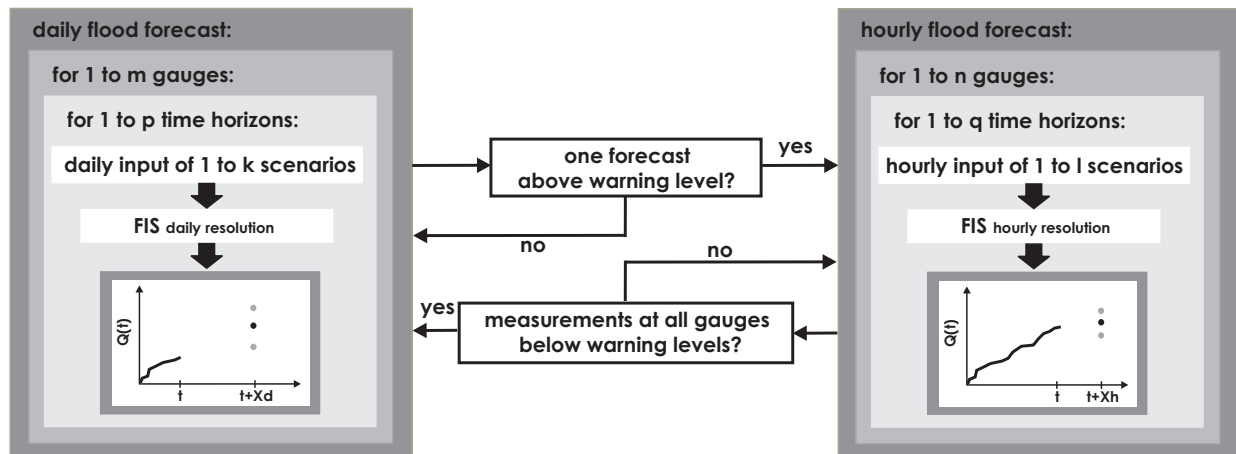


Figure 6.1: General scheme of the fuzzy rule based forecast system Expertensystem Hochwasser (ExpHo-HORIX).

During normal flow conditions the discharge forecast $Q(t + \Delta t)$ is performed on a daily resolution (Figure 6.1 left). With the help of the rating curves of the individual gauges the corresponding water level $W(t + \Delta t)$ is calculated. This is necessary due to the fact that most administrative decisions concerning the management of flood events are based on forecasted water levels. If the forecasted water level exceeds the corresponding predefined warning level threshold at least at one gauge the forecast system switches to the finer, hourly resolution and performs another forecast. As soon as measured water levels at all gauges fall below the predefined warning levels the ExpHo-HORIX system switches back to daily resolution. The user also has the possibility to chose the forecast time resolution manually. Thus, it is also possible to perform a daily forecast during a flood event and an hourly forecast during normal flow conditions.

In order to account for the uncertainties coming from the forecasted precipitation fields a statistical analysis is performed for each gauge of the considered forecast time horizon and time resolution. For this, the discharge is forecasted separately for each precipitation field (compare Figure 6.1 input of scenarios). Afterwards a statistical analysis is performed based on those forecasted discharges and different quantiles as well as the mean forecasted discharge are given to

The fuzzy based forecast system ExpHo-HORIX

- is independent of the system software and can be performed on local and high performance computers.

 - requires only one main configuration file in which all necessary information about the single fuzzy inference systems and the consideration of uncertainties are defined.

 - can handle both fuzzy inference systems, Mamdani and Takagi-Sugeno. Single fuzzy inference systems can be additionally implemented into, changed within or removed from a running ExpHo-HORIX setup without affecting other fuzzy inference systems.

 - can perform discharge forecasts for at least 99 different gauges for both temporal resolutions, daily and hourly.

 - can manage up to 24 single fuzzy inference systems concerning the forecast time horizons for each gauge and temporal resolution, daily or hourly.

 - can process 3500 predicted precipitation scenarios for each time resolution, gauge and forecast time horizon within a short computation time.

 - statistically quantifies uncertainties due to predicted precipitation scenarios by default.

 - can quantify uncertainties due to model structures if results of the SCEM analysis (Grundmann, 2009) are available.

 - calculates the corresponding water levels $W(t + \Delta t)$ of the forecasted discharges with the help of the rating curves of the individual gauges.
-

Table 6.1: General properties of the fuzzy based forecast system ExpHo-HORIX.

the user for each gauge separately (compare Figure 6.1 small diagrams). If necessary and available the uncertainty bands coming from the hydrological model are calculated based on the mean forecasted discharge as additional information.

All input and output files of the developed forecast system ExpHo-HORIX are ASCII standard files. This ensures an easy integration into an already existing environment. If no environment exists the MapServer could be used for the visualization of the forecasted discharges and if available of corresponding inundation areas (Disse et al., 2009).

6.2 Setup for the Upper Main basin

Based on the results of Chapter 5.2, 5.3, and 5.4.1 one ExpHo-HORIX system is set up for the three main gauges of the Upper Main basin (Figure 4.2): Mainleus (1166 km²), Schwürbitz (2419 km²), and Kemmern (4244 km²). In this system only Mamdani inference systems are considered for the four forecast time horizons 3 days, 6, 12, and 48 hours. Furthermore, all fuzzy inference systems for the 3 day flood forecast are trained and validated based on historical measured data and the same MS setup (Chapter 5.2.2). This is also the case for all fuzzy inference systems of the hourly flood forecast (Chapter 5.2.3, 5.2.4). Therefore, only precipitation uncertainties are statistically quantified by default. No model uncertainties as well as no overall uncertainty are statistically quantified in this system, since no MS inference system based on the generated database is implemented. However, if these MS inference systems will be implemented, model uncertainties as well as an overall uncertainty can be quantified as the results of the SCEM analysis are available (Grundmann and Schmitz, 2008, Table 6.2).

gauge	a	b
Kemmern	0.0909	0.6927
Schürbitz	0.0947	0.6937
Mainleus	0.0729	0.6963

Table 6.2: Parameters a and b of the SCEM analyse (Grundmann and Schmitz, 2008) for the three main gauges Kemmern (4244 km²), Schwürbitz (2419 km²), and Mainleus (1166 km²).

Since no real precipitation forecasts were available within the framework of this thesis the number of precipitation scenarios is set to 30. Based on those 30 forecasts the uncertainty due to precipitation inputs is quantified through the mean discharge of all inputs \bar{Q}_p , the minimal Q_{min} and maximal Q_{max} forecasted discharge and the corresponding 2.5, 5, 95, and 97.5 % quantiles $Q_{N,2.5}$, $Q_{N,5}$, $Q_{N,95}$, and $Q_{N,97.5}$.

Finally, it is planned to verify the performance of the ExpHo-HORIX system in real applications by the Bavarian administration (Bayerischer Hochwassernachrichtendienst). An example of a configuration file (ExpHo.config) for such an application is shown below (Pakosch, 2008). However, this configuration file has to be adapted to the existing environment in case of real applications.

ExpHo.config
1 (<i>windows platform</i>)
c:\UMain\ (<i>working directory</i>)
c:\UMain\gauges\currentdischarge.txt (<i>file including measured discharges</i>)
2 (<i># gauges, daily forecast</i>)
30 (<i># precipitation inputs</i>)
Kemmern (<i>1st gauge name, daily forecast</i>)
151.0 (<i>warning level [m³/s]</i>)
c:\UMain\Kemmern\W_Q_relation.txt (<i>file including W-Q-relation</i>)
0 (<i>no SCEM uncertainty</i>)
1 (<i># forecast time horizons</i>)
3 (<i>forecast horizon 3 days</i>)

```

c:\UMain\Kemmern\3d_forecast\MS.config (FIS configuration file 3 day forecast)
1 (Mamdani inference system)
1 (direct forecast of discharge)
1.0 (no normalisation of data)
Schwüribitz (2nd gauge name, daily forecast)
138.0 (warning level [m3/s])
c:\UMain\Schwuerbitz\W_Q_relation.txt (file including W-Q-relation)
0 (no SCEM uncertainty)
1 (# forecast time horizons)
3 (forecast horizon 3 days)
c:\UMain\Schwuerbitz\3d_forecast\MS.config (FIS config. file 3 day forecast)
1 (Mamdani inference system)
1 (direct forecast of discharge)
1.0 (no normalisation of data)
1 (# gauges, hourly forecast)
30 (# precipitation inputs)
Kemmern (gauge name, hourly forecast)
151.0 (warning level [m3/s])
c:\UMain\Kemmern\W_Q_relation.txt (file including W-Q-relation)
0 (no SCEM uncertainty)
3 (# forecast time horizons)
6 (forecast horizon 6 hours)
c:\UMain\Kemmern\6h_forecast\MS.config (FIS config. file 6 hour forecast)
1 (Mamdani inference system)
1 (direct forecast of discharge)
1.0 (no normalisation of data)
12 (forecast horizon 12 hours)
c:\UMain\Kemmern\12h_forecast\MS.config (FIS config. file 12 hour forecast)
1 (Mamdani inference system)
1 (direct forecast of discharge)
1.0 (no normalisation of data)
48 (forecast horizon 48 hours)
c:\UMain\Kemmern\48h_forecast\MS.config (FIS config. file 48 hour forecast)
1 (Mamdani inference system)
1 (direct forecast of discharge)
1.0 (no normalisation of data)

```

Figure 6.2: Example of the ExpHo-HORIX main configuration file (comments are given within the parentheses).

7 Summary and Outlook

People worldwide have to face flood events. In order to save goods and, more important, lives timely and reliable flood forecast systems are required. The development of such a flood warning system based on fuzzy inference systems considering extreme flood events within meso-scale catchments and with return periods of 100 years and more is the main objective of this work. For the setup of this flood forecast system three main research questions, posed in the introduction, are investigated and revisited in the following.

Can unobserved extreme flood events with return periods of 100 years or higher be simulated by classical rainfall-runoff models? In particular, is it possible to reduce the calibration time of those rainfall-runoff models by performing optimization algorithm?

Records of (extreme) flood events, which cause high damages, are seldom, but essential for a successful setup of a timely and reliable flood warning system, in particular, considering extreme flood events ($HQ_{>100}$). Since only 30 flood events are hourly recorded within the Upper Main basin between 1991 and 2004 and the highest one corresponds to a return period of around 20 years the extension of the database is absolutely necessary.

Within the HORIX project the database is extended by simulations of possible flood events. For this purpose, the hydrological model WaSiM-ETH is performed. However, before the simulations can be carried out, the hydrological model itself has to be calibrated and validated. Depending on the experience of the user this process can be very time consuming. Furthermore, if the trial-and-error method is applied the reproducibility of the results is not always ensured. Therefore, the performance of the Shuffled Complex Evolution optimization algorithm (SCE) is investigated in this work. For this, both source codes of WaSiM-ETH and SCE are coupled.

In a first step the General Sensitivity Analysis (GSA) after Madsen (2000) is carried out for the investigation of the parameter behavior of the WaSiM-ETH model and the corresponding parameter space. For this investigation three subcatchments with different catchment sizes and characteristics are chosen. Furthermore, response surfaces (Singh, 1995) based on 5000 Monte Carlo simulations are taken into account for the evaluation considering different objective functions. Based on the results the WaSiM-ETH parameter *drainage density* is indicated as a very sensitive parameter independent of the considered objective function. Therefore, it has a great impact on the model results. Considering the two parameters *recession constant for direct runoff* and *inter-flow* the investigation verifies their behavior as they are defined. Both parameters have no impact on the discharge volume (not sensitive), but on the shape of the modeled hydrograph (high sensitive). However, for the three model parameters *recession constant for hydraulic conductivity*, *recession constant for baseflow*, and *scaling factor for baseflow* no statements about their behavior and impact on the model can be drawn based on the GSA results. Considering one objective

function their sensitivities range over all three defined sensitivity classes. Furthermore, the GSA results contradict the visual interpretations of the response surface in some cases. In particular, for these three model parameters a higher dimensional sensitivity analysis should be carried out, but also for the other three, as the dimension of the investigated parameter space is extremely reduced with the applied projections of the GSA and response surface approach. Since no clear statements about the parameter sensitivities of all parameters can be derived it is not advisable to reduce the parameter space for the SCE optimization algorithm.

Beside the definition of the parameter space for the WaSiM-ETH parameters the definition of the six SCE parameters has a great impact on the optimization performance. Therefore, a special SCE-WaSiM-ETH setup and optimization strategy is developed for the Upper Main basin. Thereby, the focus of the calibration lies primarily on the good representation of flood events, and secondly on the correct simulation of the entire flow spectrum. Since WaSiM-ETH requires a long initial phase of about 2 years in case of the Upper Main basin the optimization process is performed in an iterative way. Model grids considering soil moisture, etc. are generated in advance to keep simulation times additionally low. However, a time lag of further 2 months is chosen before the objective function is calculated to reduce transient oscillation effects. The optimization is then performed considering the initial model grids. The resulting parameters are compared with the initial one. If the parameter values used for the model initialisation differ significantly, new initial model grids are generated considering the results of the SCE optimization. Afterwards a new optimization process is started considering the new initial model grids. These steps are repeated until no significant differences between the parameter values occur. The performance of this strategy and the adjusted SCE setup is compared with the default and recommended SCE setup considering the three subcatchments which are also chosen for the GSA analysis. With the special SCE-WaSiM-ETH setup optimization results of comparable quality are found. Furthermore, the optimization results are satisfying and reasonable. However, the adjusted optimization process itself requires much less computation times and man power in comparison to the default and recommended SCE setups and the classical calibration process. Considering the calibration of all subcatchments within the Upper Main basin the performance of the adjusted optimization process verifies the results. However, only for three smaller head catchments the optimization results considering flood events are not adequate which can be mainly traced back to the general WaSiM-ETH model setup for the Upper Main basin.

For the simulation of extreme flood events ($HQ_{>100}$) extreme precipitation events considering seven different frequencies (Bliefernicht et al., 2008) are taken as model inputs. Considering each season, wintertime and summertime, 100 realisations are available for each return period. In this work, two initial WaSiM-ETH model grids considering dry and wet conditions are generated for both seasons separately. Since most of the high flood events are influenced by snowmelt within the Upper Main basin, a third initial condition ensuring a certain amount of snow is generated for the winter season. For the evaluation of the simulated extreme flood events peak heights are compared to those estimated with classical statistics, although latter also contain certain uncertainties, in particular, considering higher frequencies (Pakosch, 2004). Nevertheless, the comparison shows that (realistic) extreme flood events with return periods of 100 years or more can be simulated with the generated precipitation fields and calibrated hydrological model WaSiM-ETH.

Can fuzzy inference systems ensure a reliable and continuous flood forecast for different forecast time horizons? How simple and user-friendly are these systems?

A reliable and continuous flood forecast warning system has to face both, low and medium discharge conditions as well as (extreme) flood events. Therefore, in this thesis the idea is developed to perform the forecast for different time horizons (3 days; 6, 12, and 48 hours) which have their focus on different discharge conditions, but together ensure a continuous forecast. Thereby, the focus of the 3 day forecast lies on the appropriate representation of low and medium discharge conditions as well as on reliable forecasts of trespasses considering a predefined threshold (warning level). A trespass of the warning level results in switching to the 6, 12, and 48 hour forecast systems. Therefore, the forecast of the flood hydrograph itself is less important for the 3 day forecast systems, but essential for the other three. The fuzzy inference systems are trained and validated for the three main gauges Kemmern (4244 km²), Schwürbitz (2419 km²), and Mainleus (1166 km²).

Since no reference and generally accepted statements could be found in literature which clarify the question whether one fuzzy inference system, Mamdani (MS) or Takagi-Sugeno (TS), is superior, the performance of both is investigated considering all forecast horizons and gauges in this work. Furthermore, since single response fuzzy inference systems are considered, one Mamdani or Takagi-Sugeno inference system has to be trained and validated for each time horizon. Thereby, the training of the fuzzy inference systems is carried out with the Simulated Annealing (SA) optimization algorithm without any further restrictions. The SA-MS / SA-TS setup is taken from a previous study (Reyhani-Masouleh, 2008).

In contrast to the 3 day, 6 and 12 hour forecast time horizons, no reference could be found in literature considering the 48 hour forecast. Furthermore, since the "memories" of the catchments have no great impact on the 48 hour forecast the setup of fuzzy inference systems for this time horizon is a challenge. Therefore, it is investigated in more detail than the others within the framework of this thesis.

For the 3 day forecast the performance comparison is carried out considering the direct forecast of discharge $Q(t + 3d)$ and the forecast of discharge changes $\Delta Q(t, t + 3d)$. For these investigations all daily observed data (1984 - 2004) are taken into account. In contrast to this the database for the 6, 12, and 48 hour forecast includes only hourly observed data of the 30 highest flood events (1991 - 2004). Due to the results of the daily based forecast only the direct forecast of discharges $Q(t + 6h)$, $Q(t + 12h)$ and $Q(t + 48h)$ is investigated.

In case of the 3 day, 6 and 12 hour forecast the selection of arguments is based on a previous study (Bengelstorf, 2009) and further findings in literature. Since simple and user-friendly fuzzy inference systems have to be ensured the fuzzification of the arguments is performed with a pure statistical approach. Thereby, only the minimal, maximal, and mean values of the corresponding argument are considered. In order to find the best fitted fuzzy inference system a series of rule systems is trained and validated for each fuzzy inference system (MS, TS), argument combination and forecast time horizon. The performance comparison is carried out for the gauge Kemmern. The transferability of the best fitted fuzzy inference systems for gauge Kemmern is investigated considering the gauges Schwürbitz and Mainleus.

Comparing the daily forecast of $Q(t + 3d)$ and $\Delta Q(t, t + 3d)$ and considering the well-timed forecast of trespasses, failures of the MS and TS fuzzy inference systems mostly occur if the discharge oscillates around the predefined warning level for a certain time period. However, the forecast of low and medium discharge conditions as well as the well-timed forecast of trespasses is less sat-

7 Summary and Outlook

isfying for the forecast of $\Delta Q(t, t + 3d)$. In this case far too large forecasted discharge changes cause too often the forecast of negative discharges. Considering the forecast of $Q(t + 3d)$ no negative discharges are forecasted.

The results of all three forecast time horizons (3 day, 6 and 12 hours) show that the argument *current observed discharge at the forecast gauge* can not be neglected in this work, since it contains too much information about the current catchment conditions. Furthermore, the SA-TS optimization setup shows a certain sensitivity considering the number of rules to be optimized and the chosen argument combination. Although the SA-MS optimization setup is also sensitive to a certain degree with respect to the chosen argument combination in case of the 6 and 12 hour forecast, the MS optimization process can generally be easier performed than the TS optimization. The reasons for these sensitivities could not be totally clarified in this work. Nevertheless, no significant performance differences between the two best fitted fuzzy inference systems considering the discharge forecast are recognizable. The forecasts are of comparable quality. Considering the transferability of the best fitted MS / TS inference systems the results of the gauges Schwürbitz and Mainleus verify those of gauge Kemmern: It is possible to set up simple and user-friendly MS and TS inference systems considering the forecast time horizons 3 days, 6 and 12 hours and the main gauges within the Upper Main river.

For the 48 hour forecast time horizon a fuzzification and optimization strategy is developed in a first step for gauge Kemmern to ensure simple and user-friendly forecast systems as well as low computation times. Thereby, the performance of both fuzzy inference systems are investigated considering the direct forecast of discharges $Q(t + 48h)$. As fuzzification methods the pure statistical approach as well as the combination of the statistical and equally-partitioning method are compared. Furthermore, the optimization with no further restriction and in case of MS with predefined, fixed responses are investigated. Considering the TS systems different argument combinations of the linear response functions are analysed. For the investigations a series of rule systems are trained and validated for each case. The results show that for the MS inference system a reasonable fuzzification and optimization strategy can be derived with which comparable fuzzy inference systems can be trained without investigating a certain number of rules. Therefore, low computation times are ensured. Furthermore, the fuzzification applying the combination of the statistical and equally-partitioning method leads generally to better results. Thus, it is performed throughout all investigations considering the 48 hour forecast. Due to the already mentioned sensitivities of the TS inference system no general optimization strategy can be developed. Further investigations performing this fuzzy inference system are neglected. Nevertheless, the performance of the best fitted MS and TS inference systems for gauge Kemmern are of comparable quality and ensure a satisfying 48 hour forecast of $Q(t + 48h)$.

Further investigations considering the 48 hour forecast with MS inference systems show that equally good forecast performance can be achieved considering different argument combinations. However, in order to ensure user-friendly forecast systems MS inference systems considering the simplest argument combination should be performed. Furthermore, it is proven that the information content of the arguments *current observed discharge at the forecast gauge* and *current observed discharge at the upstream gauge* are essential for the 48 hour forecast within the Upper Main basin. The results also show that no general improvement of the forecast performance of discharge is achieved if finer temporal discretized forecasts of the argument *cumulated areal precipitation* are considered.

Although some modifications are required for the gauges Schwürbitz and Mainleus the transferability of the results considering the best fitted MS inference system of gauge Kemmern is verified: It is possible to set up simple and user-friendly MS and TS inference systems considering the forecast time horizons 48 hours at the main gauges within the Upper Main river. Considering the optimization setup these systems only differ in the performed fuzzification methods from those of the three other forecast time horizons.

Further investigations show that an improvement of the developed 48 hour forecast systems considering the ten highest flood peaks is achieved by performing Tukey depth as argument. Furthermore, the limited extrapolation behavior of MS inference systems is demonstrated and discussed in conjunction with Tukey depth. Therefore, the developed MS inference systems have to be trained on a generated database in order to ensure the 48 hour forecast of extreme flood events with a return period of 100 years and higher. Considering the generated database the developed MS inference systems can be trained and validated without any further restrictions in a satisfying way and of comparable quality. However, the performance of these systems considering the observed flood events is less satisfying. Only the observed peaks of the highest flood events can be reproduced with those MS inference systems. This circumstance can be traced back to the properties of the generated and observed database and the limited extrapolation behavior of MS inference systems. The highest observed flood event (approximately HQ_{20}) belongs to the smallest ones within the generated database and is very rarely presented. Nevertheless, the MS inference systems which are trained only on the observed and generated database, respectively, complement each other. Therefore, the performance of these MS inference systems ensures a continuous forecast of flood events considering both ranges, usual and extreme.

The comparison of the classical rainfall-runoff model WaSiM-ETH and the developed MS forecast systems shows that flood forecasts of comparable quality can be performed with both modelling approaches. However, the MS inference systems are more robust considering both, the spatial distribution and the estimated amount of forecasted precipitation. Furthermore, these forecast systems are less time consuming and always applicable since no tracking of the model has to be performed between single flood events. Therefore, reliable and continuous forecasts are ensured with a simpler model setup.

Can a user-friendly and flexible warning system based on fuzzy inference systems be developed which considers precipitation and model uncertainties?

In this thesis the warning system ExpHo-HORIX (*Expertensystem Hochwasser - HORIX*) is developed. The two most important properties of this warning system are its abilities (1) to account for uncertainties, and (2) to provide the user with a manageable, transparent and fast forecast system, which ensures an easy integration into an existing environment. Two kinds of uncertainties are distinguished: precipitation forecast and model uncertainties. The quantification of precipitation uncertainties is performed by default and based on the forecast of precipitation ensembles. In contrast to this model uncertainties can only be quantified if (1) fuzzy inference systems which are trained on a generated database are implemented and (2) results of the SCEM analysis after Grundmann (2009) are available for the rainfall-runoff model with which the database has been generated. The warning system is very flexible since single MS / TS inference systems can be additionally implemented into, changed within or removed from a running ExpHo-HORIX setup without affecting other fuzzy inference systems. Furthermore, it is very user-friendly as only

one main configuration file is required in which all necessary information about the single fuzzy inference systems and the consideration of uncertainties are defined.

Outlook

Within this thesis three main research questions considering the development of a fuzzy rule based expert system for flood forecasts are investigated and answered. However, based on the presented results and developed methods new research objectives arise.

With common sensitivity analysis the high dimensional parameter space under investigation is often tremendously reduced to one or two dimensions. Therefore, one new objective could be the investigation of a multi-dimensional sensitivity analysis based on Tukey depth. Since Bárdossy and Singh (2008) considered Tukey depth to find robust parameter vectors for a hydrological model the approach to apply this data depth for a multi-dimensional sensitivity analysis is reasonable.

Considering the calibration of rainfall-runoff models and the SCE optimization algorithm the transferability of the developed iterative optimization strategy has to be verified. Thereby, the performance should be investigated for several catchments owning different catchment properties.

Since most of the time recording points at gauges are out of order and / or report wrong measurements during high flood events the arguments *current observed discharge at the forecast gauge* and *current observed discharge at the upstream gauge* are uncertain and error-prone. Therefore, other approaches and argument combinations should be investigated in which these arguments are not included. Thereby, the idea *forecast of discharge changes* should be picked up again and investigated in more detail than it is done in this work. Furthermore, the performance of spatial distributed arguments instead of mean areal ones seems promising. Disse et al. (2009) presented one possible approach for the consideration of spatial distributed information. However, their presented approach results in much more complex forecast systems than those presented in this work because the forecast at single gauges are based on a forecast chain.

Based on the presented results it seems promising to perform Tukey depth as an indicator and additional tool for the quantification of the forecast quality of fuzzy inference systems. Thereby, it has to be investigated in more detail if in general better forecast qualities correspond to higher Tukey depth values (ordinary conditions) and suboptimal qualities to low depth values (unusual conditions).

Since the sensitivity behavior of the SA-TS optimization process is not totally clarified further investigations should be carried out, in particular, considering the performance of Tukey depth as an argument as well as the generated database. In contrast to the MS inference systems TS systems own a certain extrapolation behavior due to the definition of linear response functions. In this context it would be of interest to investigate whether the performance of TS inference systems trained on the existing generated database is of comparable quality to the one of the MS inference systems if the 48 hour forecast of observed flood events is considered.

Finally, as soon as real precipitation forecasts are available, the training of all best fitted fuzzy inference systems should be repeated and their performance checked.

Bibliography

- M. B. Abbott, J. C. Bathurst, J. A. Cunge, P. E. O'Connell, and J. Rasmussen. An introduction to the European Hydrological System – Système Hydrologique Européen, "SHE", 1: History and philosophy of a physically-based, distributed modelling system. *Journal of Hydrology*, pages 45–59, 1986a.
- M. B. Abbott, J. C. Bathurst, J. A. Cunge, P. E. O'Connell, and J. Rasmussen. An introduction to the European Hydrological System – Système Hydrologique Européen, "SHE", 2: Structure of a physically-based, distributed modelling system. *Journal of Hydrology*, pages 61–77, 1986b.
- A. Abraham. Neuro fuzzy systems: State-of-the-art modeling. *Lecture Notes in Computer Science*, 2084:269–276, 2001.
- A. Abraham. Adaptation of fuzzy inference system using neural learning. In N. Nedjah and L. de Macedo Mourelle, editors, *Fuzzy systems engineering: theory and practice*. Springer, 2005.
- R. J. Abraham and L. See. Multi-model data fusion for river flow forecasting: an evaluation of six alternative methods based on two contrasting catchments. *Hydrology and Earth System Sciences*, 6(4):655–670, 2002.
- S. Alvisi, G. Mascellani, M. Franchini, and A. Bárdossy. Water level forecasting through fuzzy logic and artificial neural network approaches. *Hydrology and Earth System Sciences*, 10:1–17, 2006.
- E. A. Anderson. National weather service river forecast system - snow accumulation and ablation model. *National Oceanographic and Atmospheric Administration (NOAA), NWS-HYDRO-17, Silver Spring, MD*, page 217p, 1973.
- ASCE. Artificial neural networks in hydrology. i: Preliminary concepts. *Journal of Hydrologic Engineering*, 5:115–123, 2000a.
- ASCE. Artificial neural networks in hydrology. ii: Hydrologic applications. *Journal of Hydrologic Engineering*, 5:124–137, 2000b.
- A. Bárdossy. The use of fuzzy rules for the description of elements of the hydrological cycle. *Ecological Modelling*, 85:59–65, 1996.
- A. Bárdossy. Generating precipitation time series using simulated annealing. *Water Resources Research*, 34:1737–1744, 1998.
- A. Bárdossy and M. Disse. Fuzzy rule-based models for infiltration. *Water Resources Research*, 29:373–382, 1993.

Bibliography

- A. Bárdossy and L. Duckstein. *Fuzzy rule-based modeling with applications to Geophysical, Biological and Engineering Systems*. CRC Press, 1995.
- A. Bárdossy and S. K. Singh. Robust estimation of hydrological model parameters. *Hydrology and Earth System Sciences*, 5:1641–1675, 2008.
- A. Bárdossy, J. Stehlík, and H.-J. Caspary. Automated objective classification of daily circulation patterns for precipitation and temperature downscaling based on optimized fuzzy rules. *Climate Research*, 23:11–22, 2002.
- A. Bárdossy, U. Haberlandt, and V. Krysanova. Automatic fuzzy-rule assessment and its application to the modelling of nitrogen leaching for large regions. *Soft Computing*, 7:370–385, 2003.
- Bayer. HND. Homepage des Bayerischen Hochwassernachrichtendienst, 2005. <http://www.hnd.bayern.de/>.
- K.-M. Bengelstorf. Statistische Untersuchung der Einzugsgebiete Oberer Main, Freiberger Mulde und Fränkische Saale zur Bestimmung von Eingangsgrößen eines regelbasierten Hochwasservorhersagesystems. Diplomarbeit, Universität der Bundeswehr München, Germany, 2009.
- S. Bergström. The HBV model. In V. Singh, editor, *Computer models of watershed hydrology*, pages 443–476. Water Resources Publications, 1995.
- St. Berlik. *Computational Intelligence: 3. Optimierung*. Vorlesungsunterlagen WS 2009/2010, Fachgruppe Praktische Informatik, Universität Siegen, 2009.
- K. Beven. Changing ideas in hydrology - the case of physically-based models. *Journal of Hydrology*, 105:157–172, 1989.
- K. Beven and J. Freer. Equifinality, data assimilation, and data uncertainty estimation in mechanistic modelling of complex environmental systems using the glue methodology. *Journal of Hydrology*, 249:11–29, 2001.
- K. Beven and M. J. Kirkby. A physically based variable contributing area model of basin hydrology. *Hydrological Sciences Bulletin*, 24(1):43–69, 1979.
- K. J. Beven. *Rainfall-Runoff Modelling - The Primer*. John Wiley and Sons, Ltd, 2003.
- M. Black. Vagueness - an exercise in logical analysis. *Philosophy of Science*, 4:427–455, 1937.
- L. Blasy and H. Øverland. Modellierung des Wasserhaushalts für das Flussgebiet Oberer Main mit dem Modellsystem ASGi auf Stundenbasis. *Projektbericht, Dr. Blasy - Dr. Øverland, Beratende Ingenieure GbR*, 2004.
- J. Bliedernicht. *Probability forecasts of daily areal precipitation for small river basins*. PhD thesis, University of Stuttgart, Germany, 2010.
- J. Bliedernicht, A. Bárdossy, and C. Ebert. Stochastische Simulation stündlicher Niederschlagsfelder für Extremwertereignisse an der Freiberger Mulde, dem Oberen Main und der Fränkischen Saale. *Hydrologie und Wasserbewirtschaftung*, 52(4):168–172, 2008.
- L. N. Braun. *Simulation of snowmelt-runoff in lowland and lower alpine regions of Switzerland*, volume 21. Züricher Geographische Schriften, ETH Zürich, 1985.

- M. Bruen and J. Yang. Functional networks in real-time flood forecasting - a novel application. *Journal of Hydrology*, 28:899–909, 2005.
- W. Brutsaert. *Evaporation into the Atmosphere*. Kluwer Academic Publishers, 1982.
- M. Casper, P. Gemmar, O. Gronz, M. Johst, and M. Stüber. Fuzzy logic-based rainfall-runoff modelling using soil moisture measurements to represent system state. *Hydrological Sciences Journal*, 52(3):478–490, 2007.
- M. Castellano-Mendez. Modelling of the monthly and daily behaviour of the runoff of the Xallas river using Box-Jenkins and neural networks methods. *Journal of Hydrology*, 296:38–58, 2004.
- F. Chebana and T. B. M. J. Ouarda. Depth and homogeneity in regional flood frequency analysis. *Water Resources Research*, 44:W11422, 2008.
- K. Cramer. *Multivariate Ausreißer und Datentiefe*. Shaker, Aachen, 2003.
- N. H. Crawford and R. K. Linsley. Digital simulation in hydrology: Stanford Watershed Model iv. Technical report, 1966.
- J. Cullmann. *Online flood forecasting in fast responding catchments on the basis of a synthesis of artificial neural networks and process models*. PhD thesis, Technische Universität Dresden, Germany, 2006.
- M. Disse, S. Pakosch, P. Keillholz, A. Yörük, and T. Molnar. Endbericht zum Forschungsvorhaben Teilprojekt 1 des Verbundprojektes HORIX. *Technische Informationsbibliothek Hannover*, 3, 2009.
- DLR. Corine Land Cover Raster Data 2000. Deutsches Zentrum für Luft- und Raumfahrt, 2000.
- D. L. Donoho and M. Gasko. Breakdown properties of location estimates based on halfspace depth and projected outlyingness. *The Annals of Statistics*, 20(4):1803–1827, 1992.
- Q. Duan. Personal conversation, 2010.
- Q. Duan, S. Sorooshain, and V. K. Gupta. Effective and efficient global optimization for conceptual rainfall-runoff models. *Water Resources Research*, 28(4):1015–1031, 1992.
- Q. Duan, S. Sorooshain, and V. K. Gupta. Shuffled Complex Evolution approach for effective and efficient global minimization. *Journal of Optimization Theory and Applications*, 76(3): 501–521, 1993.
- Q. Duan, S. Sorooshain, and V. K. Gupta. Optimal use of the SCE-UA global optimization method for calibrating watershed models. *Journal of Hydrology*, 158:265–284, 1994.
- D. Dubois and H. Prade. *Fuzzy sets and systems: theory and applications*. Academic Press, 1980.
- S. Dyck and G. Peschke. *Grundlagen der Hydrologie*. Verlag für Bauwesen, 1995.
- R. Dyckerhoff. Data depths satisfying the projection property. *Allgemeines Statistisches Archiv*, 88:163–190, 2004.
- K. Eckhardt and J. C. Arnold. Automatic calibration of a distributed catchment model. *Journal of Hydrology*, 251(1/2):103–109, 2001.

Bibliography

- European Commission. Homepage of the European Commission - Environment, 2011. http://ec.europa.eu/environment/water/flood_risk/index.htm.
- C. A. Federer and D. Lash. *BROOK - a hydrologic simulation model for eastern forests*. 1983.
- D. A. K. Fernando and A. W. Jayawardena. Runoff forecasting using rbf networks with ols algorithm. *Journal of Hydrologic Engineering*, 3(3):203–209, 1998.
- J. Fleckenstein. Mathematische Modelle in der Hydrologie. Vorlesungsunterlagen, 2005. http://www.hydro.uni-bayreuth.de/lehre/files/LVDetail90/Vorlesung_Handout.pdf.
- P. Gemmar, O. Gronz, and M. Stüber. Effiziente Erstellung und praktischer Einsatz von NA-Modellen mittels Fuzzy Logic und automatisierter Entwicklungsverfahren. *Forum für Hydrologie und Wasserbewirtschaftung*, 16:27–40, 2006.
- D. E. Goldberg. *Genetic algorithm in search, optimization, and machine learning*. Addison-Wesley Publishing Company, 1989.
- J. Grundmann. *Analyse und Simulation von Unsicherheiten in der flächendifferenzierten Niederschlags-Abfluss-Modellierung*. PhD thesis, Technische Universität Dresden, Germany, 2009.
- J. Grundmann and G. H. Schmitz. Methodenentwicklung zur Bestimmung von Unsicherheiten von Niederschlags-Abfluss Modellen. 2. *Nutzerworkshop HORIX*, 2008.
- F. Guély, R. La, and P. Siarry. Fuzzy rule base learning through Simulated Annealing. *Fuzzy Sets and Systems*, 105:353–363, 1999.
- H. V. Gupta, S. Sorooshian, and P. O. Yapo. Toward improved calibration of hydrologic models: Multiple and noncommensurable measures of information. *Water Resources Research*, 34(4):751–763, 1998.
- J. Gurtz, A. Baltensweiler, and H. Lang. Spatially distributed hydrotope-based modelling of evapotranspiration and runoff in mountainous basins. *Hydrological Processes*, 13:2751–2768, 1999.
- HAP. Homepage Hochwasserrisikomanagement-Plan Bayerisches Main Einzugsgebiet, 2008. <http://www.hopla-main.de/>.
- F. Herrera, M. Lozano, and J. L. Verdegay. A learning process for fuzzy control rules using genetic algorithms. *Fuzzy Sets and Systems*, 100:143–158, 1998.
- R. Hoberg. *Clusteranalyse, Klassifikation und Datentiefe*. Eul, Lohmar, 2003.
- T. Hogue, S. Sorooshain, H. Gupta, A. Holz, and D. Braatz. A multistep automatic calibration scheme for river forecasting models. *Journal of Hydrometeorology*, 1:524–542, 2000.
- Y. Hundecha, A. Bárdossy, and H.-W. Theisen. Development of a fuzzy logic-based rainfall-runoff model. *Hydrological Sciences*, 46(3):363–376, 2001.
- R. L. Iman, J. C. Helton, and J. E. Campbell. An approach to sensitivity analysis of computer models, part 1. introduction, input variable selection and preliminary variable assessment. *Journal of Quality Technology*, 13(3):174–183, 1981.

- A. P. Jacquin and A. Y. Shamseldin. Development of rainfall-runoff models using Takagi-Sugeno fuzzy inference systems. *Journal of Hydrology*, 329:154–173, 2006.
- P. H. M. Janssen and P. S. C. Heuberger. Calibration of process-oriented models. *Ecological Modelling*, 83:55–66, 1995.
- K. Jasper, J. Gurtz, and H. Lang. Advanced flood forecasting in alpine watersheds by coupling meteorological observations and forecasts with a distributed hydrological model. *Journal of Hydrology*, 267:40–52, 2002.
- A. Kaufmann and M. M. Gupta. *Introduction to fuzzy arithmetic: theory and applications*. Van Nostrand Reinhold Company, 1991.
- S. Kirkpatrick, C. D. Gelatt, and M. P. Vecchi. Optimization by Simulated Annealing. *Science*, 220(4598):670–680, 1983.
- G. J. Klir and B. Yuan. *Fuzzy sets and fuzzy logic - theory and applications*. Prentice-Hall, 1995.
- G. Koshevoy and K. Mosler. Zonoid trimming for multivariate distributions. *The Annals of Statistics*, 25:1998–2017, 1997.
- P. Krause, D. P. Boyle, and F. Bäse. Comparison of different efficiency criteria for hydrological model assessment. *Advances in Geosciences*, 5:89–97, 2005.
- G. Kuczera. Efficient subspace probabilistic parameter optimization for catchment models. *Water Resources Research*, 33(1):177–185, 1997.
- LfU. Data exchange for the Upper Main basin. Bayerischen Landesamts für Umwelt, 2005.
- LfU. Homepage des Bayerischen Landesamts für Umwelt, 2008. <http://www.wasserrahmenrichtlinie.bayern.de>.
- LfW. Verzeichnis der Bach- und Flussgebiete in Bayern. Bayerisches Landesamt für Wasserwirtschaft, 1978.
- X. Liang, D. P. Lettenmaier, E. F. Wood, and S. J. Burges. A simple hydrologically-based model of land surface water and energy fluxes for general circulation models. *Journal of Geophysical Research*, 99:14415–14428, 1994.
- R. Y. Liu. On a notion of simplicial depth. *Proceedings of the National Academy of Sciences of the USA*, 85:1732–1734, 1988.
- R. Y. Liu and K. Singh. A quality index based on data depth and multivariate rank tests. *Journal of the American Statistical Association*, 88:252–260, 1993.
- A. K. Lohani, N. K. Goel, and K. K. S. Bhatia. Takagi-Sugeno fuzzy inference system for modeling stage-discharge relationship. *Journal of Hydrology*, 331:146–160, 2006.
- J. Lukasiewicz. *Aristoteles syllogistic: From the standpoint of modern formal logic*. Oxford University Press, 1957.
- H. Madsen. Automatic calibration of a conceptual rainfall-runoff model using multiple objectives. *Journal of Hydrology*, 235(3-4):276–288, 2000.

Bibliography

- H. Madsen. Parameter estimation in distributed hydrological catchment modeling using automatic calibration with multiple objectives. *Advances in Water Resources*, 26:205–216, 2003.
- P. C. Mahalanobis. On the generalized distance in statistics. *Proceedings of the National Academy of India*, 12:49–55, 1936.
- E. H. Mamdani. Applications of fuzzy algorithms for control of a simple dynamic plant. *Proceedings of IEEE*, 121(12):1585–1588, 1974.
- A. Mantoglou and J. Wilson. Turning bands method for simulation of random fields using line generation by a spectral method. *Water Resources Research*, 18:1397–1394, 1987.
- A. Marx. *Einsatz gekoppelter Modelle und Wetterradar zur Abschätzung von Niederschlagsintensitäten und zur Abflussvorhersage*. PhD thesis, University of Stuttgart, Germany, 2007.
- S. F. Masri, G. A. Bekey, and F. B. Safford. An Adaptive Random Search method for identification of large scale nonlinear systems. *Proceedings of 4th IFAC Symposium on Identification and System Parameter Estimation, Amsterdam, Holland*, 1978.
- J. L. Montheith. *Vegetation and atmosphere, volume 1: Principles*. Academic Press, London, 1975.
- T. J. Mulvaney. On the use of self-registering rain and flood gauges in making observations of the relations of rainfall and flood discharges in a given catchment. *Proceedings of the Institution of Civil Engineerings of Irland*, 4:19–31, 1851.
- J. E. Nash and J. V. Sutcliffe. River flow forecasting through conceptual models. Part I - a discussion of principles. *Journal of Hydrology*, 10(3), 1970.
- D. Nauck, F. Klawonn, and R. Kruse. *Neuronale Netze und Fuzzy-Systeme. Grundlagen des Konnektionismus, Neuronaler Fuzzy-Systeme und der Kopplung mit wissenbasierten Methoden*. Vieweg Verlag Braunschweig Wiesbaden, 1994.
- J. A. Nelder and R. Mead. A simplex method for function minimization. *Computational Journal*, 7:308–313, 1965.
- D. Niehoff. *Modellierung des Einflusses der Landnutzung auf die Hochwasserentstehung in der Mesoskala*. PhD thesis, Universität Potsdam, Germany, 2001.
- T. R. Oke. *Boundary Layer Climates*. Routledge, 1987.
- S. Pakosch. Statistische Methoden zur stationären und instationären Auswertung von gemessenen Maximalabflüssen mit Hilfe theoretischer Verteilungsfunktionen. Diplomarbeit, Universität Stuttgart, Germany, 2004.
- S. Pakosch. Kurzbericht zur GSA Analyse und zur SCE-Optimierung. *Unveröffentlichter Bericht, Professur für Wasserwirtschaft und Ressourcenschutz, Universität der Bundeswehr München*, 2006.
- S. Pakosch. Kurzbeschreibung zur Anwendung des Expertensystems zur Hochwasservorhersage ExpHo - HORIX. *Unveröffentlichtes Manual, Professur für Wasserwirtschaft und Ressourcenschutz, Universität der Bundeswehr München*, 2008.

- S. Pakosch and M. Disse. Systematischer Vergleich des Topmodels- und Richards-Ansatzes für die ungesättigte Bodenzone. *Forum für Hydrologie und Wasserbewirtschaftung*, 15.06(3):89–92, 2006.
- S. Pakosch and M. Disse. Half-automatic calibration of WaSiM-ETH by using the genetic evolution algorithm SCE-UA. *Geophysical Research Abstracts*, EGU2007-A-04339, SRef-ID: 1607-7962/gra/EGU2007-A-04339, 9, 2007.
- S. Pakosch, M. Disse, and A. Bárdossy. Entwicklung eines fuzzy basierten Regelsystems für die Hochwasservorhersage. *Forum für Hydrologie und Wasserbewirtschaftung*, 23.08:171–179, 2008a.
- S. Pakosch, M. Disse, and A. Bárdossy. Flood forecasting in meso-scale catchments using a fuzzy rule-based expert system. *Geophysical Research Abstracts*, EGU2008-A-05204, SRef-ID: 1607-7962/gra/EGU2008-A-05204, 10, 2008b.
- M. Pfeiffer. Simulated Annealing - Vitruval Lab. Vorlesungsunterlagen, 2003. <http://isgwww.cs.uni-magdeburg.de/sim/vilab/2003/presentations/martin.pdf>.
- E. J. Plate. *Statistik und angewandte Wahrscheinlichkeitslehre für Bauingenieure*. Ernst & Sohn Verlag, Berlin, 1993.
- A. Reyhani-Masouleh. Assessment of Simulated Annealing as a training method for a fuzzy based flood forecasting system. Master Thesis, Universität der Bundeswehr München, Germany, 2008.
- L. Richards. Capillary conduction of liquids through porous media. *Physics*, 1:318–333, 1931.
- D. Rosbjerg and H. Madsen. *Concepts of Hydrological Modeling*. John Wiley and Sons, Ltd, 2005.
- H. H. Rosenbrock. An automatic method for finding the greatest or least value of a function. *Computer Journal*, 3:175–184, 1960.
- P. J. Rousseeuw and A. Struyf. Computing location depth and regression depth in higher dimensions. *Statistics and Computing*, 8:193–203, 1998.
- B. Russel. Vagueness. *The Australasian Journal of Psychology and Philosophy*, 1:84–92, 1923.
- I. Ruts and P. J. Rousseeuw. Computing depth contours of bivariate point clouds. *Computational Statistics and Data Analysis*, 23:153–168, 1996.
- J. Schulla. *Hydrologische Modellierung von Flussgebieten zur Abschätzung der Folgen von Klimänderungen*. PhD thesis, ETH Zurich, Switzerland, 1997.
- J. Schulla. Personal conversation, 2006.
- J. Schulla and K. Jasper. Model description WaSiM-ETH. Technical report, 2002.
- L. See and R. J. Abrahart. Multi-model data fusion for hydrological forecasting. *Computers and Geosciences*, 27:987–994, 2001.
- L. See and S. Openshaw. Applying soft computing approaches to river level forecasting. *Hydrological Sciences*, 44(5):763–778, 1999.

Bibliography

- L. See and S. Openshaw. A hybrid multi-model approach to river level forecasting. *Hydrological Sciences*, 45(4):523–536, 2000.
- A. Y. Shamseldin, K. M. O'Connor, and G. C. Liang. Methods for combining the outputs of different rainfall-runoff models. *Journal of Hydrology*, 197:203–229, 1997.
- L. K. Sherman. Stream flow from rainfall by the unit graph method. 108:501–505, 1932.
- R. R. Shrestha, A. Bárdossy, and M. Roda. A hybride deterministic-fuzzy rule based model for catchment scale nitrate dynamics. *Journal of Hydrology*, 342:143–156, 2007.
- S. P. Simonović. *Managing water resources - Methods and tools for a systems approach*. UNESCO Publishing, 2009.
- K. Singh. A notion of majority depth. *Technical Report, Rutgers University, Department of Statistics*, 1991.
- V. P. Singh. *Computer models of watershed hydrology*. Water Resources Publications, Colorado, USA, 1995.
- M. B. Smith, V. I. Korena, Z. Zhanga, S. M. Reeda, J. J. Panb, and F. Moreda. Runoff response to spatial variability in precipitation: an analysis of observed data. 239:267–286, 2004.
- S. Sorooshian, Q. Duan, and V. K. Gupta. Calibration of rainfall-runoff models: Application of global optimization to the Sacramento soil moisture accounting model. *Water Resources Research*, 29(4):1185–1194, 1993.
- D. G. Sotiropoulos, V. P. Plagianakos, and M. N. Vrahatis. *An evolutionary algorithm for minimizing multimodal functions*. Technical Report TR98-03, Department of Mathematics, University of Patras, 1998.
- R. C. Spear and G. M. Hornberger. Eutrophication in peel inlet. ii: identification of critical uncertainties via generalized sensitivity analysis. *Water Resources*, 14:43–49, 1980.
- StBA. Flächennutzung in Deutschland. Statistisches Bundesamt, 2004. http://www.statistik-portal.de/statistik-portal/de_jb09_jahrtaf1.asp.
- T. Takagi and M. Sugeno. Fuzzy identification of systems and its applications to modeling and control. *IEEE Transactions on Systems, Man, and Cybernetics*, 15(1):116–132, 1985.
- J. W. Tukey. Mathematics and picturing data. *Proceedings of the 1974 International Congress of Mathematicians, Vancouver*, 2:523–531, 1975.
- M. T. Van Genuchten. A closed-form equation for predicting the hydraulic conductivity of unsaturated soils. *American Journal of Soil Sciences*, 44(5):892–898, 1976.
- H. Vernieuwe, O. Georgieva, B. De Baets, V. R. N. Pauwels, N. E. C. Verhoest, and F. P. De Troch. Comparison of data-driven Takagi-Sugeno models of rainfall-discharge dynamics. *Journal of Hydrology*, 302:173–186, 2005.
- S. Wagner. *Water balance in a poorly gauged basin in West Africa using atmospheric modelling and remote sensing information*. PhD thesis, University of Stuttgart, Germany, 2008.
- WaSiM. Homepage, 2009. <http://www.wasim.ch/en/dialog/publications.htm>.

- U. Wendling. Zur Messung und Schätzung der potentiellen Verdunstung. *Zeitschrift für Meteorologie*, 25(2):103–111, 1975.
- L. Xiong, A. Y. Shamseldin, and K. M. O’Connor. A non-linear combination of the forecasts of rainfall-runoff models by the first-order Takagi-Sugeno fuzzy system. *Journal of Hydrology*, 245:196–217, 2001.
- L. A. Zadeh. Fuzzy sets. *Information and Control*, 8:338–353, 1965.
- E. C. Özelkan and L. Duckstein. Fuzzy conceptual rainfall-runoff models. *Journal of Hydrology*, 253:41–68, 2001.
- A. Zimmermann and S. Pakosch. Kurzbeschreibung zur Anwendung des Shuffled Complex Evolution (SCE) Algorithmus für WaSiM-ETH. *Unveröffentlichtes Manual, Professur für Wasserwirtschaft und Ressourcenschutz, Universität der Bundeswehr München*, 2008.
- H.-J. Zimmermann. *Fuzzy set theory and its applications*. Kluwer Academic Publishers, 1991.
- Y. Zuo and R. Serfling. General notions of statistical depth function. *The Annals of Statistics*, 28(2):461–482, 2000.

Appendix

A Fuzzy arithmetic

For a better understanding the four defined arithmetic operators for fuzzy numbers (Chapter 3.1.2) are applied on two fuzzy numbers A and B in the following. Thereby, let A and B be two fuzzy numbers described through their triangular membership functions $\mu_A(x)$ and $\mu_B(x)$ (compare Equation 3.13 and Figure 3.1b):

$$\mu_A(x) = (2, 6, 8)_T = \begin{cases} 0 & \text{if } x \leq 2 \\ \frac{x-2}{4} & \text{if } x \in [2, 6] \\ \frac{8-x}{2} & \text{if } x \in [6, 8] \\ 0 & \text{if } x \geq 8 \end{cases} \quad \mu_B(x) = (2, 3, 4)_T = \begin{cases} 0 & \text{if } x \leq 2 \\ x-2 & \text{if } x \in [2, 3] \\ 4-x & \text{if } x \in [3, 4] \\ 0 & \text{if } x \geq 4 \end{cases}$$

Before Equation 3.19 to Equation 3.22 can be applied $x_{A,1}(\alpha)$, $x_{A,2}(\alpha)$, $x_{B,1}(\alpha)$, and $x_{B,2}(\alpha)$ (Equation 3.13) have to be determined. Considering fuzzy number A one get

$$\alpha = \frac{x_{A,1}(\alpha) - 2}{4} \rightarrow x_{A,1}(\alpha) = 4\alpha + 2 \quad \text{and} \quad \alpha = \frac{8 - x_{A,2}(\alpha)}{2} \rightarrow x_{A,2}(\alpha) = 8 - 2\alpha,$$

for fuzzy number B

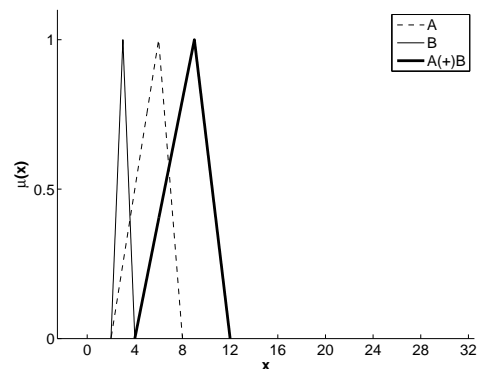
$$\alpha = x_{B,1}(\alpha) - 2 \rightarrow x_{B,1}(\alpha) = \alpha + 2 \quad \text{and} \quad \alpha = 4 - x_{B,2}(\alpha) \rightarrow x_{B,2}(\alpha) = 4 - \alpha.$$

Now, Equation 3.19 to Equation 3.22 can be calculated as:

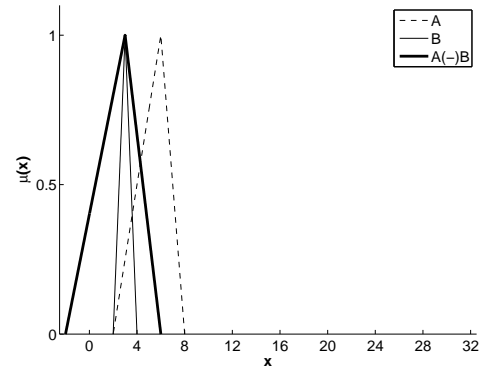
$$\begin{aligned} A(+)B &= [(4\alpha + 2) + (\alpha + 2), (8 - 2\alpha) + (4 - \alpha)] = [5\alpha + 4, 12 - 3\alpha] \\ A(-)B &= [(4\alpha + 2) - (4 - \alpha), (8 - 2\alpha) - (\alpha + 2)] = [5\alpha - 2, 6 - 3\alpha] \\ A(\cdot)B &= [(4\alpha + 2) \cdot (\alpha + 2), (8 - 2\alpha) \cdot (4 - \alpha)] = [(4\alpha^2 + 10\alpha + 4), (2\alpha^2 - 16\alpha + 32)] \\ A(/)B &= [(4\alpha + 2)/(4 - \alpha), (8 - 2\alpha)/(\alpha + 2)] \end{aligned}$$

Finally following membership functions are obtained for fuzzy addition, subtraction, multiplication, and division:

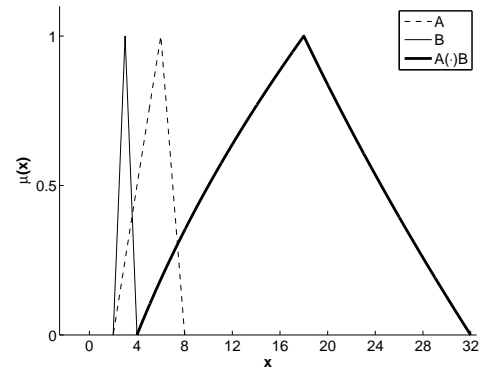
$$\mu_{A(+)B}(x) = (4, 9, 12)_T = \begin{cases} 0 & \text{if } x \leq 4 \\ \frac{x-4}{5} & \text{if } x \in [4, 9] \\ \frac{12-x}{3} & \text{if } x \in [9, 12] \\ 0 & \text{if } x \geq 12 \end{cases}$$



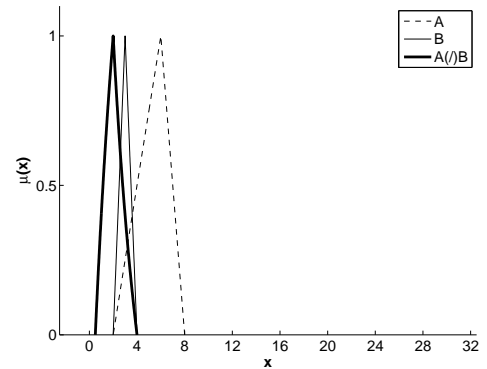
$$\mu_{A(-)B}(x) = (-2, 3, 6)_T = \begin{cases} 0 & \text{if } x \leq -2 \\ \frac{x+2}{5} & \text{if } x \in [-2, 3] \\ \frac{6-x}{3} & \text{if } x \in [3, 6] \\ 0 & \text{if } x \geq 6 \end{cases}$$



$$\mu_{A(\cdot)B}(x) = (18, 14, 14)_{LR} = \begin{cases} 0 & \text{if } x \leq 4 \\ \frac{\sqrt{9+4x}-5}{4} & \text{if } x \in [4, 18] \\ \frac{8-\sqrt{2x}}{2} & \text{if } x \in [9, 32] \\ 0 & \text{if } x \geq 32 \end{cases}$$



$$\mu_{A(/)B}(x) = (2, 1.5, 2)_{LR} = \begin{cases} 0 & \text{if } x \leq 0.5 \\ \frac{4x-2}{x+4} & \text{if } x \in [0.5, 2] \\ \frac{8-2x}{x+2} & \text{if } x \in [2, 4] \\ 0 & \text{if } x \geq 4 \end{cases}$$



Only the addition and subtraction of two triangular fuzzy numbers result in one triangular fuzzy number again, whereas for the multiplication and division LR-fuzzy numbers are obtained. Further, the following fundamental differences between classical and fuzzy arithmetic exist:

$$\text{classical arithmetic} \quad (A/B) \cdot B = A \quad (A - B) + B = A \quad (.1)$$

$$\text{fuzzy arithmetic} \quad (A(/)B)(\cdot)B \neq A \quad (A(-)B)(+)B \neq A \quad (.2)$$

This can be shown considering the given example above and the supports of A and B:

$$\begin{aligned} (A (/) B) (\cdot) B &= [0.5, 4] (\cdot) [2, 4] = [1, 16] \neq [2, 8] = A \\ (A (+) B) (-) B &= [4, 12] (-) [2, 4] = [0, 10] \neq [2, 8] = A \end{aligned}$$

B Hydrological Modelling

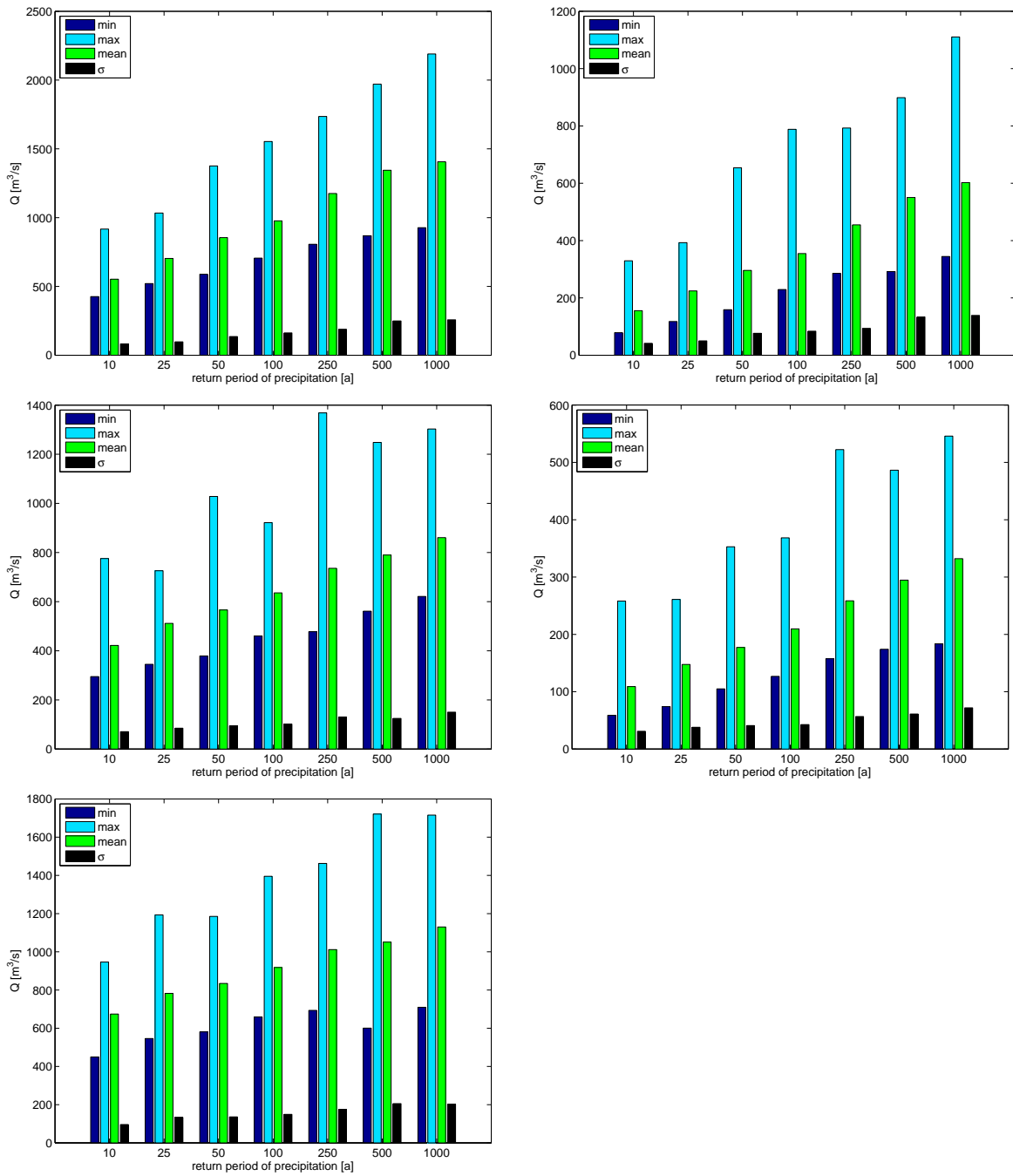


Figure B.1: Simulated minimum, maximum, and mean peak with corresponding standard deviation (σ) for each considered return period of precipitation in summer (top) and winter (middle, bottom) under wet (left), dry (right), and snowy (bottom) precondition at gauge Kemmern (4244 km²).

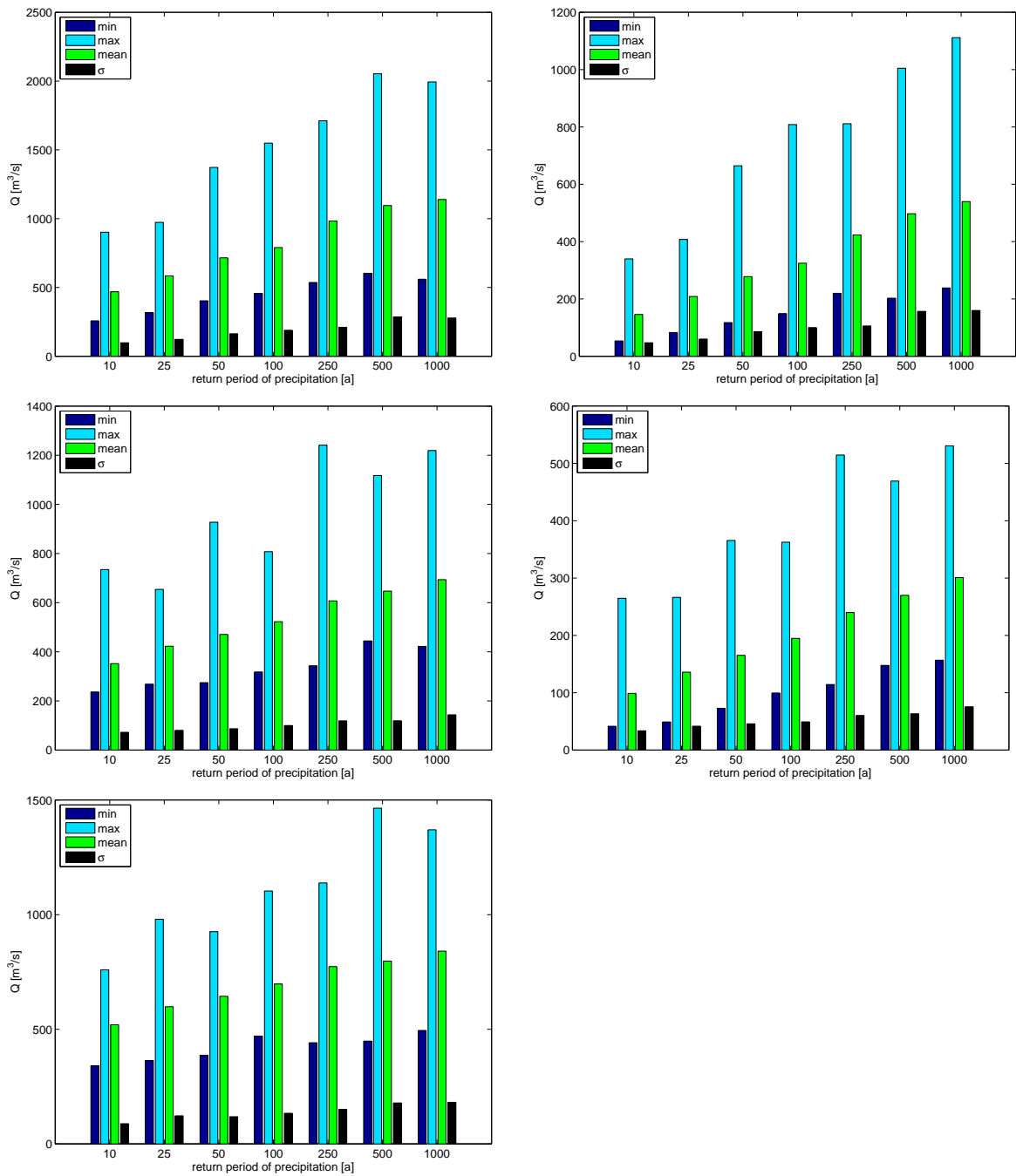


Figure B.2: Simulated minimum, maximum, and mean peak with corresponding standard deviation (σ) for each considered return period of precipitation in summer (top) and winter (middle, bottom) under wet (left), dry (right), and snowy (bottom) precondition at gauge Schwürbitz (2419 km^2).

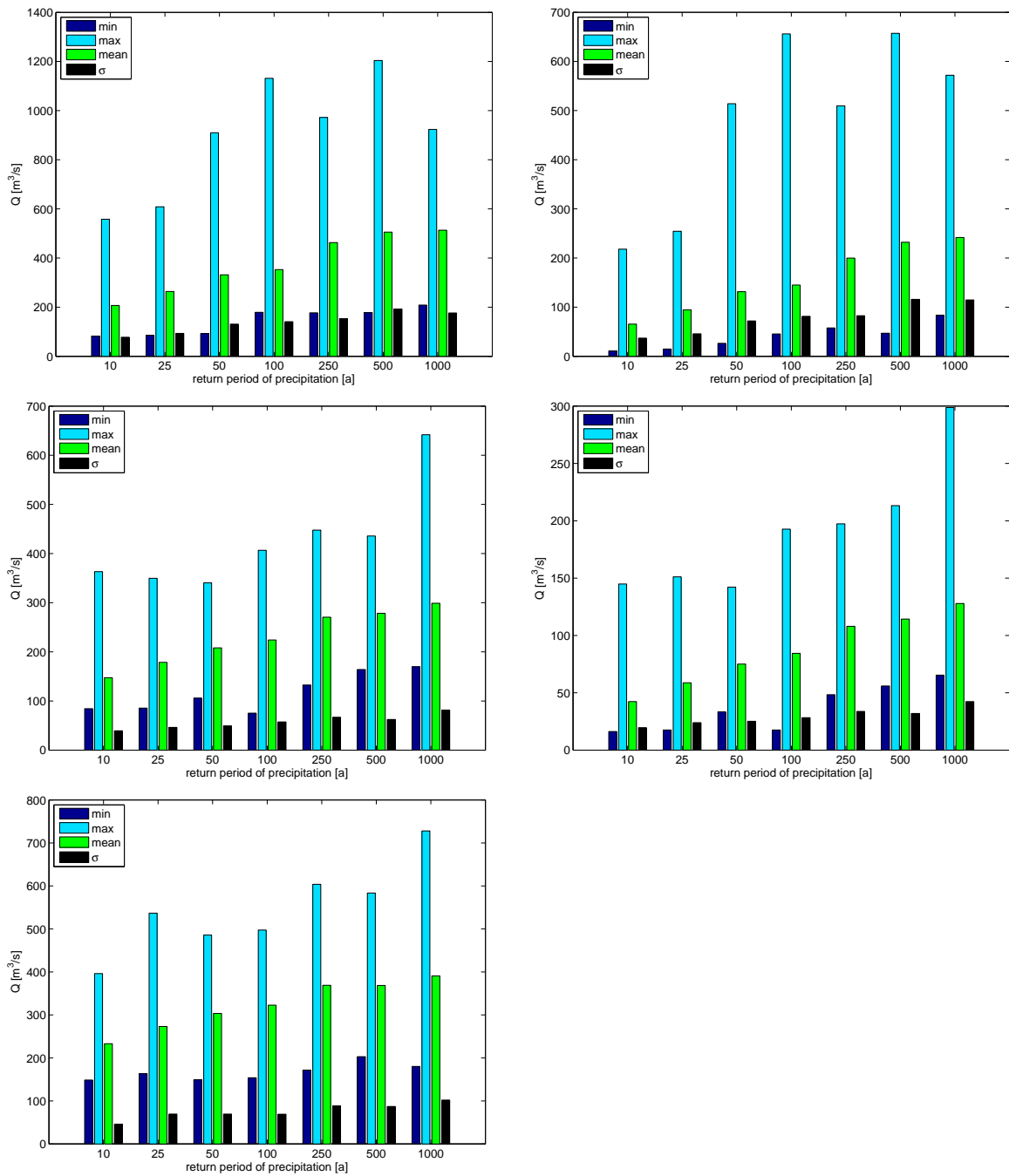


Figure B.3: Simulated minimum, maximum, and mean peak with corresponding standard deviation (σ) for each considered return period of precipitation in summer (top) and winter (middle, bottom) under wet (left), dry (right), and snowy (bottom) precondition at gauge Mainleus (1166 km²).

C Fuzzy Modelling

IF	Q(t)	&	API14d(t)	&	mT14d(t)	&	P(t)	&	fP(t+1d)	&	fP(t+2d)	&	fP(t+3d)	THEN	Q(t+3d)
IF		&	max	&	mean	&		&	mean	&	mean	&	min	THEN	min
IF	min	&		&	max	&		&		&		&		THEN	min
IF	min	&	mean	&		&		&		&		&		THEN	min
IF	min	&		&	mean	&	mean	&		&		&		THEN	min
IF	min	&		&		&		&		&	min	&		THEN	min
IF		&	mean	&	max	&		&		&		&		THEN	min
IF		&	mean	&		&	max	&	min	&		&		THEN	min
IF		&	mean	&	min	&		&	min	&	mean	&	mean	THEN	min
IF		&		&		&		&		&	min	&		THEN	mean
IF	mean	&		&		&		&	min	&	mean	&		THEN	mean
IF		&	mean	&		&		&	mean	&	mean	&		THEN	mean
IF	mean	&	trocken	&	mean	&	min	&	mean	&	mean	&	mean	THEN	mean
IF		&		&	mean	&	mean	&	mean	&	mean	&	mean	THEN	mean
IF	mean	&	mean	&	mean	&	min	&	mean	&	mean	&	mean	THEN	mean
IF	mean	&	mean	&	min	&		&		&		&	min	THEN	mean
IF	mean	&		&	mean	&	mean	&	mean	&	max	&		THEN	mean
IF		&	mean	&	max	&		&		&	max	&		THEN	mean
IF		&	max	&		&	max	&		&	mean	&	mean	THEN	mean
IF	max	&	mean	&		&		&		&		&		THEN	max
IF	max	&		&		&		&	max	&		&		THEN	max
IF	mean	&		&		&		&	max	&		&	max	THEN	max
IF	max	&		&		&	max	&		&		&		THEN	max
IF		&	mean	&	min	&		&		&	max	&		THEN	max

Figure C.1: Linguistical description of the best fitted MS inference system considering the direct 3 day forecast of discharge $Q(t + 3d)$: D3_4, 23 rules.

IF	Q(t)	& API14d(t)	& mT14d(t)	& P(t)	& fP(t+1d)	& fP(t+2d)	& fP(t+3d)	THEN	Q(t+3d) =	a1 * Q(t) +	a2 * P(t) +	a3 * fP(t+1d) +	a4 * fP(t+2d) +	a5 * fP(t+3d)
IF	min	&	&	& max	& mean	& max	& min	THEN	0.03 +	0.01 * Q(t) +	-0.03 * P(t) +	-0.02 * fP(t+1d) +	1.17 * fP(t+2d) +	-0.33 * fP(t+3d)
IF	min	&	&	&	&	& min	&	THEN	0.00 +	0.12 * Q(t) +	0.12 * P(t) +	0.21 * fP(t+1d) +	0.11 * fP(t+2d) +	0.58 * fP(t+3d)
IF	min	&	&	&	&	& min	&	THEN	0.03 +	-0.14 * Q(t) +	0.22 * P(t) +	-0.69 * fP(t+1d) +	0.13 * fP(t+2d) +	0.44 * fP(t+3d)
IF	min	&	&	&	&	& min	&	THEN	-0.33 +	23.17 * Q(t) +	-59.71 * P(t) +	2.88 * fP(t+1d) +	0.41 * fP(t+2d) +	3.81 * fP(t+3d)
IF	min	&	&	&	&	& max	&	THEN	-0.07 +	-0.04 * Q(t) +	0.11 * P(t) +	0.18 * fP(t+1d) +	0.08 * fP(t+2d) +	1.81 * fP(t+3d)
IF	min	&	&	&	&	&	&	THEN	0.00 +	0.00 * Q(t) +	0.02 * P(t) +	0.03 * fP(t+1d) +	0.02 * fP(t+2d) +	0.87 * fP(t+3d)
IF	min	&	&	&	&	& min	&	THEN	0.01 +	-0.35 * Q(t) +	0.00 * P(t) +	-0.73 * fP(t+1d) +	-4.44 * fP(t+2d) +	1.25 * fP(t+3d)
IF	min	&	&	&	&	& mean	&	THEN	0.63 +	-16.76 * Q(t) +	341.78 * P(t) +	-28.96 * fP(t+1d) +	1.36 * fP(t+2d) +	53.25 * fP(t+3d)
IF	min	&	&	&	&	& max	&	THEN	-0.18 +	0.62 * Q(t) +	-0.03 * P(t) +	0.18 * fP(t+1d) +	0.31 * fP(t+2d) +	7.33 * fP(t+3d)
IF	min	&	&	&	&	& mean	&	THEN	-0.01 +	1.12 * Q(t) +	0.03 * P(t) +	0.02 * fP(t+1d) +	0.00 * fP(t+2d) +	1.32 * fP(t+3d)
IF	min	&	&	&	&	& min	&	THEN	0.00 +	-0.13 * Q(t) +	-0.01 * P(t) +	0.01 * fP(t+1d) +	-0.17 * fP(t+2d) +	0.78 * fP(t+3d)
IF	min	&	&	&	&	& mean	&	THEN	3.98 +	57.81 * Q(t) +	178.23 * P(t) +	-4.45 * fP(t+1d) +	2.20 * fP(t+2d) +	-667.12 * fP(t+3d)
IF	min	&	&	&	&	& min	&	THEN	-0.01 +	-25.19 * Q(t) +	-0.94 * P(t) +	-4.49 * fP(t+1d) +	0.39 * fP(t+2d) +	-0.51 * fP(t+3d)
IF	min	&	&	&	&	& mean	&	THEN	-0.02 +	-1.37 * Q(t) +	0.02 * P(t) +	0.04 * fP(t+1d) +	0.05 * fP(t+2d) +	1.92 * fP(t+3d)
IF	mean	&	&	&	&	& mean	&	THEN	0.00 +	-0.01 * Q(t) +	0.02 * P(t) +	-0.04 * fP(t+1d) +	0.02 * fP(t+2d) +	0.83 * fP(t+3d)
IF	mean	&	&	&	&	& min	&	THEN	0.00 +	0.01 * Q(t) +	-0.03 * P(t) +	0.04 * fP(t+1d) +	-0.78 * fP(t+2d) +	0.99 * fP(t+3d)
IF	mean	&	&	&	&	& max	&	THEN	-0.05 +	0.06 * Q(t) +	0.24 * P(t) +	0.25 * fP(t+1d) +	0.11 * fP(t+2d) +	1.16 * fP(t+3d)
IF	mean	&	&	&	&	& mean	&	THEN	-0.11 +	0.10 * Q(t) +	0.31 * P(t) +	0.41 * fP(t+1d) +	-3.32 * fP(t+2d) +	3.15 * fP(t+3d)
IF	mean	&	&	&	&	& mean	&	THEN	0.00 +	0.00 * Q(t) +	0.20 * P(t) +	0.04 * fP(t+1d) +	0.06 * fP(t+2d) +	0.68 * fP(t+3d)
IF	mean	&	&	&	&	& mean	&	THEN	-0.02 +	-0.10 * Q(t) +	0.02 * P(t) +	0.11 * fP(t+1d) +	0.08 * fP(t+2d) +	1.03 * fP(t+3d)
IF	mean	&	&	&	&	& mean	&	THEN	0.02 +	-2.01 * Q(t) +	0.07 * P(t) +	0.02 * fP(t+1d) +	-0.04 * fP(t+2d) +	0.49 * fP(t+3d)
IF	max	&	&	&	&	& mean	&	THEN	0.04 +	-148.80 * Q(t) +	0.96 * P(t) +	0.86 * fP(t+1d) +	2.68 * fP(t+2d) +	-5.71 * fP(t+3d)
IF	max	&	&	&	&	& mean	&	THEN	-0.01 +	0.12 * Q(t) +	0.24 * P(t) +	0.16 * fP(t+1d) +	0.06 * fP(t+2d) +	0.42 * fP(t+3d)
IF	max	&	&	&	&	& mean	&	THEN	-0.01 +	-9.88 * Q(t) +	0.20 * P(t) +	0.05 * fP(t+1d) +	6.29 * fP(t+2d) +	0.46 * fP(t+3d)
IF	max	&	&	&	&	& min	&	THEN	14.10 +	3.09 * Q(t) +	-11.98 * P(t) +	-1.47 * fP(t+1d) +	2.13 * fP(t+2d) +	-1.54 * fP(t+3d)

Figure C.2: Linguistical description of the best fitted TS inference system considering the direct 3 day forecast of discharge $Q(t + 3d)$: D3_4, 25 rules.

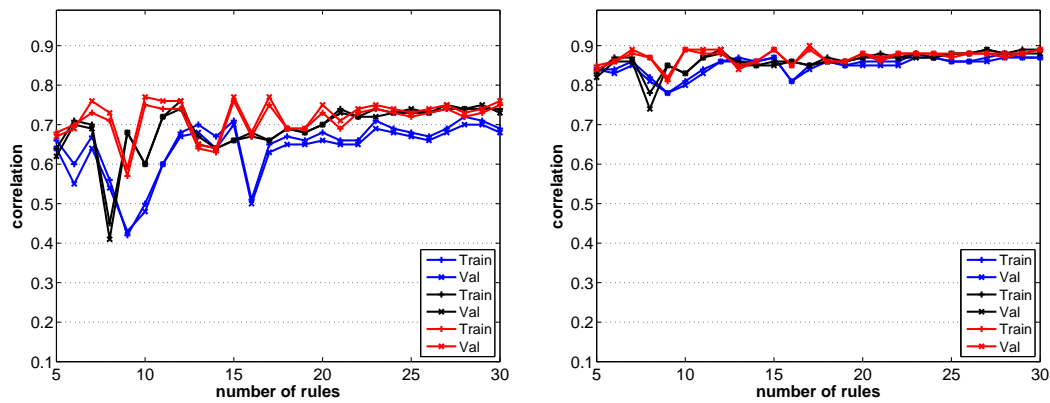


Figure C.3: Development of the correlation values for argument combinations dD3_1 (blue), dD3_2 (black), and dD3_3 (red) and MS inference systems (left: $\Delta Q(t, t + 3d)$; right: resulting $Q(t + 3d)$).

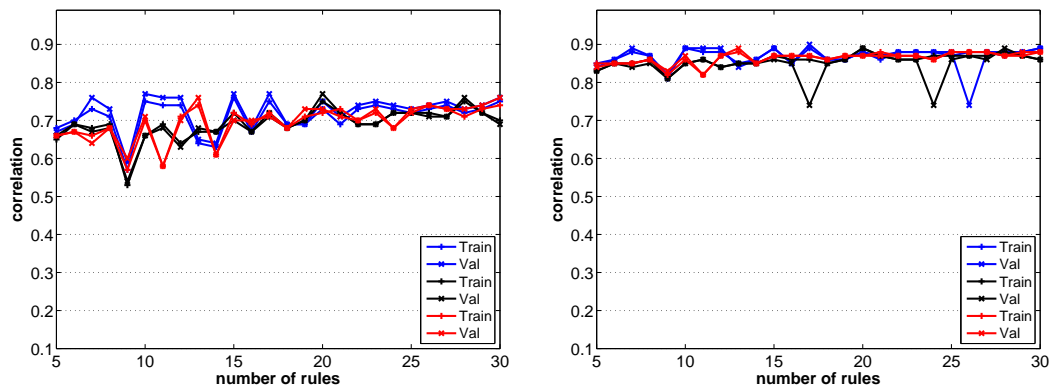


Figure C.4: Development of the correlation values for argument combinations dD3_3 (blue), dD3_4 (black), and dD3_5 (red) and MS inference systems (left: $\Delta Q(t, t + 3d)$; right: resulting $Q(t + 3d)$).

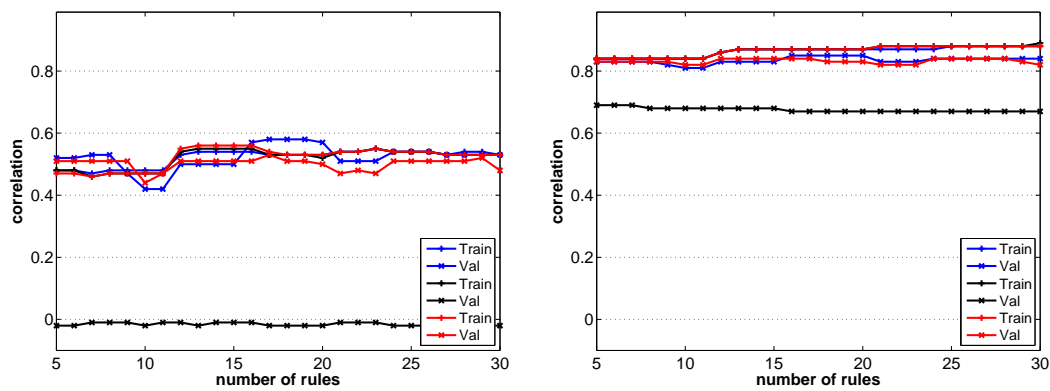


Figure C.5: Development of the correlation values for argument combinations dD3_1 (blue), dD3_2 (black), and dD3_3 (red) and TS inference systems (left: $\Delta Q(t, t + 3d)$; right: resulting $Q(t + 3d)$).

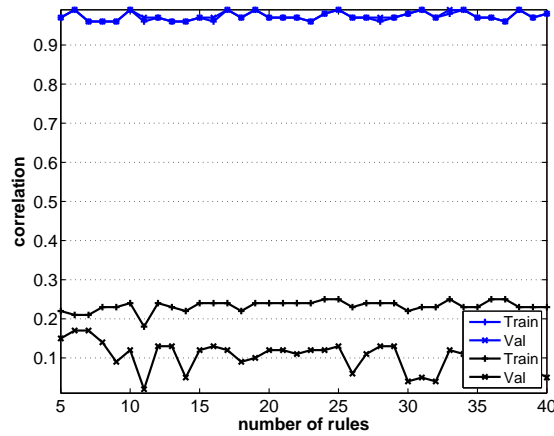


Figure C.6: Development of the correlation values for argument combinations H6_1 (blue), and H6_3 (black) and MS inference systems.

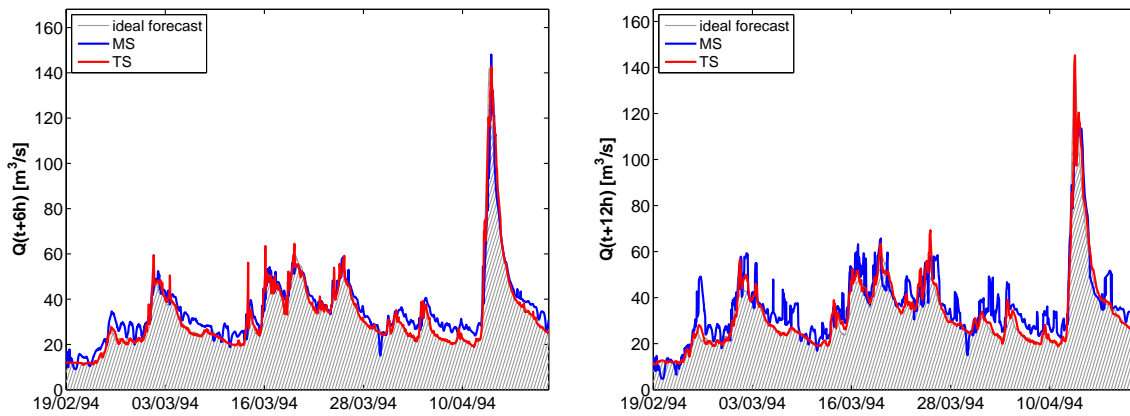


Figure C.7: Example of a flood event simulated with the best fitted MS and TS inference systems for the 6 (left) and 12 (right) hour forecast at gauge Mainleus (1166 km^2).

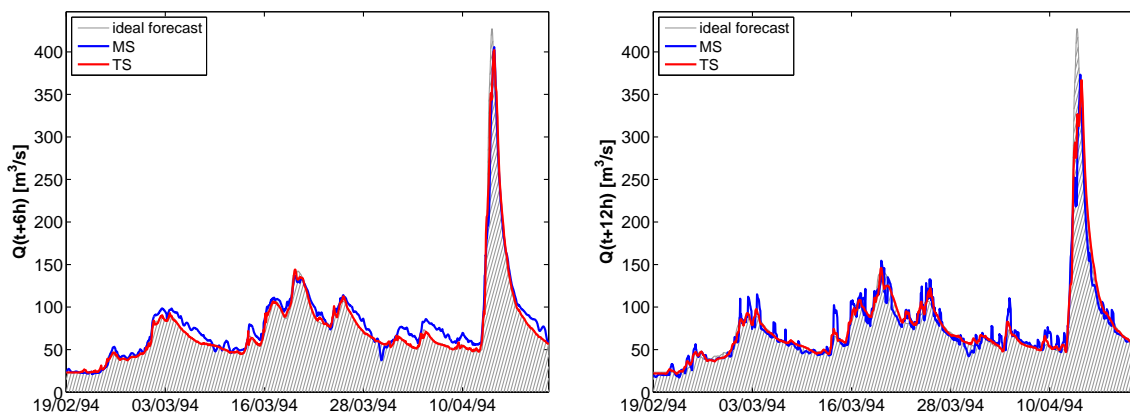


Figure C.8: Example of a flood event simulated with the best fitted MS and TS inference systems for the 6 (left) and 12 (right) hour forecast at gauge Schwürbitz (2419 km^2).

D Mamdani inference system and Tukey depth

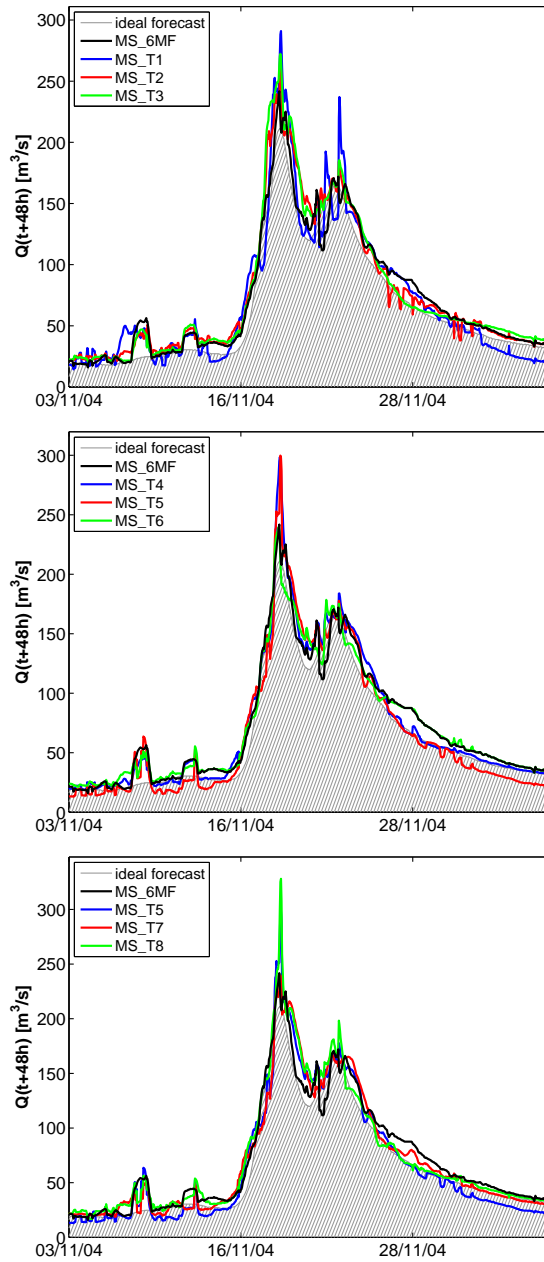


Figure D.1: Examples for a smaller flood event simulated with argument combination H48_1 and the different optimization setups MS_6MF, MS_T1, MS_T2, MS_T3, MS_T4, MS_T5, MS_T6, MS_T7, and MS_T8.

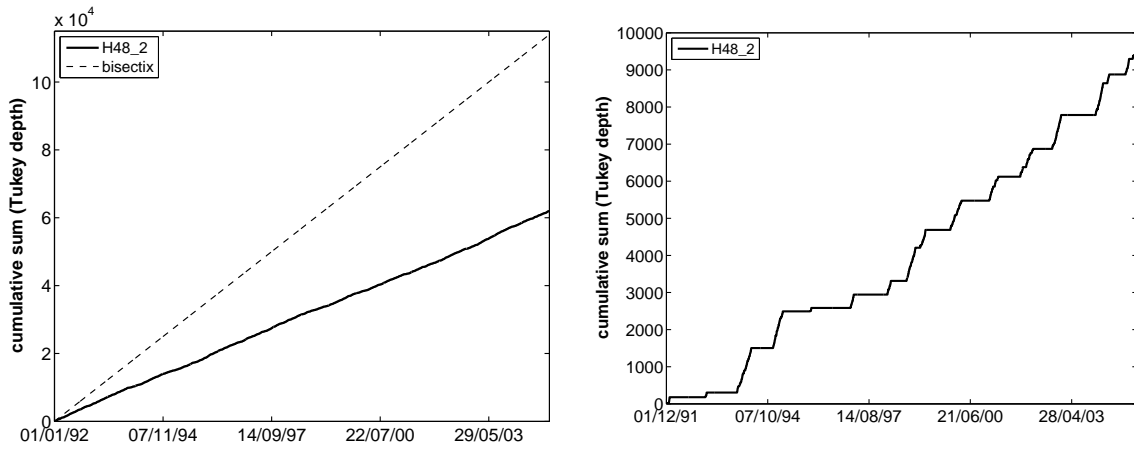


Figure D.2: Cumulative curves based on Tukey depth values calculated on hourly data considering the time period from 01.01.1992 to 31.12.2004(left) and only the 30 highest flood events (right) for the argument combinations H48_2.

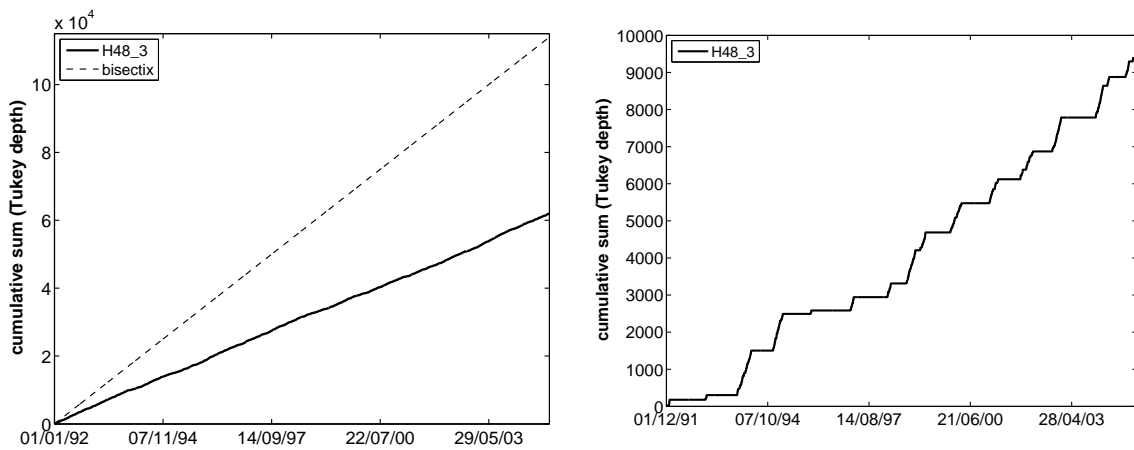


Figure D.3: Cumulative curves based on Tukey depth values calculated on hourly data considering the time period from 01.01.1992 to 31.12.2004 (left) and only the 30 highest flood events (right) for the argument combinations H48_3.

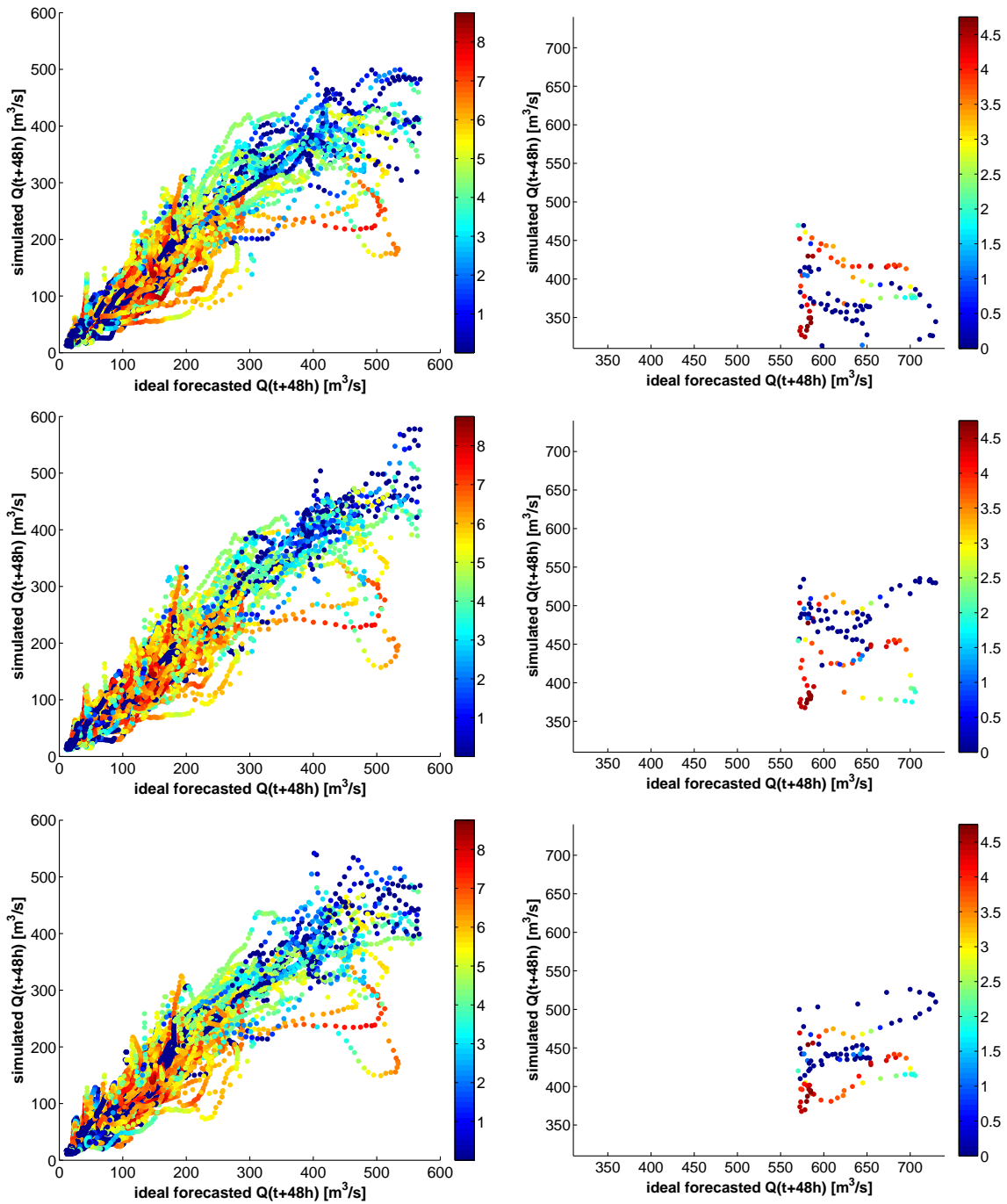


Figure D.4: Training (left) and validation (right) results considering the extrapolation behavior of MS inference systems for H48_1, MS_6MF, 20 rules (top), 40 rules (centre), and 23 rules (bottom; best optimization result in this case; marker color represents the corresponding log-scaled depth values).

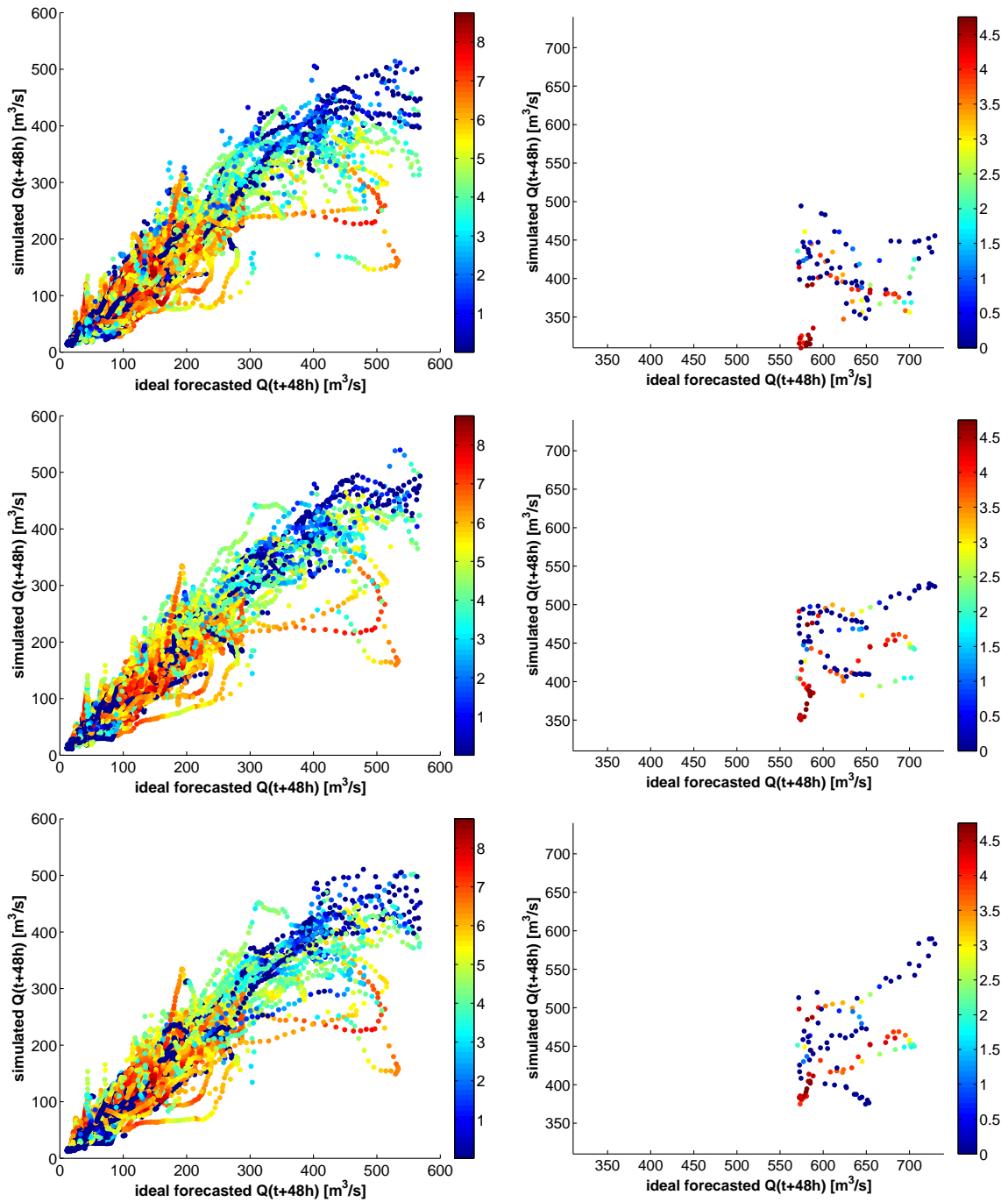
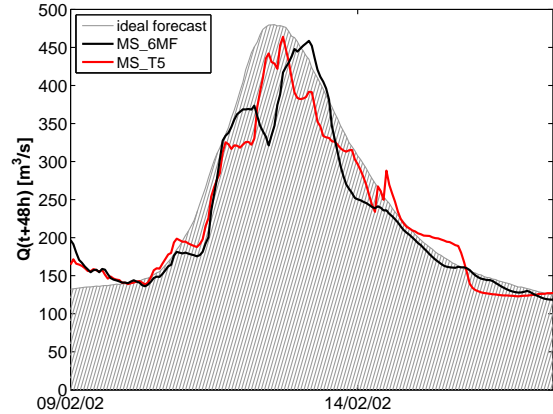
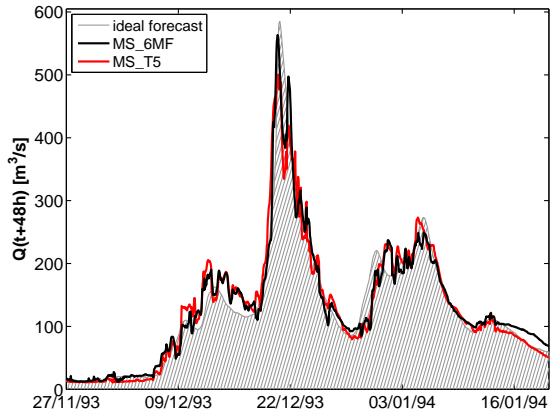
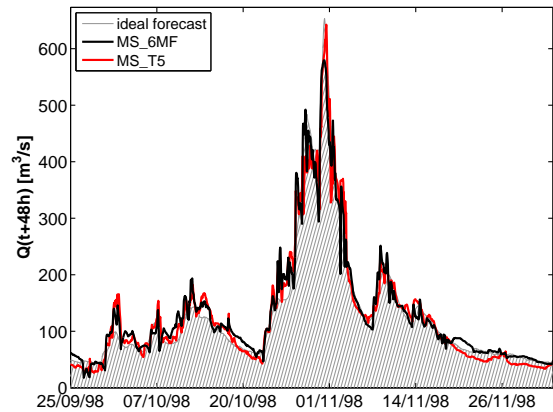
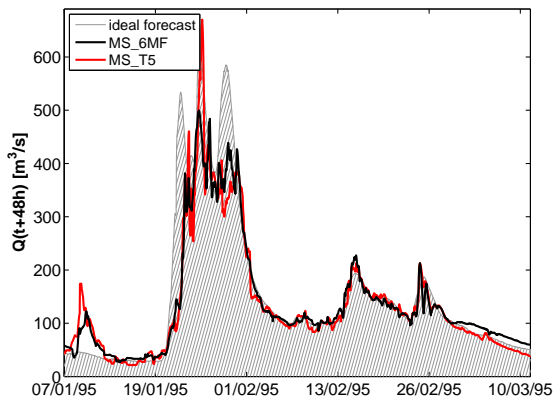
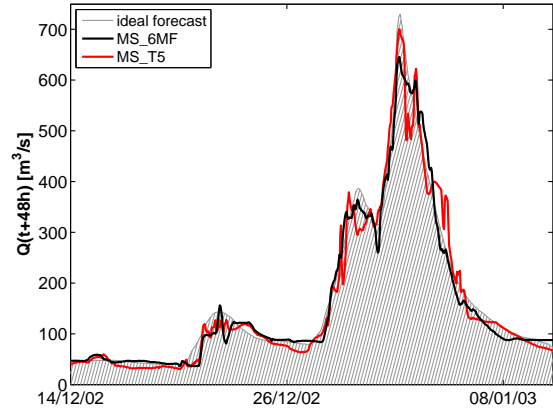
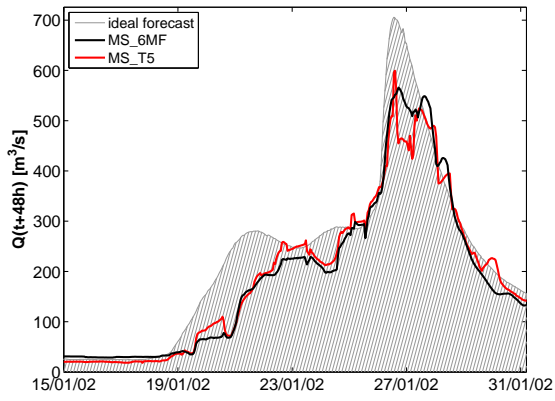


Figure D.5: Training (left) and validation (right) results considering the extrapolation behavior of MS inference systems for H48_1, MS_T5m, 20 rules (top), 40 rules (centre), and 32 rules (bottom; best optimization result in this case; marker color represents the corresponding log-scaled depth values).



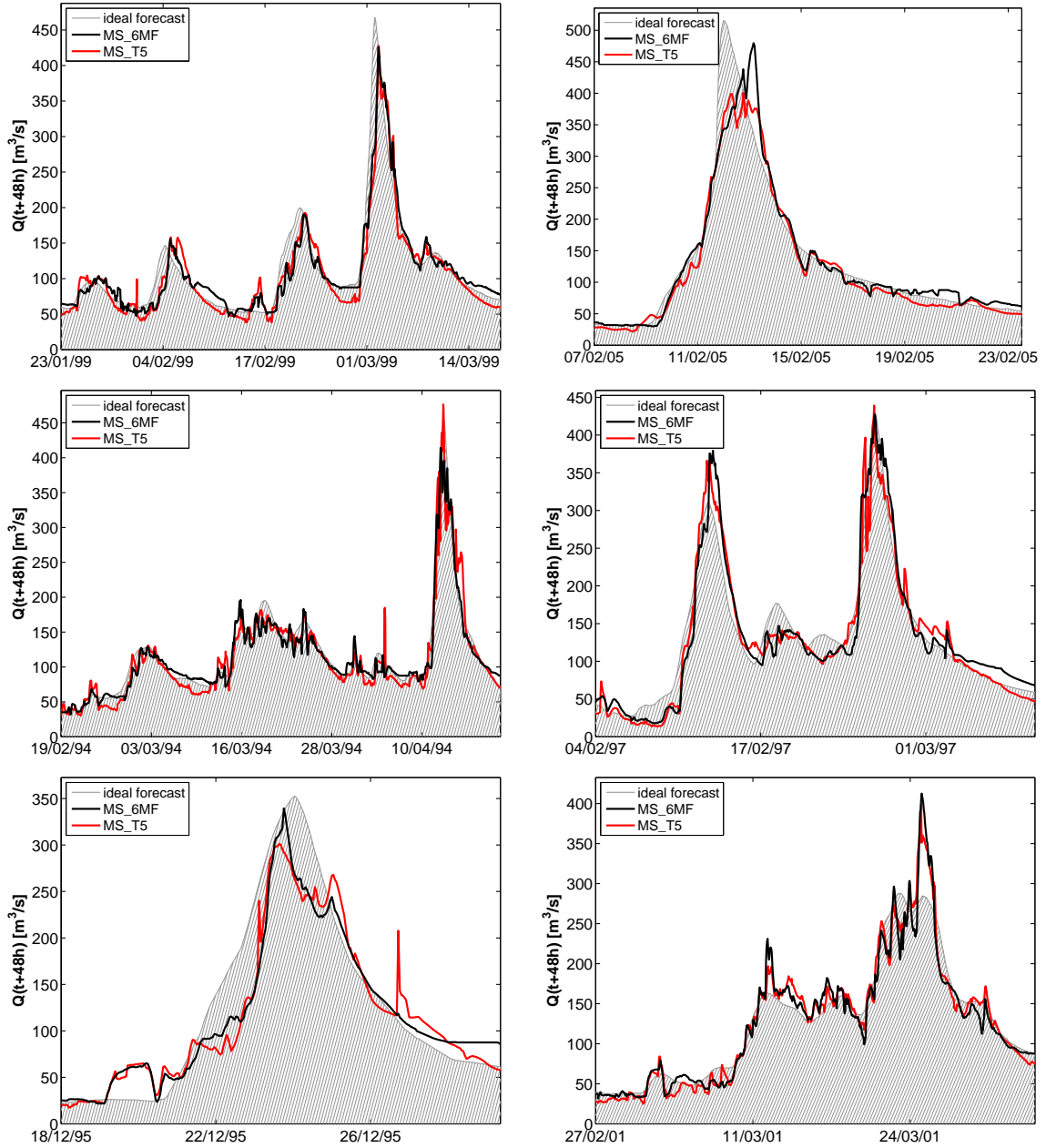


Figure D.6: Performance of the inference systems MS_6MF and MS_T5 (H48_1) considering the twelve highest observed flood events ($< HQ_1$ to HQ_{20}) and the 48 hour forecast at gauge Kemmern (4244 km^2).

E Mamdani inference systems of observed and generated database

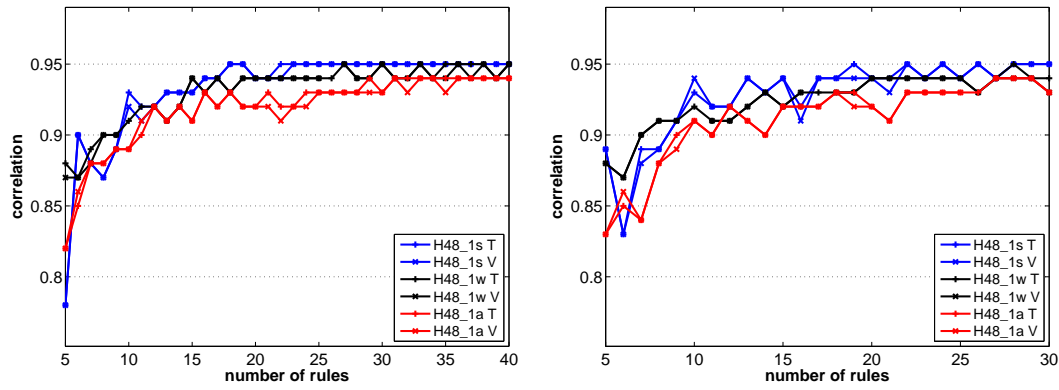


Figure E.1: Development of the correlation values for MS_6MF and MS_T5 (H48_1s, w, a) inference systems (T: training, V: validation).

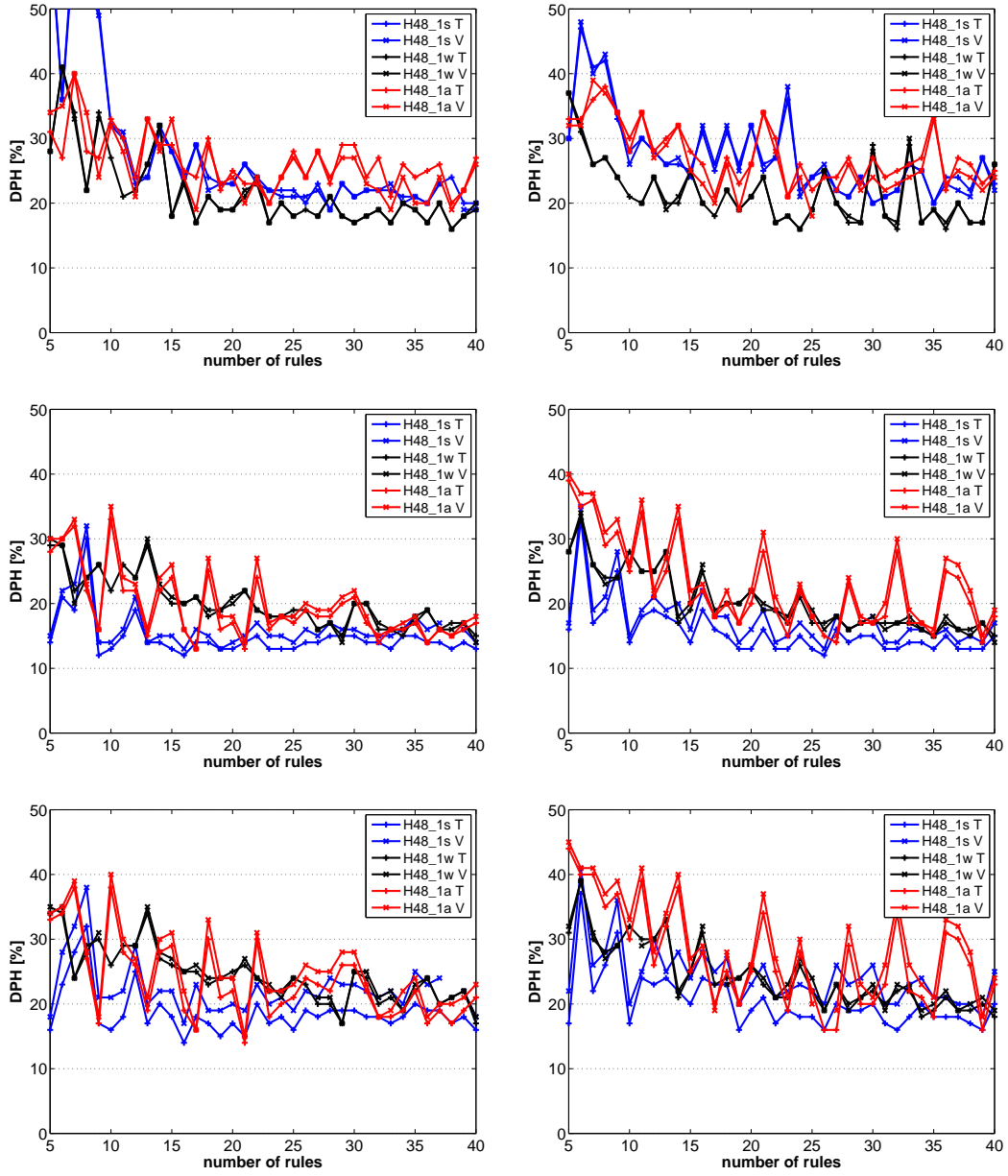


Figure E.2: Development of the DPH values for MS_6MF and MS_T5 (H48_1s, w, a) inference systems (top: all peak; centre / bottom: highest 100 / 50 peaks; T: training, V: validation).

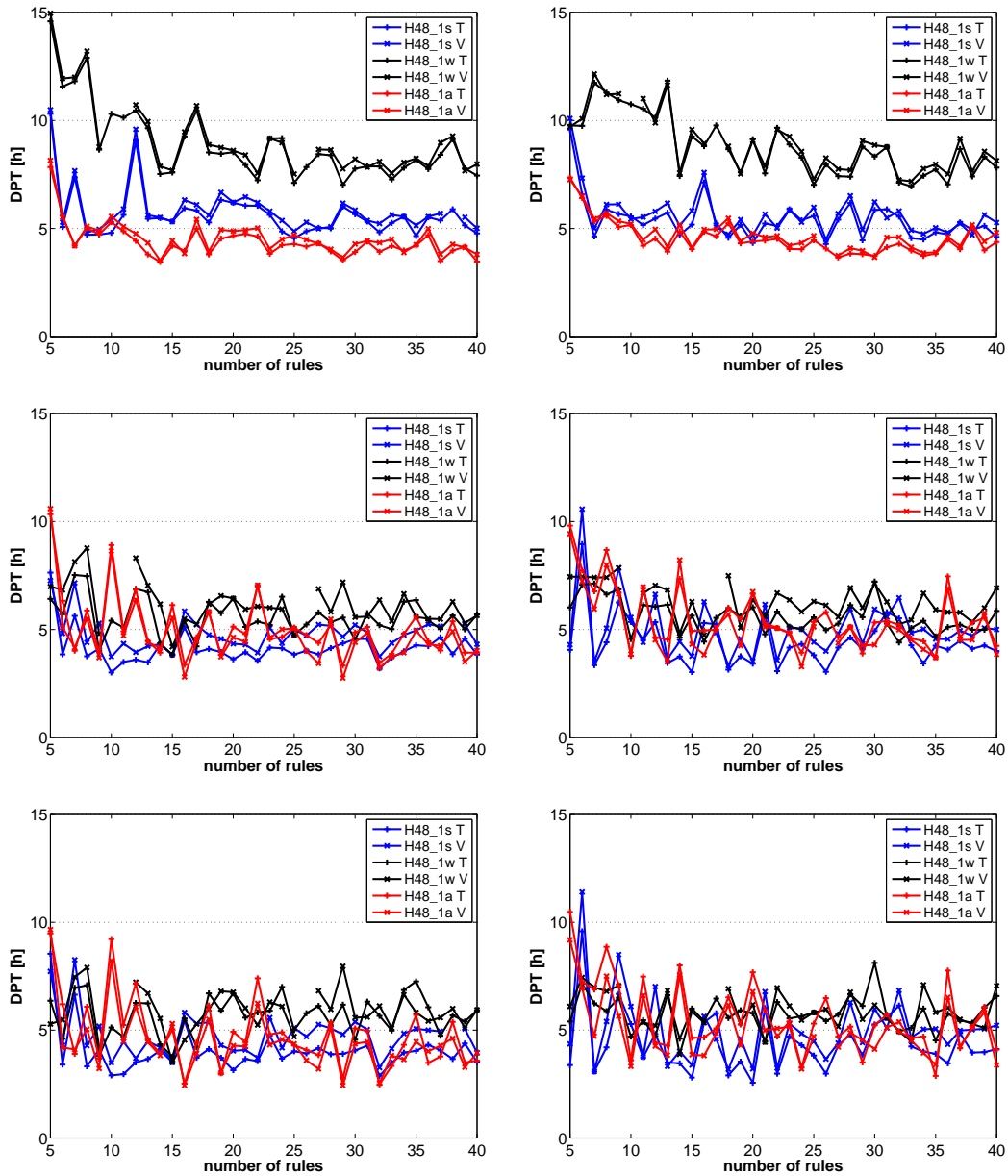


Figure E.3: Development of the DPT values for MS_6MF and MS_T5 (H48_1s, w, a) inference systems (top: all peak; centre / bottom: highest 100 / 50 peaks; T: training, V: validation).